GEOCHEMICAL MONITORING OF THE SEISMIC ACTIVITIES
AND NOBLE GAS CHARACTERIZATION OF THE GEOTHERMAL FIELDS
ALONG THE EASTERN SEGMENT OF
THE BÜYÜK MENDERES GRABEN

A THESIS SUBMITTED TO
THE GRADUATE SCHOOL OF NATURAL AND APPLIED SCIENCES
OF
MIDDLE EAST TECHNICAL UNIVERSITY

BY

SELİN SÜER

IN PARTIAL FULFILLMENT OF THE REQUIREMENTS
FOR
THE DEGREE OF DOCTOR OF PHILOSOPHY
IN
GEOLOGICAL ENGINEERING

FEBRUARY 2010

Approval of the thesis:

GEOCHEMICAL MONITORING OF THE SEISMIC ACTIVITIES AND NOBLE GAS CHARACTERIZATION OF THE GEOTHERMAL FIELDS ALONG THE EASTERN SEGMENT OF THE BÜYÜK MENDERES GRABEN

submitted by **SELİN SÜER** in partial fulfillment of the requirements for the degree of **Doctor of Philosophy in Geological Engineering Department, Middle East Technical University** by,

Prof. Dr. Canan Özgen
Dean, Graduate School of **Natural and Applied Sciences**   _____

Prof. Dr. Zeki Çamur
Head of Department, **Geological Engineering**   _____

Prof. Dr. Nilgün Güleç
Supervisor, **Geological Engineering Dept., METU**   _____

Prof. Dr. Jörg Erzinger
Co-Supervisor, **GeoForschungsZentrum-Potsdam**   _____

Examining Committee Members:

Prof. Dr. Şakir Şimşek
Geological Engineering Dept., Hacettepe University   _____

Prof. Dr. Nilgün Güleç
Geological Engineering Dept., METU   _____

Prof. Dr. Mahmut Parlaktuna
Petroleum and Natural Gas Engineering Dept., METU   _____

Prof. Dr. Erdin Bozkurt
Geological Engineering Dept., METU   _____

Dr. Thomas Wiersberg
GeoForschungsZentrum-Potsdam   _____

Date: February 5, 2010

I hereby declare that all information in this document has been obtained and presented in accordance with academic rules and ethical conduct. I also declare that, as required by these rules and conduct, I have fully cited and referenced all material and results that are not original to this work.

Name, Last name: Selin Süer

Signature   :

ABSTRACT

GEOCHEMICAL MONITORING OF THE SEISMIC ACTIVITIES AND NOBLE GAS CHARACTERIZATION OF THE GEOTHERMAL FIELDS ALONG THE EASTERN SEGMENT OF THE BÜYÜK MENDERES GRABEN

Süer, Selin

Ph.D., Department of Geological Engineering

Supervisor: Prof. Dr. Nilgün Güleç

Co-Supervisor: Prof. Dr. Jörg Erzinger

February 2010, 253 pages

This study aims the real-time monitoring of gases (CO_2, N_2, O_2, H_2, H_2S, CH_4, He, Ar) discharging from natural pools in the Tekke Hamam geothermal field (Denizli) in addition to the geochemical characterization of the field along with the Kızıldere geothermal field, both located at the eastern segment of the Büyük Menderes Graben.

The continuous gas monitoring experiment (November 2007-October 2008) conducted in the Tekke Hamam geothermal field has revealed temporal variations in the gas compositions, gas flow rate and pool temperature. Different variation components, such as daily variation profiles and peak/Multi-day signals, are detected in the monitored data, which are mainly correlated with shallow and deep processes involving mainly meteorological factors and seismicity induced variations, respectively. Particularly, the coupled variations in the gas compositions and flow rate seem to correlate with seismicity induced permeability modifications within the subsurface during the absence of significant meteorological factors, such as high rainfall and varying atmospheric pressure.

The noble gas characterization of the fields have revealed both high ^{3}He/^{4}He and ^{4}He/^{20}Ne isotopic ratios, suggesting a mantle contribution of about 18% for Kızıldere and 34% for Tekke Hamam, whereas the other noble gases (Ar, Ne, Kr, Xe) are of atmospheric nature. The different mantle contributions observed in both fields can suggest a different mantle-He flux variably contaminated by crustal helium. The chemical (cation-trace element-anion) and stable isotopic (δ^{18}O-δD) contents of the thermal waters reveal high temperature water-rock interaction accompanied by the effects of deep origined gases (mainly CO_2 and H_2S) discharging from the fields.

ÖZ

BÜYÜK MENDERES GRABENİNİN DOĞU KESİMİNDEKİ SİSMİK ETKİNLİĞİN JEOKİMYASAL OLARAK İZLENMESİ VE JEOTERMAL SAHALARIN ASAL GAZ KARAKTERİZASYONU

Süer, Selin

Doktora, Jeoloji Mühendisliği Bölümü

Tez Yöneticisi: Prof. Dr. Nilgün Güleç

Ortak Tez Yöneticisi: Prof. Dr. Jörg Erzinger

Şubat 2010, 253 sayfa

Bu çalışma, Tekke Hamam jeotermal sahasında (Denizli) yer alan doğal göletlerden çıkan gazların gerçek-zamanlı izlenmesine ek olarak, bu saha ile yine Büyük Menderes Grabeninin doğu kesiminde konumlanan Kızıldere jeotermal sahasının jeokimyasal karakterizasyonunu amaçlamaktadır.

Tekke Hamam jeotermal sahasında gerçekleştirilen sürekli gaz izleme çalışması (Kasım 2007-Ekim 2008), gaz bileşimleri, gaz akış hızı ve gölet sıcaklığında zamansal değişimlerin olduğunu göstermiştir. İzlenen parametrelerde günlük değişim profilleri ve Ani artış-azalış/Çoklu-gün sinyalleri gibi farklı değişim bileşenleri tespit edilmiş ve bunlar meteorolojik etkiler ve sismisiteye bağlı değişimler gibi sırasıyla, sığ ve derin kökenli süreçlerle ilişkilendirilmiştir. Özellikle, gaz bileşimleri ve akış hızında kimi zaman eşleşen değişimler, yüksek yağış gibi önemli olabilecek meteorolojik etkilerin yokluğunda, sismisiteye bağlı yeraltındaki geçirgenlik değişimleri ile bağdaştırılmıştır.

Sahaların asal gaz karakterizasyonu, yüksek $^3He/^4He$ ve $^4He/^{20}Ne$ izotopik oranları için mantosal katkının Kızıldere sahası için %18 ve Tekke Hamam sahası için de %34 civarında olduğunu göstermekte, diğer asal gazlar için ise (Ar, Ne, Kr, Xe) atmosferik

kökene işaret etmektedir. Her iki sahada gözlenen farklı manto katkıları, sahalarda farklı mantosal-He akısının değişik oranlarda kabuksal helyum ile karıştığını düşündürmektedir. Termal suların kimyasal (katyon-iz-anyon) ve izotopik ($\delta^{18}O$-δD) bileşimleri ise sahalarda genellikle derin kökenli gazların (CO_2 ve H_2S) eşlik ettiği yüksek sıcaklıklı akışkan-kayaç etkileşimlerinin varlığını göstermektedir.

Anahtar Kelimeler: Gerçek-zamanlı Gaz İzleme, Sismisite, Asal Gaz Karakterizasyonu, Kızıldere ve Tekke Hamam Jeotermal Sahaları, Büyük Menderes Grabeni

ACKNOWLEDGMENTS

TABLE OF CONTENTS

LIST OF TABLES

TABLES

LIST OF FIGURES

FIGURES

CHAPTER 1

INTRODUCTION

Earthquake prediction via geochemical monitoring studies in the seismically active regions of the crust have become popular especially in the last several decades. Such studies have focused mainly on the mechanisms inducing earthquakes and the associated response in the affected region of the crust (Thomas, 1988; Toutain and Baubron, 1999). Especially with the development of new and more precise geochemical analysis techniques, geochemical surveys have provided valuable insights into the possible physical and chemical processes prevailing in the crust during seismically active periods.

In the context of geochemical monitoring studies aiming earthquake prediction, both fluid and gas components from different compartments of the Earth (such as groundwaters, soil, atmosphere, etc.) have been monitored either periodically, comprising intervals of weekly and/or monthly monitoring, or continuously, that is, monitoring in real-time, with data acquisition within minutes or even seconds. In this regard, particularly gases dissolved in geothermal fluids, owing to their highly mobile nature in the subsurface, have proved to be very useful tracers of seismicity-induced variations. Variations in dissolved gases in geothermal waters have been reported before, during, and after seismic activities and were considered to reflect physical and chemical processes occurring at depth, such as fluid pressure, fluid-mixing, micro-fracture formation and permeability modifications (Hirabayashi and Kusakabe, 1985).

Amongst the gases of interest, the quite responsive and sensitive ones are the noble gases (He, Ne, Ar, Kr, Xe, with particular focus on the ^{3}He/^{4}He-ratio), whose concentrations and isotopic compositions have frequently been used as natural tracers in the investigation of the origin of geothermal fluids, in understanding the reservoir processes and in the monitoring of seismicity (Lupton, 1983; King, 1986; Thomas, 1988; Kennedy and Truesdell, 1996; Kipfer et al., 2002; Lippmann et al., 2003, 2005; Wiersberg and

Erzinger, 2007). Changes in gas compositions, such as CO_2, H_2S, CH_4, H_2, and variations including He/Ar, CH_4/Ar, N_2/Ar, and ^{3}He/^{4}He ratios, were also proposed to be potential precursors of seismic activities (Sugisaki, 1978; Kawabe, 1985; Sano et al., 1998; Italiano and Martinelli, 2001).

Turkey is a very rich country in terms of geothermal energy and has several geothermal sites associated with frequent seismic activities. Especially western Anatolia, in this respect, houses several high-enthalpy geothermal fields, and has been a site of frequent low-medium magnitude earthquakes in the past decades.

The present thesis study concentrates mainly on two major aspects: i) real-time gas monitoring in an attempt to predict earthquakes and ii) geochemical characterization of geothermal fluids. In this regard, two geothermal fields were selected to be studied in this thesis, namely, the Kızıldere and the Tekke Hamam geothermal fields, both located in the Western Anatolian Extensional Province (Figure 1.1). The Kızıldere geothermal field is located on the northern boundary fault, whereas the Tekke Hamam geothermal field is located on the southern boundary fault of the Büyük Menderes Graben (Figure 1.1b and 1.2), one of the major grabens representing the horst-graben tectonics of the Western Anatolian Extensional Province. The Kızıldere geothermal field comprises the biggest field with one of the highest geothermal energy potential in Turkey and is the first field in Turkey from which electricity is produced from a geothermal power plant with a total installed capacity of 20MWe. The Tekke Hamam geothermal field, on the other hand, has also been a site of importance in terms of geothermal energy and is currently famous for its natural mud pools (having intense gas emissions), and is a center of balneological facilities, housing several thermal resorts and curing centers.
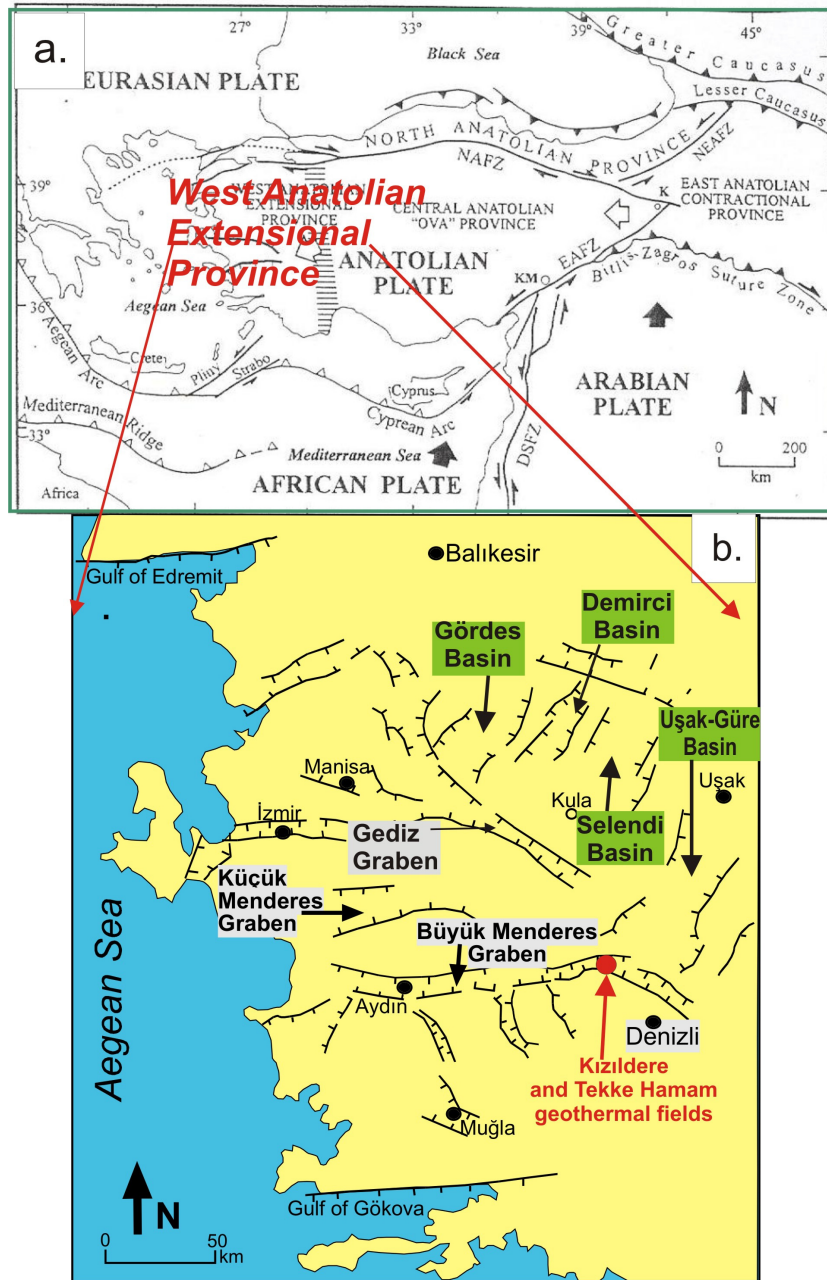
Figure 1.1 a). Tectonic map of Turkey (Bozkurt, 2001), b). Simplified major structural elements of Western Anatolia (Bozkurt, 2001).
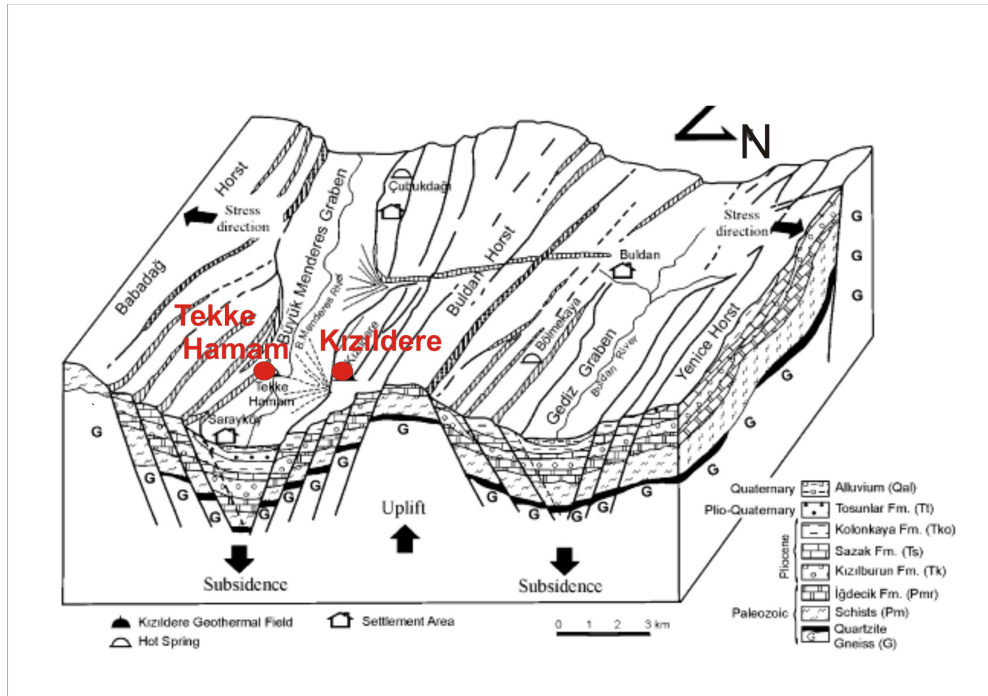
Figure 1.2 Location of the Kızıldere and Tekke Hamam geothermal fields in the Büyük Menderes Graben (Şimşek, 1985).

1.1 Purpose and Scope

The purpose of this thesis study is

    (i)   the continuous/real-time monitoring of the compositions of gases discharged from the ground of a bubbling pool in the Tekke Hamam geothermal field and the further evaluation of any possible compositional variations in relation to seismicity occurring nearby

    (ii)   the geochemical characterization of both the Tekke Hamam and the Kızıldere geothermal fields.

Within the framework of the real-time gas monitoring part of the thesis, after a major reconnaissance survey in the vicinity of the geothermal fields, the natural gas discharging pools in the Tekke Hamam geothermal site were selected for the operation of the real-

time monitoring study. The main criteria for the selection of the natural pools in the Tekke Hamam geothermal site, instead of the production wells in the Kızıldere geothermal field, was to avoid any possible man-influence on the gases, which can be more pronouncable in the gases discharging from wells, as opposed to the natural emissions. Therefore, as a major aim to detect the most earth-related, pure gas compositional/flux variations that can be correlated with seismicity, the natural gas discharging pools (Pool 2 and Pool 3) in the Tekke Hamam geothermal field were selected as the target sites for the real-time gas monitoring experiment. In this regard, a Quadrupole Mass Spectrometer (QMS) was used in the monitoring of gas compositions from a bubbling pool in the Tekke Hamam geothermal field. The nearly year round continuous, on-site gas monitoring experiment was started in late November 2007, and was operated till the end of October 2008. During monitoring, possible temporal variations in the dissolved gas compositions of CO_2, CH_4, H_2, H_2S, N_2, O_2, He and Ar were continuously recorded along with the flow rate of the gas fluxes and the pool temperature. As possible external factors, seismic events and some meteorological parameters relevant to geochemical changes were compiled during the course of monitoring.

In addition to the real-time gas monitoring experiment performed in the Tekke Hamam geothermal field, a chemical-isotopic survey, mainly concentrating on the noble gas characterization of both Tekke Hamam and Kızıldere geothermal fields, was conducted via the off-line analysis of both gas and fluid samples collected from wells and/or springs/natural bubbling pools. Although there exists many other medium-to high enthalpy geothermal fields within western Anatolia, the main selection criteria of the two fields for the geochemical characterization part of the thesis was to i) get a full set of noble gas analyses which was not conducted so far in the region, and ii) to see if there is any major difference in the noble gas character of the two fields, both located at different boundary faults of the graben. In addition, since previous studies (Güleç and Hilton, 2006) have also shown that the highest heat flow of western Anatolia, accompanied by the highest mantle helium component, is localized at the eastern end of the Büyük Menderes Graben, where the Kızıldere and Tekke Hamam geothermal fields coexist, the two fields were taken into the scope of the present thesis to better evaluate and constrain any possible crustal-mantle interactions within the subsurface.

1.2 Materials and Methods

The methods that were utilized in this thesis study are shortly summarized as follows:

i. *Real-time Gas Monitoring*

The gas monitoring station was constructed near a natural bubbling pool in the Tekke Hamam geothermal field. The gas compositions were monitored by means of a Quadrupole Mass Spectrometer (QMS), where gas discharged at the ground of the pool was collected in a funnel and was continuously transferred to the measuring devices. The QMS was set to measure the CO_2, CH_4, H_2, H_2S, N_2, O_2, He and Ar compositions. In addition to the QMS, a flowmeter and a temperature sensor were also used for the online recording of the gas flux rate and the pool temperature, respectively. All of the monitored parameters were measured within one minute intervals. Data storage was done via the operation of the QUADSTAR and the LABVIEW computer softwares for the gas compositions and the gas flow rate and pool temperature, respectively. Some other additional devices, such as UPS (Uninterrupted Power Supply) and air conditioning units, were also used in the monitoring station for the avoidance/minimization of power cut offs and the maintanance of the suitable insitu ambient temperature conditions in the station, respectively.

During the course of monitoring, routine field visits (nearly once every month) were also performed in order to check the performance of the equipment in the monitoring station and perform gas calibrations when necessary.

In addition to the monitored gas data, the seismic events (epicenter, focal depth, magnitude) that occurred in the vicinity of the monitoring site were compiled from the website records of the Kandilli Observatory and Earthquake Research Institute in İstanbul. The daily meteorological data, on the other hand, comprising atmospheric pressure (mbar), rainfall amount (mm) and air temperature (maximum, minimum, average ºC) were taken from the Turkish State Meteorological Service.

ii. Chemical and Isotopic Analyses

Water and gas sampling was performed during 3 main sampling campaigns conducted in the Kızıldere and Tekke Hamam geothermal fields. Water and gas samples were taken from wells and/or pools/springs in the geothermal fields. The water samples were analysed for their cation-trace element-anion and stable isotope contents. The gas samples, on the other hand, were analysed for their noble gas compositions and isotopic ratios (He (^{3}He/^{4}He), Ne (^{20}Ne/^{22}Ne, ^{21}Ne/^{22}Ne), Ar (^{40}Ar/^{36}Ar, ^{38}Ar/^{36}Ar), Kr, Xe).

- Cation-trace element and Anion analyses: Cation-trace element and anion analyses of the water samples were conducted at the ACME Laboratories (CANADA) for the first sampling campaign and at the SRC Laboratories (CANADA) for the second and third sampling campaigns.
- ^{18}O/^{16}O and D/H analyses: The stable isotope analyses of the samples were conducted at the Environmental Isotope Laboratories of the University of Waterloo (CANADA).
- Noble gas analyses: The noble gas analyses of the gas samples collected from the fields were performed at the GFZ-Potsdam Noble Gas Laboratories (GERMANY).

iii. Data Evaluation

The data gathered during the thesis study were evaluated with two separate aims: (i) evaluation of gas monitoring results from the Tekke Hamam geothermal site and (ii) evaluation of the geochemical properties of both Kızıldere and Tekke Hamam geothermal fields. The continuous gas monitoring results were evaluated in terms of:

- investigation of the gas compositional variations and their possible relations to the meteorological factors and seismic activities occurring in the field,
- interpretation of the possible sources/mechanisms of the gases discharging from the pools in the Tekke Hamam geothermal field.

The geochemical evaluation stage of the thesis study concentrated on:

- Characterization of the hydrogeochemical facies of the Kızıldere and Tekke Hamam geothermal waters and their possible physico-chemical evolution in the subsurface.
- Stable isotopic evaluation of the fields; origin of geothermal waters (meteoric, magmatic, palaeo) and the possible physico-chemical processes occurring at depth.
- Noble gas characterization of the two fields: the possible origins of the noble gases, and evaluation of the possible interactions prevailing between crust-mantle-atmospheric compartments; that is, the source provenance of the gases dissolved in the geothermal fluids.

1.3 Layout of Thesis

This thesis is divided into 9 chapters. Following this introduction chapter (Chapter 1):

Chapter 2 is concerned with the regional geology, as well as the geologic and hydrogeologic outline of the studied geothermal fields.

Chapter 3 gives an overview of the geochemical monitoring studies dealing with earthquake prediction.

Chapter 4 is a brief summary of the major principles of noble gases and their applications.

Chapter 5 gives information about the online monitoring station construction and sampling procedures performed during the study.

Chapter 6 presents the results of the chemical and isotopic analyses, together with a discussion of the results with regard to the hydrogeochemical facies and possible subsurface processes.

Chapter 7 is about the noble gas characterization of the Kızıldere and Tekke Hamam geothermal fields.

Chapter 8 discusses the temporal variations recorded during the real-time monitoring study and their possible relations with seismic activities and meteorological factors, plus the possible source provenance of the gases emitted from the Tekke Hamam geothermal site.

Chapter 9 gives the conclusions derived from the thesis study, as well as the recommendations for future studies aiming similar purposes.

CHAPTER 2

KIZILDERE AND TEKKE HAMAM GEOTHERMAL FIELDS:
GEOLOGICAL AND HYROGEOLOGICAL BACKGROUND

2.1 Tectonic Setting and Regional Geology

Kızıldere and Tekke Hamam geothermal fields are located within the western Anatolian region of Turkey whose tectonic evolution has been, in the simplest terms, the result of the destruction of Paleo-Tethys and the birth and the subsequent demise of Neo-Tethys. The sequence of events has been much more complicated, however, and were mainly characterized by a number of mini-oceans that have repeatedly opened and closed since Permian (Şengör and Yılmaz, 1981).

Turkey's present geologic framework was established during the Alpine orogeny as a result of the collision between the African and the Arabian plates. The collision between these two plates was associated with the separation, rotation, collision and deformation of small continental fragments in the intervening area. During this orogeny, various suture zones, forming the boundaries of several micro-continents, were developed in Turkey (Şengör and Yılmaz, 1981; Okay, 1986; Bozkurt and Mittwede, 2001). Throughout the evolution of Neo-Tethys in the general area of Turkey, the microcontinents constantly changed shape and position as a result of a semi-continuous series of rifting, shearing and collision phenomena (Şengör and Yılmaz, 1981).

One of the earliest tectonic subdivisions of Turkey was by Ketin (1966) who differentiated 4 major belts, namely, Pontides, Anatolides, Taurides and Border Folds. Later, several subdivisions were proposed by several authors (e.g. Şengör and Yılmaz, 1981; Şengör, 1984; Okay, 1986; Okay and Tüysüz, 1999). The tectonic units differentiated in these subdivision schemes are the microcontinental fragments the boundaries of which are formed by the Neo-Tethyan suture zones.

According to the division scheme of Şengör (1984), there are four major paleotectonic units of Turkey, which are from north to south, the Rhodope-Pontide fragment, Sakarya continent, Kırşehir block and the Menderes-Taurus Platform. These units are separated from each other by various Neo-Tethyan suture zones (Figure 2.1).

Western Anatolia covers the Sakarya Continent to the north and the Menderes-Taurus platform to the south (Figure 2.1). These paleotectonic units are separated from each other by the İzmir-Ankara Suture, which represents a branch of the Neo-Tethys (Şengör, 1984).

The Sakarya continent is delimited in the north by the Intra Pontide, and in the south by the İzmir-Ankara suture zones. The basement, which is mostly represented by the Karakaya complex, consists of unmetamorphosed to variably metamorphosed rocks ranging in age from Late Paleozoic to Late Triassic. Jurassic to Tertiary clastics and carbonates unconformably overlie the basement.

The oldest unit of the Menderes-Taurus block is the Menderes Massif, consisting of metamorphic rocks of various grade. The Menderes Massif (Bozkurt and Park, 1994; Hetzel et al., 1995; Gessner et al., 2001) represents a well developed metamorphic core complex located in Western Turkey. The massif also represents one of the oldest basements in Turkey and is mainly composed of orthogneisses forming the core (known as 'core augen gneiss') and an overlying low-grade metasediments, known as the 'cover series' (Satır and Friedrichsen, 1986). Geological and geochronological evidence indicates different episodes of deformation and metamorphism in different parts of the massif (Şengör et al., 1984).

The Western Anatolian Graben system (WAGS), in other words, the West Anatolian Extensional Province, is one of the most important structural features representing the neotectonic period of Turkey which has been governed since the late Miocene by the collision and further convergence of the Arabian Block in the south, and the Eurasian block in the north (Mc Kenzie, 1972; Dewey and Şengör, 1979; Bozkurt, 2001) (Figure 1.1a).
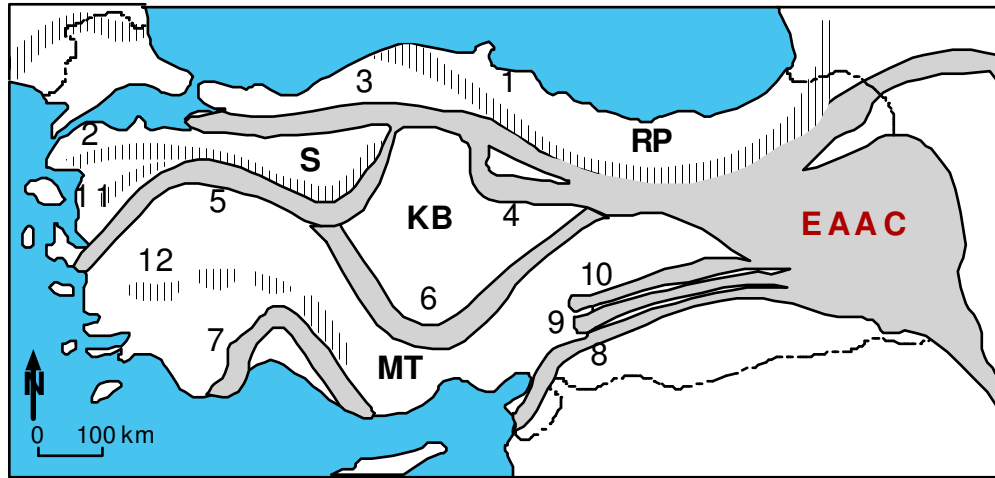
Figure 2.1 Palaeotectonic units and suture zones of Turkey (RP: Rhodope-Pontide Fragment, KB: Kırşehir Block, S: Sakarya Continent, MT: Menderes-Taurus Platform, EAAC: East Anatolian Accretionary Complex, 1: Main Palaeo-Tethys Suture, 2: Karakaya Suture, 3: Intra Pontide Suture, 4: Erzincan Suture, 5: İzmir-Ankara Suture, 6: Inner Tauride Suture, 7: Antalya Suture, 8: Asurid Suture, 9: Çüngüş Suture, 10: Maden Suture, 11: Hercinian Suture, 12: Pan-African Suture) (Şengör, 1984).

The Western Anatolian Graben System is an area of intense seismic activity which is related to the east-west trending graben complexes in the Aegean region. The broad tectonic framework of the Aegean is dominated by the rapid westward motion of the Anatolian Plate relative to the Black Sea plate and west-southwestward motion relative to the African Plate (McKenzie, 1972). Fault plane solutions and maps of surface breaks suggest that the motion is taken up to the west on a number of E-W grabens and that the N-S component of the motion increases southwestward. The westward movement of Turkish plate carries western Turkey through an extensional zone where the continent is streched and its thickness halved. The streching in Western Turkey is not confined to a small number of faults, but occurs throughout large regions (McKenzie, 1978). According to Dewey and Şengör (1979), the tectonics of the Aegean region involves complex slip patterns across the boundaries of several microplates that segment the end of the Anatolian Plate. The westward escape is faciliated by the subduction of the oceanic floor of the eastern Mediterranean at the Hellenic Trench. Although the westward motion is accomplished simply at the Hellenic Trench and along the East and North Anatolian

12

transform faults, the motion is retarded by intracontinental locking between the Sea of Marmara and the northern end of the Hellenic Trench. This locking results in a complex pattern of grabens and trust and strike-slip deformation that segment the western end of the Anatolian plate and the southwestern corner of the Black Sea plate into a number of small scholles.

Western Turkey is known to be a site of widespread active continental extension and has been experiencing approximately N-S-directed extension since, at least, latest Oligocene-Early Miocene, and is currently under the influence of forces exerted by northward subduction of the African plate beneath the southern margin of the Anatolian plate along the Aegean-Cyprean subduction zone and dextral slip on the North Anatolian fault system (Bozkurt and Mittwede, 2005) (Figure 1.1a).

The E-W trending grabens (e.g., the Gediz Graben, the Küçük Menderes Graben, the Büyük Menderes Graben) in Western Anatolia constitute the most prominent neotectonic features of the region (Figure 1.1b). These grabens and their bounding high-angle normal faults are the most seismically active elements of western Turkey, and their activity is evidenced by previous historical earthquakes that occurred in the region. In addition to the E-W grabens, NE-SW-trending basins, such as the Gördes, Demirci and Selendi basins, are also found in the region (Bozkurt, 2003) (Figure 1.1b).

The age of the major E-W trending grabens within the western Anatolian extensional province has been an issue of considerable debate among scientists for the last decades. Some authors stated that the E-W trending grabens commenced to exist during the Tortonian (Şengör and Yılmaz, 1981; Şengör et al., 1985; Şengör, 1987). Later, other authors, based on the palynological data from the Gediz and Büyük Menderes grabens, stated that the basins commenced to exist during the Early Miocene and continued their evolution since then (Seyitoğlu and Scott, 1991, 1992, 1996; Seyitoğlu et al., 2002). Other studies, on the other hand, proposed a different view on the possible age of the grabens. They stated that the prevailing N-S neotectonic extension in western Turkey and the resulting E-W grabens began to develop in or later than 5Ma (Plio-Quaternary) (Bozkurt and Park, 1994; Bozkurt and Park, 1997; Koçyiğit et al., 1999; Bozkurt, 2000, 2001, 2002).

Therefore, studies conducted until now proposed different ideas and models on the origin, timing and evolution of Neogene crustal extension prevailing in western Turkey. In this regard, mainly four different models have been proposed in relation to the possible mechanisms controlling the origin of extension prevailing in the region: 1) the back-arc spreading model: this model argues that the back-arc extension is caused by south-southwestward migration of the Hellenic Trench System (McKenzie, 1978; LePichon and Angelier, 1979), 2) the orogenic collapse model: this model argues that the localized extension is related to the spreading and thinning of over thickened crust, following the latest Palaeocene collision across Neotethys during the Late Oligocene-Early Miocene (Seyitoğlu and Scott, 1991; McClusky et al., 2000), 3) the tectonic escape model: this model argues that extension in western Turkey resulted from westward extrusion of Anatolia between its bounding structures, the dextral North and the sinistral East Anatolian fault zones, since the late Serravalian (12Ma) (Dewey and Şengör, 1979; Şengör et al., 1985), and 4) the episodic, two-stage graben model: this model argues that the extension occurs in two distinct structural styles of different timing: an Early-Middle Miocene phase of core-complex formation and a subsequent modern phase of Plio-Quaternary normal faulting and graben formation, with an intervening phase of N-S short-term compression and accompanying N-S crustal shortening during late Serravalian-late Early Pliocene times. The two stages of extension proposed in the final model are attributed to orogenic collapse and westward escape of the Anatolian block (Koçyiğit et al., 1999; Bozkurt, 2000, 2001, 2003, 2004; Yılmaz et al., 2000, Westaway, 2003; Bozkurt and Rojay, 2005).

In addition to its tectonic significance, the Western Anatolian Graben system (WAGS) houses many of the important high enthalpy geothermal fields of Turkey. The Kızıldere and Tekke Hamam geothermal fields, in this respect, are the two most important geothermal fields located within the Western Anatolian Graben System (Figure 1.1b and Figure 1.2). The Kızıldere geothermal field is located on the northern, whereas the Tekke Hamam geothermal field is located on the southern boundary faults of the Büyük Menderes Graben, which is one of the major grabens characterizing the WAGS (Figure 1.2).

2.2 Recent Seismic Activities

Western Anatolian region is characterized by several, recent low-to-medium magnitude seismicity associated with the active tectonism. In other words, the occurrence of geothermal activity is very much related to the faults bounding the major grabens in Western Anatolia, that is, to the seismic remnants of the extensional tectonics prevailing in the region since the Miocene.

During the course of the real-time gas monitoring conducted in the Tekke Hamam geothermal field (from November 2007 to October 2008), no major destructive seismic event, exceeding M= 5.0, occurred within the vicinity of the area. However, several seismic activities (having magnitudes dominantly changing between 3.0<M<4.0) were recorded in the vicinity of the geothermal fields, especially concentrated along the Çameli-Denizli district, nearly 100 km south of the Kızıldere and Tekke Hamam geothermal fields.

2.3 Volcanism

Volcanism in western Anatolia has been active since the Eocene. The most voluminous products of volcanism in western Anatolia is represented by the calc-alkaline Miocene – Pliocene volcanics, which consist of lava flows, domes and agglomerates of mainly andesitic-dacitic composition (Innocenti et al., 1982; Ercan et al., 1983; Savaşçın and Güleç, 1990). Pliocene to Quaternary volcanics are mainly exposed in the southern Aegean forming the typical island arc associated with the subduction along the Hellenic Trench, and they are mainly calc-alkaline in nature with basaltic to rhyolitic composition (Fytikas et al., 1984). Quaternary volcanism in western Anatolia, on the other hand, is mainly represented by the Kula volcanics, observed as lava flows, cones and craters, and are mainly characterized by silica-undersaturated alkali olivine basalt having typical intraplate characteristics (Güleç, 1991).

2.4 Stratigraphy

The region of interest is characterized by the presence of three major rock units: the metamorphic rock series (Menderes Massif Metamorphics) which form the basement of the area, the fluvial and lacustrine Pliocene units and finally the Quaternary deposits representing the youngest units of the area.

In Figure 2.2, the generalized stratigraphic section common to both Kızıldere and Tekke Hamam geothermal fields is shown. Figure 2.3 gives the geological map of the area.

2.4.1   The Menderes Massif Metamorphics

The oldest units in the study area are the widely distributed metamorphics of the Menderes Massif which form the basement of the geothermal fields located along the whole range of the Büyük Menderes Graben.

The Menderes Massif (Bozkurt and Park, 1994; Hetzel et al., 1995; Gessner et al., 2001) is a well developed metamorphic core complex located in Western Turkey. It comprises three submassifs (northern, central and southern), each of which is interpreted as a core-complex exhumed at different times during the Neogene history of southwest Turkey. The E-W trending Gediz Graben in the north and the Büyük Menderes Graben in the south form the boundaries of the three submassifs (Bozkurt, 2007).

The Menderes massif comprises two major rock associations: a core and cover series. The core rocks are composed of augen gneisses, migmatites, gabbros with some granulite and eclogite relics, and medium- to high-grade metamorphic schists (Şengör et al., 1984; Satır and Friedrichsen, 1986; Oberhänsli et al., 1997; Candan et al., 2001). The cover series is represented by a Palaeozoic schist envelope and a Mesozoic to Cenozoic marble envelope. The Palaeozoic schist envelope comprises garnet, kyanite, staurolite-bearing micaschists, graphite-rich quartzitic phyllite–schists, garnet amphibolites, and marble intercalations (Dürr, 1975; Akkök, 1983; Satır and Friedrichsen, 1986; Bozkurt, 1996; Hetzel et al., 1998; Whitney and Bozkurt, 2002). The thick marble envelope of the cover series overlie the schist sequence. The core of the Menderes Massif is dated as

16

Precambrian (Gessner et al., 2004), whereas the cover sequence is dated as Palaeozoic to Early Tertiary (Graciansky, 1965; Bozkurt and Park, 1994). The rocks of the Menderes Massif were metamorphosed during the Eocene, coeval with major Alpine collision in Anatolia (Whitney and Bozkurt, 2002).

Below is a brief description of the metamorphic stratigraphy in the Kızıldere and Tekke Hamam geothermal fields. From bottom to top, the stratigraphy is represented by gneisses, quartzite-gneiss-schist alternations, schists (micaschist unit), and an alternation of quartzites, micaschists and marbles known as the İğdecik formation (Figure 2.2) (Şimşek, 1984).

Gneiss (Pgny)

The gneiss unit, which forms the core and basement of the Menderes Massif metamorphics, outcrops along the Buldan and Yenice horsts. The gneisses differ according to the composition and metamorphism degree of their parent rock. They are classified by names such as augen, biotite-bearing and migmatitic gneiss accoring to their texture and mineral contents (Schuiling, 1962; Ayan, 1973; Dora, 1975), whereas they are classified as ortho-(Graciansky, 1965) and para- (Schuiling, 1962; Dora, 1975) according to their origin.

Quartzite-gneiss-schist alternations

At the upper levels of the gneisses, there are quartzite levels which appear to alternate with the gneisses below and the schists above. The thickness of this alternation reaches 150 m in some places, and the alternation appears to be intensely fractured.

Micaschist (Pm)

The quartzite-gneiss-schist alternation is overlain by a thick unit of micaschists. The micaschist unit consists of quartz, biotite, muscovite, chlorite, albite, calcite and garnet schists, all laterally and vertically gradational within their range. The mica schist levels

are seen mostly in the uplift zones, outcroping along the Buldan horst (Figure 2.3) (Şimşek, 1984).

İğdecik Formation (Pmr)

The alternation of quartzites, micaschists and marbles is named as the İğdecik formation, and it represents the uppermost unit of the Menderes Massif metamorphics (Şimşek, 1984) (Figure 2.2, 2.3). The rocks forming the İğdecik formation are intensely faulted and fractured, and represent the second geothermal reservoir in the field (Şimşek, 1984). This unit widely outcrops along the eastern part of the Menderes Massif.

The marbles of the formation are generally white to dark-gray coloured, coarsely grained, and abundantly jointed and fractured (Şimşek, 1984). The marbles outcrop along the horsts in the area and they are seen as thick layers (25-75 m) along the Büyük Menderes River. The micashist levels within the formation are generally white colored, locally coarse grained, locally garnet bearing, shiny, and jointed and fractured. The quartzites, on the other hand, are white to yellow in color, hard, mica bearing, fractured and abundantly jointed (Şimşek, 1984). The thick marble layers within the formation are seen as intercalations with schists and quartzites at the topmost levels of the schists. Within the schists, first the calcschists, and above are the thick layered marbles. The quartzite, micaschist and marble layers of the İğdecik formation are both vertically and laterally gradational.

The whole metamorphic complex of the Menderes Massif passes to the sedimentary sequence above through an erosional surface, represented by an angular unconformity.

2.4.2   Tertiary Formations

The basin fill above the metamorphic basement is divided into different names by various researchers.

According to Koçyiğit (2005), in the region covering the Kızıldere and Tekke Hamam geothermal fields (Denizli Horst Graben System (DGHS)) the graben fills overlying the

metamorphic rocks of the Menderes Massif are divided into categories as pre-graben, ancient graben and modern graben fill. The pre-graben fill, represented by the Gökpınar sequence (Late Oligocene-Early Miocene), overlies the metamorphic rocks of the Menderes Massif, and is a shallow-marine to terrestrial sequence consisting of reddish-brown, unsorted to poorly sorted conglomerate, grey sandstone, and a yellow-brown sandstone and mudstone alternation. Above the pre-Graben fill, ancient and modern graben fills exist. The ancient graben fill consists of two major sequences: the Hacıbekir and the Denizli sequences. The first major unit of the ancient graben fill, the Hacıbekir sequence, begins with a basal conglomerate and then continues upward with an alternation of various lithologies which comprise a 600-m-thick fluvio-lacustrine volcano-sedimentary sequence. The second major unit of the ancient graben fill is the Denizli sequence and consists of two subsequences, namely the eastern sequence and the western sequence. The eastern sequence is exposed east of the city of Denizli, beginning with a basal conglomerate and continuing upward with a thin-bedded to laminated yellow-reddish mudstone, siltstone, sandstone, finer-grained conglomerate and marl alternating with channelized conglomerate intercalations. The western sub-sequence is exposed to the west of the city of Denizli and begins with a basal conglomerate which are succeeded by sandstone, siltstone, and mudstone and marl alternation with channelized conglomerate intercalations. A late Middle Miocene-Middle Pliocene age is proposed for the Denizli sequence. Finally, the modern graben fill consists of two major successions: (1) coarser-grained lateral marginal deposits (fan-apron deposits, older travertines) and (2) finergrained axial depocentral (alluvial-plain-travertine) deposits.

In the studies done by Çemen et al (2006), the sedimentary sequence above the metamorphic basement around the Denizli region is divided into different namings. The Hasköy formation is the oldest sedimentary sequence along the northern margin of the Büyük Menderes Graben, and is mainly composed of sandstone, claystone, limestone, and lenses of coal. The Hasköy formation is conformably overlain by the Kızılcagedik formation and this formation is unconformably overlain by the Asartepe formation. All the sedimentary formations are unconformably overlain by Quaternary alluvium.

Other lithostratigraphic divisions of the area were also made by other authors (Westaway et al., 2005; Kaymakçı, 2006).

Below is a brief summary of the lithostratigraphic units observed in the vicinity of the study area, according to the lithostratigraphic division given by Şimşek (1984). The Tertiary units, from bottom to top, are represented by the Lower-Pliocene Kızılburun, Sazak and Kolankaya formations and the Upper Pliocene Tosunlar formation.

2.4.2.1 Kızılburun Formation (Tk, Pl_1)

The Kızılburun formation is the first unit to overlie the Menderes Massif metamorphics with an angular unconformity (Figure 2.2). The Kızılburun formation outcrops mostly along the horsts and consists of mainly conglomerate, sandstone and claystone alternation, with intercalations of lignite layers at some levels.

The unit starts with coarse grained basal conglomerates, which are generally loosely compacted, red to brown colored, bearing schist, quartzite and marble fragments. The conglomerate basement is overlain by alternating beds of fine-grained conglomerate, fine- to medium-grained and yellow colored sandstone and red claystone, intercalated with lignite lenses. There exists also clayey limestone and marl levels along the lignite beds which are characterized by abundant macrofossils such as Gastropods (Şimşek, 1984).

The thickness of the Kızılburun formation varies around 200 m (0-400m) and increases towards the north from the center of the Büyük Menderes Graben and decreases towards the east and west (Şimşek, 1984; Şimşek et al., 2005). The age of the Kızılburun formation is accepted as Early-Pliocene (Şimşek, 1984).

2.4.2.2 Sazak Formation (Ts, Pl_2)

The Sazak formation overlies the Kızılburun formation and it is vertically gradational with this formation below and the Kolankaya formation lying above (Figure 2.2). The Sazak formation is mainly composed of limestone, marl, siltstone, claystone and diatomite (Şimşek, 1984).

The type locality of the Sazak formation is the Sazak village, located in the northeast of the Kızıldere geothermal field. The formation is composed of mainly limestone and marl at this section. The limestones of the formation are gray colored, fractured, hard egded, definitely layered, algea and gastropod bearing, and contain gypsum. Marl layers are light yellow in color and contain Gastropods. The thickness of the formation varies in the range of 150 to 350 m (Figure 2.2).

According to the fossils it bears, such as Radix, Congeria and Dreissensia, the formation represents the fresh water environment of the Pliocene. The Sazak formation is accepted as the unit which forms the first, uppermost reservoir for the geothermal fields; however, due to the lateral facies changes observed in the formation, the continuity of the reservoir is reduced (Şimşek, 1984). The age of the Sazak formation is accepted as Early Pliocene (Şimşek, 1984).

2.4.2.3 Kolankaya Formation (Tko, Pl₃)

The Kolankaya formation overlies the Sazak formation and is the uppermost unit representing the Lower Pliocene (Figure 2.2). The Kolankaya formation is mainly composed of alternations of sandstone, marl and siltstone, and shows lateral facies changes.

According to the typical stratigraphic section taken from the Kolankaya site at the east of the Sazak village, the transition zone of the Sazak and Kolankaya formations starts with sandstone and clayey limestone levels. In this section, towards the upper parts, the unit passes into sandstone-limestone alternation and towards the upper levels it passes into sandstone and marl. The sandstones are yellow colored, fine to medium grained, definitely layered and abundantly gastropod bearing. Marl and clayey limestone levels are generally gray in color and abundantly fossil bearing. The fact that the unit alternates with clayey and marly layers imposes this formation a good cap rock characteristic (Şimşek, 1984). The total thickness of the formation cut along this section is nearly 500 m, however, the thickness varies around the range of 350 to 500 m (Şimşek, 1984; Şimşek et al., 2005).

The Kolankaya formation generally outcrops along the grabens and partly along the horsts. It represents the low energy, lacustrine, fresh water environment (Şimşek, 1984). According to the analysis of fossils, the Kolankaya formation is accepted as Early Pliocene in age.

2.4.2.4 Tosunlar Formation (Tt, Pl$_4$)

The Tosunlar formation represents the uppermost unit of the Pliocene formations, and overlies the Lower Pliocene units with an angular unconformity (Şimşek, 1985) (Figure 2.2).

The Tosunlar formation mainly consists of alternations of gray, poorly consolidated, partly bouldery, reddish and yellowish conglomerate, sandstone, siltstone and fossiliferous clayey limestone. The conglomerates in this unit consist of gneiss, schist, marble and quartzite fragments from the Menderes Massif, and gravel fragments of the Lower Pliocene Kızılburun, Sazak and Kolankaya formations. The Tosunlar formation directly lies disconcordantly over the Paleozoic gneiss and schist levels along the western part of Kızıldere. Close to Kızıldere, the contact of the Tosunlar formation and gneisses of the Paleozoic is faulted. The thickness of the Tosunlar formation is about 500 m (Şimşek, 1984).

The Tosunlar formation outcrops generally within the graben and in the hanging wall of the faults. The typical outcrop of the formation is seen around the eastern part of Kızıldere geothermal field, and in the Tekke Hamam geothermal field. The Tosunlar formation is Late Pliocene-Quaternary in age.

2.4.3 Quaternary

The Quaternary is represented by alluvium, terrace deposits, alluvial fans, slope debris and travertine (Figure 2.2, 2.3).

Alluvium (Qal)

The alluvium of the Menderes river covers a very broad area. Between the Kızıldere village and Tekke Hamam, the thickness of the alluvium reaches nearly 3 km. The thickness of the alluvial cover increases towards east and is thickest at the site where the Gediz and Büyük Menderes grabens intersect. The alluvial deposits are mainly composed of pebble, sand and clay alternations.

At the sites where rivers meet grabens, broad alluvial fans can be observed. Slope debris in the area is represented by loosely compacted, coarsely blocked, gravelly, sandy and clayey units.

Travertine deposits are also seen in the area, especially found in the vicinity of Yenice town, in Tekke Hamam and near Kızıldere hot springs. The travertines are reddish to yellowish in color, and porous and low in strength. The main composition is $CaCO_3$, but at some parts silica becomes dominant. In the eastern part of the study area, in Pamukkale and Karahayıt sites, broad travertine formations are also observed. In Pamukkale the travertines are white colored, whereas in Karahayıt, because of the high iron and manganese contents of the waters, travertines are observed as yellow to brown in color.

Terrace Deposits (Qtr)

The terrace deposits consist of weakly cemented flat or edgy gravel, sand, clay and silt (Figure 2.2). The gravel fragments are basically the Menderes Massif metamorphics and the Pliocene limestones. In the south of Sarayköy, E-W trending two terrace deposits at different levels are observed.
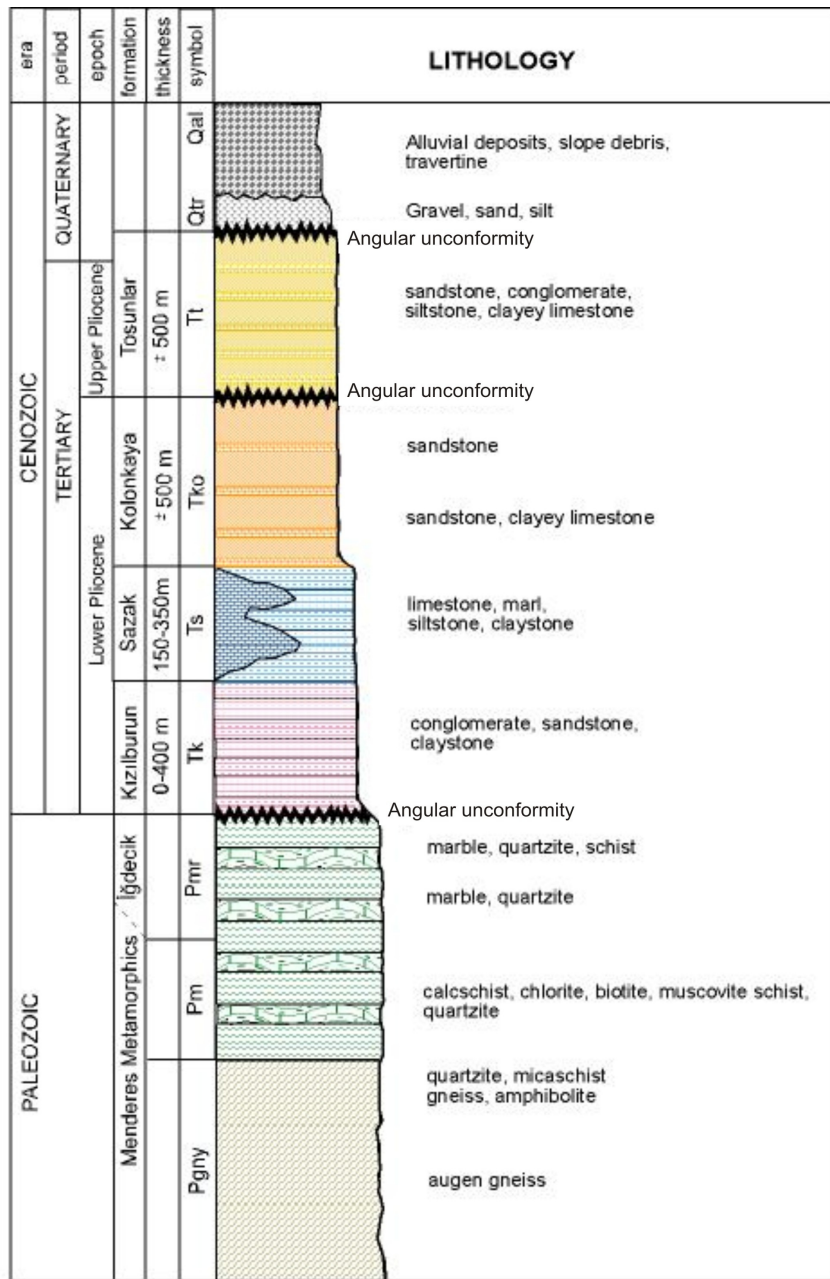
Figure 2.2 General stratigraphic succession common to both Kızıldere and Tekke Hamam geothermal fields (Şimşek, 1984).
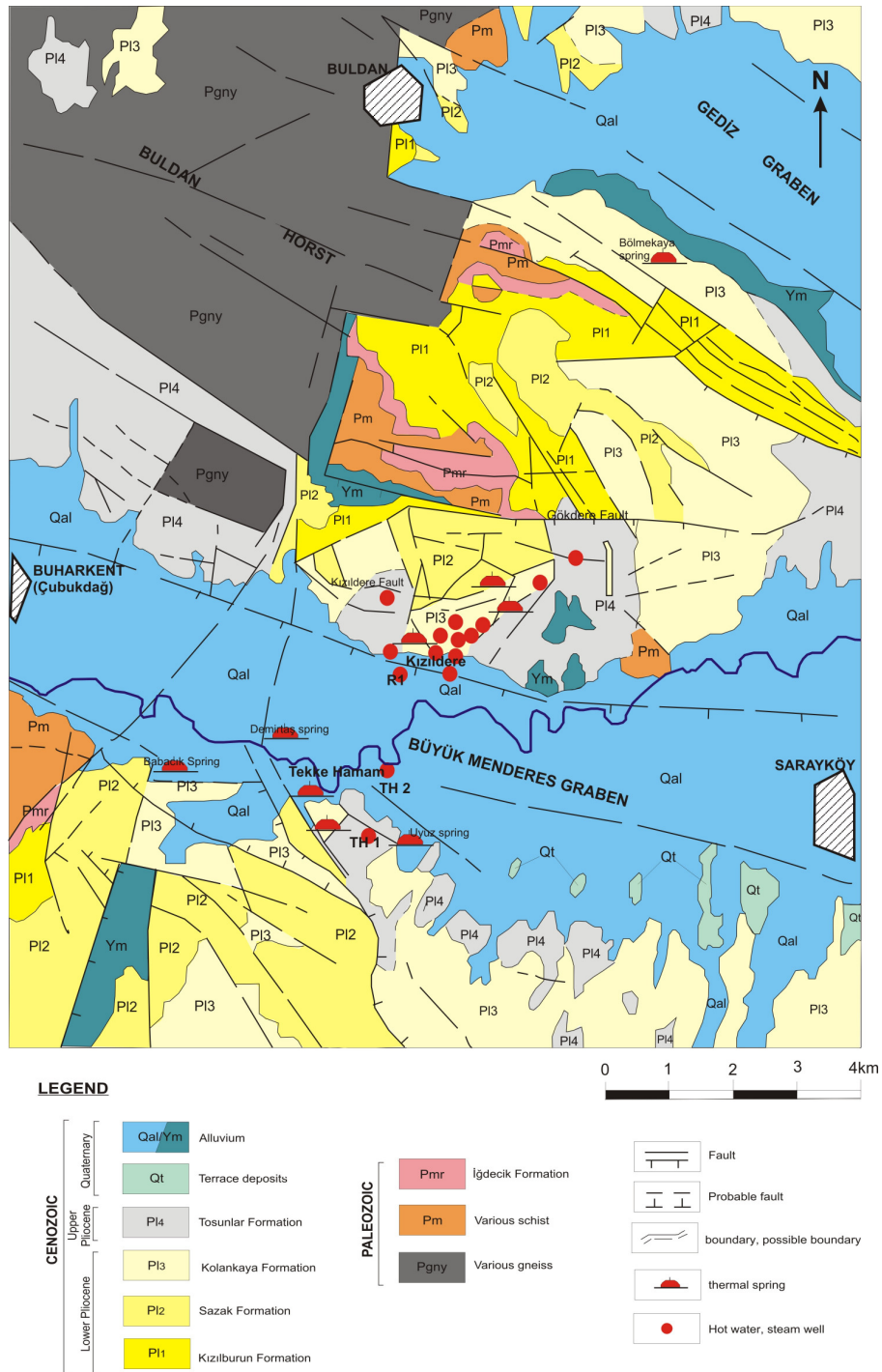
Figure 2.3 Geological map of the area (Şimşek, 1984).

2.5 Structural Geology

The Kızıldere and Tekke Hamam geothermal fields lie in the Western Anatolian Extensional Province characterized by E-W trending horst-graben structures and normal fault patterns.

The two major E-W trending grabens in the region, from north to south, are the Gediz (also called as Alaşehir Graben) and the Büyük Menderes grabens, bounded by the Yenice, Buldan and the Babadağ horsts (from north to south) (Figure 1.2).

The Büyük Menderes Graben, bounded by the Babadağ horst to the south and the Buldan horst to the north, reaches Denizli-Honaz towards the east, and Aydın and finally the Aegean sea towards the west (Figure 1.1b). The Büyük Menderes Graben is nearly 140 km long and 2.5-14 km wide, with an E-W trend along its length (Gürer et al., 2009). The graben is bounded to the north and south by the Menderes Massif metamorphics.

The Gediz graben is a 150 km long, 3-30 km wide, approximately E-W trending broad arc-shaped graben which is located between the Buldan and Yenice horsts (Arpat and Bingöl, 1969) (Figure 1.2).

The Buldan horst forms the highest topography in the field and represents the uplifted block in the footwall of Quaternary normal faults. The alignment of the Buldan horst is in conformity with the faults and is E-W and NNE-SSW trending. The Buldan horst is bounded by several step faults to the south and north, towards the Büyük Menderes and Gediz grabens, respectively. The step faults are generally E-W trending along the Büyük Menderes Graben, and WNW-ESE trending along the Gediz Graben.

The area is dominated by two sets of faults: i) approximately NE- and NW-trending subvertical oblique faults and ii) E-W faults: a major E- trending low angle fault, the Büyük Menderes Detachment Fault, and secondary listric high-angle faults, which are the dominant structural features of the region, and are confined mostly to the northern margin of the graben. On the southern margin of the graben, there are a few high-angle faults antithetic to the main northern margin fault system (Gürer et al., 2009).

The E-W trending Büyük Menderes Detachment Fault is the most prominent S-dipping normal fault with a small strike-slip component and forms the northern sector of the Büyük Menderes Graben. The fault is mainly composed of several fault segments of different orientations striking E and NW to NE. The Büyük Menderes Detachment Fault separates highly metamorphosed mid-crustal footwall rocks from shallow-level, brittlely deformed metamorphic rocks of the hangingwall and overlying sedimentary rocks (Gürer et al., 2009). The E-W trending secondary listric high angle faults, on the other hand, occur in a step-like pattern dominated by second-order synthetic to antithetic faults with respect to the dip of the master Büyük Menderes Detachment Fault (Gürer et al., 2009).

The total throw of the faults of the northern shoulder of the Büyük Menderes Graben, between the Buldan horst and the graben center, is around 3000 m (Şimşek, 1984) and exceeds the total throw of the faults in the southern shoulder. The fault steps observed along the shoulders of the Büyük Menderes Graben probably extend below the alluvial plain.

Both Kızıldere and Tekke Hamam geothermal fields are situated within the Büyük Menderes Graben. The Kızıldere geothermal field is located on the northern boundary fault of the graben, and is roughly bounded by the geothermally inactive listric-type Gökdere fault from the north and by the geothermally active, nearly E-W trending, Kızıldere fault from the south (Eşder et al., 1994) (Figure 2.3). The Tekke Hamam geothermal field, on the other hand, is located on the southern boundary fault of the Büyük Menderes Graben.

The young tectonism in the field is the major source for the occurrence of geothermal resources. Along young and large throw faults, lots of hot springs and natural steam discharges reach the surface. Due to the intense tectonic activities in the field, the hard and fragile lithologies in the stratigraphy gained secondary permeability, which resulted in the occurrence of reservoir rocks for the geothermal fluids. The recharge to reservoir rocks are mainly through the faults penetrating to depth (Şimşek, 1984).

2.6 Hydrogeology

In the area, vast amounts of groundwater resources exist in the broad alluvial plains of the Büyük Menderes river, and along the Çürüksu and Buldan streams. There exists artesian groundwater in places where plains meet stream beds and in alluvial fans reaching the plains. There are also confined aquifers at some levels within the alluvium in the Büyük Menderes plain. The cold waters mainly issue from alternating permeable and impermeable layers, or from fractures. Especially, along the horsts covered by dense forests, there are a lot of cold springs issuing with low flow rates.

In the Kızıldere geothermal field, thermal activity is characterized by a variety of surface manifestations such as steam vents and hot springs having temperatures changing between 36 and 100 ºC. Hot springs generally issue along the major east-west-trending faults, or from the intersection of the east-west-trending faults with faults of differing trends. There are hot water discharges where faults cut the valleys, and natural steam discharges along the ridges and hills. Especially steam discharges from the faults which cut the fractures of the limestones belonging to the Sazak formation. Intense young hydrothermal alteration is also observed where natural steam and hot springs rise along the faults.

In the Kızıldere geothermal field, owing to the installation of the power plant, the hot springs that were initially observed dried out completely, but there are still some steam discharges seen in the area. In the Tekke Hamam geothermal field, however, there are a number of hot water springs and mud pools having gas emissions with temperatures changing between 30 and 98 ºC and a total discharge varying around 30 l/s.

2.6.1 Reservoir Rocks

The drilling studies conducted so far in the field have shown the existence of three productive zones for both Kızıldere and Tekke Hamam geothermal fields.

The limestones of the Pliocene Sazak formation, which are intensely faulted and fractured, represent the first, upper reservoir rock in the field. The thickness of the

limestones (approximately 50 m in the central part of the stratigraphic sequence) within the Sazak formation varies, and shows both lateral and vertical gradations to marl and sandstone. The lateral facies changes, observed in the Sazak formation, limit the continuity of the reservoir, and therefore reduces its reservoir rock characteristics (Şimşek, 1984).

The alternations of marble, quartzite and schist layers of the İğdecik formation (Menderes Massif metamorphics) are characterized by a high secondary porosity and permeability evolved in relation to tectonic activity prevailing in the region, and represent the second and main reservoir rock in the field. Unlike the first, upper reservoir, this reservoir shows a broad lateral continuity over a large area. Since this reservoir is deeper than the first one, it gives relatively higher temperatures. A maximum bottomhole temperature of 212 ºC was encountered at the KD-16 well (Şimşek, 1985).

The deep drilling studies conducted in the Kızıldere geothermal field (Ölmez et al., 1998, 2001) have shown the existence of a third productive zone, as was also stated earlier by Keskin (1972) and Şimşek (1984). This productive zone is represented by the gneisses, which are the lowermost unit of the Menderes Massif metamorphics. The various schists above the gneisses act as cap rock for this reservoir. In some previous geothermometry studies done by cation and silica geothermometers, the reservoir temperatures were estimated to be around 250 and 260 ºC for the third reservoir in the field. This reservoir is associated with the main graben boundary fault line at depth. The 2261 m deep well R-1 produces from this reservoir and is associated with a temperature of 242 ºC, the highest reservoir temperature encountered so far in Turkey.

2.6.2 Cap Rocks

The siltstone and sandstone alternations of the Tosunlar formation, and the Kolankaya formation act as cap rocks for the upper limestone reservoir (Sazak formation). This cap rock forms gentle slopes in the topography and has a thickness changing between 350-650 m (Şimşek, 1984).

The well-consolidated conglomerates, sandstone and claystone alternations of the Kızılburun formation lying below the first upper reservoir act as the second cap rock in the field for the second and main reservoir (İğdecik Formation). The thickness of this formation changes between 100-250 m. In addition, in areas where the limestone levels are thin, the marl and claystone alternations of the Sazak formation act as a cap rock. In the Kızıldere geothermal feld, the Pliocene formations constitute cap rocks having thicknesses changing between 440 and 1105 m (Şimşek, 1984).

The micashists lying above the gneisses of the Menderes metamorphics act as cap rock for the third, deep reservoir.

2.6.3 Reservoir Recharge

Reservoir recharge in the area is mainly related to the permeability of the rocks forming the horsts and grabens. The reservoir rocks in the field are mainly recharged by meteoric waters penetrating to depths along the major fault zones. The waters, after being heated during their journey at depth, rise to the reservoirs via the major faults zones and flow towards the center of the graben where they mix with increasing amounts of shallow cold groundwaters (Şimşek, 1985, 2005) (Figure 2.4).

2.7 Geothermal Studies

2.7.1 Geophysical Surveys

Geophysical studies, including gravity, resistivity, geothermal gradient and seismicity surveys, were conducted in the years between 1965 and 1970 in order to delineate the subsurface geology, cap rock thicknesses and the distribution of the reservoir.

2.7.1.1 Gravity Surveys

Gravity surveys, covering a total area of 1500 km^2, were conducted near Denizli, covering Kızıldere, Tekke Hamam, Sarayköy, Babadağ and Pamukkale areas (Tezcan, 1967; Ekingen, 1970).
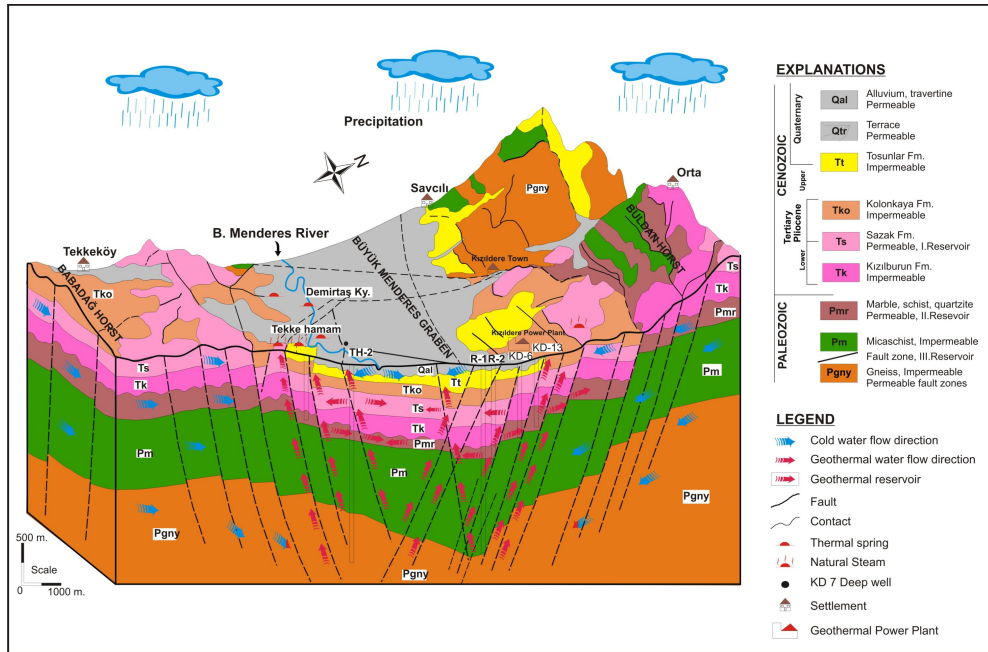
Figure 2.4 Sketch section of the hydrothermal system in the Kızıldere and Tekke Hamam geothermal fields (Şimşek, 2005).

The Bouguer anomaly map generated within the framework of the studies delineated the general tectonic structure of the region and the major horts-graben sites. In the gravity studies, negative gravity anomalies were related to the graben sites, whereas positive gravity anomalies revealed the horst structures in the area, which are Buldan, Yenice and Babadağ horsts (Tezcan, 1967). The strip of Bouguer contours with steep gradient along E-W and SE-NW directions were correlated with major faults at the boundaries of horsts and grabens. The distribution of geothermal manifestations along the convergence zones of positive and negative anomalies revealed the close relation between the geothermal system and the horst-graben boundaries.

The second order derivative map delineated three gravity highs (positive): one lying between Kızıldere and Buldan with an E-W trend, other lying in the south towards Tekke Hamam with an E-W trend and the third in the NE lying with a NW-SE trend, correlated

31

with the Buldan, Babadağ and Yenice horsts, respectively. The gravity lows (negative), on the other hand, were correlated with the grabens (Tezcan, 1967).

In the detailed gravity survey aimed to delineate the fault locations (Ekingen, 1970) NE-SW trending step faults, lined from NW to SE, were identified. By the help of the Bouger and second derivative maps, possible fault locations were delineated and important uplifts were identified.

2.7.1.2 Resistivity Surveys

Resistivity surveys in the forms of deep electrical soundings were conducted in an area of about 60 km^2 in the western part of Sarayköy, where the Kızıldere and Tekke Hamam geothermal fields exist (Tezcan, 1967). With the resistivity measurements carried out, 70, 150, 300, 500, and 900 m deep resistivity maps and cross-sections, together with basement map, were prepared. In the resistivity maps, two low resistivity zones were identified in the south and the north of the Büyük Menderes Graben. These show up as low resistivity closures pointing to the existence of hot water bearing rocks, and involve around Tekke Hamam and Kızıldere thermal manifestations (Tezcan, 1967). According to the data, the lowest value of resistivity was recorded as 5 ohm/m, and the sites showing values close to this were evaluated as the most suitable sites for drilling (Tezcan, 1967).

In the studies done by Özgüler et al (1984), the resistivity lows in Pliocene just over the step faulted basement were interpreted as they were the results of resistivity drop caused by the superheated geothermal fluid in the reservoir, and they were classified as geothermal anomalies. The resistivity surveys reflected the horst and graben tectonics of the region and their boundaries. The study revealed the low resistivity mediums (geothermal anomalies) which are the imprints of the basement geothermal reservoir in Pliocene sediments. The anomalies detected in Kızıldere were found to be closely associated with the major fault and fracture systems developed at the interface of horsts and grabens.

In the studies done by ENEL (1988), the geoelectric sounding was performed with the aim of reconstructing the trend of the resistive substratum beneath the cover constituted by the clastic terrains of the Quaternary and Tertiary. In particular, the aim was to identify any conductive zones of potential geothermal interest possibly present inside the metamorphic complex. On the basis of the results obtained from MT (Magnetotelluric) soundings integrated with the VES (Vertical Electrical Sounding), a conductive layer (5-20 ohn.m) was identified inside the metamorphic formations.

2.7.1.3 Geothermal Gradient Survey

A total of 130 geothermal gradient wells were drilled in the years between 1965 and 1968 within the cap rock, at depths changing between 80 and 250 m. 100 of these drillings were carried out in the Kızıldere field, whereas the rest were carried out in the Tekke Hamam field (Demirörer, 1967; Şimşek,1978). The geothermal gradient in the sites were found to be varying between 1 and 10 ºC/10 m, revealing high gradient anomaly contours evenly spaced over the geothermal reservoir (Şimşek, 1978). In the isogradient maps generated by Şimşek (1978), the best site for geothermal development in Tekke Hamam was selected as the Hamam tepe horst and its vicinity.

In Kızıldere and Tekke Hamam geothermal fields, for every 100 m depths, isotemperature contours were drawn. The anomalies identified from the isotemperature maps were in conformity with the isogradient anomalies. The anomaly values at a depth of 100 m reached up to 92 ºC and 110 ºC in Kızıldere and Tekke Hamam, respectively. The lowest values were found to be around 30 ºC.

2.7.1.4 Seismic Measurements

The seismic fault map of Kızıldere was prepared by Alparslan (1970) and faults and their observed throws were calculated. According to the seismic fault map of Kızıldere geothermal field, some of the faults coincided with the ones previously identified from geology, gravity and resistivity maps.

The seismic surveys in the area were utilized to find out the locations of the faults buried under the plain (ENEL, 1988). The seismic reflection profiles done by ENEL (1988) were carried out with the goal of reconstructing the deep geologic structures and determining the orientation of the main tectonic discontinuities. The sedimentary/metamorphic contact was represented by the change in amplitude and frequency of the seismic signal along the contact surface between the two formations. Reflected events were also present inside the metamorphic basement and these reflections, characterized by anomalous amplitude and frequency, were linked to densely fractured zones which were likely to be of geothermal interest (ENEL, 1988).

2.7.2 Drilling Activities

Kızıldere geothermal field is the first field from which electricity is produced in Turkey. In 1984, the Kızıldere geothermal power plant was installed with an installation capacity of 20,4 MWe. In the Kızıldere geothermal field, since 1968, a total of 22 wells have been drilled by MTA (General Directorate of Mineral Research and Exploration), having depths ranging from 370 to 2261 m. The Kızıldere geothermal power plant currently produces 15 MWe from 9 of these wells which are in production (KD-6, KD-13, KD-14, KD-15, KD-16, KD-20, KD-21, KD-22, R-1); the well no. R-1 was first drilled as a re-injection well, but later was adopted for production. The bottom-hole temperature of the wells in production varies between 194 and 242 ºC. In addition to the production wells, reinjection is performed via the R-2 well in the Kızıldere geothermal field.

In the Kızıldere geothermal field, in addition to electricity production, heating applications (district heating of Sarayköy and greenhouse heating) are also performed with the waste water discharging from the power plant. As a by product, on the other hand, CO_2 is produced from the hot fluid, at an amount of 120000 tones of liquid CO_2 annually, and is mainly used for the production of carbonated soft drink and dry ice. During production from Kızıldere geothermal field, scaling is mainly encountered in the wells, and it is minimized by controlling the pressure, mechanical cleaning of the deposits, and by the use of chemical inhibitors.

In the Tekke Hamam geothermal field, on the other hand, there exists TH-1 (615 m depth) well drilled in the late 1960's and TH-2 (2001m depth) well drilled for re-injection purpose in 1997 by MTA. The bottom hole temperature in TH-1 well was measured as 116 ºC. The bottom hole temperature of TH-2 re-injection well, on the other hand, was measured as 170 ºC, but this well could not be used for re-injection purposes due to insufficient permeability at depth. In the recent years, 4 shallow wells have been drilled by the private sector, reaching temperatures up to 120 ºC.

In Table 2.1, the information relevant to the wells drilled in the Kızıldere and Tekke Hamam geothermal fields is given. In Figures 2.5 (a,b), the well logs belonging to the sampled wells in the Kızıldere geothermal field are shown.

Table 2.1 The list of wells drilled in the Kızıldere and Tekke Hamam geothermal fields.

	Well	Year	Depth (m)	[#]Temperature (°C)	Discharge (l/s)	[*]Well Type
KIZILDERE	KD-1	1968	540	203	Observation	-
	KD1/A	1968	451	198	Observation	A
	KD-2	1968	705	175	Observation	A
	KD-11	1969	505	164	Abandoned	-
	KD-3	1969	370	155	-	P
	KD-4	1969	368	166	-	P
	KD-12	1970	405	160	Dry	-
	KD-14	1970	597	210	41.6	-
	KD-6	1970	851	194	38	A
	KD-7	1970	645	204	Observation	A
	KD-8	1970	576	180	-	-
	KD-9	1970	1241	170	Observation	A
	KD-13	1971	760	198	35.8	A
	KD-15	1971	510	208	43.3	A
	KD-16	1973	667	211,5	57.2	A
	KD-17	1975	350	157	-	A
	KD-20	1986	810	204	45.5	A
	KD-21	1985	898	205	82.5	A
	KD-22	1985	888	204	55	A
	R-1	1998	2261	242	81.1	A
	R-2	1999	1428	204	83	R
	R-3	2006	2250	241	111	P
TEKKE HAMAM	TH-1	1968	615	116	15	-
	TH-2	1997	2001	170	12	A
	KB-1	2001	115	120	20	A
	KB-2	2001	202	100	20-25	A
	KB-3	2002	161	100	10	A
	KB-4	2002	253	100	20	A

[*]A: Artesian well; P: Production well; R: Reinjection well
[#] Values represent bottomhole temperatures of the wells
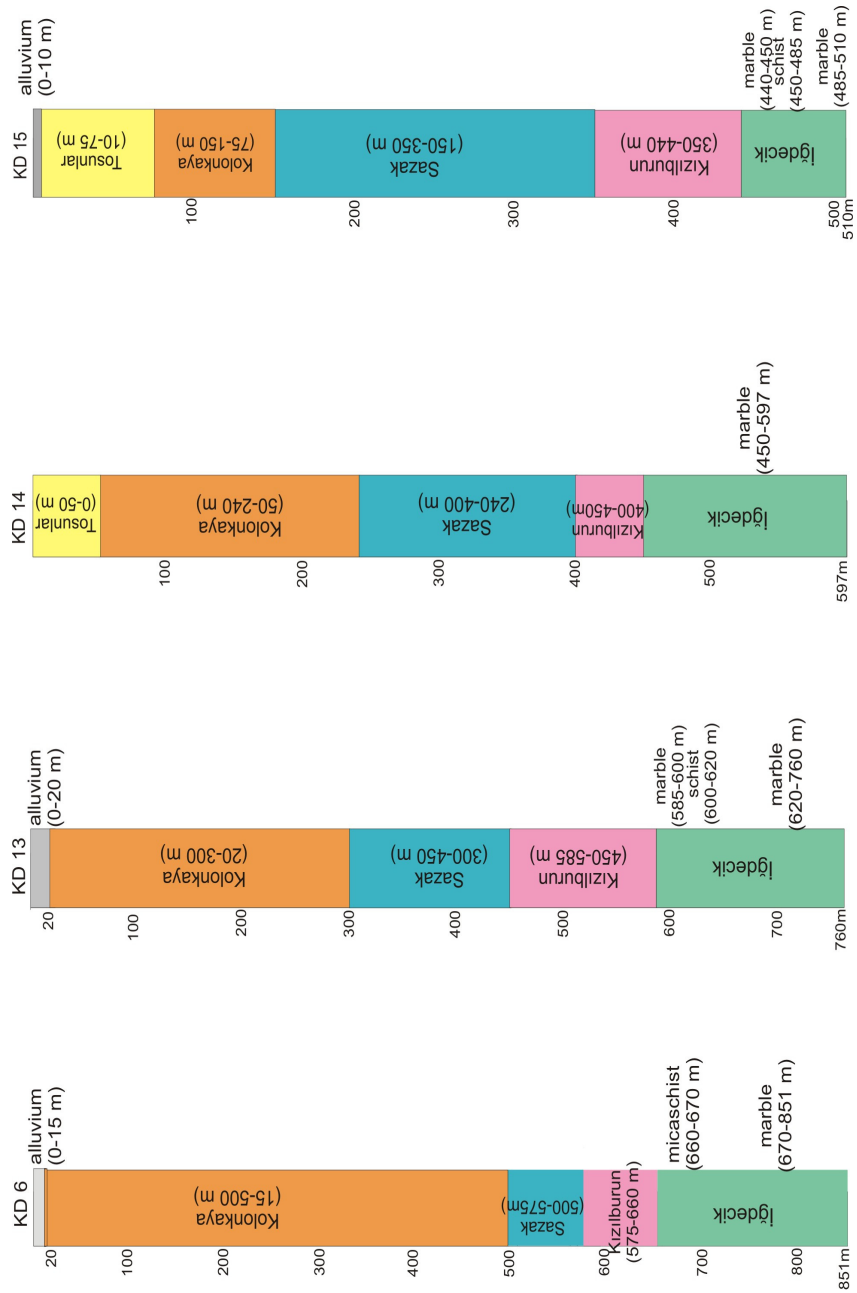
Figure 2.5a Simplified well logs of KD6, KD13, KD14 and KD15 (Uysallı and Keskin, 1971).
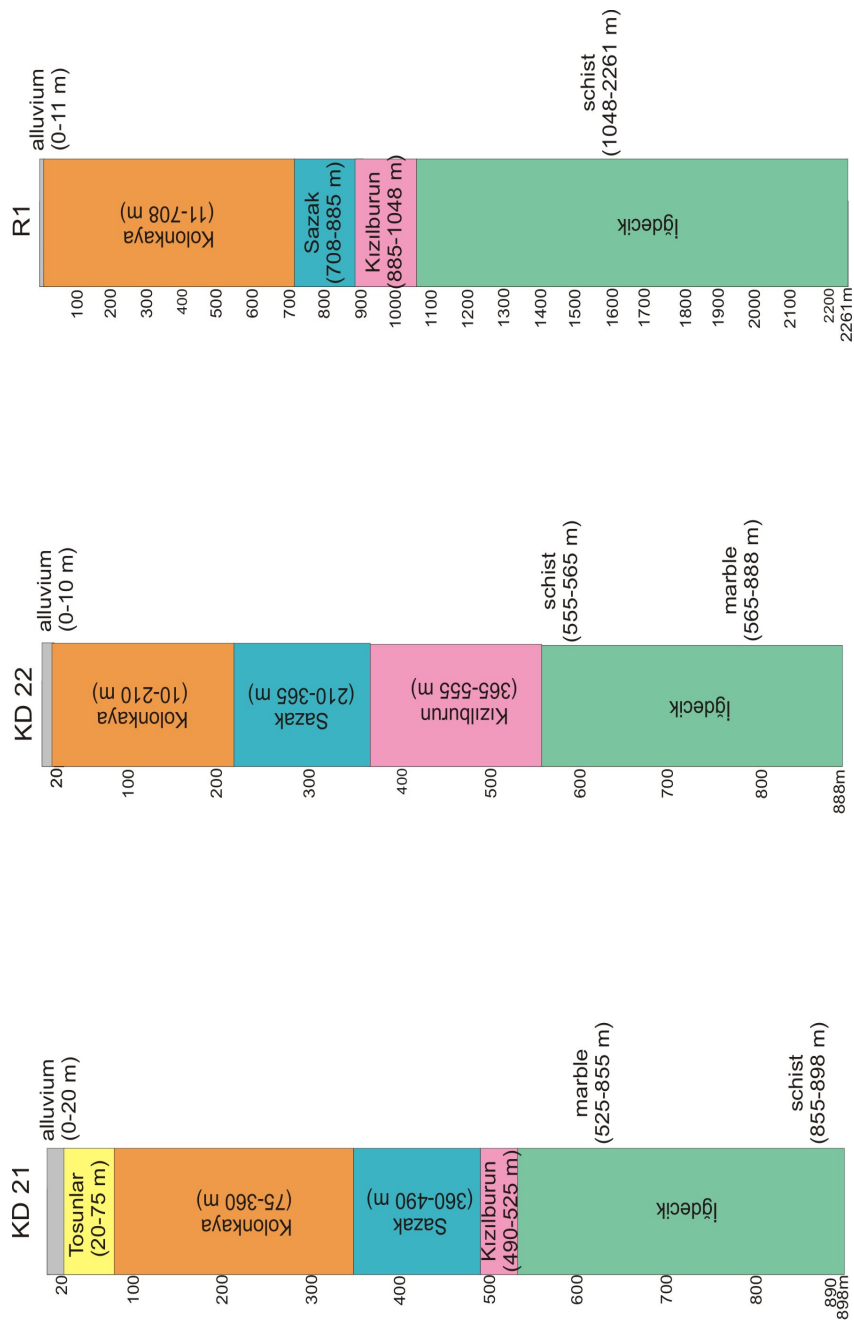
Figure 2.5b Simplified well logs of KD21, KD22 and R-1(Eşder et al., 1994; Ölmez et al., 1998).

38

CHAPTER 3

GEOCHEMICAL MONITORING STUDIES IN RELATION TO EARTHQUAKE PREDICTION

Earthquakes constitute a severe source of human disasters all around the world. In the last several decades, earthquake prediction studies have recieved great attention by several geoscientists throughout the world, especially from USA, Japan, Russia and China.

The previous research concerning the prediction of earthquakes were mostly concentrated on the geophysical phenomena behind what was happening in the subsurface (Jin and Aki, 1986). Later, in addition to geophysical methods, geochemical methods have increasingly been adopted by geoscientists for earthquake prediction. Geochemistry has provided some high-quality signals, especially since the 1960's, mainly as the result of instrumental developments. However, the utilization of geochemical methods in earthquake prediction is rather preliminary and there is a lot that still remains to be highlighted. Yet, several new aspects of earthquake prediction are being developed and with the new and more precise geochemical methods, a better visualization of such events are being introduced.

3.1 Geochemical Parameters of Interest in Earthquake Prediction

Geochemical monitoring in earthquake prediction studies are mainly focused on water and/or gaseous species within different compartments of the Earth (groundwater, thermal springs, fumaroles, soil-air, etc.).

Within the water species, especially chlorine and sulphate (Tsunogai and Wakita, 1995; Toutain et al., 1997; Nishizawa et al., 1998; Favara et al., 2001; Song et al., 2005), tritium (Sano et al., 1998) and trace metals have recieved the most attention in

earthquake prediction studies. The temporal variations detected in these parameters were mostly attributed to changes in the mixing ratios of subsurface waters in relation to crustal stress/strain modifications possibly triggered by seismicity.

Several years of seismicity monitoring via geochemical methods showed that, by far, the variations detected in subsurface gases proved to be the most useful in such studies. This is possibly due to the more and fast responsive nature of gases to instant variations within the Earth and their better tracebility.

Gases in groundwater and soil have been examined to search for precursory phenomena of earthquakes (Sato et al., 1985; King, 1986; Thomas, 1988). Especially gases like radon, helium, carbon dioxide, hydrogen, nitrogen and methane have been used widely in this respect. Among these gases, Radon (Rn), a radioactive noble gas (half life=3.8 days), is the most widely and early examined element, and a number of Rn anomalies in relation to earthquakes have been reported by various researchers (e.g. King, 1978; Igarashi et al., 1995; Wakita, 1996; Heinicke and Koch, 2000). A temporal association between earthquakes and anomalous radon flux has been suggested in these studies, Rn anomalies either preceeding or following them.

Gas ratios have also proved to be useful in earthquake prediction studies. For example, Sugisaki (1978) investigated He/Ar and N_2/Ar ratios in spring gas. Sugisaki and Sugiura (1986) and Kawabe (1985) have continuously monitored subsurface gas compositions with gas chromatographs and observed conspicuous anomalies in He/Ar, N_2/Ar and CH_4/Ar ratios prior to earthquakes. Continuous monitoring of He/Rn ratio has also been used widely (Walia et al., 2006) in the recent years due to the contrasting sources of helium and radon since they are expected to mark deep and superficial gas transfers, respectively.

Besides the chemical composition of gases, the isotopic compositions of the dissolved gases in natural waters have also been utilized widely in earthquake prediction. In this respect, helium isotope compositions have been used effectively in monitoring seismicity due to its distinct variations between mantle and crustal reservoirs. For example, Hilton (1996) reported large variations in ^{3}He/^{4}He isotope ratios correlated with the regional

seismicity in the Long Valley Caldera (USA) in between the years 1978 and 1985. Another study from Sano et al. (1998) reported decrease in the helium isotope ratio, interpreted as being due to the release of radiogenic ^{4}He as a result of micro-fracturing, which occurred in response to a large magnitude earthquake (M: 7.2). The different origin of the isotopes of helium, therefore, enabled the recognition of interaction between different compartments of the earth in response to seismicity triggering.

Gases such as ^{222}Rn, CH_4, CO_2 and He, owing to their low abundances in air, have also proved to be the most useful indicators of fluid inflows into crustal environments and have enabled the detection of fluid-bearing horizons such as shear zones, open fractures and sections of enhanced permeability within the crust (Zimmer and Erzinger, 1995; Erzinger et al., 2004; Tretner et al., 2008; Wiersberg and Erzinger, 2008).

3.2 Geochemical Monitoring Techniques

Earthquake prediction studies using geochemical parameters involve monitoring of water and/or gaseous species either in a discontinuous way (discrete sampling), that is, monitoring over days, weeks or months, or, in terms of continuous/real-time monitoring, within a couple of minutes or even seconds.

Previous earthquake prediction studies mostly adopted a discontinuous strategy of sampling of both gas and/or water species from different geological compartments of the Earth. These studies involved offline sampling and later chemical/isotopic analysis in laboratories. In the recent years, however, especially with the advancement of automatic instrumental devices (e.g. fully automated Quadrupole Mass Spectrometers, Gas Chromatographs), continuous, real-time multiparameter monitoring studies have increasingly been adopted and were accompanied by the monitoring of several helpful external parameters in addition to seismic activity. In this respect, meteorological parameters (air pressure, air temperature, rainfall etc.), hydrologic controls (flow rate of springs, groundwater level in wells) and tidal effects (Earth tide levels/fluctuations) have been recorded in monitoring studies as accompanying evidence for earthquake prediction. With the adoption of real-time monitoring strategies, the capability of performing statistical techniques have also increased significantly and is gaining wide

acceptance as one of the most important ways for evaluating real, temporal variations purely occurring due to seismicity and the further discrimination of other possible external effects as mentioned above.

Below is a brief summary of some of the recent geochemical monitoring studies dealing with earthquake prediction.

In the study done by Toutain et al. (1997), anomalies in Cl concentrations in the Alet spring mineral waters were identified 5 days prior to the 5.2 magnitude Pyrenean earthquake in France. About 36 % of increase in the Cl content relative to the mean value in the mineral water was observed, accompanied by a slight increase in sulphate content (reaching to about 14 % above the mean value), prior to the earthquake. The Cl anomaly was attributed to mixing of Cl-rich waters rising between the epicentre of the earthquake and the Alet area, induced by changes in pre-seismic strain. This study revealed the importance of mineral springs as suitable sites for investigation of seismic precursors.

In the study done by Nishizawa et al. (1998), Cl and SO_4 anomalies were detected in the Yugano hot spring waters, 12 days after the onset of the 1995 seismic swarm activity in Izu Peninsula, central Japan. The anomalies suggested that variations were related to a simple 2-component mixing process, that is, mixing with high Cl and SO_4 waters, triggered by the associated seismic swarm activities resulting in crustal stress modifications.

According to the study done by Sano et al. (1998), significant decrease in $^3He/^4He$ ratios, accompanied by concomittant increase in the $^4He/^{20}Ne$ ratios were found in groundwaters at Nishinomiya city after the 1995 Kobe Earthquake in Japan. The variations observed in the isotopic compositions of the waters were attributed to the degassing of stored radiogenic helium due to micro-fracturing in aquifer host rocks. The degassing He flux was also quantified and the importance of earthquake triggering in He degassing from the solid earth was emphasized.

In the study done by Favara et al. (2001), temporal variations were detected in temperature and some chemical species in waters of the thermal springs of Western

Sicily during the seismically active period between 1966 and 1969, coinciding with the 1968 Belice Valley earthquake. The temperature, Na, Cl, SO_4 and TDS of the thermal springs showed minimum values before the 1968 earthquake, and maximum values after the event. The changes in these parameters were attributed to permanent change in aquifers caused by tectonic activities.

Italiano et al. (2001a) reported strong anomalies in the flow rate and the chemical composition of gases (CH_4, N_2, CO_2) discharged from the Tramutola thermal well located in Campano-Lucano Apennine in coincidence with the 1996 Irpinia earthquake (M: 4.9). Contrastingly, no effect was recorded in coincidence with the 1998 seismic event (M: 5.5), although the Tramutola well is located at comparable distances from the two epicentres. The recorded variations were proposed to be caused by an earthquake-related transient modification of the permeability of the shallow crust. The different crustal response of the well to the two seismic events, on the other hand, was related to different stress distributions around the epicentres or to a different tectonic connection between the site and the locations of the earthquakes.

In the studies done by Italiano et al. (2001b), anomalous $^3He/^4He$ ratios, together with an increase in the fluid outflow, were observed in the gas samples taken from CO_2 dominated mofettes, corresponding to the seismic crisis that shook the region between September 1997 and July 1998 in Central Apennines, Italy. The increase observed in the $^3He/^4He$ ratio indicated an increase in the deep mantle derived contribution compared to the crustal one. The observed anomalies were stated to be driven by stress-induced crustal deformations affecting micro-fracturing and bulk permeability and, in turn, by a seismogenic induced modification of the crustal permeabilty of rocks.

In the studies done by Braüer et al. (2003), gas and isotopic composition of the free gas of the Eisenquelle mineral spring and mofette were monitored (weekly) for 2 years. The time series of data showed that there were significant shifts in $\delta^{13}C$ and $^3He/^4He$ for several months after the occurrence of the earthquake swarms in December 2004. The isotopic shifts were attributed to a seismically induced admixture of crustal fluids released at the hypocenter below Novy Kostel (Czech Republic) to a magmatically dominated gas flux.

In the geochemical monitoring study done by Federico et al. (2004), between 1998 and 2001, temporal variations in two distinct groups of water bodies were studied in the Vesuvius volcano area in Italy. During the monitoring study, in response to the October 1999 earthquake, seismicity related variations covering a great decrease in pH, a corresponding fall in redox potential, an increase in dissolved CO_2 and a rise in $^3He/^4He$ ratio were detected in the Olivella cold spring, with values later turning back to their original levels. The significant variations in the spring were attributed to enhanced magmatic influx of CO_2 and He to the aquifer feeding the spring, through rock fracturing and increased permeability, associated with the seismic activities in the area.

Caracausi et al. (2005) performed a long-term geochemical monitoring study in the seismic area of the Umbria-Marche region of Italy, in order to create a model of the circulation of fluids and interpret the temporal chemical and isotopic variations of both the thermal springs as well as the gas vents. Coincident with the seismic crisis, which struck the region in 1997-1998, an enhanced CO_2 degassing on a regional scale, a pH-drop in all the thermal waters as a consequence of CO_2 dissolution, higher $^3He/^4He$ isotope ratios pointing to a slight mantle-derived contribution and an increase in radon activity were detected. The anomalous CO_2 discharge was closely related to the extensional movement of the normal faults responsible for the M: 5.7, 6.0 and 5.6 main shocks that characterized the earlier seismic phase. In contrast, a clear compressive sign was recognized in the transient disappearance of the deep-originating components related to the M: 5.3, 51 km-deep event that occurred on March 26, 1998. The data collected during a rather quiet seismic period (1999-2002) allowed to identify the background values for some geochemical parameters that could characterise the study area. The observed geochemical anomalies were argued to be driven by rock permeability changes induced by crustal deformations.

In the studies done by Hartmann et al. (2005), a methodological approach was tested with a hydrochemical data set collected from a deep well monitored for two years in the seismically active Vrancea region, Romania, in order to analyse the possibility of an interdependency between changes in the chemical composition and the regional seismotectonic activity of the area. To allow a rigorous comparison with hydrochemistry, the regional earthquake time series were aggregated into an univariate time series by

expressing each earthquake in the form of a parameter "e", taking into consideration both energetic (magnitude of a seismic event) and spatial parameters (position of epi/hypocentrum relative to the monitoring site). The earthquake and the hydrochemical time-series were synchronised aggregating the e-parameters into "earthquake activity" functions "E", which takes into account the time of sampling relative to the earthquakes which occurred in the area. The set of earthquake functions "E" was then grouped by means of factor analysis to select a limited number of significant and representative earthquake functions to be used in the relation analysis with the multivariate hydrochemical data set. From the hydrochemical data a restricted number of hydrochemical factors were extracted. Finally, regression analysis was applied to detect the hydrochemical factors which significantly correlate with the aggregated earthquake functions. Three of the hydrochemical factors were found to correlate significantly with the considered earthquake activities. A screening with different time combinations revealed that correlations were strongest when the cumulative seismicity over several weeks was considered.

In the study done by Süer et al. (2008), the geothermal waters along the North Anatolian Fault Zone (NAFZ) were monitored within nearly 3 months intervals and temporal variations were detected in the chemical and isotopic compositions of some waters. The chemical/isotopic changes observed in the geothermal waters were reported to have a possible correlation with the seismic activities of moderate magnitude ($3<M<5$). In this respect, Cl, ^{3}H and Ca were found to be the most sensitive tracers of seismically-induced crustal perturbations in the area.

Song et al. (2006) performed weekly measurements of cation and anion concentrations in both hot and artesian springs in Taiwan in order to establish background concentrations and to identify geochemical earthquake-related anomalies. Here, short-term, reversible precursory geochemical anomalies, comprising sudden increases in chloride and sulfate ions, were recorded in hot and artesian springs prior and subsequent to the major earthquakes which occurred in September 1999 in the Kuantzeling area of west-central Taiwan. The anomalies were interpreted as stress/strain induced pressure changes in the subsurface water system, followed by limited precursory geochemical discharges

generated by limited changes in the levels of the subsurface reservoirs, finally leading to the mixing of previously isolated subsurface water bodies.

In the study done by Degragario et al. (2005), a new methodology for the separation of dissolved gaseous phase from water was developed and was tested in a volcanic area (Vulcano Island) from which several samples of dissolved gases were collected and analyzed for both chemical and isotopic composition (CO_2, $^3He/^4He$). Temporal variations were recorded in the helium isotopic composition and CO_2 contents of the dissolved gases (between the two sampling campaigns). The increase in the compositions of nearly all samples between the sampling campaigns were attributed to increase in the input of deep ^3He, also indicated by an increase in the CO_2 partial pressure, and were linked to an earthquake (M: 3) which occurred very close to the island only 24 hours prior to the second sampling survey.

Italiano et al. (2009) reported the results of a long term geochemical monitoring study carried out in the area hit by the 1997–98 Umbria–Marche seismic sequence (Northern Apennines, Italy). The observed modifications detected in the gas phase (CO_2, $^3He/^4He$, CH_4) during the 1997–98 period were mainly related to faulting activity, while those recorded after the end of the seismic crisis were interpreted as being a consequence of the crustal relaxation. The authors argued that the seismic events provoked modifications because of the sudden release in the accumulated mechanical stress. However, the observed geochemical anomalies did not appear to be linked to single seismic events, but were reported to be mainly driven by both rock permeability changes and microfracturing induced by crustal deformation.

In addition to the discontinuous monitoring studies, several researchers have adopted continuous monitoring strategies in dealing with earthquake prediction. These studies were initially focused mainly on the monitoring of Radon alone, however, later, with the introduction of multiparameter measurement devices, the combined monitoring of different gaseous and/or water species dissolved in different compartments of the earth has become widely adopted. Below is a brief summary of some of the continuous, real-time gas monitoring studies.

In the studies done by Steinitz et al. (1999), radon flux monitoring in soil gas was carried out for 3 years (1992-1994) in the northwestern sector of the Dead Sea area, along an approximately 20 km section of the western boundary fault of the Dead Sea rift. High radon flux levels were encountered showing large temporal variations with different components: multi year, yearly cycle (maximum values recorded during the summer seasons), and shorth term (3-14 days) Rn flux variations (termed Rn events). The relation between Rn events and earthquakes was investigated by testing for correlation between populations of radon events and populations of earthquakes. The results showed that the correlation of the Rn events with earthquakes was significantly higher for earthquakes which occurred in the rift close to the monitoring sites (particularly for earthquakes with M>2).

According to the studies done by Heinicke et al. (2000), coseismic geochemical variations were detected in some gaseous vents and natural springs during the seismic crisis in Umbria region (Central Apennines) that commenced on September 26, 1997 with several moderate earthquakes (up to M: 5.8). The adopted monitoring strategy was based on both continuous monitoring of the gas flow rate and discontinuous (weekly sampling) data acquisition. Advanced statistical methods (Spectral analysis and Run theory) were applied to identify anomalous patterns in the geochemical time series and to pick out cyclic components possibly induced by meteo-climatic variations. Finally, the relationships among results concerning the detected temporal variations in the chemical compositions of the gas and water samples, together with the analysed flow rate time-series, were evaluated altogether with the seismic activity record of the area. The variations observed in the water (pH and major ions) and gaseous species (He/CO_2, CH_4/CO_2), combined with the continuous monitoring of the gas flow rate nearby the gas vent site, suggested that the observed geochemical variations were related to changes in crustal permeability probably due to crustal deformations associated with subductive processes which characterise the Apenninic chain.

In the studies done by Zimmer and Erzinger (2003), a continuous monitoring setup was operated in order to monitor H_2O, CO_2 and Rn concentrations at fumaroles on the summit of Merapi Volcano (Indonesia), as well as the fumarole temperature, extending from July 2000 to the end of January 2001. The composition and temperature of the gases emitted

at Merapi Volcano showed significant systematic variations. Especially Rn activity of the gases emitted from the fumaroles showed a clear positive correlation with the daily variations in the atmospheric pressure. The increase observed in the Rn activity was also coupled with an increase in the water concentration of the fumarole due to high rainfall and a drastic drop in the fumarole temperature. Several seismic events recorded at Merapi were also correlated with the variations observed in the gas temperature of the fumaroles.

Das et al. (2006) installed an experimental continuous, automated, multi-parametric geochemical monitoring set-up in order to monitor possible variations in radon and radon progeny concentrations in the gases from the thermal springs at Bakreswar, West Bengal, India. During the monitoring, concurrent anomalous changes in concentration profiles of ^{222}Rn, ^{218}Po and ^{214}Bi occurred beyond 2sigma level. The monitored anomalies were mainly attributed to precursory dilatation responses arising due to earthquakes that had occurred subsequently in Indonesia, and revealed evidence of pre-seismic radioactive heterogeneities in the escaping subsurface fluids from the monitored thermal spring gases.

In the studies done by Yang et al. (2006), an automatic multiparameter monitoring system was set-up for long-term monitoring of gas composition at Chung-lun mud-pool, SW Taiwan. The multiparameter automatic gas station was built on the bank of one of the largest mud pools at an active fault zone of southwestern Taiwan, for continuous monitoring of CO_2, CH_4, N_2 and H_2O, the major constituents of its bubbling gases. After one year of continuous monitoring from October, 2001 to October, 2002, the gas composition, especially, CH_4 and CO_2 of the mud pool showed systematic variations and appeared to be independent of the meteorological factors. Taking the variations of CO_2/CH_4 ratio as the main indicator, precursory anomalies were recognized from a few days to a few weeks before an earthquake. Gas flow rate of the bubbling gases showed positive correlation with CH_4 and radon concentrations, indicating that CH_4 may be the major carrier gas for radon migrating from deep sources in the area. It was concluded that the gas composition in the area was sensitive to the local crustal stress/ strain conditions.

In the studies done by Walia et al. (2006), two major earthquakes in Garhwal Himalaya were recorded during the last decade and correlated with radon anomalies. The helium anomaly for Chamoli earthquake was also recorded and the helium to radon ratio model was tested on it. Anomalous values were recorded in both soil gas and groundwater almost simultaneously, which clearly indicated that the degassing system was only disturbed by the ongoing stress before the major event. Further, during the time window of June 1992 to August 1995 and June 1996 to September 1999, about 142 microseismic events, with magnitudes ranging between 2.1 and 4.8, were correlated with radon anomalies at both Dalhousie and Palampur stations. This study showed the efficiency of both radon and helium as seismic precursors and constituted a preliminary test for the usage of helium/radon ratio model in earthquake prediction.

Weinlich et al. (2006) constructed a continuously operated (8-month) gas monitoring station for radon and CO_2 within the epicentral area of the NW Bohemian swarm earthquakes overlying directly the active Mariánské Lázně fault. The variations in radon concentrations were detected to be similar to the variations in CO_2, i.e. CO_2 was considered to be the carrier gas for radon. Very small diurnal variations in gas concentration were proposed to be caused by the earth tides. Sudden changes in gas concentration, exceeding diurnal variations, were detected and were always linked with seismic events. The authors also reported that, decreased gas concentration might indicate compression resulting in reduced fault permeability as was implied by negative peaks following local earthquake swarms. Therefore, the sudden increase in CO_2 and Rn concentrations were interpreted as indicating an increased fault permeability caused by stress redistribution, giving rise to opening of migration pathways, before local earthquake swarms.

In the studies done by Koch and Heinicke (2007), the seismo-hydrological effects were evaluated by monitoring changes in the free gas flow throughout springs and mofettes. Since 2000, a slight upward trend in the gas flow of three Bad Brambach mineral springs (NW Bohemia) were observed, which became stronger after the 'Eisenquelle' spring capture reconstruction. Accounting for all influencing effects, a slight upward trend of the gas flow was detected for the last 5 years at the Bad Brambach measuring site. Moreover, increase was also observed in the $^3He/^4He$ mantle ratio in gases at mofettes,

and were reported to indicate a higher degassing activity of the magma body below the Cheb Basin. The detected non-seasonal pulsing of the gas flow rate was assumed to be caused by a periodicity of the fluid transport through the crust which could be based upon varying geotectonically induced hydrofracturing processes possibly due to slight pore pressure perturbations.

Ciancabilla et al. (2007) carried out a long term (2001 to 2006) multiparameter geochemical monitoring in the thermal springs of Porretta, with the aim of detecting the behaviour of the circulating fluids possibly coinciding with seismic activity. The collected data revealed a sensitivity of the thermal waters to the activity of the main fault crossing the village of Porretta. Temporal variations were recorded in the conductivity, water level and temperatures of the springs. The observed anomalous hydrologic and geochemical signals were mainly related to crustal strain phenomena due to local seismic events.

In the studies done by Cioni et al. (2007), a continuous automatic monitoring network was designed and built in Tuscany (Italy), in order to investigate and define the geochemical response of the aquifers to the local seismic activity. In August 2004, a sharp increase was detected in the CO_2 composition in the dissolved gas 12 days prior to a M: 3.7 earthquake that occurred at a distance of 3 km north of the installation site. The anomaly detected appeared independent of the variations recorded in the accompanying rainfall data and was accepted as a precursory event of seismicity.

3.3 Possible External Perturbations in Monitoring Studies

Geochemical monitoring studies dealing with earthquake prediction have also shown the effects of external factors such as atmospheric pressure, air temperature variations, soil humidity and earth tides on significant geochemical perturbations, especially in the compositions of subsurface gases. These studies demonstrated that the geochemical composition of soil and/or springs may strongly vary with time without any tectonic/seismic effect, and that the variations can be purely related to either meteorological or tidal effects.

3.3.1 Meteorological Factors

Several authors have reported the severe influence of atmospheric pressure on radon emanation (Clements and Wilkening, 1974; Duenas and Fernandez, 1987; Chen et al., 1995). Pressure variations controlling methane fluxes from sediments have been also reported (Mattson and Likens, 1990). The atmospheric pressure response is interpreted to be the result of the compression and expansion of the soil gas column between the surface and the top of the water table (Chen and Thomas, 1994).

In addition to atmospheric pressure induced variations, temperature-related fluctuations of gas concentrations have also been discussed by several authors. In the study conducted by Shapiro et al. (1985), the annual cycle of radon concentration was related to the thermo-elastic strains in the vicinity of a borehole. Reimer (1980), suggested that variations in air temperature affects the soil moisture contents and therefore partially controls He concentrations in soil. King (1980), on the other hand, in his long term monitoring study conducted in the San Andreas fault reported that there was not any significant control of temperature on the recorded radon concentrations.

Some studies have concentrated on the effects of wind as an external factor affecting the gas composition and behaviour. In the studies done by Chen and Thomas (1994), it was reported that wind did not have any deep influence on the gas behaviour. Reimer (1980) suggested that wind can affect gas emission through atmospheric pumping effects. In the studies done by Teschner et al. (2006), gas concentrations of CO_2, H_2S and CO in fumarolic emissions, as well as the temperatures of the hydrothermal steam and soil in close vicinity of the fumarole and steam pressure were measured in short-time intervals (typically 15 seconds). From the data it was concluded that environmental conditions, such as the direction and strength of wind and precipitation will interact with some of the parameters monitored and showed a strong influence on the long term variation of the parameters.

Besides such effects, serious variations of gas composition of thermal springs have been pointed out as the result of fluctuations of local hydrologic regime (Klusman and Webster, 1981; Borchiellini et al., 1991). In the studies done by King and Minissale

(1994), the seasonal trend in radon concentration in high permeability soil was reported to be affected differently by rainy and dry seasons, resulting in the reduction and increase of gas permeability, respectively, in the water saturated soil.

3.3.2 Tidal Effects

Tides are the rising of Earth's ocean surface caused by the tidal forces of the Moon and the Sun acting on the oceans. While tides are most commonly associated with oceans and large bodies of water, gravity creates tides in the atmosphere and even in the lithosphere (Earth tide). Earth tides are cyclical, small, and slow ground movements, and are caused by the gravitational attraction of the solar system bodies; primarily the Moon and the Sun, and, to a much lesser extent, the other planets. Since this attraction varies with the paths of the Moon and the Sun, tidal phenomena are typically observed on a diurnal and semi-diurnal time scale. The Earth's crust shifts (up/down, east/west, north/south) in response to the Moon's and Sun's gravitation, ocean tides, and atmospheric loading (Reddy and Affholder, 2001).

Tidal induced variations were also reported to be active on gas compositions in monitoring studies. For example, Sugisaki (1981) suggested the existence of a positive correlation between fluctuations of the He/Ar ratio of spring gases and earth tide-related strain. The author argued that successive phases of compression and expansion of the crust due the earth tides caused the periodic variation in the He/Ar ratio of the spring gas. Some studies also showed that radon concentration variations in escaped gases from groundwater showed better correlation with solid earth tides than in dissolved gases (Shi and Zhang, 1995). Groundwater radon was also reported to respond to minute crustal stress changes, with amplitudes comparable to tidal amplitude.

3.4 Concluding Remarks

The geochemical monitoring studies conducted so far have revealed that temporal variations in the geochemical time series, especially those of gases, can arise from different perturbations within the crust in response to natural earth processes, the most dominant being seismicity. The occurrence of any seismic event may trigger

modifications in the crustal stress/strain distribution of the crust and may therefore induce temporal variations in the chemical and/or isotopic composition and behaviour of the circulating terrestrial fluids/gases within different geological compartments of the Earth.

In order to better visualize the response of terrestrial fluids to seismicity, long term and continuous/real-time monitoring techniques should be adopted. Thus, long-term geochemical monitoring will enable the generation of the background distribution of any geochemical parameter of interest and will therefore lead to the detection of anomalies in the time series which are occurring due to seismo-tectonical processes, after the elimination of possible external factors. It should be noted, however, that, only the combined analysis and interpretation of all available geochemical, geophysical and meteorological data will allow a comprehensive evaluation of the assessment of earthquake prediction potential.

CHAPTER 4

AN OVERVIEW OF NOBLE GAS GEOCHEMISTRY

4.1 Introduction to Noble Gases

4.1.1 Helium

Helium, the lightest noble gas in nature, has two naturally occurring stable isotopes: ^{3}He and ^{4}He. ^{4}He is by far the most abundant of the two isotopes, making up about 99.9% of the helium on Earth. Nearly all terrestrial ^{4}He has been produced as alpha-particles from the radioactive decay of ^{238}U, ^{235}U and ^{232}Th over geological time (Ozima and Podosek, 2002). ^{3}He, on the other hand, is mainly considered as a primordial isotope, because it has not been produced in large quantities since the Big Bang, and is considered to have become entrapped within the Earth during planetary formation (Ozima and Podosek, 2002). In addition to its primordial background, other sources of ^{3}He are also present which include auroral precipitation of solar wind, accretion from cosmic rays, and flux of cosmic dust and meteorites (Graham, 2002). Small amounts of ^{3}He are also produced within the crust by the lithium spallation reactions which involve the bombardment of lithium atom by high energy neutrons (Ozima and Podosek, 2002; Graham, 2002).

Both helium isotopes provide significant information on the evolution of the Earth. The primordial nature of helium-3 basically provides important clues regarding the differentiation and outgassing of the Earth, while helium-4, being the radiogenic helium isotope, is mainly used as a tool for groundwater dating. The separate budgets for ^{3}He and ^{4}He are not closely linked; their sources are geochemically distinct, and their primary loss mechanisms are also different. They both have different atmospheric lifetimes, of the order of 1Ma for ^{4}He and of the order half of that for ^{3}He (Ozima and Podosek, 2002).

4.1.2 Neon

The second lightest isotope of noble gases is neon, which has three stable isotopes: ^{20}Ne, ^{21}Ne and ^{22}Ne. The isotopic composition of Ne changes mainly through the nuclear, so-called Wetherill reactions: ^{17}O(α,n)^{20}Ne, ^{18}O(α,n)^{21}Ne, ^{24}Mg(n,α)^{21}Ne, and ^{19}F(α,n)^{22}Ne, involving alpha particles and neutrons derived from U, Th radioactive decays (Wetherill, 1954; Yatsevich and Honda, 1997; Ballentine and Burnard, 2002; Ozima and Podosek, 2002). Isotopic analysis of exposed terrestrial rocks has demonstrated the cosmogenic production of ^{21}Ne (Marty and Craig, 1987). Neon, therefore, is a powerful tool in especially determining the cosmic exposure ages of surficial rocks and meteorites.

4.1.3 Argon

Argon is present in the Earth's atmosphere at an abundance of 0.94% which leads it to be the most abundant noble gas in the terrestrial environment. Argon has three stable isotopes: ^{36}Ar, ^{38}Ar, and ^{40}Ar. The two light isotopes are not produced in significant quantities in the mantle. The heavier isotope, which is the decay product of the naturally occurring ^{40}K (half-life of $1.25 * 10^9$ years), is almost entirely produced in the mantle, with subsequent degassing and accumulative storage in the atmosphere (Allègre et al., 1996; Ozima and Podosek, 2002).

Argon isotopes mainly provide important information on the evolution of the atmosphere, and on the geodynamics and isotopic evolution of the mantle. Most of the argon isotope literature also deals with measurement of ^{40}Ar for use in K-Ar age-dating of rocks (Faure, 1986).

4.1.4 Krypton

Krypton has six stable isotopes (^{78}Kr, ^{80}Kr, ^{82}Kr, ^{83}Kr, ^{84}Kr, ^{86}Kr) and two radioisotopes; ^{81}Kr and ^{85}Kr. The ^{81}Kr isotope, with a half-life of 229 000 years, is the product of atmospheric reactions with the other naturally occurring isotopes of krypton and from decay of ^{238}U, and has several unique advantages for dating old groundwaters (Lehmann

et al., 2003). Krypton-85 is an inert radioactive noble gas with a half-life of 10.76 years, produced by fission of uranium and plutonium.

Fission of ^{238}U provides the dominant mechanism for the production of $^{83,\,84,\,86}$Kr in the crust today, while production of shielded isotopes ^{80,82}Kr can be neglected (Ballentine and Burnard, 2002). Fission products of ^{244}Pu and the decay products of ^{129}I, both now extinct, also contribute important Kr isotopic components to both the terrestrial mantle and atmosphere (Porcelli and Ballentine, 2002).

4.1.5 Xenon

Xenon has nine stable isotopes: ^{124}Xe, ^{126}Xe, ^{128}Xe, ^{129}Xe, ^{130}Xe, ^{131}Xe, ^{132}Xe, ^{134}Xe and ^{136}Xe, five of which are radiogenic. Production of ^{131,132,134,136}Xe has occurred over geological time by the spontaneous fission of ^{238}U and extinct ^{244}Pu (halflife: 82Ma), while ^{129}Xe production occurred by radioactive decay of extinct ^{129}I($t_{1/2}$: 17Ma) (Graham, 2002).

Xenon isotopes are used as a powerful tool mainly for understanding terrestrial differentiation of our planet and the formation of the atmosphere (Graham, 2002).

4.2 Noble Gases in Terrestrial Reservoirs

4.2.1 Noble Gases in the Atmosphere

Noble gases are naturally occurring and present in the Earth's atmosphere. The noble gas elemental abundances (together with the other major and minor gases that exceed the natural abundance of Xe) and the list of the stable isotopes in the noble gas family and their abundances per element in the atmosphere are given in Tables 4.1 and 4.2, respectively. As can be seen from Table 4.1, the noble gases are present as trace constituents in the atmosphere, except for Ar which is dominated by its radiogenic component (Ozima and Podosek, 2002).

Table 4.1 Composition of the terrestrial atmosphere (Porcelli et al., 2002).

Constituent	Volume Mixing Ratio	Total Inventory (ccSTP)
Dry Air	1	$(3.961\pm0.006)*10^{24}$
N_2	$7.81*10^{-1}$	
O_2	$2.09*10^{-1}$	
Ar	$(9.34\pm0.01)*10^{-3}$	$(3.700\pm0.004)*10^{22}$
CO_2	$3.7*10^{-4}$	
Ne	$(1.818\pm0.004)*10^{-5}$	$(7.202\pm0.016)*10^{19}$
He	$(5.24\pm0.05)*10^{-6}$	$(2.076\pm0.020)*10^{19}$
CH_4	$1-2*10^{-6}$	
Kr	$(1.14\pm0.01)*10^{-6}$	$(4.516\pm0.040)*10^{18}$
H_2	$4-10 *10^{-7}$	
N_2O	$3*10^{-7}$	
CO	$0.1-2*10^{-7}$	
Xe	$(8.7\pm0.1)*10^{-8}$	$(3.446\pm0.040)*10^{17}$
Rn	$6*10^{-20}$	$2*10^{5}$

It has long been recognized that the Earth's atmosphere is not primary, in other words solar, and therefore is not composed of gases captured as gases from the solar nebula by the gravitational field of an accreting solid planet, or perhaps even by nebular gases' self-gravity (Ozima and Podosek, 2002). The Earth's present atmosphere is believed to be secondary, which means that the constituents of the atmosphere were originally part of the solids that accreted to form our planet. The secondary origin for the atmosphere is also evident from the similarities with volcanic emanations, that is, atmospheric volatiles

are derived from degassing of the solid Earth. The characteristics of the atmosphere therefore reflect the acquisition of volatiles by the solid Earth during formation, as well as the history of degassing from the mantle. Unlike He, which is lost to space, the principal sink for heavy noble gases is the Earth's atmosphere. Therefore, the composition of the atmosphere represents an integrated mixture of noble gases degassed from the mantle and crust over 4.5 billion years of Earth history.

Losses of noble gases from the atmosphere to space can also modify noble gas compositions. Under present conditions only He is able to escape from the top of the atmosphere due to its light weight, and therefore the relative abundance of He is greatly depleted when compared to the other noble gases. The isotopic composition of He in the atmosphere thus reflects the isotopic composition of He leaking from the solid Earth. The helium that is currently present in the earth's atmosphere represents mainly the product of alpha decay of heavy isotopes (to ^{4}He) and the beta decay of cosmogenic tritium (to ^{3}He).

The composition of the terrestrial atmosphere is utilized as a standard for noble gas measurements; measurements of other media are typically normalized to the atmospheric values. Within the noble gases, the He isotopic composition of terrestrial samples is often expressed in units of R_a, and the He isotope ratios are reported relative to the atmospheric value (R/R_a notation) as shown below in Equation 4.1 (Ozima and Podosek, 2002; Anderson, 2007).

$$R/R_a = (^{3}He/^{4}He)_{sample} / (^{3}He/^{4}He)_{atmosphere} \qquad (4.1)$$

4.2.2 Noble Gases in Mantle

Noble gases have proved to be useful tracers in providing significant insights into the chemical heterogeneity of the Earth's mantle. The low background inventory of noble gases in terrestrial environments, owing to their exclusion from solid materials during planetary formation in the inner solar system, has lead to the utilization of these gases as excellent tracers of mantle reservoirs.

Table 4.2 Noble gas isotope composition of the atmosphere (Porcelli et al., 2002).

Isotope	Relative Abundances	Percent molar abundance
^{3}He	$(1.399\pm0.013)*10^{-6}$	0.000140
^{4}He	1	100
^{20}Ne	9.80 ± 0.08	90.50
^{21}Ne	0.0290 ± 0.0003	0.268
^{22}Ne	1	9.23
^{36}Ar	1	0.3364
^{38}Ar	0.1880 ± 0.0004	0.0632
^{40}Ar	295.5 ± 0.5	99.60
^{78}Kr	0.6087 ± 0.0020	0.3469
^{80}Kr	3.9599 ± 0.0020	2.2571
^{82}Kr	20.217 ± 0.004	11.523
^{83}Kr	20.136 ± 0.021	11.477
^{84}Kr	100	57.00
^{86}Kr	30.524 ± 0.025	17.398
^{124}Xe	2.337 ± 0.008	0.0951
^{126}Xe	2.180 ± 0.011	0.0887
^{128}Xe	47.15 ± 0.07	1.919
^{129}Xe	649.6 ± 0.9	26.44
^{130}Xe	100	4.070
^{131}Xe	521.3 ± 0.8	21.22
^{132}Xe	660.7 ± 0.5	26.89
^{134}Xe	256.3 ± 0.4	10.430
^{136}Xe	217.6 ± 0.3	8.857

In order to obtain information on the noble gas state in the Earth's mantle, it is necessary to analyze mantle-derived materials, such as volcanic rocks, volcanic gases, mantle xenoliths, and diamonds, which trapped mantle noble gases. Among these various mantle-derived materials, submarine volcanic rocks (oceanic basalts) proved to be the most useful owing to their wide occurrence and their relatively large (for mantle samples) amounts of trapped noble gases (Graham, 2002).

The two most important oceanic basalts in noble gas studies of mantle are the MORBs (Mid Ocean Ridge Basalts) and the OIBs (Ocean Island Basalts). Mid-ocean ridge basalts

(MORB) form by partial melting as the ascending mantle beneath spreading ridges reaches its solidus temperature, and they are generally accepted to represent a broad sampling of the convecting mantle. Ocean island basalts (OIBs), on the other hand, represent melting anomalies that are mainly associated with mantle upwelling (Graham, 2002).

Until now, the studies related to the investigation of mantle heterogeneity were best highlighted by the helium isotope measurements in MORB and OIB. Measurements on helium isotopes have shown that mantle derived materials are mainly dominated by the presence of excess ^{3}He, that is, primordial helium, and the ubiquitous presence of excess ^{3}He reveals that primordial volatiles are still escaping from the Earth's interior (Lupton and Craig, 1975). Since helium undergoes gravitational escape from the thermosphere and has an atmospheric residence time of 1 to 10 million years, it is not recycled back to the Earth's interior. These properties gives the ^{3}He/^{4}He ratio a unique character among isotopic tracers of mantle sources involved in volcanism (Lupton, 1983). The helium isotope ratios of the MORBs and OIBs revealed that they are characterized by different mantle sources, although they are both derived from the mantle. It is generally believed that MORBs represent depleted upper mantle and have relatively uniform ^{3}He/^{4}He ratios which clusters tightly around a characteristic value of ^{3}He/^{4}He : $1* 10^{-5}$ (R/Ra: 8). OIB (hot spot or plume), on the other hand, represent less degassed and therefore less depleted mantle, and exhibit a wide variation in ^{3}He/^{4}He (between 3.5 and 43 Ra), ranging from sub-MORB values up to values a few times higher than in MORBs (Graham, 2002).

In addition to the differences observed in ^{3}He/^{4}He ratios between MORB and OIB, some differences are also evident from the study of other noble gas isotopic ratios such as ^{40}Ar/^{36}Ar, ^{20}Ne/^{22}Ne, ^{21}Ne/^{22}Ne, and ^{129}Xe/^{130}Xe. For example, the ^{40}Ar/^{36}Ar ratio in MORB is very high, up to nearly 25000 (Ozima and Podosek, 1983; Sarda et al., 1985; Allegre et al., 1986). The high ratio is an indication of extensive degassing of MORB-source mantle, that is, high K/Ar leading to high ^{40}Ar/^{36}Ar ratios. The ^{40}Ar/^{36}Ar ratio in OIB source mantle, on the other hand, is considerably less than in MORB-source mantle, and reveals the less extensively degassed nature of their source (Ozima and Podosek, 2002).

For Ne, the mantle is characterized by elevated ratios of $^{20}Ne/^{22}Ne$ and $^{21}Ne/^{22}Ne$ compared to the atmosphere (Sarda et al., 1988). In a plot of $^{20}Ne/^{22}Ne$ vs $^{21}Ne/^{22}Ne$, MORBs lie on a fairly well-defined array, anchored by the atmospheric point, and extend to values as high as 13 for $^{20}Ne/^{22}Ne$ (vs 9.8 in air) and 0.07 for $^{21}Ne/^{22}Ne$ (vs 0.029) (Figure 4.1). The "MORB array" is most readily interpreted as the result of air contamination of a MORB composition lying at or beyond the high end of the array. In comparison to MORBs, some OIBs show a much steeper correlation in the Ne three-isotope diagram. These steep trends reveal that these OIB mantle sources have less nucleogenic Ne (lower $^{21}Ne/^{22}Ne$) than the MORB mantle source. The difference between the Ne isotopic composition of the MORBs and OIBs probably results from differences in the dilution, by primordial Ne, of the nucleogenic ^{21}Ne that is produced in their mantle sources. Even a small amount of nucleogenic production can markedly shift the mantle $^{21}Ne/^{22}Ne$ ratio because ^{21}Ne is so scarce. Therefore Ne in mantle samples represents a mixture of three sources: "solar" Ne captured by the Earth during accretion and characterized by $^{20}Ne/^{22}Ne$ and $^{21}Ne/^{22}Ne$ ratios of 13.6 and 0.032, respectively; nucleogenic Ne (nearly pure ^{21}Ne); and atmospheric contamination (Honda et al., 1991). In this view, the Earth accreted with solar-like Ne, and radioactive decay simply moves the mantle composition to the right (higher $^{21}Ne/^{22}Ne$) as a function of time and degree of outgassing.

As an overview, the upper mantle source of MORBs is characterized by higher radiogenic/primordial noble gas isotope ratios due to its degassed nature. In this regard, the difference between MORB and OIB noble gas isotope compositions is the most fundamental geochemical evidence for the presence of some mode of stratification existing within the Earth's mantle (Graham, 2002).
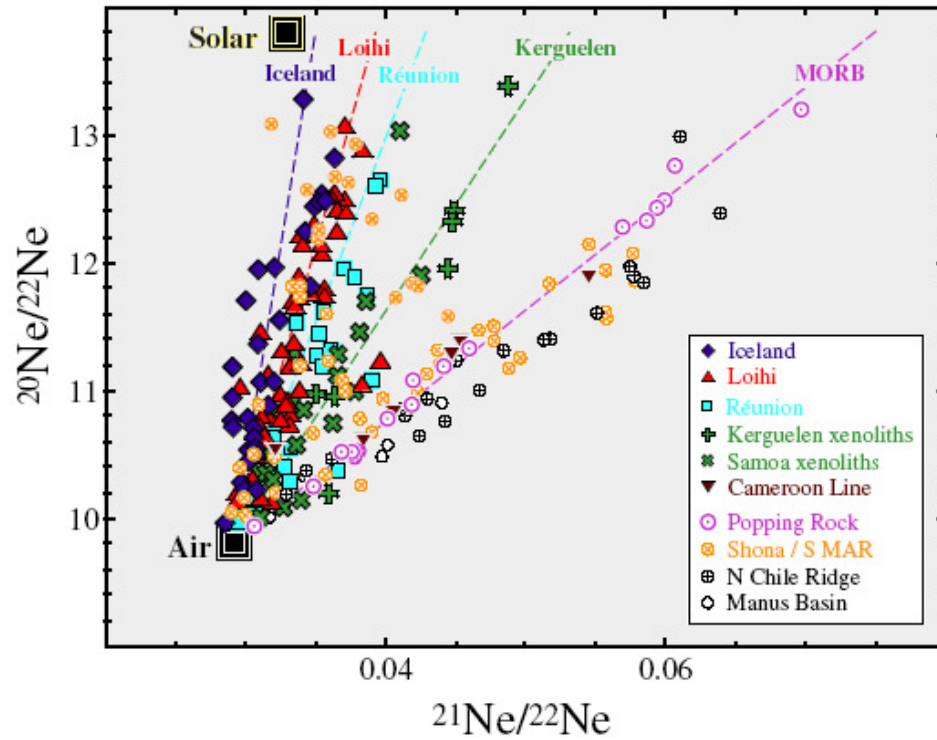
Figure 4.1 The Ne three isotope diagram ($^{20}Ne/^{22}Ne$ vs. $^{21}Ne/^{22}Ne$) (Graham, 2002).

Regarding the degassing mechanism of noble gases, many models have been created for the evolution of the atmosphere and degassing of the solid Earth. Within the noble gases, He proved to represent a quantifiable degassing flux. This flux could be identified owing to the escape of He from the atmosphere and its resulting low background level in air and air saturated water. If the He escape rate from the Earth's upper atmosphere is known, an independent estimation of the mantle He flux would be possible. Since He is too light to be gravitationally bound to the Earth, the present He concentration in the atmosphere can possibly represent a stationary value in balance between the He influx from mantle and its outflow from the upper atmosphere. The present best estimate of the He escape flux is still based on the mantle He flux (Ozima and Podosek, 2002).

According to their solubility characteristics, noble gases generally prefer to be partitioned essentially in the melt (magma) phase. Once in magma, noble gases are easily transported with the ascending magma to the Earth's surface, where they are then released into the atmosphere. Therefore, consecutive noble gas partitions, first between melt and crystal in a mantle source and then between gas (bubble) and melt at the surface, would result in a large scale mantle degassing (Ozima and Podosek, 2002).

4.2.3 Noble Gases in the Crust

Noble gases within the crust originate from three main sources: the atmosphere, mainly introduced into the crust via dissolution in groundwater; the mantle, where magmatic activity exists; and those produced in the crust by the result of radioactive decay processes. Noble gases originating from interplanetary dust particles (IDP) and cosmic ray interaction with the crustal surface may also in some cases contribute to the noble gas inventory of crustal materials.

Neutron flux plays an important role for the production of noble gases within the crust. There are three main types of reaction that produce neutrons within the crust: cosmic ray interactions (only important within the top few meters of the crust), spontaneous fission, and alpha particle interaction with light nuclei (Ballentine and Burnard, 2002).

4.2.3.1 Helium Production in the Crust

The isotopes of ^{3}He and ^{4}He are both produced by radiogenic processes in terrestrial rocks.

^{4}He in the crust is produced from the alpha-decay of the ^{235,238}U and ^{232}Th decay chains, and is therefore directly proportional to the concentration of these elements in the crust (Ballentine and Burnard, 2002). These reactions can be summarized as follows (Equation 4.2, 4.3, 4.4).

$$^{238}\text{U} \longrightarrow {}^{206}\text{Pb} + 8\,{}^{4}\text{He} \qquad (4.2)$$

$$^{235}\text{U} \longrightarrow {}^{207}\text{Pb} + 7\,{}^{4}\text{He} \qquad (4.3)$$

$$^{232}\text{Th} \longrightarrow {}^{208}\text{Pb} + 6\,{}^{4}\text{He} \qquad (4.4)$$

The production of ^{3}He within the crust is essentially due to the neutron capture reaction of Li given in Equation 4.5 below,

$$^{6}\text{Li}(n,\,\alpha){}^{3}\text{H}(\beta^{-}){}^{3}\text{He} \qquad (4.5)$$

where neutrons are derived from a spontaneous fission of ^{238}U and from reactions of light elements such as Na, Mg, Al, and Si, with alpha particles emitted from U, Th decays. However, in a very shallow surface region, the secondary cosmic ray neutrons would be more important (Ozima and Podosek, 2002).

Therefore, the production of ^{3}He is concomitant with the production of ^{4}He, giving a nearly constant production ratio of $^{3}\text{He}/^{4}\text{He}$ in the average crust (Ozima and Podosek, 2002).

4.2.3.2 Neon Production in the Crust

Both ^{21}Ne and ^{22}Ne can be produced in a significant amount in crustal materials such as granite by nuclear reactions involving neutrons and alpha particles derived from U, Th radioactive decays. Except for $^{18}\text{O}(\alpha,n){}^{21}\text{Ne}$ and $^{19}\text{F}(\alpha,n){}^{22}\text{Na}(T_{1/2}: 2.605a){}^{22}\text{Ne}$ reactions, however, other reactions are unlikely to be important in Earth's noble gas inventory (Ozima and Podosek, 2002). Their rate of production is therefore related to radioelement and target-element concentrations as well as the distribution of the target element with respect to any radioelement heterogeneity (Ballentine and Burnard, 2002).

4.2.3.3 Argon

^{40}Ar production in the crust is dominated by the decay of ^{40}K, which is characterized by a branched decay mode, producing ^{40}Ca by beta decay and ^{40}Ar by electron capture. ^{36}Ar

production in the crust is generally neglected owing to its small production compared to the atmospheric derived ^{36}Ar introduced into the crust via dissolution in groundwater.

4.2.3.4 Krypton and Xenon

Fission of ^{238}U provides the dominant mechanism for the production of $^{83, 84, 86}$Kr and ^{129,131,132,134,136}Xe in the crust today, while production of shielded isotopes ^{80,82}Kr and ^{124,126,128,130}Xe can be neglected (Ballentine and Burnard, 2002). Fission products of ^{244}Pu and the decay products of ^{129}I, both now extinct, contribute important Kr and Xe isotopic components to both the terrestrial mantle and atmosphere (Porcelli and Ballentine, 2002). Kr and Xe derived from these extinct radionuclei are not produced in the crust and therefore do not contribute to the crustal system except where carried in as components of magmatic or atmosphere-derived fluids (Ballentine and Burnard, 2002).

4.3 Noble Gases in Groundwater

The chemical inertness of the noble gases, coupled with their distinctive isotopic and solubility characteristics, makes them ideal tracers in groundwater-related studies. The applicability of noble gases extends across topics such as groundwater dating, paleoclimatology, mechanisms of recharge, and mantle and seismic studies.

4.3.1 Solubility Characteristics of Noble Gases in Water

The noble gas abundance in groundwaters are dominated by air-derived noble gases. Atmospheric noble gases enter the meteoric cycle by gas partitioning during air/water exchange with the atmosphere. In groundwaters gases partition between the water phase and the soil air of the quasi-saturated zone. Groundwater equilibrates with air during its infiltration and it dissolves atmospheric He, Ne, Ar, Kr, and Xe in amounts defined by the local altitude and temperature. Owing to their inert nature, the equilibrium concentrations of the noble gases can record the physical conditions prevailing during air/water partitioning, such as changes in soil temperature, altitude or pressure, and salinity (Kipfer et al., 2002).

On the whole, noble gases exhibit about the same order of magnitude of solubility in water as do other gases that do not react chemically with the water. Within the noble gases, Ar is approximately as soluble as the major atmospheric gases; its solubility for pure water at 0 ℃ is 2.26 times that of N_2 and 1.09 times that of O_2. The noble gases as a group, however, exhibit a fairly wide range in solubilities, with the characteristic features of strongly increasing solubility and temperature dependence of solubility with increasing atomic weight. Therefore, the solubilities for noble gases is smallest for helium and increases towards xenon (Ozima and Podosek, 2002).

The noble gas solubilities in water generally decrease with increasing temperature. However, for temperatures higher than 60 ℃ noble gas concentrations increase dramatically with increasing temperature (Crovetto et al., 1982). Another major important solubility characteristic of noble gases is that they become less soluble with increasing salinity (Smith and Kennedy, 1985). The temperature and salinity dependence increases with the atomic mass of the noble gas and is therefore more pronounced for Xe.

As a whole, noble gases behave as ideal gases during dissolution and partitioning processes in meteroic water (Kipfer et al., 2002). The lack of chemical interactions in the noble gases makes them ideal gases, and their solubility in water is directly proportional to their partial pressure in air. This, in turn, depends on the barometric pressure, which is linearly correlated to the altitude. The higher the altitude, the lesser the noble gases dissolve in water (Mazor, 1997).

The most important source of noble gases in natural waters is the solution of atmospheric gases according to the Henry's law given in the Equation 4.6 below:

$$p_i = k_i (T,S) x_i \qquad\qquad (4.6)$$

where p_i is the partial pressure of the noble gas in the gas phase; k_i is a proportionality coefficient, known as the Henry coefficient, which is dimensionless and can simply be assumed to depend only on temperature (T) and salinity (S) of the water (Aeschbach-Hertig et al., 1999); and x_i is the equilibrium concentration of the dissolved gas in water (or other liquid) as a mole fraction. Noble gas concentrations in water are usually

reported in cm^{3}STP/gH$_2$O notation. Noble gas concentrations in gas samples, on the other hand, can be expressed as mbar or ppmv.

4.3.2 Components of Noble Gases in Terrestrial Fluids

The abundance of noble gases in groundwater is generally understood as a mixture of two distinct noble gas components – a well constrained atmospheric component and a residual component of non-atmospheric origin. The non-atmospheric component in groundwaters derive from different geochemical compartments of the Earth (Kipfer et al., 2002). The major components in groundwaters can therefore be summarized as follows:

4.3.2.1 Atmospheric Component

Atmospheric noble gases constitute a major component in groundwaters. The atmospheric signals of noble gases are inherited by groundwaters upon infiltration and equilibration in the subsurface. An additional atmosphere-derived component is ubiquitous in groundwater: the so-called "excess air" (Heaton and Vogel, 1981). Excess air originates from the dissolution of air bubbles that are trapped in the quasi-saturated soil zone, i.e. the zone affected by periodic fluctuations of the groundwater table. Although the noble gas excess is air-like in composition, there still is a lot that remains unclear about the formation processes responsible for the observed gas excess in groundwater. There are basically two different models: the partial re-equilibration and closed system equilibration models, which describe the relative abundances of dissolved atmospheric noble gases as well as the possible fractionation relative to pure air (Stute et al., 1995; Aeschbach-Hertig et al., 2000).

Atmospheric noble gases can also be derived due to sampling, that is, air contamination. In this regard, within the noble gases, especially Ar is very susceptible to atmospheric contamination owing to its high abundance in air.

4.3.2.2 Non-atmospheric Noble Gas Components

Non-atmospheric noble gases originate from well-defined geochemical reservoirs with a distinct geochemical composition. There are basically two non-atmospheric components in natural waters: noble gases of crustal/radiogenic and of mantle origin (Kipfer et al., 2002).

Radiogenic noble gases are generated by all kinds of disintegration of radioactive precursors and succeeding nuclear reactions. Only $^4He_{rad}$, $^3He_{rad}$, occasionally $^{40}Ar_{rad}$ and $^{21}Ne_{rad}$ have sufficiently large production yields that these isotopes can be observed in natural waters. The continental crust is dominated by radiogenic He (^4He) that is produced by nuclear reactions in crustal rocks and minerals. The decay of the atmospheric tritium (^3H) to tritiogenic helium ($^3He_{trit}$), constitutes an important radiogenic source for ^3He for groundwaters that are younger than 50 years, that is, waters that were affected by nuclear bomb testings applied in the early 1960s (Attendorn and Bowen, 1997). All other noble gas isotopes have such low production yields that they are hardly detectable against their atmospheric background. The mantle, on the other hand, is dominated by ^3He (primordial He) kept entrapped since the formation of the Earth. Each non-atmospheric component is distint in their $^3He/^4He$ ratio (Kipfer et al., 2002).

Within the noble gases, helium has proved to be the best tracer of in-situ additions of gases into groundwater related systems, thereby making it as studied by many researchers. Until now many studies involved the separation of helium components in groundwaters (Kulongoski et al., 2003, 2005, 2008; Castro, 2004; Morikawa et al., 2008). There are basically two components for helium in groundwater: atmospheric and non-atmospheric. The atmospheric components of helium can be introduced during air equilibrium or during sampling. The non-atmospheric components of helium, on the other hand, can originate from different terrestrial reservoirs, such as lithospheric mantle, asthenospheric mantle, continental crust etc.

The individual components of ^3He can be represented by

     i)   in situ production from the reaction $^6Li\ (\alpha,n)\ ^3H\ (\beta^-)\ ^3He$ in the aquifer or the host rock (nucleogenic ^3He),

ii)   fluxes from the mantle (terrigenic ^{3}He),

iii)   air-equilibrated helium,

iv)   excess air (dissolved air bubbles), and

v)   tritiogenic helium, the decay product of the radioactive tritium (^{3}H).

The individual components of ^{4}He, on the other hand, can include:

    i)   in situ production from the radioactive decay of U and Th in crustal rocks (radiogenic ^{4}He),

ii)   fluxes from the mantle (terrigenic ^{4}He),

iii)   air-equilibrated helium, and

iv)   excess air (dissolved air bubbles).

In groundwater, due to additions from the above mentioned sources, the helium content is not conserved (Torgersen and Clarke, 1985; Andrews, 1992; Mahara et al., 2001). The isotopic ratio of helium can be drastically changed by the addition of isotopically different He components: mantle He which has a high ratio (^{3}He/^{4}He = 1*10^{-5}; Ozima and Podosek, 2002; Graham, 2002); radiogenic helium which has a low ratio (^{3}He/^{4}He = 2*10^{-8}; Mamyrin and Tolstikhin, 1984), and atmospheric helium which exhibits an intermediate value (^{3}He/^{4}He = 1.4*10^{-6}; Lupton, 1983).

$$^3He_s = {}^3He_{atm} + {}^3He_{ea} + {}^3He_{tri} + {}^3He_{exc} \qquad (4.7)$$

$$^3He_s = {}^3He_{atm} + {}^3He_{ea} + {}^3He_{tri} + {}^3He_{man} + {}^3He_{crus} \qquad (4.8)$$

$$^4He_s = {}^4He_{atm} + {}^4He_{ea} + {}^4He_{exc} \qquad (4.9)$$

$$^4He_s = {}^4He_{atm} + {}^4He_{ea} + {}^4He_{man} + {}^4He_{crus} \qquad (4.10)$$

where ^3He_s and ^4He_s are the helium-3 and helium-4 concentrations measured in a groundwater sample, He_{atm} and He_{ea} are the amounts of He resulted from equilibrium solubility with the atmosphere and that from excess air, respectively. $^3He_{exc}$ ($^3He_{man}$ and $^3He_{crus}$) and $^4He_{exc}$ ($^4He_{man}$ and $^4He_{crus}$) represent the terrigenic components of helium

derived from the earth's mantle and crust. $^3\mathrm{He}_{trit}$ denotes the tritiogenic component of helium produced by the radioactive decay of tritium (Morikawa et al., 2008).

In component separation to identify the non-atmopsheric components in a gas sample, first atmospheric correction should be applied. $^{20}\mathrm{Ne}$ and $^{36}\mathrm{Ar}$ are generally used as a measure for the degree of atmospheric contamination since both nuclides are enriched in air compared with other reservoirs such as Earth's mantle and crust.

The measured $^3\mathrm{He}/^4\mathrm{He}$ ratios can be corrected assuming that the measured $^{20}\mathrm{Ne}$ is completely atmospheric. Therefore, the measured $^3\mathrm{He}/^4\mathrm{He}$ ratios are corrected, assuming a $^4\mathrm{He}/^{20}\mathrm{Ne}$ ratio of 0.319 (Ballentine et al., 2002) for the atmospheric component, by using the Equations 4.11 and 4.12 given below (Poreda and Craig, 1989).

$$(^3\mathrm{He}/^4\mathrm{He})_{cor} = [(^3\mathrm{He}/^4\mathrm{He})_m - (^3\mathrm{He}/^4\mathrm{He})_{air} * r] / (1 - r) \qquad (4.11)$$

$$r = (^4\mathrm{He}/^{20}\mathrm{Ne})_{air} / (^4\mathrm{He}/^{20}\mathrm{Ne})_m \qquad (4.12)$$

where the subscript cor is the corrected value; and m is the measured value.

After correction for air contamination, the separate contributions of mantle and crustal percentages can be calculated assuming a simple binary mixing between a mantle (R/Ra = 8) and a crustal (R/Ra =0.02) endmember component, utilizing the formula given below (Equation 4.13):

$$R_c = 8.0\,a + 0.02\,(1 - a) \qquad (4.13)$$

where the subscript c is the corrected $^3\mathrm{He}/^4\mathrm{He}$ ratio; a is the percentage of mantle component involved in the sample and $(1 - a)$ denotes the percentage of crustal contribution.

In dealing with the identification of non-atmospheric derived components, noble gas isotopic ratios such as $^4\mathrm{He}/^{20}\mathrm{Ne}$, $^{40}\mathrm{Ar}/^{36}\mathrm{Ar}$, $^{21}\mathrm{Ne}/^{22}\mathrm{Ne}$ and $^{20}\mathrm{Ne}/^{22}\mathrm{Ne}$ higher than the characteristic atmospheric ratios, can also be an indication of the existence of non-

atmospheric derived components in gases and fluids. Especially, the ^{4}He/^{20}Ne ratio of samples, significantly higher than that characteristic for air (0.319), suggests the existence of non-atmospheric derived components.

4.4 Other Applications of Noble Gases in Groundwater

4.4.1 Dating Young Groundwater

Tritium, the short-lived radioactive isotope of hydrogen (half-life of 12.43 years), together with its daughter isotope ^{3}He$_{trit}$ has been used to determine the true ages of water parcels in many studies (Schlosser et al., 1989). As ^{3}H decays, tritiogenic helium is produced. As long as the water is in contact with the atmosphere, the resulting excess ^{3}He$_{trit}$ can continuously escape into the air. However, as soon as a water parcel is isolated from the gas exchange with the atmosphere, the ^{3}H decay starts and leads to a corresponding increase in ^{3}He$_{trit}$ content of the water, thereby leading to the quantitative measurement of the isolation time of the water parcel.

4.4.2 Dating Old Groundwater

Groundwater accumulates helium that is continually released from the radioactive decay of uranium and thorium within the crust. The basic assumption is that the groundwater acts as a sink for the helium evolved from the local crustal rocks. After corrected for atmospheric helium that is basically introduced during recharge, the measured ^{4}He in a groundwater sample should then reflect the groundwater residence time, which is of only qualitative nature, at a practical limit of 10^4 and 10^8 years (Mazor, 1997; Clark and Fritz, 1997). Many studies have shown the use of radiogenic helium accumulation rates as a tool for groundwater dating (Mahara and Igarashi, 2003).

4.4.3 Paleotemperature Reconstruction

Groundwaters contain dissolved noble gases in concentrations that were defined by the ambient temperature that prevailed during the time of recharge (Mazor, 1972; Stute et al., 1992). Owing to their chemical inertness, the dependency of noble gas solubility

equilibrium on the physical conditions during gas exchange, in particular the sensitivity of the Henry coefficient on temperature, has been used for the reconstruction of the soil temperature that prevailed during recharge of groundwater. Therefore, if an aquifer contains groundwater that recharged during different climatic conditions in the past, noble gas concentrations can thus provide valuable information on the past temperature evolution (Mazor, 1972; Andrews and Lee, 1979).

In summary, the evaluation of the noble gas concentrations in groundwaters can be translated into

1.   geochemical fingerprints on the different terrestrial components of noble gases, especially helium
2.   climatic conditions prevailing during groundwater recharge (atmospheric noble gas component),
3.   groundwater residence times (qualitative and quantitative).

4.5 Tectonic Control on the Distribution of Mantle-Helium in Crustal Fluids

The study of noble gases, particularly helium and its isotopes, in areas void of recent volcanism have shown the evidence for the existence of mantle-derived volatiles in crustal fluids, such as groundwaters, geothermal waters and gases, and natural gas fields (Ballentine et al., 1991; Torgersen, 1993; Güleç et al., 2002; Erzinger et al., 2004; Kulongoski et al., 2005; Güleç and Hilton, 2006; Wiersberg and Erzinger, 2007; Gilfıllan et al., 2008).

In crustal environments, mantle derived helium can represent a major helium component, even though there is no recent remnant volcanic activity associated with mantle upwelling. The generally accepted view suggests that the occurrence of mantle helium in continental environments is restricted to volcanically or tectonically active regions, especially to extension zones (Oxburgh et al., 1986; Oxburgh and O'Nions, 1987; Ballentine et al., 1991; Torgersen, 1993). It is believed that the source of excess helium is an enhanced flux of mantle volatiles up into the basin due to processes such as crustal thinning, crustal underplating by mantle melts related to extensional regimes. Many

studies have investigated the crustal fluids in regions undergoing active extension, such as the Upper Rhine graben (Clauser et al., 2002), Western Anatolia –Turkey (Güleç, 1988; Güleç et al., 2002) and the Great Hungarian Plain (Stute et al., 1992). These studies have shown the association of crustal fluids with high ^{3}He/^{4}He isotopic ratios, exceeding the ones characteristic to crustal production, and have revealed the existence of mantle derived helium, which was related to mantle volatile degassing.

Several models have been proposed regarding the transport mechanisms of mantle helium into the shallow levels of the crust. The major transport models were mainly attributed to the regional tectonic background of the studied fields, that is, faults were accepted to be acting as major conduits for the flow of mantle volatiles into the crust, and therefore, the introduction of mantle helium anomalies (Güleç et al., 2002; Clauser et al., 2002; Erzinger et al., 2004; Kulongoski et al., 2005; Kennedy and Van Soest, 2006; Güleç and Hilton, 2006; Erzinger et al., 2006; Mutlu et al., 2008). Kennedy et al (1997) showed that elevated ^{3}He/^{4}He ratios (i.e., greater than crustal production values) in deep pore fluids from the San Andreas Fault (SAF) could be used to estimate the flow rate of mantle fluids through the SAF zone. However, recently published studies, dealing with the noble gas analyses of mud gas samples from the SAFOD (San Andreas Fault Observatory at Depth) Main Hole, have shown that the permeability of the section of the SAF core intersected by the borehole was relatively low, and that the SAF did not play a major role as a conduit for fluids coming from the mantle (Wiersberg and Erzinger, 2007). It was further suggested that, rather than acting as a permeable conduit, the SAF appeared to be considerably less permeable than the surrounding crust and acted as a barrier for fluid flow.

Mantle helium reaching the shallow levels of the crust through tectonic pathways will be continuously diluted by the addition of crustal and/or atmospheric components due to the constant radioactive decay of Uranium and Thorium (producing mainly ^{4}He) and continuous atmospheric recharge, respectively. Therefore, continental fluids are mainly interpreted to represent variable admixtures of mantle components reaching through faults and crustal components continuously being produced within the crust (Torgersen, 1993).

Within the noble gases, the study of helium and its isotopes has led to the better understanding and visualization of possible interactions between mantle-crustal processes prevailing in crustal fluids. In addition, helium, along with other gases such as Radon and CO_2, has also enabled the detection of fluid-bearing horizons such as shear zones, open fractures, and sections of enhanced permeability (Erzinger et al., 2006). Therefore, the isotopes of helium, remain as one of the major tools of choice for detecting mantle volatile input into crustal fluids, and have shown the importance of tectonic and/or hydrologic controls on the input of mantle volatiles in regions devoid of recent volcanism.

CHAPTER 5

METHODS OF STUDY

This thesis study was realized through 3 major steps:

i) field studies; consisting of continuous gas monitoring in the Tekke Hamam geothermal field, and fluid and gas sampling from Kızıldere and the Tekke Hamam geothermal fields,

ii) chemical and isotopic analyses of fluid and gas samples collected from both fields and

iii) overall data evaluation regarding the on-line gas monitoring results and the chemical and isotopic analyses.

The methods that were utilized in this thesis study are summarized as follows:

5.1 Field Studies

Three major sampling campaigns were conducted in the Kızıldere and the Tekke Hamam geothermal fields. The first sampling campaign was conducted between 19 - 26 November 2007, and was realized in two main steps: (i) set-up of the on-line gas monitoring station in the Tekke Hamam geothermal field and (ii) gas and fluid sampling from the selected wells and/or springs/pools in the Kızıldere and the Tekke Hamam geothermal fields. The second sampling campaign, conducted between 28 August and 2 September 2008, involved gas and fluid sampling from the previously sampled sites and an overall control of the on-line gas monitoring station. The third and final sampling campaign, conducted between 21 – 25 July 2009, covered only sampling studies and involved mainly cold water sampling from the vicinity of the fields in addition to the water sampling from the pools in Tekke Hamam and some wells in Kızıldere; gas

sampling, on the other hand, was only conducted in R-1 well in the Kızıldere geothermal field.

In addition to the sampling campaigns mentioned above, routine field visits (nearly once every month) were also conducted during the continuous gas monitoring campaign (November 2007 – October 2008) in the Tekke Hamam geothermal field and involved the control of the equipment in the station and the data storage.

5.1.1 Construction of the On-line Gas Monitoring Station (19 - 26 November 2007, Sampling Campaign I)

After a reconnaissance field survey conducted in the Tekke Hamam and the Kızıldere geothermal fields in early 2007, a gas discharging pool (mofette) with intense gas emissions at ambient temperature in the Tekke Hamam geothermal field was selected as site for on-line gas monitoring, and later a station was built near the pool (Pool 2 for the time interval between November 2007 – August 2008 and, later, Pool 3 for the time interval between September 2008 – October 2008, see Figure 5.1). The on-line gas monitoring station constructed for the Tekke Hamam geothermal field measured the gases released at the ground of the pool and recorded the compositions of gases as well as the gas flow rate and the pool temperature at one minute intervals.

The equipment used in the on-line monitoring station consists of a Quadrupole Mass Spectrometer (Pfeiffer Omnistar©) for on-line gas analysis, a flowmeter for the recording of the gas flow rate coming from the pool, a field computer and a data logger for data storage.

Air condition was used to stabilize the temperature of the station and 2 UPS (Uninterrupted Power Supply) units were used for data retrieval in case of power cut off. Silicon tubings, a temperature probe, an inverted plastic funnel and some additional devices (eg. Water trap, connection plastics, metal rings) were also used during the construction of the gas line between the station and the bubbling pool.

5.1.1.1 Construction of the Gas Line

For the construction of the gas line, a plastic funnel with 20 cm diameter was placed inversely at the ground of the pool where gas was discharged (Figure 5.2). The inverted funnel was then fixed at the bottom of the pool with some lead rings and connected with 10 m plastic tube (PE) that led into the station. The flow rate of the discharged gas, introduced into the station via the plastic tubing, was determined with a flowmeter (Ritter ©) placed in the flow line (Figure 5.3). Behind the flowmeter, some gas was introduced into the QMS by a capillary and the remaining gas was designed as the gas line exhaust which was mounted on the outer wall of the station (Figure 5.4). The temperature probe connected to the data logger was also inserted into the pool and was covered with rocks. Between the station and the pool, a trench was digged and a pipeline was placed in which the gas tube and the temperature probe cable were placed (Figure 5.5). Figure 5.6 shows a simplified configuration of the automated monitoring station.

Figure 5.1 The bubbling pool (Pool 2 and later Pool 3) and the monitoring station in Tekke Hamam (Pool 3 is located behind the wooden fence).

Figure 5.2 Insertion of the inverted funnel and checking the gas flow with a water trap.
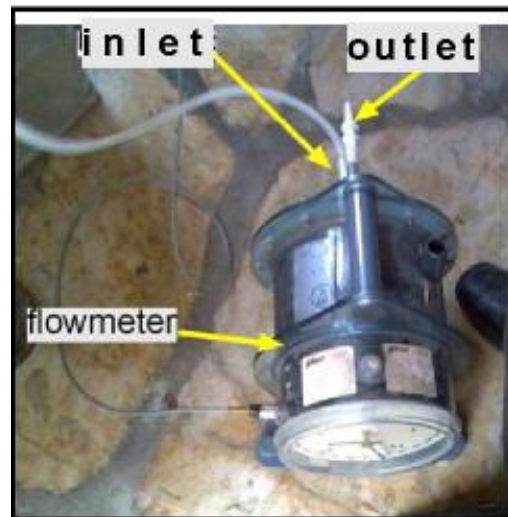
Figure 5.3 Inlet and outlet of the flowmeter.
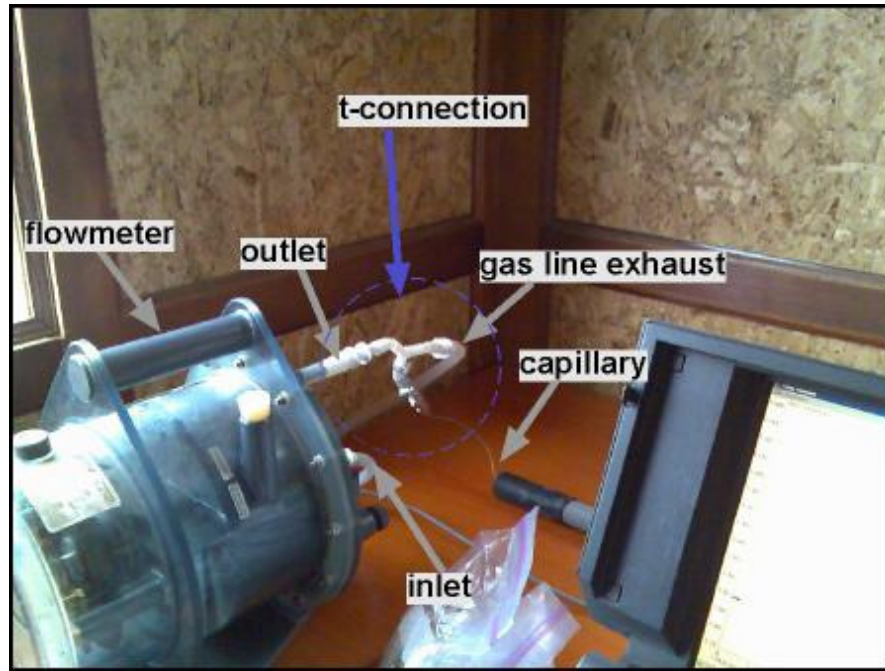
Figure 5.4 T-connection between the flowmeter and the QMS.

Figure 5.5 Sealing of the gas tube and the temperature probe.
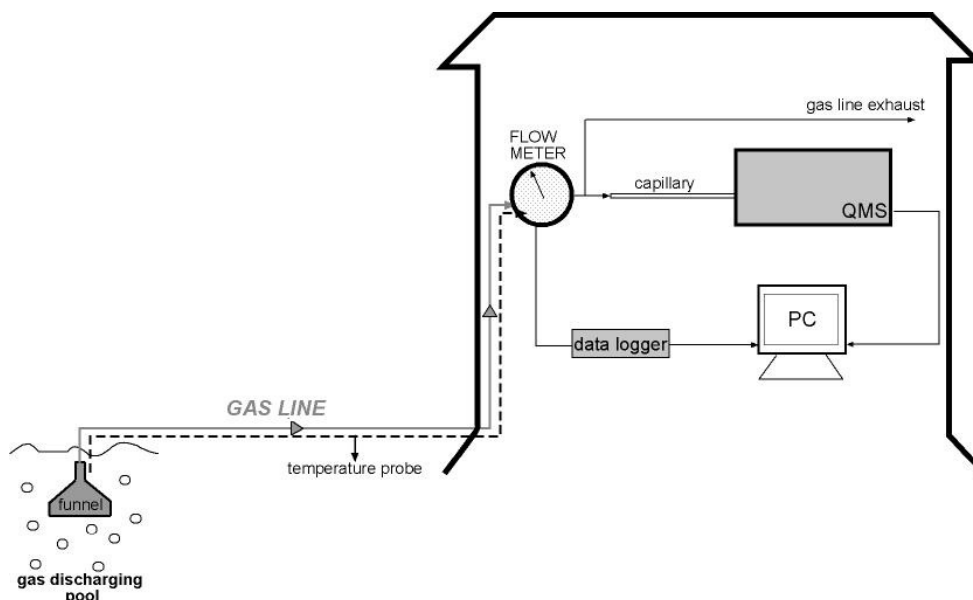
Figure 5.6 Simplified sketch of the automated monitoring station.

5.1.1.2 Installation of the Quadrupole Mass Spectrometer

After setting up all the electrical connections, the QMS and the computer were turned on. The flowmeter was filled with water until some level to make it function. After turning on the QMS and waiting for some time for the Turbo Molecular Pump to reach its maximum speed, we were ready to begin monitoring gases from the pool/mofette.

For the operation of the QMS and the flowmeter-temperature probe, the Quadstar 422 and Labview software were installed on the computer, respectively. The Quadstar and the Labview programs generated daily files consisting of gas compositions (vol.%) and gas flow rate (l/min)-pool temperature (ºC), respectively. During the routine field visits performed nearly within monthly intervals, the data regarding the gas composition measured by the QMS and the gas flow rate and pool temperature recorded by the computer were all downloaded and compiled in separate monthly EXCEL files.

The QMS was arranged to analyze the composition of gases in an interval of 23 seconds. However, to reduce the amount of data generated, measurements were performed at the interval of every one minute. The system was set to measure H_2 (on mass 2), He (on mass 4), CH_4 (on mass 15), N_2 (on masses 14, 15 and 28), O_2 (on masses 32 and 33), Ar (on masses 36 and 40), CO_2 (on masses 28 and 44) and H_2S (on mass 33).

Brief technical description on the working principles of the Quadstar software- used to handle the gas monitoring files measured by the QMS- is given in Appendix A.

5.1.1.3 Calibration of the QMS

For quantitative analysis, the QMS was calibrated with air, pure CO_2, and certified gas mixtures, the composition of which are selected according to the expected nature of gas. With calibration, the measured ion currents are put to a solution matrix and the individual concentrations of the components in the gas to be analyzed are determined via calibration factors. For calculating the gas concentrations from ion currents, the mass spectrometer sensitivity for the individual gas components must be known. Those relative mass spectrometer sensitivities are determined by the measurement and stored as calibration factors.

Calibration gas files were prepared via the PARSET menu of the Quadstar software. After the preparation of the calibration files, from MEASURE menu, the QMS was calibrated with air and the calibration gas. With these calibrations, a table containing the gases and their respective calibration factors was generated.

During air calibration, the capillary of the QMS was disconnected from the gas line and exposed to air. Air was used to calibrate for Oxygen, Nitrogen, and Argon. As internal standard, Ar was used (all sensitivity factors are relative to the sensitivity for ^{40}Ar, which is set as 1).

During calibration with gas standards, the QMS was disconnected from the gas line and then connected to the calibration gas flask. After establishing the connection, the "dead volume", i.e. the space between the inlet capillary of the QMS and the calibration flask

was evacuated by using the QMS for some time until a pressure inside the chamber of $<10^{-7}$ mbar was achieved. Then the calibration gas flask was opened to the QMS for measuring.

The composition of the standard gases used in the calibration were as follows:

Standard Gas 1: CO_2 (98.64 vol.-%), Ar (0.986 vol.-%), Kr (0.1008 vol.-%), CH_4 (0.1012 vol.-%) and H_2 (0.1080 vol.-%).

Standard Gas 2: N_2 (98.88 vol.-%), H_2S (0.1011 vol.-%) and Ar (1.018 vol.-%).

In addition to calibrations with the gas standards and air, the QMS was also calibrated for the masses of the gases (Mass Scale Calibration). Mass scale calibration was applied in order to overcome any problem regarding the ion current values. The individual mass spectral peaks produced by a quadrupole mass spectrometer are asymmetric; they exhibit a 'tail' on the low mass side. In some cases a definite structure is observed in the tail. The mass scale calibration can be performed with one peak in the upper and one in the lower region of the mass scale. If no special calibration gas is available, the peaks of air can be used.

Once calibrated, the QMS was ready to proceed with the quantitative analysis.

5.1.2   Fluid and Gas Sampling in Kızıldere and Tekke Hamam Geothermal Fields

For the geochemical characterization studies, gas and fluid samples were collected from both the Kızıldere and the Tekke Hamam geothermal fields.

The sampling localities in Tekke Hamam include a bubbling mud pool that is also used for health purposes (pool 1), bubbling intermediate temperature pools (pool 2, 3, 4, 5, 6, TH-8) one drilling well (Umut-1), and 2 hot water discharges connected to the drilling well (TH-6 and TH-7) (Figure 5.7, 5.8, 5.9). Gas samples in Tekke Hamam were taken from the bubbling pools (except for Pool 6 and TH-8), whereas the water samples were taken from all sites. In the Kızıldere geothermal field, a total of 8 wells (KD-6, KD-13, KD-14, KD-15, KD-16, KD-21, KD-22, R-1) have been sampled for both water and gas

analyses (Figure 5.10). Cold/warm water samples were also taken from the vicinity of the geothermal fields.

The physical parameters (temperature, pH, Electrical Conductivity (EC), Dissolved Oxygen (DO), Total Dissolved Solid (TDS)) of the samples were measured by a Multiparameter measurement device (Figure 5.11) directly in the field for each sampling point. The UTM coordinates, on the other hand, were recorded for each sampling site using a GPS (Global Positioning System).

Table 5.1 (a,b,c,d) presents the UTM coordinates and the physical parameters related to the samples taken from both the Kızıldere and the Tekke Hamam geothermal fields during the three major sampling campaigns.

5.1.2.1 Fluid Sampling

In the Tekke Hamam geothermal field, water samples were taken directly from the gas discharging pools (mofettes) and well discharges, whereas in the Kızıldere geothermal field, water samples were taken from the water depots near the production wells which represent the residual water left after the steam separation in the power plant (Figure 5.10).

During fluid sampling, three sets of 100 ml high density polyethylene bottles were used (for each sample) separately for cation-trace element, anion and stable isotope ratio ($^{18}O/^{16}O$ and D/H) analyses. The samples were filtered for anion and cation analyses. Filtration was carried out through a 0.45 μm membrane filter to prevent algal growth, which may bring about removal of dissolved chemical constituents, such as NH_3, and SO_4, and clogging of laboratory instruments during water analysis. The cation samples were also further acidified with nitric acid (10% of 1000 ml Nitric acid diluted with distilled water) to avoid the precipitation of metals (1ml of HNO_3 was added to 100 ml of sample). Samples for isotope analyses, on the other hand, were not filtered, except for the gas discharging pools in Tekke Hamam which were muddy. For all samples, the bottles were filled completely until no space was left for a possible air exchange of the water, and sealed tightly to avoid leaking.

Figure 5.7 Gas discharging pools in the Tekke Hamam geothermal field.

Figure 5.8 Drilling well (Umut-1) and well discharge through pipe (TH-7) in the Tekke Hamam geothermal field.

Figure 5.9 TH-8 in the Tekke Hamam geothermal field.

Figure 5.10 A photo of the two Kızıldere wells, KD-13 and KD-21, and one of the water depots from which water samples were taken.
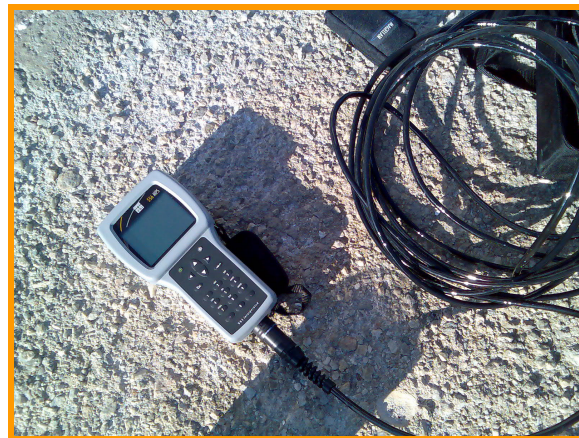
Figure 5.11 The Multiparameter measurement device used in the geothermal fields.

Table 5.1a Physical parameters of samples taken from Kızıldere and Tekke Hamam geothermal fields (19-26 November 2007).

	Sample No	UTM(E)	UTM(N)	Altitude (m)	T(°C)	pH	#EC (μs^c/cm)	EC (μs/cm)	DO (%)	DO (mg/l)	TDS (mg/l)	Sal	Sample type
	Pool 1	660686	4198572	141	-	-	-	-	-	-	-	-	natural pool
	Pool 2	660685	4198555	141	-	-	-	-	-	-	-	-	
	Pool 3	660685	4198547	141	-	-	-	-	-	-	-	-	
	Pool 4	660697	4198566	146	-	-	-	-	-	-	-	-	
Tekke Hamam	Pool 5	660701	4198583	145	-	-	-	-	-	-	-	-	
	TH-8	660751	4198608	137	53.82	7.0	5246	8134	12.80	0.6	3410	2.69	
	Umut-1	660564	4198691	138	-	-	-	-	-	-	-	-	drilling well
	TH-6	660697	4198630	150	51.48	8.7	3606	5583	54.20	3.4	2489	1.96	well discharge
	TH-7	660670	4198626	132	57.42	8.5	3992	6455	2.30	0.1	2595	2.00	well discharge
	TH-cold	660564	4198691	137	15.52	7.8	5226	4281	70.70	6.9	3398	2.83	cold discharge

#Conductivity at 25 °C

accuracy for T is ±0.15°C, EC is ±0.001ms/cm, DO is ±2% or 0.2mg/l, Sal is ±1.0%, pH is ±0.2 units

Table 5.1a (continued).

	Sample No	UTM(E)	UTM(N)	Altitude (m)	T(°C)	pH	#EC (µs^c/cm)	EC (µs/cm)	DO (%)	DO (mg/l)	TDS (mg/l)	Sal	Sample type
	KD-6	661906	4202419	175	-	9.3	2861	3884	56.60	3.4	1859	1.44	
	KD-13	661882	4202637	195	-	9.3	5451	6829	70.40	4.6	3541	2.88	
	KD-14	662002	4202868	197	-	9.3	5693	7660	39.40	2.4	3698	2.99	
Kızıldere	KD-15	662170	4203002	202	-	9.0	5780	8017	64.30	3.8	3764	3.04	drilling well
	KD-16	662094	4202888	196	-	9.2	5938	8060	44.99	2.7	3850	3.12	
	KD-21	662172	4202781	200	-	9.2	3851	5363	64.50	3.7	2491	1.92	
	KD-22	661983	4202735	198	-	9.2	5673	7260	51.00	3.2	3680	2.99	
	R-1	661036	4201912	148	-	9.1	6745	9126	63.90	3.8	4385	3.58	

#Conductivity at 25 °C

accuracy for T is ±0.15°C, EC is ±0.001ms/cm, DO is ±2% or 0.2mg/l, Sal is ±1.0%, pH is ±0.2 units

Table 5.1b Physical parameters of samples taken from Kızıldere and Tekke Hamam geothermal fields (28 August-2 September 2008).

	Sample No	UTM(E)	UTM(N)	Altitude (m)	T(°C)	pH	#EC (μs°/cm)	EC (μs/cm)	DO (%)	DO (mg/l)	TDS (mg/l)	Sal	ORP	Sample Type
	Pool 1	660686	4198572	141	43.00	6.6	5325	7139	7.80	0.4	3480	2.81	-256	
	Pool 2	660685	4198555	141	32.32	6.5	10035	11439	21.00	1.5	6528	5.60	-78	
	Pool 3	660685	4198547	141	34.15	6.3	8028	9437	2.50	0.2	5228	4.40	-111	natural pool
	Pool 4	660697	4198566	146	38.65	6.1	9230	11634	9.70	0.6	6008	5.07	-109	
	Pool 5	660701	4198583	145	33.71	6.4	10853	12676	6.20	0.4	7063	6.08	-105	
Tekke Hamam	Pool 6	660708	4198564	142	-	-	-	-	-	-	-	-	-	
	TH-8	660751	4198608	137	30.82	7.5	6539	7241	4.60		4242	3.53	-263	
	Umut-1	660564	4198691	138	85.02	8.5	4118	8834	2.40	0.1	2677	2.01	-378	drilling well
	TH-6	660697	4198630	150	54.19	8.9	3586	5580	35.80	1.8	2331	1.80	-136	well discharge
	TH-cold	660564	4198691	137	29.40	8.0	4716	5107	57.60	4.3	3068	2.50	-22	cold discharge

#Conductivity at 25 °C

accuracy for T is ±0.15°C, EC is ±0.001ms/cm, DO is ±2% or 0.2mg/l, Sal is ±1.0%, pH is ±0.2 units, ORP is ±20mV

Table 5.1b (continued).

	Sample No	UTM(E)	UTM(N)	Altitude (m)	T(°C)	pH	#EC (µs°/cm)	EC (µs/cm)	DO (%)	DO (mg/l)	TDS (mg/l)	Sal	ORP	Sample Type
	KD-6	661906	4202419	175	73.74	9.3	5813	11211	31.50	1.2	3777	2.93	-208	
	KD-13	661882	4202637	195	72.35	9.3	5860	11153	18.40	0.7	3808	2.96	-227	
	KD-14	662002	4202868	197	78.40	9.3	6325	12772	45.70	1.6	4108	3.19	-241	
Kızıldere	**KD-15**	662170	4203002	202	79.60	9.1	6189	12636	22.60	0.8	4021	3.12	-246	drilling well
	KD-16	662094	4202888	196	74.48	9.1	6154	11962	31.60	1.2	4001	3.11	-219	
	KD-21	662172	4202781	200	76.51	9.1	6056	11994	32.00	1.2	3954	3.08	-233	
	KD-22	661983	4202735	198	80.32	9.2	5496	11284	75.60	2.5	3575	2.75	-229	
	R-1	661036	4201912	148	77.62	9.3	6778	13528	69.40	2.4	4406	3.44	-264	

#Conductivity at 25 ºC

accuracy for T is ±0.15ºC, EC is ±0.001ms/cm, DO is ±2% or 0.2mg/l, Sal is ±1.0%, pH is ±0.2 units, ORP is ±20mV

Table 5.1c Physical parameters of samples taken from Kızıldere and Tekke Hamam geothermal fields (21- 25 July 2009).

	Sample No	UTM(E)	UTM(N)	Altitude (m)	T(°C)	pH	#EC (µsᶜ/cm)	EC (µs/cm)	DO (%)	DO (mg/l)	TDS (mg/l)	Sal	ORP	Sample Type
	Pool 1	660686	4198572	141	40.70	6.5	2854	3713	23.80	1.5	1856	1.44	-224	natural pool
	Pool 2	660685	4198555	141	32.52	6.3	4544	5194	25.70	1.8	2952	2.39	79	
Tekke Hamam	**Pool 3**	660685	4198547	141	34.83	6.0	3834	4565	37.10	2.6	2499	2.00	12	
	Pool 4	660697	4198566	146	36.75	5.8	8225	10075	26.20	1.7	5346	4.49	48	
	Pool 6	660708	4198564	142	42.98	6.5	4935	6626	29.50	1.8	3207	2.57	-253	
	TH-8	660751	4198608	137	33.06	7.4	5778	6669	33.50	2.4	3758	3.09	-45	
	KD-13	661882	4202637	195	77.93	9.2	5988	11995	17.20	0.6	3887	3.01	-271	
	KD-14	662002	4202868	197	71.01	9.3	3336	6326	13.60	0.5	2168	1.62	-328	drilling well
Kızıldere	**KD-15**	662170	4203002	202	71.49	9.6	6217	11714	19.80	0.8	4054	3.16	-268	
	KD-16	662094	4202888	196	67.40	9.0	5268	9503	17.70	0.7	3412	2.64	-284	
	KD-20	661867	4202798	198	71.10	9.2	5950	11169	23.00	0.9	3862	3.01	-262	
	R-1	661036	4201912	148	53.62	9.4	3691	5677	23.00	1.3	2395	1.85	-304	

#Conductivity at 25 °C

accuracy for T is ±0.15°C, EC is ±0.001ms/cm, DO is ±2% or 0.2mg/l, Sal is ±1.0%, pH is ±0.2 units, ORP is ±20mV

91

Table 5.1d Physical parameters of cold water samples (21- 25 July 2009).

Sample No	UTM(E)	UTM(N)	Altitude (m)	T(°C)	pH	#EC (μsᶜ/cm)	EC (μs/cm)	DO (%)	DO (mg/l)	TDS (mg/l)	Sal	ORP	Sample Type
Asarlık	657234	4198642	205	27,76	7.4	1101	1154	32.80	2.6	711	0.54	75	
Kaplanpost	656599	4198473	217	27,29	6.8	1885	1969	22.50	1.8	1225	0.95	58	
Tekke	655218	4196955	397	15.08	6.9	1214	984	30.30	3.0	789	0.61	42	
Değirmendere	653967	4194072	682	16.84	7.0	795	671	25.80	2.5	517	0.39	48	cold spring
Acısu	666630	4197500	181	28.28	7.5	746	793	21.50	1.7	485	0.36	34	
Acıpınar	661264	4194200	430	18.50	6.4	2568	2257	17.70	1.6	1670	1.33	70	
Yukarı Tırkaz	655570	4194365	644	21.71	7.2	728	682	20.50	1.8	473	0.36	54	
Savcıllı	655154	4202244	157	27.29	7.5	990	1033	18.30	1.5	644	0.49	51	
Çatak	655527	4206493	798	28.67	6.8	239	256	16.60	1.3	155	0.11	57	
Yukarı Sazak	665298	4205746	616	21.00	6.7	4928	4554	20.10	1.8	3202	2.65	83	
Yukarı Sazak-DW	665692	4204483	473	33.42	7.2	5321	6176	18.30	1.3	3459	2.83	75	drilling well

#Conductivity at 25 °C

accuracy for T is ±0.15°C, EC is ±0.001ms/cm, DO is ±2% or 0.2mg/l, Sal is ±1.0%, pH is ±0.2 units, ORP is ±20mV

5.1.2.2 Gas Sampling in Kızıldere and Tekke Hamam Geothermal fields

5.1.2.2.1 Sampling from Gas Discharging Pools in Tekke Hamam

Gas sampling from the pools in Tekke Hamam (for noble gas analyses) was conducted during the first two sampling campaigns.

All gas samples were collected as the free gas phase from the pools in Tekke Hamam. For gas sampling from the pools (3, 4, 5, 6) (Figure 5.12), a plastic inverted funnel was dipped inside the pools to capture the bubbles coming out, similar as gas sampling for on-line analysis. Cu-tubes were connected to the inverted funnel via plastic tubings. A water trap was used as the last unit of the sampling to avoid air entrance into the gas line.

Pool 1 (Mud Pool), on the other hand, was sampled in a slightly different way (Figure 5.13). At this sampling point, the inverted funnel was first connected to the water trap with a plastic tube to trap the water from the water-gas mixture coming out from the pool. The remaining gas was let into the Cu-tube. The other end of the cu-tube was connected to a plastic tubing which was dipped inside the pool to avoid air contamination. By this way, only the gas coming from the pool was let inside the Cu-tube.

In Pool 2, which was also utilized in online gas monitoring, the gas sample was collected directly from the gas line exhaust of the station (Figure 5.14). The one end of the Cu-tube was connected to the exhaust, whereas the other end was connected to the water trap via plastic tubings, the same design as in pools 3, 4, 5 and 6.

In all sampling procedures, the Cu-tubes were first closed from the end close to the inverted funnel to avoid the accumulation of pressure inside the Cu-tube.
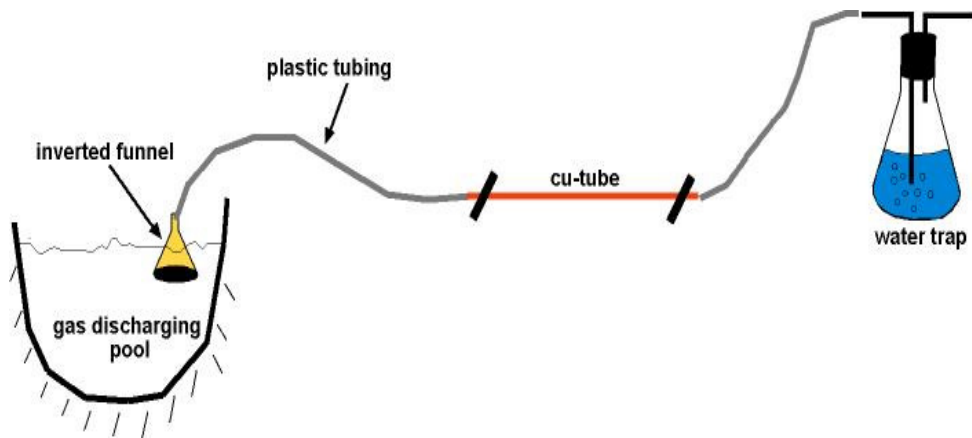
Figure 5.12 Sketch of gas sampling from pools (pool 3, 4, 5, 6) in the Tekke Hamam geothermal field.
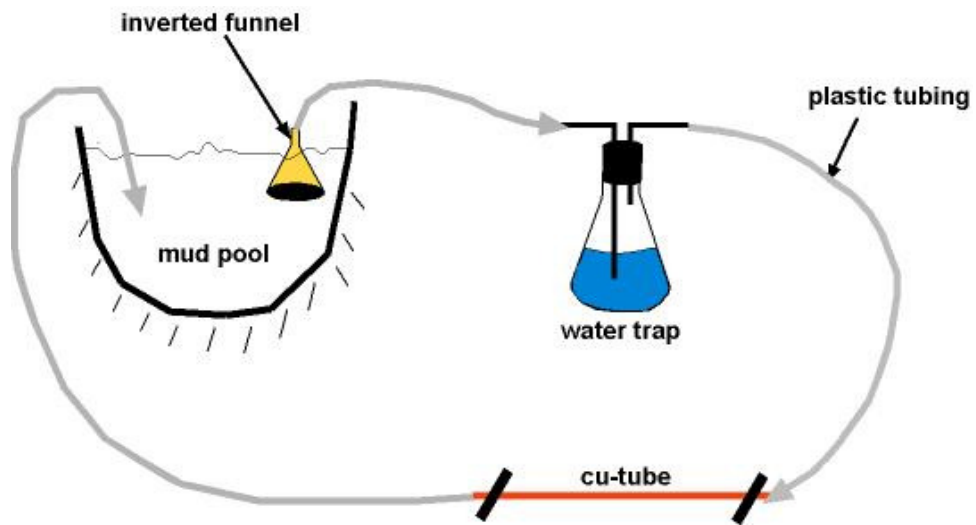
Figure 5.13 Sketch of gas sampling from pool 1 in the Tekke Hamam geothermal field.
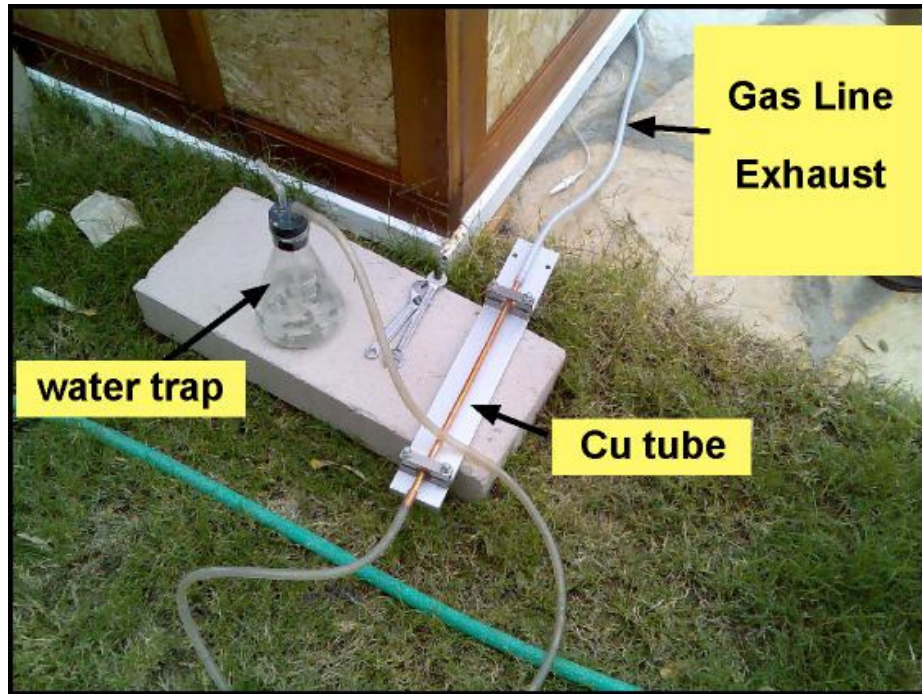
Figure 5.14 Sampling from the gas line exhaust of the station, representing pool 2.

5.1.2.2.2 Gas Sampling from Wells in Kızıldere Geothermal Field

Gas sampling from wells was conducted mainly during the first two sampling periods. Only one well (R-1) was sampled for gas during the third sampling campaign.

During sampling from the wells in Kızıldere, a steam separator (Figure 5.15) was used to get only the gas component found together with the steam phase. In this design, the steam separator was directly connected to the gas discharge of the well with tight silicon tubings. The steam entering the separator was cooled by continuously pouring cold water over the separator to enhance the separation of gas from the steam via steam condensation. After the condensation of the steam, the non-condensed gas phase accumulating over the condensed steam phase was captured into Cu-tubes via plastic tubings. A water trap was also used at the end of the sampling design to avoid air

contamination. During sampling, the Cu tubes were closed from the end near the separator to avoid overpressure. Figure 5.16 shows the photo of gas sampling from the Kızıldere wells.

Figure 5.15 Steam Separator used in the Kızıldere geothermal field.

Figure 5.16 Gas sampling from wells in Kızıldere via steam separation.

5.2 Analytical Techniques

The cation-trace element and anion contents of the samples were analysed in the ACME-Canada Laboratories for the first sampling campaign, and in the SRC-Canada

laboratories for the second and third sampling campaigns. The stable isotope compositions of the water samples were analysed in the Environmental Isotope Laboratories of the University of Waterloo for all the sampling periods. The noble gas analysis of the gas samples, on the other hand, were conducted in the GFZ-Potsdam noble gas laboratory.

The noble gas analysis of the samples were done via the MM5400 sector field mass spectrometer optimized for noble gas analyses. The MM 5400 noble gas mass spectrometer is fitted with (i) an ultrahigh vacuum furnace for heating and melting of rock samples (ii) a gas preparation line for removal of active gases (iii) a cryogenic adsorber for the separation of noble gases from each other and (iv) pipette systems for calibration using noble gas standards.

5.3 Data Evaluation

5.3.1 Online Monitoring Data Evaluation

As a first step before data evaluation, the seismic events and meteorological data were all compiled. The seismic data (magnitude ($M > 3.0$), focal depth, epicentral distance) were routinely compiled from the website records of the Kandilli Observatory and Earthquake Research Institute of Turkey. The meteorological data, comprising the daily air temperature (maximum, minimum, average, ºC), air pressure (mbar) and precipitation (mm) belonging to the Denizli Meteorology Station, were obtained from the Turkish State Meteorological Service.

The temporal variations recorded in gas compositions as well as the gas flow rate and temperature were evaluated on a monthly basis for each parameter. The raw data (comprising gas compositions (in ASCI format), gas flow rate and pool temperature) from the QMS and the data logger were all gathered in separate monthly files using the EXCEL software. In addition to these data, the compiled meteorological data and the seismic events relevant to the site were also incorporated into the monthly raw data files. The data files in EXCEL were then transformed into temporal variation diagrams for every single monitored parameter using the GRAPHER (graphical design) software.

Further statistical analyses (eg. running average) were performed on some of the data such as helium to eliminate insignificant variations complicating the temporal variation diagrams.

While dealing with the presentation of seismic events in the temporal variation diagrams, a new arbitrary parameter, **"Relative Seismicity",** was created and calculated for each seismic event simply by using the equation M/d^2, where M is the magnitude of the event and d the distance from the epicenter to the station (in km). For the sake of presentation, this arbitrary value was shown on a logarithmic scale in the temporal variation diagrams.

5.3.2 Evaluation of the Chemical and Isotopic Analyses

- The cation-trace element and anion analyses results on the water samples were used for the characterization of the hydrogeochemical facies of the Kızıldere and Tekke Hamam geothermal waters and the further evaluation of their possible physico-chemical evolution within the subsurface.

- The stable isotopic analyses of the samples were used for the evaluation of the possible origins (meteoric, magmatic, palaeo) of the waters and physico-chemical processes occurring at depth.

- The noble gas results of the gas samples were used for the noble gas characterization of the two fields and for the evaluation of the possible origins of the noble gases, especially He, and the further evaluation of the possible interactions prevailing between crust-mantle-atmospheric compartments; that is, the source provenance of the gases dissolved in the geothermal fluids.

CHAPTER 6

CHEMICAL AND STABLE ISOTOPIC COMPOSITIONS OF THE KIZILDERE AND TEKKE HAMAM WATERS

Three major sampling campaigns were conducted in the Kızıldere and the Tekke Hamam geothermal fields to search for possible temporal changes in water compositions. The first sampling campaign was conducted between 19 - 26 November 2007, the second sampling campaign was conducted between 28 August and 2 September 2008, and the third and final sampling campaign was conducted between 21 – 25 July 2009. During the sampling studies, drilling wells and springs/natural pools were sampled for chemical (cation-trace element and anion) and stable isotopic analysis ($\delta^{18}O$ and δ^2H). The chemical analyses of the samples from the first sampling campaign were conducted in the ACME Laboratories (CANADA), whereas the chemical analyses of the samples for the second and third sampling campaigns were conducted in the SRC Laboratories (CANADA). The stable isotope analyses of the samples, on the other hand, were conducted in the Environmental Isotope Laboratory of the University of Waterloo.

6.1 Chemical Compositions

The results of chemical analysis of the water samples (thermal/cold) collected during the sampling campaigns are given in Table 6.1 (a,b,c,d) together with their pH, temperature and TDS values measured in the field.

As can be seen from the tables, the temperatures of the bubbling pools in the Tekke Hamam geothermal field range between 30.8 – 43.0 °C, whereas the samples from drilling wells (Umut-1, TH-6, TH-7) have temperatures reaching a maximum of 85.0 °C. The temperatures of the Kızıldere well waters, on the other hand, range between 53.6 – 80.3 °C. The cold to slightly warm waters sampled from the vicinity of the geothermal fields have temperatures varying between 15.1 – 33.4 °C. The pH of the pool samples in

the Tekke Hamam geothermal field are slightly acidic to neutral in character with pH values ranging between 5.8 and 7.5, whereas the waters from the well discharge (Umut-1, TH-6, TH-7) are alkaline in character (8.5-8.9). The well waters sampled in the Kızıldere geothermal field have a dominant alkaline character, with pH values varying around 9.2. The cold to warm waters, on the other hand, have pH values varying around the neutral pH border (6.4-7.5). The TDS values (**T**otal **D**issolved **S**olid content) of the bubbling pools in Tekke Hamam range between 1856 – 7063 mg/l (the highest TDS observed in Pool 5) and are generally higher than those of the well samples from both the Kızıldere (1859 – 4406 mg/l) and the Tekke Hamam (2331 - 2677 mg/l) fields. The cold to warm waters, on the other hand, are characterized by lower TDS contents, ranging between 155 – 3459 mg/l (the highest TDS observed in Y.Sazak waters).

6.1.1 Hydrogeochemical Facies

Based on the major anion and cation contents of the samples collected from the Tekke Hamam and the Kızıldere geothermal fields during the second and third sampling campaigns, the hydrogeochemical facies of the samples are presented in Figures 6.1 (a,b) and Figures 6.2 (a,b) as Piper diagrams and Schoeller plots, respectively. The Piper and Schoeller diagrams for the cold/warm waters, on the other hand, are shown in Figures 6.3a and 6.3b, respectively.

6.1.1.1 Tekke Hamam Waters

As can be seen from the Piper and Schoeller diagrams, the bubbling pools in the Tekke Hamam geothermal field show Na-Ca-SO_4 character for Pools 2 and 3, Na-SO_4 type for Pools 1, 4, 5, TH-8, and Na-HCO_3-SO_4 type for Pool 6. The samples taken from the hot water well (Umut-1) and well discharge (TH-6) are characterized by a Na-HCO_3-SO_4 type. The cold water sample (TH-cold), representing the water sourced from the vicinity of the field and collected from the distribution pipe near the well Umut-1, is of Ca-Mg-SO_4 type. Therefore, as an overall inspection, there are mainly 4 types of waters identified for Tekke Hamam: Na-Ca-SO_4, Na-HCO_3-SO_4, Na-SO_4 and Ca-Mg-SO_4. The different types of waters observed in the same geothermal system of the Tekke Hamam geothermal field can point to the existence of possible mixing processes of deep-hot and

shallow-cold waters and the accompanied effects of deep origined gases (mainly CO_2 and H_2S). The possible mixing relations in the waters are also evident from distribution of the samples in the Piper diagrams, appearing as a linear trend.

In deep origined geothermal fluids, the SO_4 concentrations are generally low (<50 mg/kg), however, with the oxidation of H_2S, SO_4 concentration increases (Nicholson, 1993). The SO_4 dominancy in the Tekke Hamam waters may evolve as a result of the H_2S contents of the gases discharging from the field, as it is also evident from the sulfur smell. Steam condensation in the upper levels of the crust can lead to near surface oxidation of deep H_2S, producing sulfuric acid which further dissociates to form high sulfate contents. In general, steam heated waters have very low pH values (varying around 2-3), however, the higher pH values of the Tekke Hamam pools, close to neutral waters, possibly point to a substantial neutralization of acidity basically by mineral-fluid reactions. In addition to the high SO_4 contents, the acidic waters might have intensified the water-rock interaction whereby the dissolved cations and silica of the waters were leached from the surrounding rocks. Another contribution for the SO_4 dominancy in the pool waters of Tekke Hamam can be related to the interaction with gypsum levels in the Neogene sedimentary sequence, which are especially found in the upper geothermal reservoir (Sazak Formation). Therefore, the SO_4 dominancy in the Tekke Hamam waters is probably derived from the interaction with gypsum levels and the near surface H_2S oxidation (the latter possibly representing a minor component).

In addition to the dominant Na contents, the high Ca and Mg contents of the Tekke Hamam pool waters can possibly point to low temperature interaction of the deep rising fluids with shallow waters as Ca and Mg solubility is inversely proportional to temperature. The well samples from Tekke Hamam also have high Ca and Mg contents (when compared with those from Kızıldere). Therefore, the high Ca and Mg content in these sulfate waters can be attributed to near-surface low-temperature reactions leaching local rocks and/or dilution by surface waters rich in both Ca and Mg.

It is also worth to note that, although the pools in Tekke Hamam have low temperatures (mainly changing around 30.8 – 43.0 °C), they are characterized by very high Total Dissolved Solid (TDS) contents, reaching up to nearly 7063 mg/l (Pool 5). The high TDS

contents of the Tekke Hamam pool waters are possibly related to intense leaching of rocks due to the gases coming from depth (especially high CO_2 contents, together with H_2S). In addition, the continuous bubbling in the pools associated with the release of gases, as well as steam, can lead to the enrichment of the residual liquid phase.

The compositional variations in the Tekke Hamam waters appear to be significant especially for the pool samples. Since the natural pools in the field are shallow surface manifestations of the deep hot geothermal reservoir, they are under the effects of shallow surface processes, such as surface boiling and/or dilution with meteoric recharge.

6.1.1.2 Kızıldere Waters

The waters from wells in the Kızıldere geothermal field are all sodium bicarbonate type, relatively high in sulfate and low in Cl.

Bicarbonate-rich waters in nature generally originate through either dissolution of CO_2-bearing gases or condensation of geothermal steam in relatively deep, oxygen-free groundwaters (Ellis and Mahon, 1977). Because the absence of oxygen prevents oxidation of H_2S, the acidity of these aqueous solutions is due to dissociation of H_2CO_3. Although it is a weak acid, it converts feldspars to clays, generating neutral aqueous solutions, which are typically rich in sodium and bicarbonate, particularly at medium-high temperature. Therefore, the HCO_3 content of the Kızıldere waters can possibly evolve as a result of the dissolution of deep rising CO_2 within the reservoir rocks that are dominated by limestones/marble-quartzite-schist alternations.

The major hydrogeochemical processes in the geothermal fields controlling the cation dominance is the ion exchange reactions, which is also referred to as natural water softening and occurs between Na and Ca and/or Mg cations. Solution of calcareous materials in geothermal systems leads to an increase in Ca which is then exchanged for Na from clay minerals (a number of clayey levels are associated with the cap rocks of the Kızıldere geothermal system). Such a process yields a Na-HCO_3 type groundwater.

The high SO_4 content in the well samples from the Kızıldere geothermal field, on the other hand, can point to an interaction with gypsum levels in the Neogene sedimentary sequence, since at high temperatures, sulfate concentrations are limited by $CaSO_4$ solubility. The very low Ca and Mg contents of the Kızıldere waters, on the other hand, is probably in accordance with the deep high temperature conditions prevailing in the geothermal reservoirs. Since both Ca and Mg are higher in colder waters due to their increased solubility with decreasing temperature (retrograde solubility), they are highly insoluble in high temperature waters and prefer the mineral phases during water-rock interaction. The very low Ca-Mg contents observed in the Kızıldere waters can also be related to the scaling problems encountered in the wells during production. When the geothermal fluid flashes there is a loss of CO_2, which increases the pH of the fluid and leads to precipitation of Ca in the wells before the fluid reaches the surface.

Therefore, the thermomineral waters of the Kızıldere geothermal site possibly reflect the combination of high temperature water-rock interaction and ion exchange reactions in the presence of deep CO_2 rich gases.

There is no major compositional difference between the waters sampled from Kızıldere, however, well R-1 is characterized by a relatively higher TDS content (except for sampling campaign III) when compared with the other samples. The compositional difference in well R-1 can be possibly related to its higher bottom-hole temperature (242 ºC; highest reservoir temperature ever recorded in the Kızıldere geothermal field). Also, since R-1 is the only sample producing from the third and deepest reservoir in the field (the gneisses of the Menderes Massif metamorphics), different than the other wells which produce mainly from the second and main reservoir (marble-schist-quartzite alternation of the İğdecik formation), there may be slight differences in their chemical contents.

There appears to be no significant variation in the composition of the chemical constituents of the thermomineral waters in the Kızıldere geothermal field between the two sampling campaigns. This may reveal the fact that the Kızıldere geothermal field is characterized by a deep groundwater circulation not affected by shallow surface processes.

6.1.1.3 Cold/Warm Waters

The cold water samples collected from the vicinity of the geothermal fields have a broad distribution of water types. Mg and Ca are the dominant cations, whereas HCO_3 and SO_4 are the dominant anions. The samples Asarlık, Değirmendere, Acısu köyü and Y.Tırkaz are Mg-HCO_3, Kaplanpost and Y. Sazak are Ca-Mg-SO_4, Tekke and Y.Sazak-DW are Mg-SO_4, Acıpınar is Ca-SO_4, Savcıllı is Ca-Mg-HCO_3 and Çatak is Ca-HCO_3 in character (Figure 6.3).

The differences observed in the cold waters collected from the vicinity of the geothermal fields may possibly reflect different lithologic and mineralogic controls on water chemistry due to differing flow patterns and recharge sources. The cold waters having a HCO_3 character possibly evolve through shallow and short duration of fluid circulation, as also supported by their lower TDS contents. The high SO_4 contents of some of the waters (Yukarı Sazak waters, Acıpınar and Tekke) can possibly be due to the interaction of these waters with sulfate bearing lithology, since they are also accompanied by high Ca and/or Mg contents. The high Cl contents of the Y.Sazak waters, on the other hand, can possibly point to relatively deeper circulation of these fluids and their further mixing with deep rising thermal fluids, as also supported by their high TDS contents (comparable to those of thermal waters of the region).

Table 6.1a Results of chemical analyses for Sampling Campaign I (19-26 November 2007) (concentrations are in mg/l).

Sample Name	Sample Type	*T(ºC)	*pH	Na	K	Ca	Mg	€Alk	*TDS
Pool 2	natural pool	-	-	921	79	650	394	303	-
Pool 3		-	-	781	87	506	261	513	-
Pool 4		-	-	1077	116	500	194	517	-
Pool 5		-	-	1354	114	808	378	638	-
TH-8		53.8	7.0	1024	102	64	42	963	3410
TH-6	drilling well	51.5	8.7	764	89	75	7	750	2489
TH-7		57.4	8.5	793	91	76	5	858	2595
TH-cold	cold spring	15.5	7.8	336	16	523	529	318	3398
R-1	drilling well	-	9.1	1595	196	32	5	2233	4385
KD-6		-	9.3	1247	128	1	1	1863	1859
KD-13		-	9.3	1277	128	3	1	1860	3541
KD-14		-	9.3	1342	143	1	0	1717	3698
KD-15		-	9.0	1364	136	2	0	1623	3764
KD-16		-	9.2	1388	145	1	0	1783	3850
KD-21		-	9.2	1318	133	2	1	2033	2491
KD-22		-	9.2	1296	132	2	0	1967	3680

*T, pH and TDS represent field measurements
€Alkalinity of waters are the lab measurements
 dash symbol (-) represents the measurements which were not conducted during sampling

Table 6.1b Results of chemical analyses for Sampling Campaign II (28 Aug- 2 Sept 2008) (concentrations are in mg/l).

Sample Name	Sample Type	*T(ºC)	*pH	HCO$_3$	CO$_3$	Cl	SO$_4$	Na	K	Ca	Mg	*TDS
Pool 1	natural pool	43.00	6.6	1200	<1	167	1860	978	120	150	102	3480
Pool 2		32.32	6.5	891	<1	482	5000	1360	206	548	504	6528
Pool 3		34.15	6.3	648	<1	266	4500	1100	198	652	291	5228
Pool 4		38.65	6.1	179	<1	273	4700	1470	284	395	220	6008
Pool 5		33.71	6.4	959	<1	478	5600	1580	253	460	534	7063
Pool 6		-	-	1630	<1	97	1500	1230	161	29	19	-
TH-8		30.82	7.5	1650	<1	177	2200	1290	171	112	105	4242
Umut-1	drilling well	85.02	8.5	1110	11	101	1040	747	107	81	7.8	2677
TH-6		54.19	8.9	1120	<1	83	950	702	93	77	9.9	2331
TH-cold	cold spring	29.40	8.0	478	<1	209	2590	349	20	426	384	3068
R-1	drilling well	77.62	9.3	1850	739	143	1120	1740	311	1	0.1	4406
KD-6		73.74	9.3	1470	464	113	930	1340	192	0.8	0.2	3777
KD-13		72.35	9.3	1400	536	105	870	1310	194	1	0.6	3808
KD-14		78.40	9.3	1510	541	119	1020	1410	230	0.7	<0.1	4108
KD-15		79.60	9.1	1520	469	117	1130	1410	202	1.1	0.1	4021
KD-16		74.48	9.1	1620	476	116	1040	1380	222	1	0.3	4001
KD-21		76.51	9.1	1890	451	113	1000	1370	217	1	0.3	3954
KD-22		80.32	9.2	1150	359	81	580	895	124	0.6	0.3	3575

*T, pH and TDS represent field measurements
dash symbol (-) represents the measurements which were not conducted during sampling

Table 6.1c Results of chemical analyses for Sampling Campaign III (21-25 July 2009) (concentrations are in mg/l).

Sample Name	Sample Type	*T(ºC)	*pH	HCO$_3$	CO$_3$	Cl	SO$_4$	Na	K	Ca	Mg	*TDS
Pool 1	natural pool	40.70	6.5	1170	<1	193	1800	980	103	177	97	1856
Pool 2		32.52	6.3	804	<1	432	4700	1090	125	790	407	2952
Pool 3		34.83	6.0	478	<1	224	3700	860	129	570	248	2499
Pool 4		36.75	5.8	326	<1	268	4500	1140	191	590	254	5346
Pool 6		42.98	6.5	1720	<1	89	1200	1070	124	59	21	3207
TH-8	drilling well	33.06	7.4	1500	<1	155	1800	1160	120	130	51	3758
R-1		53.62	9.4	1640	815	155	860	1610	210	2	<1	2395
KD-13		77.93	9.2	1620	496	115	730	1300	140	1	<1	3887
KD-14		71.01	9.3	1590	586	128	810	1400	160	5	<1	2168
KD-15		71.49	9.6	1610	397	126	1000	1350	140	2	<1	4054
KD-16		67.40	9.0	1960	384	152	800	1370	150	9	<1	3412
KD-20		71.10	9.2	1570	499	132	890	1370	140	10	<1	3862

*T, pH and TDS represent field measurements

Table 6.1d Results of chemical analyses for Sampling Campaign III (21-25 July 2009) (cold waters-concentrations are in mg/l).

Sample Name	Sample Type	*T(ºC)	*pH	HCO$_3$	CO$_3$	Cl	SO$_4$	Na	K	Ca	Mg	*TDS
Asarlık	cold spring	27.76	7.4	418	<1	16	260	16	2.9	81	94	711
Kaplanpost		27.29	6.8	426	<1	27	680	20	4.4	209	123	1225
Tekke		15.08	6.9	451	<1	15	1170	15	2.8	91	93	789
Değirmendere		16.84	7.0	437	<1	8	74	6.1	1.5	63	51	517
Acısu köyü		28.28	7.5	451	<1	12	31	8.6	1.4	46	51	485
Acıpınar		18.50	6.4	156	<1	10	1590	7.1	4.5	638	37	1670
Yukarı Tırkaz		21.71	7.2	462	<1	7	31	4.9	1.6	54	50	473
Savcıllı		27.29	7.5	320	<1	31	170	33	15	77	44	644
Çatak		28.67	6.8	120	<1	10	9.8	10	2.9	31	3	155
Yukarı Sazak		21.00	6.7	337	<1	141	2700	155	121	560	372	3202
Yukarı Sazak-DW	well	33.42	7.2	372	<1	82	3600	230	27	510	640	3459

*T, pH and TDS represent field measurements
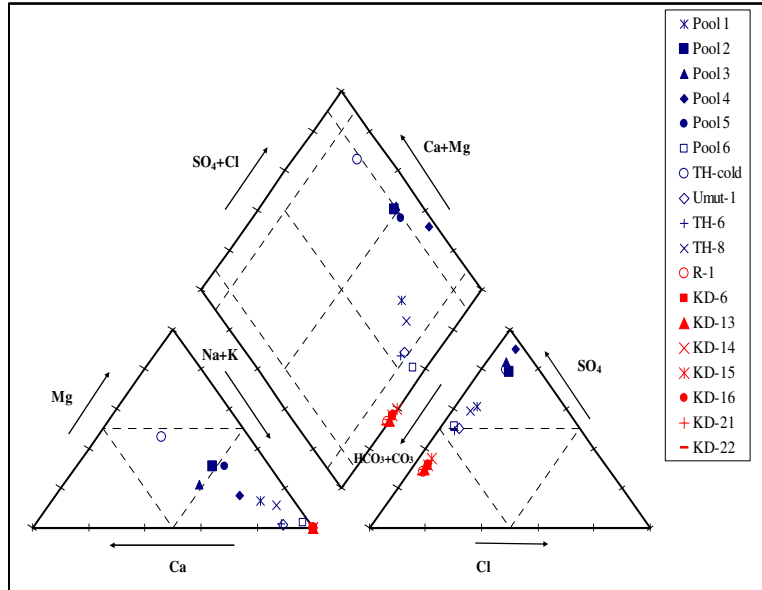
Figure 6.1a Piper diagram of the waters from Kızıldere and Tekke Hamam geothermal fields (Sampling Campaign II).
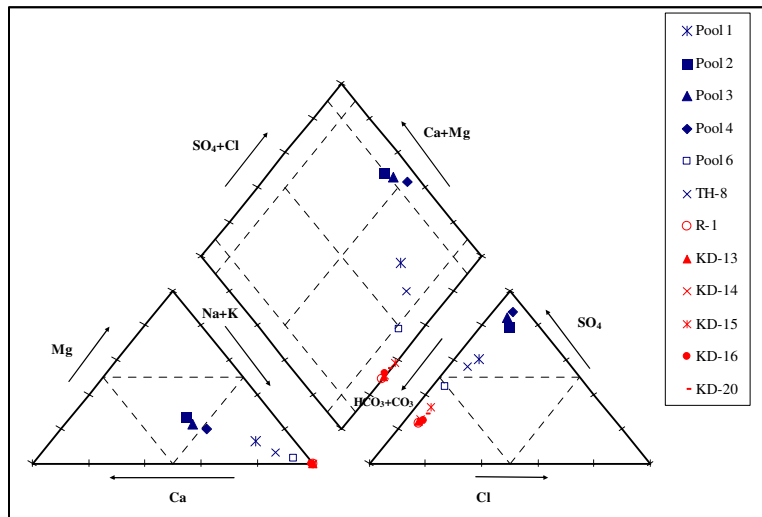
Figure 6.1b Piper diagram of the waters from Kızıldere and Tekke Hamam geothermal fields (Sampling Campaign III).
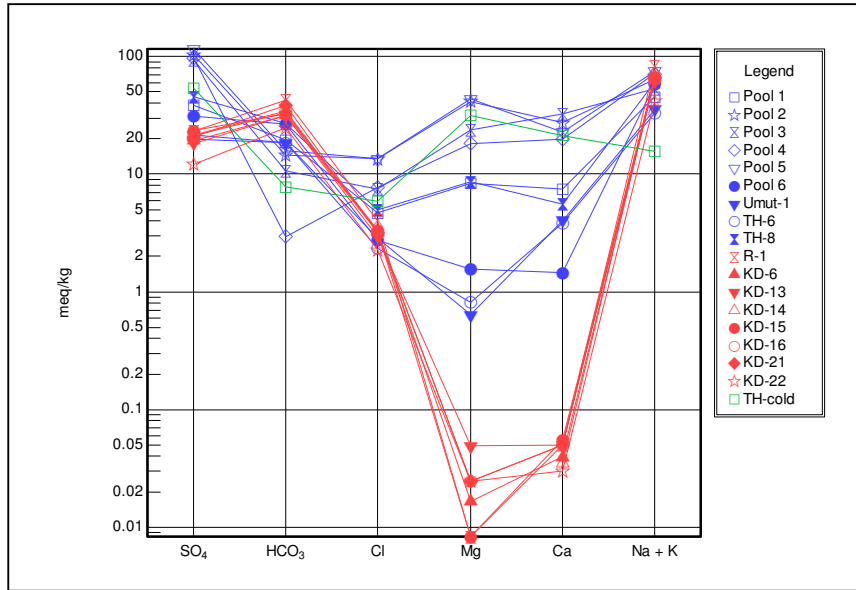
Figure 6.2a Schoeller plot for sampling campaign II.
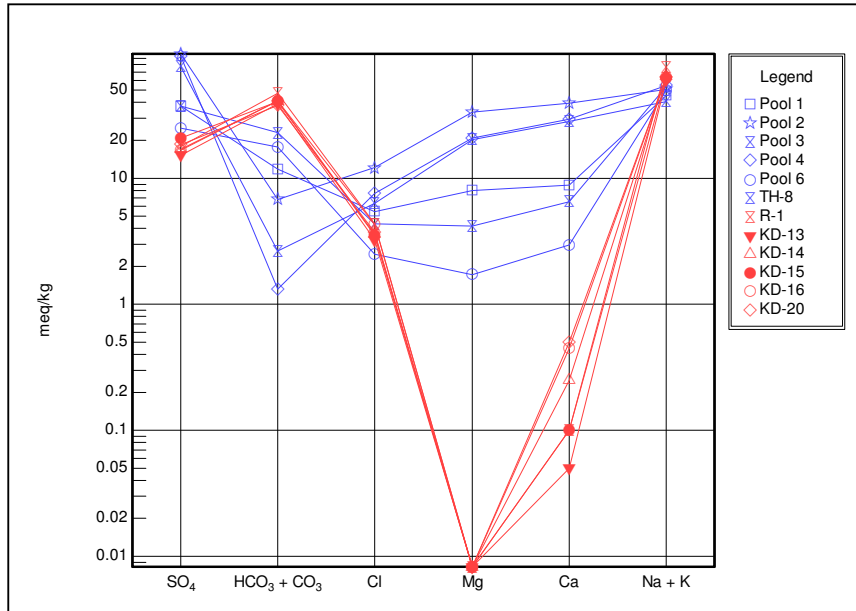
Figure 6.2b Schoeller plot for sampling campaign III.

111
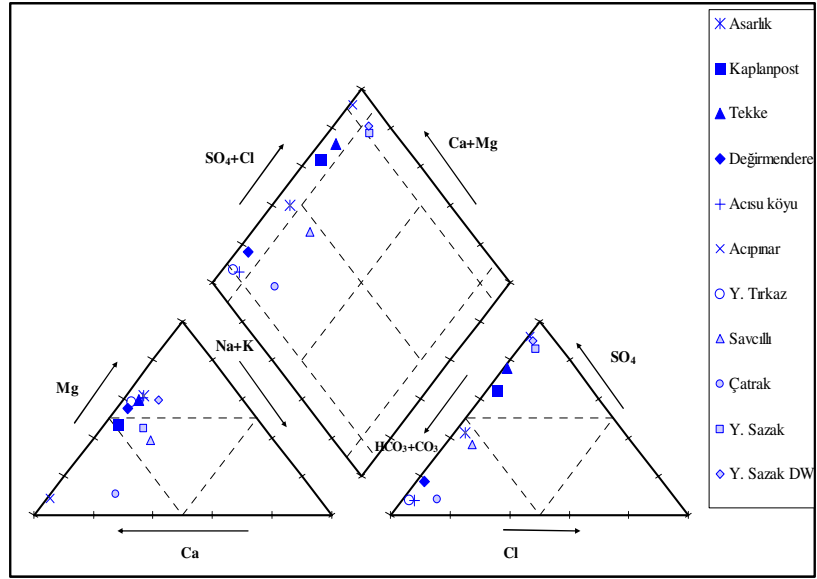
Figure 6.3a Piper diagram of the cold waters from the vicinity of the geothermal fields (Sampling Campaign III).
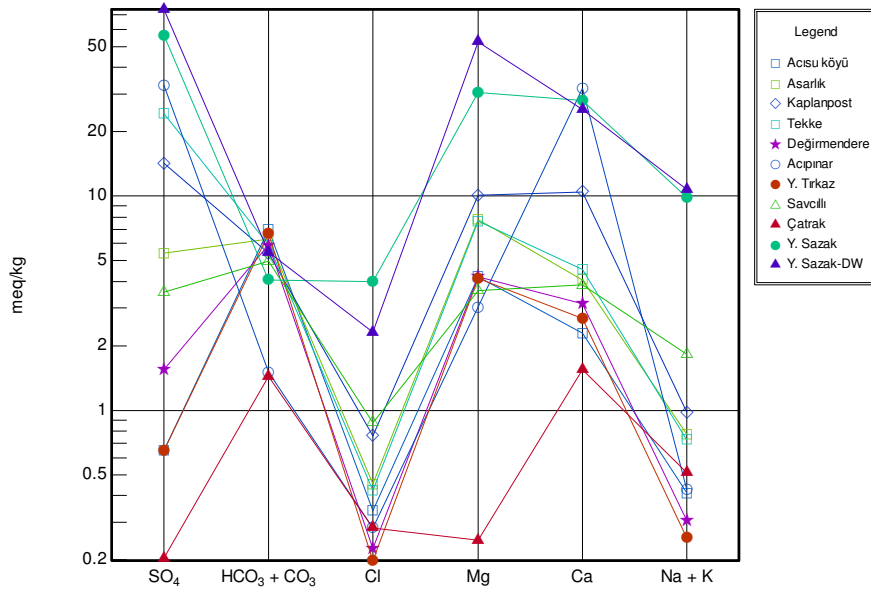
Figure 6.3b Schoeller plot for sampling campaign III-cold waters.

6.1.2 Trace Element Contents

The analysis of the trace element contents of the waters collected from the Tekke Hamam and Kızıldere geothermal fields revealed very low concentrations, some elements near or below their specific detection limits. The trace elements which were measured above the detection limits and which appear to be important in terms of possible environmental concerns (B, NO_3) and fluid-mineral equilibria are shown in Table 6.2 (a,b,c,d) separately for each sampling campaign.

As can be seen from the tables, the pool samples from Tekke Hamam are rich in terms of NO_3 and display a wide range (0.04-75 mg/l; low contents for the second and high contents for the third sampling campaigns), which possibly suggests their interaction with shallow surface processes, such as agricultural activity. The low NO_3 content of the well sample Umut-1 is also similar to the NO_3 contents of Kızıldere wells (0.09-0.31 mg/l) and can therefore point to the insignificant amounts of NO_3 in deep, hot waters. The wide variation in the NO_3 concentration of the pool waters in Tekke Hamam can possibly suggest a temporal variation in relation to shallow surface processes, which can be differently activated due to different recharge or man-influence conditions for the second and third sampling campaigns.

Within the trace elements, boron, is a natural source of environmental problems associated with geothermal waters; surface waters have been reported to be contaminated by the discharged geothermal fluids in many geothermal sites all around the world. High concentrations of boron exist in geothermal waters from areas with widely different tectonic, lithologic, and hydrologic regimes (Ellis and Mahon, 1977). Experimental studies and comparisons of water/rock ratios derived from B concentrations and heat flow rates reveal that B is readily leached from volcanic and sedimentary rocks with comparatively little partitioning of B into secondary minerals. Especially the high content of CO_2 and high temperature increases the solubility of boron bearing minerals. Both Tekke Hamam and Kızıldere waters have high boron contents which is a feature characteristic of geothermal waters in general. The boron contents of the Kızıldere and Tekke Hamam waters range between 20.1 and 34.9 mg/l, and 7.0 and 20.9 mg/l, respectively. The high boron contents mainly point to high temperature water-rock

interaction since the concentration of boron increases with increasing temperature. The slight differences observed in the boron contents of Tekke Hamam and Kızıldere samples can arise from slightly different water-rock interaction processes and/or different temperature conditions. According to the study done by Özgür (2001), the high boron contents in the thermal waters of Kızıldere geothermal field were mainly attributed to: (i) unstable boron-bearing mineral phases (e.g., feldspars, muscovites, tourmalines, hornblends, and biotites) in the metamorphic rocks, proven by experimental leaching tests of various rocks, (ii) a magmatic input, corroborated by isotope analyses of $\delta^{11}B$, $\delta^{13}C$, and $\delta^{34}S$ of thermal waters. However, the origin of the high boron contents in the Kızıldere thermal waters is still debatable (Özgür, 2001). As an environmental precaution for the minimization of the contamination induced by the high boron content, the thermal waters discharged from the Kızıldere geothermal field are being reinjected via the reinjection wells.

The high amounts of Sr (over 1 mg/l) in the Tekke Hamam waters probably originates from aragonite in Cretaceous carbonate rocks and/or interaction with shallow cold water since the solubility of Sr bearing minerals increases with decreasing temperature. The low contents of Sr in the Kızıldere waters (generally below 1 mg/l), on the other hand, can be possibly related to scaling observed in the wells, as it has been shown by previous studies (Şimşek et al., 2005) that the calcium carbonate scales also have an appreciable $SrCO_3$ component.

The Al contents of the Tekke Hamam waters appear to be slightly lower than those of Kızıldere. The Fe contents of the Tekke Hamam waters are higher than those of Kızıldere. Both fields are characterized by high Si contents, although in higher amounts for the Kızıldere waters which can possibly derive from their deeper and higher reservoir temperature conditions.

The trace element contents of the cold waters which appear to be significant and above the detection limits are given in Table 6.2d. The nitrate content of the cold waters change between 0.15 and 4.3 mg/l. The boron contents of the cold waters are low (in accordance with their lower temperatures) and range between 0.012-0.75 mg/l. The Si content of the cold waters range between 7.7-30.9 mg/l and are significantly lower than the hot waters.

The Sr contents of the cold waters (0.13-22.8 mg/l) are significantly higher than the Kızıldere well waters and higher/close to those of the Tekke Hamam waters. The Fe contents of the cold waters change between 0.012 – 0.063 mg/l and are similar to the hot waters.

Table 6.2a Trace element contents of the samples (Sampling Campaign I: 19-26 November 2007, mg/l).

Sample Name	Al	B	Fe	Si
Pool 2	0.25	12.0	1.592	91.1
Pool 3	0.31	7.0	0.617	88.0
Pool 4	2.49	16.2	5.607	41.9
Pool 5	0.10	17.9	3.86	74.7
TH-6	0.08	14.7	<0.1	99.5
TH-7	0.04	15.1	<0.1	92.8
TH-8	0.03	19.1	0.103	85.2
TH-cold	0.04	3.4	<0.1	35.3
R-1	2.54	34.8	2.769	311.2
KD-6	0.35	22.4	<0.1	138.5
KD-13	0.46	22.0	<0.1	147.8
KD-14	0.65	27.2	<0.1	203.7
KD-15	0.55	27.2	<0.1	177.5
KD-16	0.40	28.7	<0.1	194.6
KD-21	0.69	24.6	<0.1	174.0
KD-22	0.51	23.6	<0.1	171.3

Table 6.2b Trace element contents of the samples (Sampling Campaign II: 28 Aug-2 Sept 2008, mg/l).

Sample Name	Al	B	Fe	Si	Sr	NO₃
Pool 1	0.63	16.6	0.79	87.2	6.4	37
Pool 2	0.076	16.2	0.63	104	17.2	49
Pool 3	0.13	8.4	0.33	101	14	75
Pool 4	0.53	15.9	0.47	100	9.7	124
Pool 5	0.14	20.6	0.43	103	19.6	0.04
Pool 6	<0.005	18.7	0.005	91.5	1.62	44
TH-cold	<0.005	2.3	0.052	24.1	9.12	<0.04
Umut-1	0.039	13.5	0.033	85.6	4.19	0.18
TH-6	<0.005	11.6	0.026	74	3.78	4.2
TH-8	<0.005	20.9	0.099	75.2	5.1	23
R-1	0.62	22.3	0.001	142	0.15	0.11
KD-6	0.29	20.6	0.004	119	0.26	0.13
KD-13	0.37	20.1	0.054	128	0.21	0.09
KD-14	0.52	25.9	0.01	159	0.29	0.09
KD-15	0.47	24.3	0.043	145	0.36	0.31
KD-16	0.57	25.2	0.008	161	0.55	0.13
KD-21	0.52	23.8	0.004	154	0.33	0.22
KD-22	0.51	21.4	0.016	144	0.24	0.13

Table 6.2c Trace element contents of the samples (Sampling Campaign III: 21-25 July 2009, mg/l).

Sample Name	Al	B	Fe	Si	Sr	NO₃
Pool 1	<0.005	15.3	0.028	83.5	7.33	0.24
Pool 2	0.019	11.5	0.31	120	14.5	0.41
Pool 3	0.086	7.3	0.42	99.5	12.4	0.16
Pool 4	0.47	12.9	0.37	100	11.4	0.21
Pool 6a	<0.005	15.7	0.016	100	1.85	33
TH-8a	<0.005	19.6	0.085	81.4	5.65	9.7
R-1	1.5	32.2	0.032	260	0.23	0.09
KD-13	0.40	20.1	0.042	120	0.24	0.16
KD-14	0.57	26.4	0.075	160	1.41	0.09
KD-15	0.49	23.9	0.032	140	0.42	0.13
KD-16	0.56	25.8	0.072	160	1.92	0.1
KD-20	0.56	22.3	0.076	160	1.64	0.09

Table 6.2d Trace element contents of the cold/warm water samples (Sampling Campaign III: 21-25 July 2009, mg/l).

Sample Name	B	Fe	Si	Sr	NO₃
Asarlık	0.16	0.022	27	16.9	3.1
Kaplanpost	0.21	0.012	24.9	22.8	0.55
Tekke	0.14	0.031	26.9	16.8	2.7
Değirmendere	0.06	0.04	23.6	16	2.9
Acısu koyu	0.082	0.022	24.7	7.08	0.8
Acıpınar	0.073	0.048	30.9	11.1	0.84
Y. Tırkaz	0.055	0.063	25.1	6.86	0.68
Savcıllı	0.039	0.014	7.7	1.1	4.3
Çatak	0.012	0.052	16.9	0.13	0.15
Y. Sazak	0.45	0.024	19.6	12.1	1.4
Y. Sazak DW	0.75	0.013	27.9	9.88	0.36

6.2 Stable Isotope Compositions

The results of the stable isotopic compositions of the water samples collected from the Kızıldere and Tekke Hamam geothermal fields are given in Table 6.3 for the three sampling campaigns. The $\delta^{18}O$ and δD values of the waters from Kızıldere range between -6.25‰ and -4.23‰, and -54.55‰ and -51.01‰, respectively. The Tekke Hamam waters have values ranging from -8.60‰ to 0.89‰ for $\delta^{18}O$ and -65.12‰ to -8.97‰ for δD. The cold/warm waters, on the other hand, have $\delta^{18}O$ values changing between -8‰ and -5.8‰ and δD values changing between -47.35‰ and -39.88‰.

In Figure 6.4 (a,b,c), the isotope compositions of the waters are presented separately as $\delta^{18}O$ vs. δD diagram for the sampling campaigns. As can be seen from the figures, the $\delta^{18}O$ and δD compositions of the geothermal waters reveal an essentially meteoric origin for both Kızıldere and Tekke Hamam geothermal waters.

When examined for the Tekke Hamam waters, it is readily seen from Figure 6.4 that, for the first sampling period, the pool samples lie along and/or close to the Global Meteoric Water Line (GMWL). For the second and third sampling periods, the Tekke Hamam pool

waters significantly deviate from the GMWL and are aligned along an evaporation line. The different distribution of the pool waters for the sampling periods is possibly related to the different seasonal conditions prevailing during the sampling periods (first during the rainy season, and second and third sampling during the dry and hot season), and most probably reflects the effects of intense evaporation processes during the hot season. The well waters (Umut-1 and TH-6) appear to have more negative $\delta^{18}O$ and δD values and can therefore point to recharge from higher altitudes.

The Kızıldere well waters, on the other hand, generally lie to the right of the GMWL and reflect the effects of intense water-rock interaction processes under high temperature conditions. The Kızıldere waters show similar distributions for the three sampling periods and suggest that these waters are not affected by seasonal conditions. Within the Kızıldere samples, R-1 appears to have the most positive values, in conformity with its high temperature. KD-13 and KD-6 show lower ^{18}O concentrations, again in conformity with their lower bottom hole temperatures.

In Figure 6.4c, the distribution of the cold waters relative to the hot waters is seen. As can be seen from the figure, the cold waters collected from the region lie between the MMWL (Mediterranean Meteoric Water Line) and the GMWL. It is seen that the Kızıldere waters have more negative deuterium values than the cold waters collected from the vicinity of the region, suggesting recharge from higher altitudes for the hot water aquifers. The less negative $\delta^{18}O$ values (as opposed to the expected more negative values that should couple the negative δD values), however, probably stand from the intense water-rock interaction in deep reservoir conditions. The Tekke Hamam pool waters, on the other hand, seem to follow the same trend with the cold water samples, deviating from the trend as a result of intense evaporation during higher ambient temperatures.

The Tekke Hamam well samples have slightly lower $\delta^{18}O$ values than those of the Kızıldere waters, possibly reflecting less intense water-rock interaction. The similar deuterium values of both fields can point to similar recharge altitudes. In any case, the Kızıldere waters appear to be influenced by higher temperature water-rock interaction and longer fluid circulation, leading to more positive $\delta^{18}O$ compositions.

Table 6.3 The results of the isotopic analyses of water samples ($\delta^{18}O$ and δD values are given in ‰; the errors for $\delta^{18}O$ and D are 0.20 ‰ and 0.80 ‰, respectively).

	Sampling campaign I		Sampling campaign II		Sampling campaign III	
	19-26 November 2007		28 Aug - 2 Sept 2008		21-25 July 2009	
Sample Name	$\delta^{18}O$	$\delta^{2}H$	$\delta^{18}O$	$\delta^{2}H$	$\delta^{18}O$	$\delta^{2}H$
Pool 1	-	-	-5.49	-43.22	-5.33	-48.03
Pool 2	-3.80	-29.69	2.52	-9.18	-0.42	-20.43
Pool 3	-6.53	-38.80	-1.95	-22.76	-3.90	-30.88
Pool 4	-3.41	-25.81	0.89	-17.03	-0.67	-21.78
Pool 5	-4.53	-25.60	0.45	-8.97	-	-
Pool 6	-	-	-3.46	-41.34	-5.97	-50.78
Umut-1	-	-	-6.71	-55.75	-	-
TH 6	-6.76	-57.11	-6.49	-53.35	-	-
TH 7	-6.92	-57.15	-	-	-	-
TH 8	-4.57	-47.66	0.65	-23.68	-2.12	-34.72
TH -cold	-6.02	-43.26	-5.34	-40.56	-	-
R-1	-4.27	-53.48	-4.23	-51.06	-4.25	-52.10
KD 6	-5.88	-54.34	-5.62	-53.80	-	-
KD 13	-5.53	-53.98	-6.25	-53.25	-6.18	-54.70
KD 14	-4.75	-51.85	-5.30	-52.23	-5.10	-53.12
KD 15	-5.05	-53.70	-5.26	-52.87	-5.44	-53.45
KD 16	-4.41	-52.99	-5.18	-53.18	-5.19	-53.42
KD 21	-5.58	-54.55	-5.60	-53.81	-	-
KD 22	-5.18	-53.43	-5.09	-53.44	-	-
Asarlık	-	-	-	-	-7.53	-46.83
Kaplanpost	-	-	-	-	-7.33	-45.22
Tekke	-	-	-	-	-7.44	-45.04
Değirmendere	-	-	-	-	-7.82	-47.05
Acısu köyu	-	-	-	-	-7.89	-47.35
Acıpınar	-	-	-	-	-5.90	-39.88
Y. Tırkaz	-	-	-	-	-7.88	-46.92
Savcıllı	-	-	-	-	-7.27	-42.92
Çatak	-	-	-	-	-8.00	-45.51
Y. Sazak	-	-	-	-	-7.18	-46.57
Y. Sazak DW	-	-	-	-	-5.80	-41.39
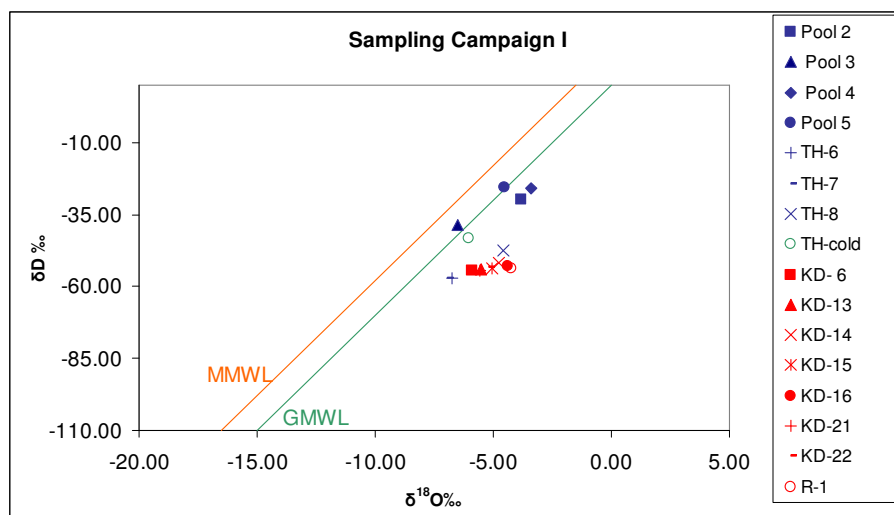
Figure 6.4a $\delta^{18}O$ vs. δD diagram for Kızıldere and Tekke Hamam samples (Sampling campaign I) (blue symbols represent Tekke Hamam, red symbols represent Kızıldere samples, GMWL: Global Meteoric Water Line Craig (1961); MMWL: Mediterranean Meteoric Water Line (Gat and Carmi, 1970)).
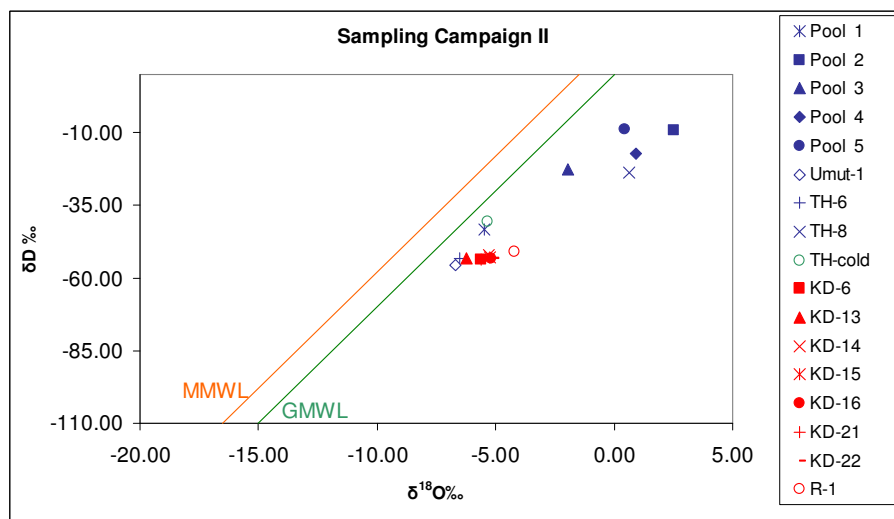
Figure 6.4b $\delta^{18}O$ vs. δD diagram for Kızıldere and Tekke Hamam samples (Sampling campaign II) (blue symbols represent Tekke Hamam, red symbols represent Kızıldere samples, GMWL: Global Meteoric Water Line Craig (1961); MMWL: Mediterranean Meteoric Water Line (Gat and Carmi, 1970)).
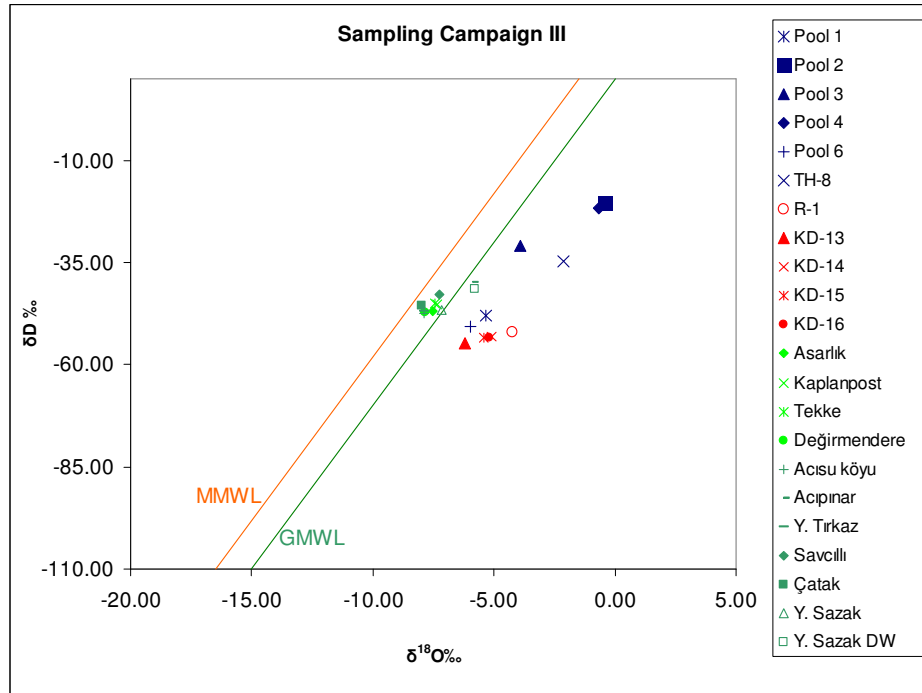
Figure 6.4c $\delta^{18}O$ vs. δD diagram for Kızıldere and Tekke Hamam samples (Sampling campaign III) (blue symbols represent Tekke Hamam, red symbols represent Kızıldere samples, green symbols represent cold waters; GMWL: Global Meteoric Water Line Craig (1961); MMWL: Mediterranean Meteoric Water Line (Gat and Carmi, 1970)).

6.3 Possible Subsurface Processes

Dissolved constituents may be subdivided into two major groups according to their behavior: Conservative (mobile) constituents are those conserved in water-rock systems and provide information about the origin of both geothermal fluid and the tracer itself (e.g. Cl, Br, B, Li, Rb and Cs). These tracers are effectively used in geothermal investigations since they highlight many processes, such as mixing and boiling, due to their ability to remain in the fluid phase without being changed once they are introduced into the system. Compatible constituents (e.g. Ca, Mg, Na, K, HCO_3, SO_4, F, SiO_2), on the other hand, are those whose activity is controlled by saturation with respect to a solid or a gas phase; they tend to equilibrate with other reactive constituents and/or minerals of

121

the rock in the geothermal system and may respond to thermochemical changes along the upflow path of the geothermal water.

Within the major ions, Cl, owing to its mobile behavior in most natural waters, is used in order to identify any possible interaction between deep-hot and shallow-cold waters. Since saturation with respect to halite, which determines a compatible behavior of chloride, is in fact attained only in very peculiar natural environments, chloride can be confidently used as the mobile species of reference to investigate the behavior of other dissolved constituents. Such an investigation is conveniently carried out by means of binary diagrams, where each chemical species of interest is plotted against chloride. These diagrams are particularly useful to detect mixing and boiling processes. In Figure 6.5, the binary diagrams for Cl vs B, Cl vs Si and Cl vs $\delta^{18}O$ of both fields are shown for sampling campaign III along with the cold waters. As can be seen from the diagrams, the Kızıldere samples plot along a well-defined linear trend with the cold waters (R^2: ~ 0.7 for all diagrams), suggesting the presence of a possible subsurface mixing in the field. The Tekke Hamam waters, on the other hand, display a scattered distribution in the diagrams, with a wide range of Cl concentration at somewhat constant B and Si contents and fluctuating $\delta^{18}O$ values, suggesting the effects of a boiling/evaporation process rather than mixing.

6.4 Fluid-Mineral Equilibria

In order to evaluate the fluid-mineral equilibria in waters, the saturation index with respect to minerals should be calculated. A saturation index of zero indicates that thermodynamic equilibrium exists with the solid phase. A negative or positive index indicates undersaturation and oversaturation, respectively.

Mineral saturation indices for the well samples from the Kızıldere geothermal field were calculated using the measured surface temperatures via the PHREEQC (Parkhurst ve Appelo, 1999) computer program (Table 6.4). As can be seen from the table, all of the Kızıldere well waters are undersaturated with respect to Alunite, anhydrite, gibbsite, gypsum and siderite. The waters are oversaturated with respect to geothite, hematite and

calcite. For aragonite and dolomite, on the other hand, the waters show both types of saturation, either oversaturated or undersaturated.
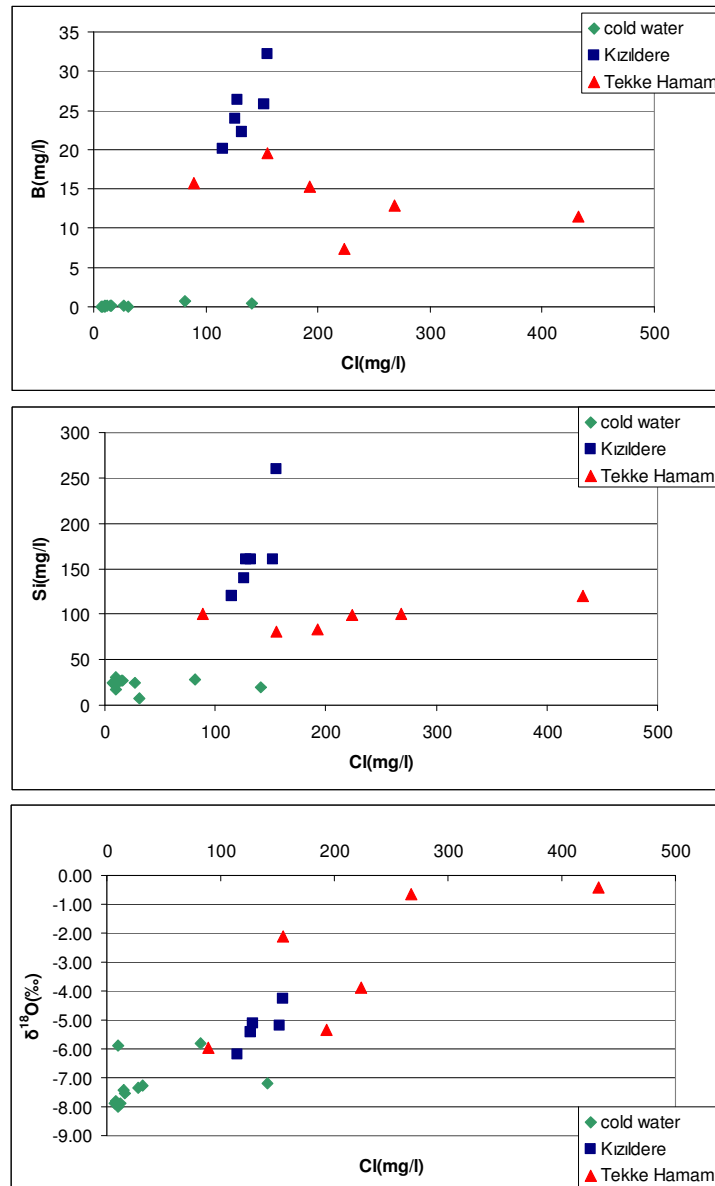
Figure 6.5 B vs Cl, Si vs Cl and δ^{18}O vs Cl binary diagrams for Kızıldere and Tekke Hamam geothermal fields (Sampling Campaign III; concentrations are in mg/l).

Table 6.4 Saturation indices for minerals (Kızıldere geothermal waters).

	Alunite	Anhydrite	Aragonite	Calcite	Dolomite	Gibbsite	Geothite	Gypsum	Siderite	Hematite
KD-6	-24.4	-3.21	0.03	0.15	-0.08	-3.04	2.97	-3.37	-15.28	8.14
KD-13	-22.95	-3.19	0.16	0.28	0.7	-2.72	4.31	-3.33	-13.31	10.82
KD-14	-23.01	-3.21	-0.01	0.1		-2.75	3.41	-3.42	-14.47	9.03
KD-15	-23.85	-2.93	0.15	0.26	-0.39	-2.93	3.91	-3.15	-14.39	10.04
KD-16	-23.9	-3.08	0.12	0.24	0.12	-2.84	3.18	-3.24	15.31	8.56
KD-21	-25.08	-3.06	0.12	0.23	-0.04	-3.07	2.69	-3.24	-16.29	7.59
KD-22	-23.7	-3.37	-0.06	0.05	0.01	-2.79	3.59	-3.6	-14.36	9.4
R-1	-22.31	-3.1	0.16	0.27	-0.14	-2.62	2.47	-3.3	-15.19	7.15

6.5 Concluding Remarks

The chemistry of the waters from the Kızıldere and Tekke Hamam geothermal fields are possibly controlled by temperature dependent water-rock interaction in addition to dissolution of deep gases, mainly CO_2 and H_2S (deep and shallow surface interaction of gases with the surrounding lithology). The wells in both fields are dominated by a Na-HCO_3 type, although not so dominant in the well samples from the Tekke Hamam geothermal field. The HCO_3 nature in all well samples is probably imposed by the marble-limestone lithology and the accompanying reaction with gases such as CO_2 and H_2S. Regarding the chemistry of the pool waters in the Tekke Hamam geothermal field, the SO_4 dominated nature appears to be derived mainly from the interaction with the gypsum levels and a minor component from the near surface H_2S oxidation.

It is apparent from both the chemical and isotopic analysis that the Kızıldere waters do not display significant compositional differences within time, however, the pool waters, possibly owing to their shallow nature, show significant variations within time, possibly reflecting the effects of seasonal changes.

CHAPTER 7

NOBLE GAS CHARACTERIZATION
OF THE
KIZILDERE AND TEKKE HAMAM GEOTHERMAL FIELDS

7.1 Results of Analyses

The abundances of the five stable noble gas nuclides: ^{4}He, ^{20}Ne, ^{40}Ar, ^{84}Kr and ^{132}Xe are presented as mbar in Table 7.1 and as ppmv in Table 7.2, together with their associated analytical 2σ errors. The isotopic ratios of the gas samples, along with the air-corrected ^{3}He/^{4}He ratios, are shown in Table 7.3.

As can be seen from the Tables 7.1 and 7.2, the abundance of ^{4}He ranges from 0.001576 ± 0.000079 to 0.00330 ± 0.00017 mbar (2.5 to 3.2 ppmv), ^{20}Ne ranges from 0.0403 ± 0.0020 to 0.1636 ± 0.0080 * 10^{-3} mbar (64 to 162*10^{-3} ppmv), ^{40}Ar ranges from 0.0627 ± 0.0036 to 0.204 ± 0.014 mbar (99 to 201 ppmv), ^{84}Kr ranges from 1.67 ±0.17 to 10.26 ± 0.75 * 10^{-6} mbar (16 to 244 *10^{-4} ppmv), and ^{132}Xe ranges from 0.063 ± 0.018 to 1.12 ± 0.29 *10^{-6} mbar (9 to 161 *10^{-5} ppmv) for the Tekke Hamam gas samples. For the Kızıldere samples, ^{4}He ranges from 0.000479 ± 0.000024 to 0.00407 ± 0.00020 mbar (0.69 to 4.0 ppmv), ^{20}Ne ranges from 0.01043 ± 0.00053 to 0.609 ± 0.030 *10^{-3} mbar (10 to 605 *10^{-3} ppmv), ^{40}Ar ranges from 0.01640 ± 0.00094 to 0.3854 ± 0.0266 mbar (16 to 385 ppmv), ^{84}Kr ranges from 0.372 ± 0.019 to 3.22 ± 0.32 * 10^{-6} mbar (4 to 37 * 10^{-4} ppmv) and ^{132}Xe ranges from 0.0288 ± 0.0015 to 0.1675 ± 0.0325 *10^{-6} mbar (3 to 21 *10^{-5} ppmv). The errors associated with the ppmv abundances are in the range of ±20% due to uncertainties in the inlet pressure determination when admit the gas to the mass spectrometer.

The measured ^{3}He/^{4}He ratio varies between 2.46 Ra and 2.86 Ra (where Ra stands for the atmospheric ^{3}He/^{4}He ratio of 1.40 * 10^{-6}), ^{20}Ne/^{22}Ne varies between 9.845 and 9.919,

$^{21}Ne/^{22}Ne$ varies between 0.02859 and 0.02908, $^{40}Ar/^{36}Ar$ varies between 293.0 and 304.2, and $^{38}Ar/^{36}Ar$ varies between 0.1858 and 0.1885 for the Tekke Hamam gas samples (Table 7.3). For the gas samples taken from the Kızıldere geothermal field, on the other hand, the $^{3}He/^{4}He$ ratio varies between 0.96 Ra and 1.92 Ra, $^{20}Ne/^{22}Ne$ varies between 9.810 and 9.879, $^{21}Ne/^{22}Ne$ varies between 0.02843 and 0.02961, $^{40}Ar/^{36}Ar$ varies between 289.0 and 310.1, and $^{38}Ar/^{36}Ar$ varies between 0.1867 and 0.1883.

The distribution of the measured isotopic ratios relative to their air-crust-mantle equivalents are shown separately in Figure 7.1(a,b,c,d,e).

All samples, except well R1 from the Kızıldere geothermal field, have R/Ra ratios higher than the atmospheric value (R/Ra = 1; $^{3}He/^{4}He$ = 1.40 * 10^{-6}; Lupton, 1983) and the radiogenic helium production in crustal rocks (R/Ra = 0.02; $^{3}He/^{4}He$ = 2 * 10^{-8}; Mamyrin and Tolstikhin, 1984) (Figure 7.1a). The high $^{3}He/^{4}He$ ratios of the samples from the geothermal fields suggest the existence of mantle volatile degassing. Therefore, the gases discharging from both fields possibly represent an admixture of crustal and mantle-derived helium.

The argon ($^{40}Ar/^{36}Ar$, $^{38}Ar/^{36}Ar$) and neon isotopic ratios ($^{21}Ne/^{22}Ne$ and $^{20}Ne/^{22}Ne$) of the samples are generally, within the analytical error, indistinguisable from the atmospheric ratios ($^{40}Ar/^{36}Ar$ = 295.5 (Ozima and Podosek, 2002); $^{38}Ar/^{36}Ar$ = 0.188 (Ozima and Podosek, 2002); $^{21}/^{22}Ne$ = 0.029, $^{20}Ne/^{22}Ne$ = 9.80 (Ballentine et al., 2002; Ballentine et al., 2005))(Figure 7.1b,c,d,e).

As an inspection for the air contamination in the gas samples, the $^{4}He/^{20}Ne$ ratio of the samples were calculated and are shown in Figure 7.2. As can be seen from the figure, the Tekke Hamam samples have a $^{4}He/^{20}Ne$ ratio varying between 12.68 (Pool 4) and 39.11 (Pool 1), whereas the Kızıldere samples have a much more distributed ratio, with values ranging from 2.07 (KD-21) to 198.63 (R-1). The $^{4}He/^{20}Ne$ ratio of all the samples is significantly higher than that of air (0.319; Ozima and Podosek, 2002), suggesting the existence of non-atmospheric derived components in both of the geothermal fields, and little but varying contamination with air or air saturated water.

Table 7.1 Noble gas abundances in mbar and their associated errors.

Sample No	Sampling Campaign	⁴He (mbar)	+/-	²⁰Ne (10⁻³mbar)	+/-	⁴⁰Ar (mbar)	+/-	⁸⁴Kr (10⁻⁶ mbar)	+/-	¹³²Xe (10⁻⁶ mbar)	+/-
Pool 1	I	0.001576	0.000079	0.0403	0.0020	0.0627	0.0036	8.09	0.50	0.59	0.15
Pool 2	I and II	0.00300	0.00015	0.1636	0.0082	0.180	0.009	10.3	0.8	0.617	0.147
Pool 3	I	0.00330	0.00017	0.1246	0.0071	0.204	0.014	1.67	0.17	0.112	0.011
Pool 4	I	0.001817	0.000091	0.0947	0.0095	0.1267	0.0063	1.76	0.18	0.063	0.018
Pool 5	I	0.00204	0.00010	0.0952	0.0048	0.1385	0.0076	17.0	1.0	1.12	0.29
R-1	III	0.00407	0.00020	0.02049	0.00100	0.0308	0.0015	0.372	0.019	0.0288	0.0015
KD-6	I and II	0.0017435	0.000087	0.6087	0.0304	0.385	0.027	3.14	0.28	0.168	0.033
KD-13	I	0.001466	0.000073	0.371	0.019	0.221	0.011	1.41	0.15	0.0668	0.0071
KD-14	I	0.000492	0.000025	0.0815	0.0041	0.0678	0.0034	0.601	0.062	0.0428	0.0043
KD-15	I	0.00206	0.00010	0.01043	0.00053	0.01640	0.00094	2.14	0.14	0.147	0.039
KD-16	I	0.000479	0.000024	0.0224	0.0011	0.0387	0.0019	0.440	0.044	0.0346	0.0035
KD-21	II	0.000927	0.000046	0.4485	0.0224	0.257	0.013	3.22	0.32	0.0689	0.0073
KD-22	II	0.001129	0.000056	0.1516	0.0076	0.0941	0.0047	0.639	0.071	0.0341	0.0037

Table 7.2 Noble gas abundances in ppmv (error for ppmv is 20%).

	Sample No	Sampling Campaign	^{4}He	^{20}Ne	^{40}Ar	^{84}Kr	^{132}Xe
			ppmv	10^{-3} ppmv	ppmv	10^{-4} ppmv	10^{-5} ppmv
Tekke Hamam	Pool 1	I	2.5	64	99	128	93
	Pool 2	I and II	3.0	162	177	101	61
	Pool 3	I	3.3	123	201	16	11
	Pool 4	I	2.6	136	182	25	9
	Pool 5	I	2.9	137	199	244	161
Kızıldere	R-1	III	4.0	20	30	4	3
	KD-6	I and II	2.0	605	385	37	21
	KD-13	I	1.4	366	218	14	7
	KD-14	I	0.7	117	97	9	6
	KD-15	I	2.0	10	16	21	15
	KD-16	I	0.7	32	56	6	5
	KD-21	II	0.9	443	254	32	7
	KD-22	II	1.1	150	93	6	3

Table 7.3 Noble gas isotopic ratios of the samples, along with the air corrected R/Ra ratios.

Sample No	Sampling Campaign	[R/Ra] Measured	+/-	*[R/Ra] cor	$^{20}Ne/^{22}Ne$	+/-	$^{21}Ne/^{22}Ne$	+/-	$^{40}Ar/^{36}Ar$	+/-	$^{38}Ar/^{36}Ar$	+/-	$^{4}He/^{20}Ne$
Pool 1	I	2.79	0.08	2.80	9.850	0.020	0.02908	0.00030	304.2	2.1	0.1885	0.0028	39.11
Pool 2	I and II	2.46	0.05	2.49	9.845	0.037	0.02877	0.00039	295.9	2.5	0.1872	0.0021	19.76
Pool 3	I	2.74	0.04	2.76	9.919	0.044	0.02859	0.00038	298.1	2.1	0.1884	0.0019	26.48
Pool 4	I	2.86	0.06	2.89	9.874	0.049	0.02861	0.00086	293.0	2.4	0.1858	0.0009	19.19
Pool 5	I	2.78	0.08	2.80	9.883	0.041	0.02901	0.00042	301.6	3.4	0.1873	0.0018	21.43
R-1	III	0.96	0.01	0.95	9.866	0.041	0.02895	0.00050	297.7	1.4	0.1875	0.0012	198.63
KD-6	I and II	1.92	0.06	1.93	9.879	0.198	0.02878	0.00054	298.7	3.2	0.1879	0.0024	37.23
KD-13	I	1.71	0.04	1.75	9.859	0.039	0.02856	0.00028	292.4	1.7	0.1880	0.0016	3.95
KD-14	I	1.31	0.07	1.33	9.851	0.045	0.02864	0.00025	294.4	1.6	0.1883	0.0016	6.04
KD-15	I	1.18	0.04	1.18	9.810	0.023	0.02905	0.00042	310.1	5.4	0.1873	0.0031	197.51
KD-16	I	1.14	0.05	1.14	9.869	0.062	0.02961	0.00047	289.0	1.6	0.1867	0.0025	21.38
KD-21	II	1.49	0.12	1.56	9.841	0.039	0.02843	0.00028	291.7	1.4	0.1880	0.0016	2.07
KD-22	II	1.48	0.07	1.49	9.857	0.080	0.02908	0.00028	292.5	1.6	0.1880	0.0016	7.45

*(R/Ra)$_{cor}$ stands for the air-corrected R/Ra value.
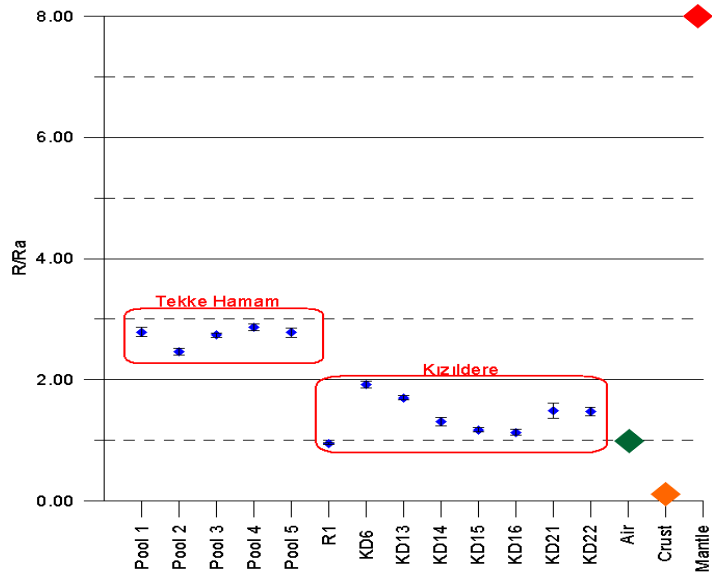
Figure 7.1a Distribution of R/Ra values of the samples relative to air-crust-mantle (air R/Ra = 1.0, Lupton, 1983; crust R/Ra = 0.02, Mamyrin and Tolstikhin, 1984; mantle R/Ra =8.0, Ozima and Podosek, 2002, error bars are within the symbol limits).
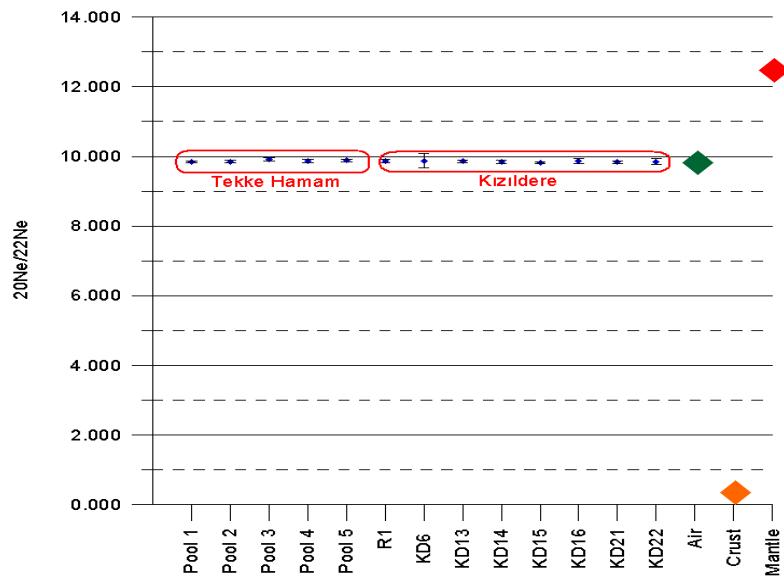
Figure 7.1b Distribution of $^{20}Ne/^{22}Ne$ ratio of the samples relative to air-crust-mantle (air $^{20}Ne/^{22}Ne$ = 9.8; mantle $^{20}Ne/^{22}Ne$ = 12.5, crust $^{20}Ne/^{22}Ne$ = 0.30; Ballentine et al., 2002; Ballentine et al., 2005, error bars are within the symbol limits).
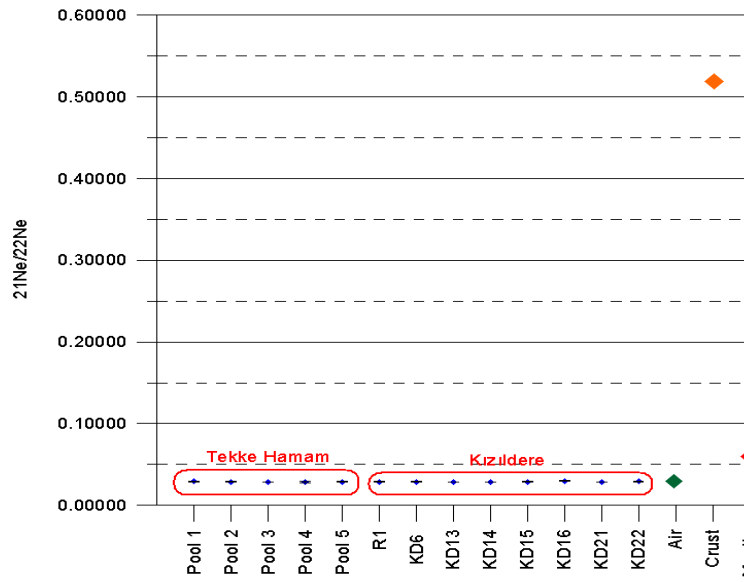
Figure 7.1c Distribution of ^{21}Ne/^{22}Ne ratio of the samples relative to air-crust-mantle (air $^{21}/^{22}$Ne = 0.029, mantle ^{21}Ne/^{22}Ne = 0.06, crust ^{21}Ne/^{22}Ne = 0.52; Ballentine et al., 2002; Ballentine et al., 2005), error bars are within the symbol limits).
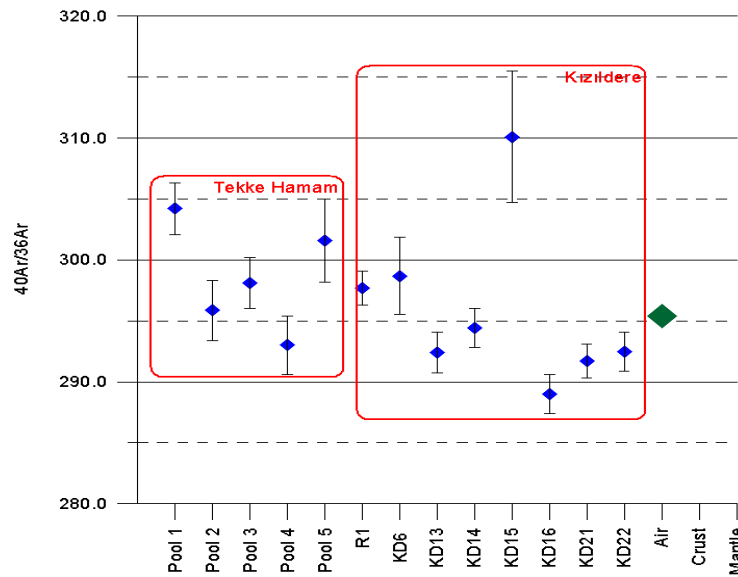
Figure 7.1d Distribution of ^{40}Ar/^{36}Ar ratios of the samples relative to air-crust-mantle (air ^{40}Ar/^{36}Ar =295.5, mantle and crust ^{40}Ar/^{36}Ar = 40000 (Ozima and Podosek, 2002)).
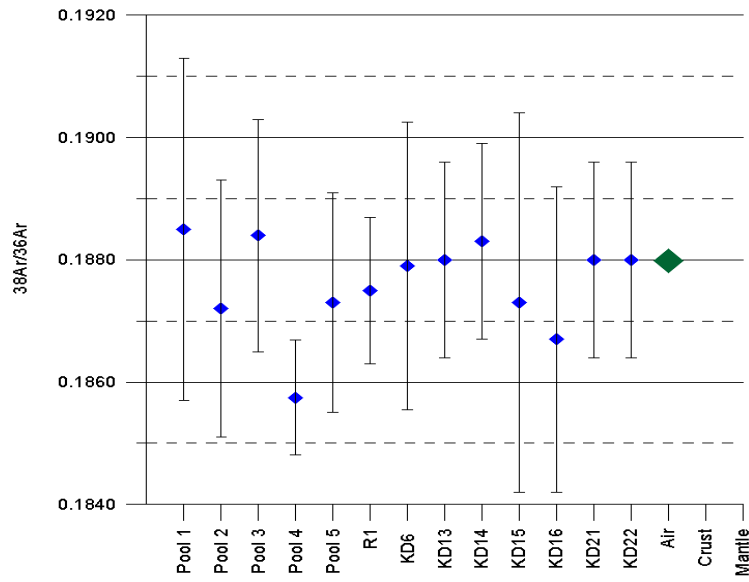
Figure 7.1e Distribution of $^{38}Ar/^{36}Ar$ ratios of the samples relative to air-crust-mantle (air $^{38}Ar/^{36}Ar = 0.188$, mantle and crustal $^{38}Ar/^{36}Ar = 40000$ (Ozima and Podosek, 2002)).
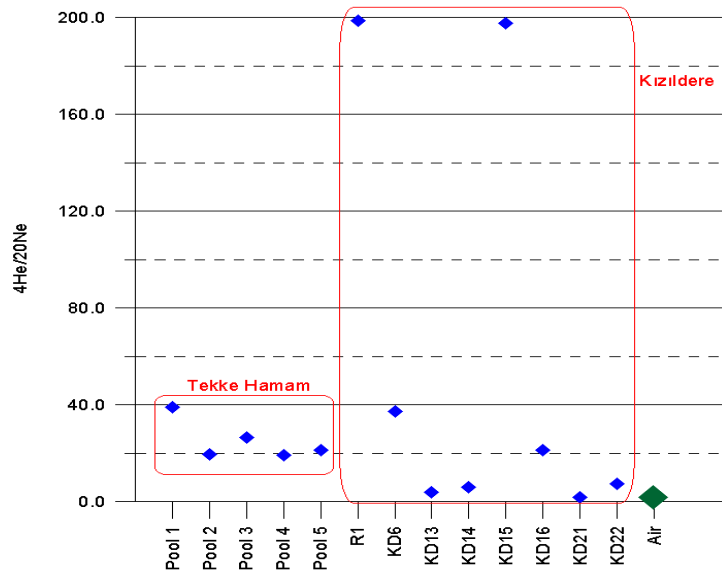
Figure 7.2 Distribution of $^{4}He/^{20}Ne$ ratios of the samples relative to air (air $^{4}He/^{20}Ne = 0.319$; Ozima and Podosek, 2002).

7.2 Isotopic/Nuclide Fractionation Possibilities

Although the Ne and Ar isotope ratios show values similar to that of air, there are still some samples which slightly differ from the air value. The differences, although within the error bars equivalent to air, can possibly arise from fractionation events affecting deep rising gases. Isotopic fractionation in gas samples from geothermal wells is generally shown by enrichment (compared to air) of lighter noble gas isotopes relative to heavier ones.

The mechanism for isotopic fractionation is still under debate. The effects of isotopic fractionation generally decrease with increasing atomic mass, that is, it is more severely observed for the isotopes of Helium and less severely observed for the isotopes of Xenon. Generally, there is a little mass dependence in solubility that plays a role in the isotope ratios (e.g. the solubility for ^{3}He and ^{4}He is slightly different), but this discrepancy is very little, even for helium with the greatest possible mass difference between two isotopes among the noble gases (25%). However, the progressive solubility increase He<Ne<Ar<Kr<Xe is larger to be explained by increasing masses and mass depending solubility only.

Fractionation can occur due to different sampling procedures or different physical processes affecting gases while rising to the surface. For example, the gas samples taken from the Tekke Hamam geothermal site represent the bubbling free gases directly discharging from the pool, not the samples taken from deep wells like those in Kızıldere, and they may not be severely affected by possible fractionation events encountered during sampling, however, they may show the effects of isotopic fractionation during their rise to the surface. In Kızıldere, on the other hand, the use of a steam separator during sampling may have triggered isotopic fractionation. In any case, the air-like isotopic ratios for both Neon and Argon can reflect the existence of atmospheric contamination during sampling, which is likely to be observed mostly in argon, being the most abundant noble gas in air and hence the most affected, or can suggest contamination by atmospheric Ar and Ne which dissolved in groundwater during air/water equilibration.

Within the isotopic ratios, the most significant deviation from the air value is displayed by the $^{40}Ar/^{36}Ar$ isotopic ratio of the gas samples, that is, most of the samples appear to align outside the value of air. The lower $^{40}Ar/^{36}Ar$ ratios, compared to that of air, can call for the existence of an isotopic fractionation event leading to the enrichment of the lighter Ar isotope, that is, ^{36}Ar, with respect to the heavier Ar isotope, ^{40}Ar. This is more prominently observed in the gas samples taken from the Kızıldere site, however, there are samples in Kızıldere which also show higher values, although dominantly lower. In the Tekke Hamam geothermal site, dominantly higher values on the average are seen and can point to either (i) a lower amount of atmospheric contamination for the Tekke Hamam samples or (ii) a higher amount of radiogenic Ar input. Keeping in mind that the Tekke Hamam samples also show relatively higher helium abundances, the second alternative seems to be more likely, however, still the low values close to that of air does not rule out the possibility of atmospheric contamination in the samples, attained either during sampling or during air dissolution.

In a three isotope plot of $^{20}Ne/^{22}Ne$ vs. $^{21}Ne/^{22}Ne$ shown in Figure 7.3, it is seen that samples generally plot to the left of the air value in the diagram. Most of the samples seem to have higher $^{20}Ne/^{22}Ne$ and generally lower $^{21}Ne/^{22}Ne$ when compared with those of air.

The distribution of the neon isotopic ratios in the three isotope plot can be related to two possible alternatives, as follows:

i. an isotopic fractionation process, enriching the lighter isotope of Ne, ^{20}Ne, relative to ^{22}Ne and ^{21}Ne in the gas phase. Since nucleogenic neon, mainly ^{21}Ne, is produced in fairly constant proportions to radiogenic helium, crustal neon would shift the points to the right. However, the opposite is observed for most of the samples. Therefore, the alignment of the samples can indicate that they originally had an atmospheric isotopic composition and later were possibly affected by a mass-dependent fractionation process enriching them in the light isotopes of neon. Mass-dependent fractionation is a process which is related to molecular diffusion and generates higher $^{20}Ne/^{22}Ne$ ratios in an escaped phase from a reservoir and complementary lower $^{20}Ne/^{22}Ne$

ratios in the residual phase, thus, light elements are more likely to exhibit isotopic fractionation than heavy isotopes. If mass-dependent fractionation had occurred at the time of the degassing of fluids from depth, this process would have led to higher ratios in $^{20}Ne/^{22}Ne$ in the gas discharging, as opposed to lower $^{20}Ne/^{22}Ne$ ratios in the fluid. Therefore the increase in the light isotope ^{20}Ne and the decrease in ^{21}Ne can call for the existence of isotopic fractionation. Isotopic fractionation can occur either during the migration of gases underground or during sampling, possibly occurring due to different sampling procedures.

ii.   Another alternative for the existence of slightly higher $^{20}Ne/^{22}Ne$ and slightly lower $^{21}Ne/^{22}Ne$ than the value of air can be related to an additional component other than air, that is, a non-atmospheric component. The higher $^{20}Ne/^{22}Ne$ ratios can call for the existence of a mantle derived component, as can be also strengthened by the high helium isotopic ratios observed in the gas samples. However, the low $^{21}Ne/^{22}Ne$ ratios can be related to a lower amount of nucleogenic production accompanied by radiogenic helium.

Both Tekke Hamam and Kızıldere samples have similar neon isotopic ratios. However, all samples seem to stay within the error limits around the value of air, therefore the variations in the ratios cannot be significant enough to be affected by mantle components. Therefore, it is more likely that there exists an isotopic fractionation event, rather than a mantle input for neon.

Regarding the correlations between the elemental nuclide abundances, especially the correlation plots of ^{20}Ne versus ^{40}Ar (elemental nuclide fractionation)(Figure 7.4) and ^{84}Kr vs ^{132}Xe (Figure 7.5) display very well defined correlation plots. It seems that all data points for Kızıldere and Tekke Hamam appear to lie on linear mixing trends, with a stronger correlation coefficient for the Kızıldere samples, and possibly display the existence of a non-fractionated atmospheric component. However, there seems to be no significant correlation identified between Kr and Xe relative to Ar and Ne. Especially in the plot of Kr vs. Ar and Xe vs. Ar, four data points out of 13 fall out of this correlation.

In the nuclide vs. nuclide diagrams shown in Figures 7.4 and 7.5, the different slopes for the fields are either related to

   i)   different recharging temperatures when atmospheric gases were buried in meteoric waters and drawn down and/or

   ii)   different interaction with shallow, cold aquifers during rising (before sampling).

The further process is unlikely to affect such large solubility differences, and therefore the latter alternative can possibly explain the different mixing trends. The Kızıldere samples were hot, whereas the Tekke Hamam samples have already undergone interaction with the shallow water table and hence gas recharging temperatures where much colder.
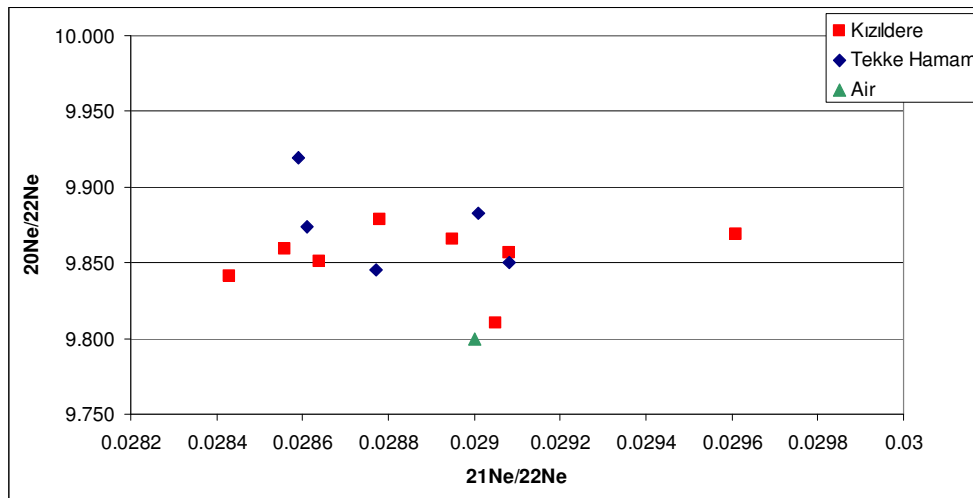
Figure 7.3 $^{20}Ne/^{22}Ne$ versus $^{21}Ne/^{22}Ne$ diagram, the three isotope Ne diagram.
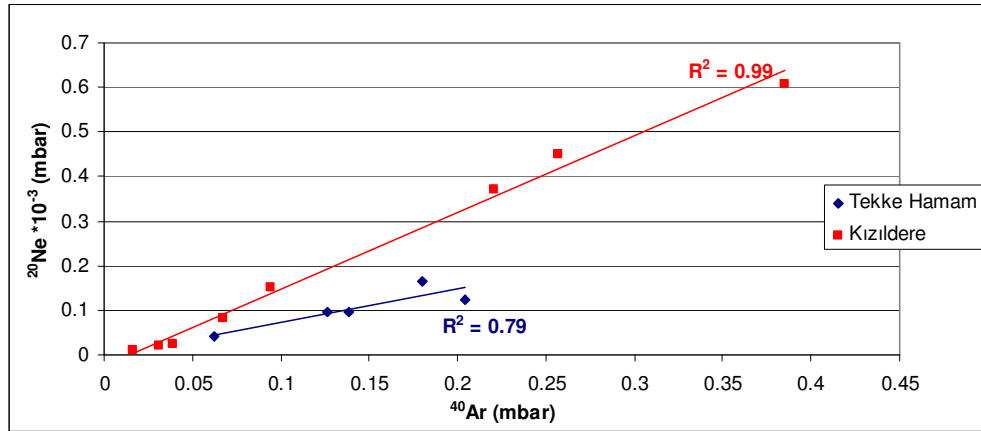
Figure 7.4 ^{20}Ne versus ^{40}Ar for the Kızıldere and Tekke Hamam samples.
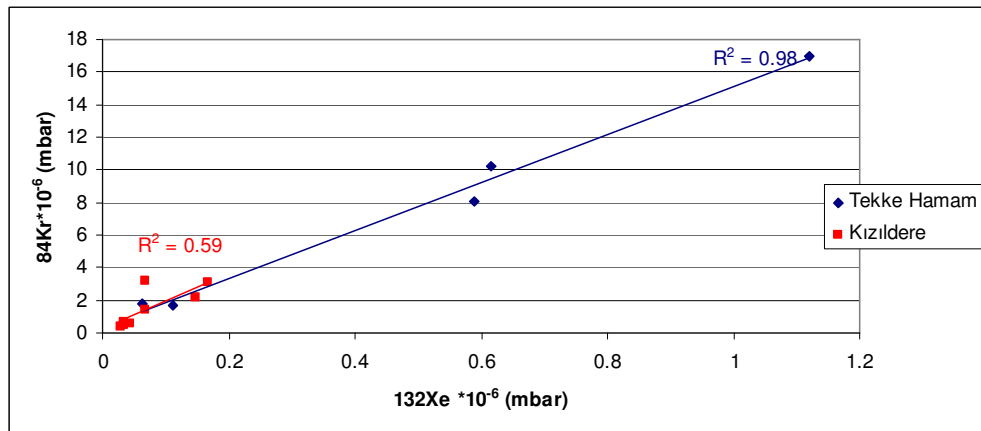
Figure 7.5 ^{84}Kr versus ^{132}Xe for the Kızıldere and Tekke Hamam samples.

7.3 R/Ra versus Helium-4 and ^{4}He/ ^{20}Ne

When making a comparison between the fields, it can be seen that the Tekke Hamam samples have both relatively higher R/Ra ratios and ^{4}He abundances when compared

with those of Kızıldere. The possible explanations for this coupling can be either related to a common mantle helium flux variably contaminated by crustal helium or a different mantle helium flux variably contaminated by crustal helium. In the former, we would expect a lowering in the helium isotope ratio due to interaction with shallow crustal radiogenic helium. Generally higher helium abundances lead to lower helium isotopic ratios. However, in the samples taken from Tekke Hamam and Kızıldere, just the reverse is observed, that is, a high helium isotope ratio is accompanied by higher helium abundances. In a plot of helium abundance versus helium isotope ratio for both fields this situation can be seen better (Figure 7.6). In the figure, each field seems to be defined by a characteristic helium isotope ratio accompanied by helium abundances, however, there exists a poor correlation for both fields.

In case of the latter possibility (different mantle-He flux), different scenarios can be suggested:

i.   A lower mantle helium flux for the Kızıldere site and a higher mantle flux for the Tekke Hamam site (leading to lower R/Ra ratios in Kızıldere and higher R/Ra values in Tekke Hamam). The admixing with crustal Helium in this case should be lower in Kızıldere than in Tekke Hamam (leading to lower helium abundances accompanied by lower $^{40}Ar/^{36}Ar$ ratios).

ii.   Different solubility situations may have led to the different helium abundances in addition to the different mantle helium fluxes for both fields. Since the solubility of helium decreases with increasing temperature, as also for the other noble gases, the abundance of helium within the Kızıldere waters may be low, whereas those in Tekke Hamam may have increased due to shallow level interaction accompanying an increase in solubility due to lowering temperatures.

iii. Different residence times may have led to the differences in the helium abundances. For example, a longer residence time of fluid in the reservoir will enrich it in the radiogenic helium due to radiogenic helium ingrowth. The samples taken from Tekke Hamam possibly represent free gases

138

following pathways towards the surface. The Kızıldere samples, on the other hand, represent gases dissolved in the deep hot reservoir, not in significant interaction with the shallow crustal conditions. Since the gas samples taken from Kızıldere represent gases dissolved in water in the reservoir, they may have time to incorporate radiogenic helium, however, just the reverse case is observed.

iv.   The Tekke Hamam hydrothermal reservoir may be fed by a less degassed and a deeper mantle source, having relatively high ^{3}He/^{4}He ratios and higher helium concentrations. Kızıldere samples, on the other hand, may indicate mixing of two mantle sources, from which one can be as mentioned above and the other possibly representing a shallower mantle source that has already undergone degassing processes. A degassed mantle source like this could, for example, be an isolated plutonic/magmatic body. Such a shallow mantle reservoir in closer distance to the hydrothermal reservoir may also explain the higher reservoir temperatures observed in the Kızıldere samples. Moreover, a degassed mantle reservoir is more sensitive to magma-rock interaction and can therefore explain the lower ^{3}He/^{4}He ratios and the lower helium abundances at Kızıldere. The spatial heterogeneity in temperature and ^{3}He/^{4}He ratios at Kızıldere is probably due to the mixing processes between two mantle sources at hydrothermal depths.

Therefore, it is possible that the different ^{3}He/^{4}He ratios and the accompanying differences in the abundances of helium for both fields can possibly be related to the existence of a different mantle-He flux variably contaminated by crustal helium.

As a further evaluation of the possible evolution of the mantle and crustal signatures, the R/Ra ratios of the samples were plotted against the ^{4}He/^{20}Ne ratios in Figure 7.7. In this diagram, binary mixing curves are drawn for three possible endmembers, namely, air, mantle and crust. The compositions assigned to these endmembers are as follows:

Air................... R/Ra = 1.0 (Lupton, 1983), $^4He/^{20}Ne = 0.319$ (Ballentine et al., 2002)
Mantle...................... R/Ra = 8.0, $^4He/^{20}Ne = 10000$ (Ozima and Podosek, 2002)
Crust...............R/Ra = 0.02 (Mamyrin and Tolstikhin, 1984), $^4He/^{20}Ne = 10000$

A plot of the measured R/Ra versus $^4He/^{20}Ne$ ratios reveals mixing hyperbolas between air and two distinct endmembers (Figure 7.7) for the Kızıldere and Tekke Hamam samples. The evolutionary trends for both Tekke Hamam and Kızıldere samples seem to be slightly different, with a higher mantle end-member component for Tekke Hamam and a slightly lower mantle end-member component for Kızıldere. Samples R-1 and KD-15 from the Kızıldere geothermal field appear to be more influenced by the radiogenic helium component, as it is already evident by their lower helium isotopic ratios coupled with a higher abundance of ^4He (they also have higher $^{40}Ar/^{36}Ar$ ratios, maximum observed in KD-15). The distributed alignment of the Kızıldere well samples can further suggest the possiblity of a common magmatic or mantle source for the field differently contaminated by local surficial helium-4 rich sources. The Tekke Hamam samples, on the other hand, appear to be tightly clustered suggesting that either the crustal and mantle He components are well mixed before input into the field or have been homogenized within the reservoir subsequent to filling, or have mixed in the shallow groundwater table before gas migration to the surface.

Therefore, two end members can be suggested: a surficial one, the atmosphere, with lower $^4He/^{20}Ne$ and $^3He/^4He$ ratios, and a deeper one, a mixing between magmatic and crustal fluids. The observed trends in the diagram can possibly suggest that gases emitted from both geothermal fields are fed by different deep magmatic/mantle source variably contaminated by local surficial helium-4 rich sources, owing to differing shallow level interaction with groundwater and/or air and different subsurface pathways leading the gases to the surface.

Another interesting point to mention is that, within the samples, especially the helium isotope ratio of R-1 is almost indistinguisable from the ratio of air and has a correspondingly higher concentration of ^4He. Given that faults have proved to be acting as conduits (Kennedy et al., 1997) or barriers (Wiersberg and Erzinger, 2007) for mantle volatile transport from depth, the low R/Ra ratio and the higher ^4He abundance of sample

R1 can be related to a possible non-active fault constituting a barrier between R1 and the other wells in the Kızıldere field. Hence, in the absence of an enhanced permeability via an active fault, the accumulation of ^{4}He during slow migration through the less permeable wall rocks could be the reason for this situation. Therefore, mantle volatile gases degassing from depth can evolve towards more crustal components owing to their interaction with different subsurface conditions, and can lead to differences in the discharging gases within a similar tectonic province. Currently, it is hard to estimate the effects of mantle/deep gas and crustal/shallow gas interactions in the subsurface.
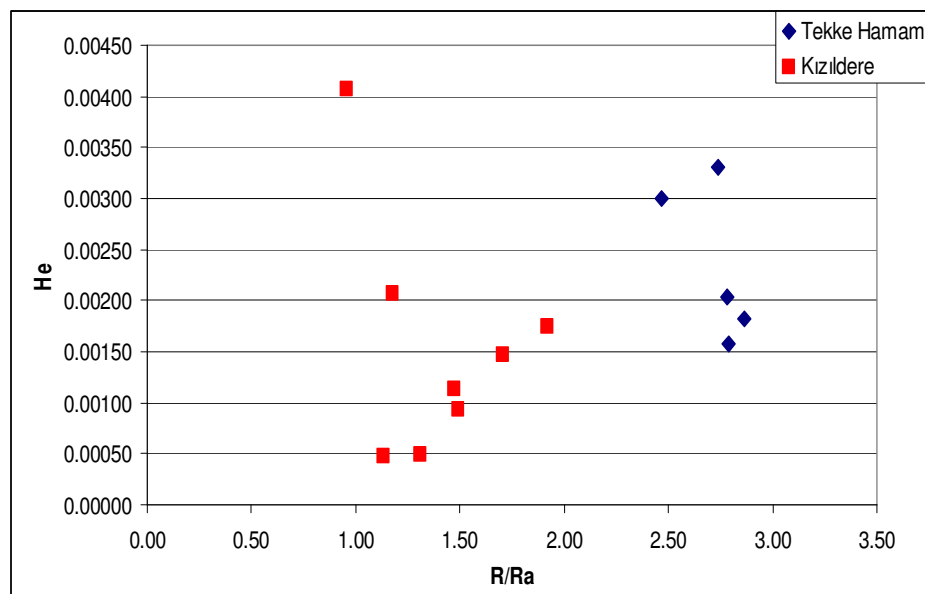
Figure 7.6 Correlation diagram between He abundance and R/Ra values for the Kızıldere and Tekke Hamam fields.
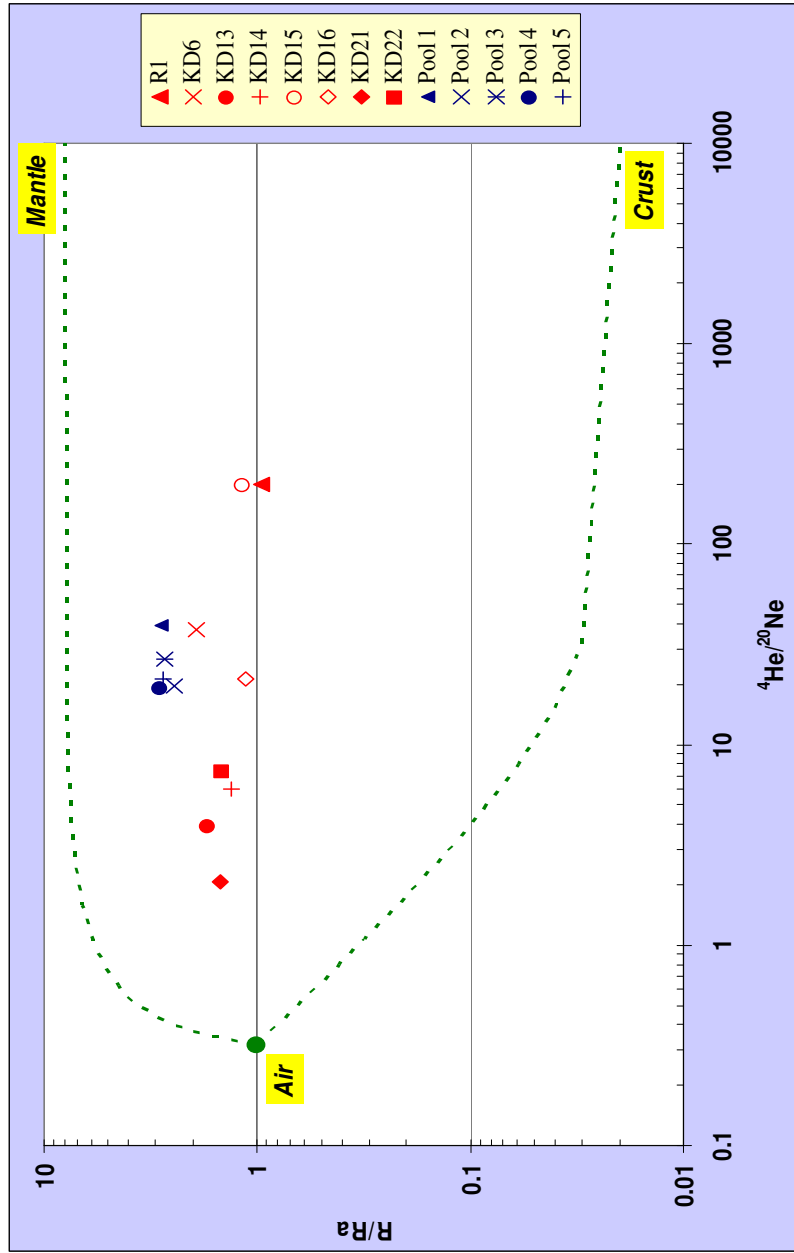
Figure 7.7. R/Ra values plotted against $^4He/^{20}Ne$ ratios of the gas samples from the Kızıldere and Tekke Hamam geothermal fields (Mixing trajectories between air (R/Ra = 1), mantle (R/Ra = 8) and radiogenic (R/Ra = 0.02) He bound these data).

7.4 Spatial Correlation of Samples in terms of R/Ra Ratios

The distribution of the R/Ra ratios are shown in Figure 7.8 (a, b) for the Kızıldere and Tekke Hamam geothermal fields, respectively. In the Kızıldere geothermal field, excluding well R-1, a SW-NE reaching trend to lower R/R_a values can be observed. In the Tekke Hamam geothermal field, on the other hand, there seems to be a very slight decreasing trend towards the west of the area.

In Figure 7.9, the overall distribution of the R/Ra ratio is seen for both fields. As can be seen from the figure, there appears to be a slight increasing trend in the R/Ra ratio from the north of the graben (where Kızıldere geothermal field is located) to the south (where Tekke Hamam geothermal fields is located). However, it should be kept in mind that, since there is no known geothermal field existing at the centre of the graben, between the zone covering both Tekke Hamam and Kızıldere, it is not clear whether the trend in the R/Ra ratio is a continuously increasing trend (from the north of the graben to the south) or if there is a discontinuity hiding within the trend.

In the Kızıldere geothermal field, there appears to be a strong negative linear trend ($R^2=0.70$) between the bottom-hole well temperatures and the R/Ra values of the Kızıldere samples, that is, higher temperatures are coupled with lower R/Ra values (Figure 7.10).

7.5 Components of Helium in the Geothermal Fluids

The inert nature of the noble gases, coupled with their distinctive isotopic and solubility characteristics, makes them ideal tracers in identifying the sources of gases coming from depth. Among the noble gases, helium has proved to be very successful in identifying the possible sources of gases, owing to its low atmospheric abundance coupled with its low solubility in water, and large and diagnostic variations in its isotopic composition ($^3He/^4He$ ratios).
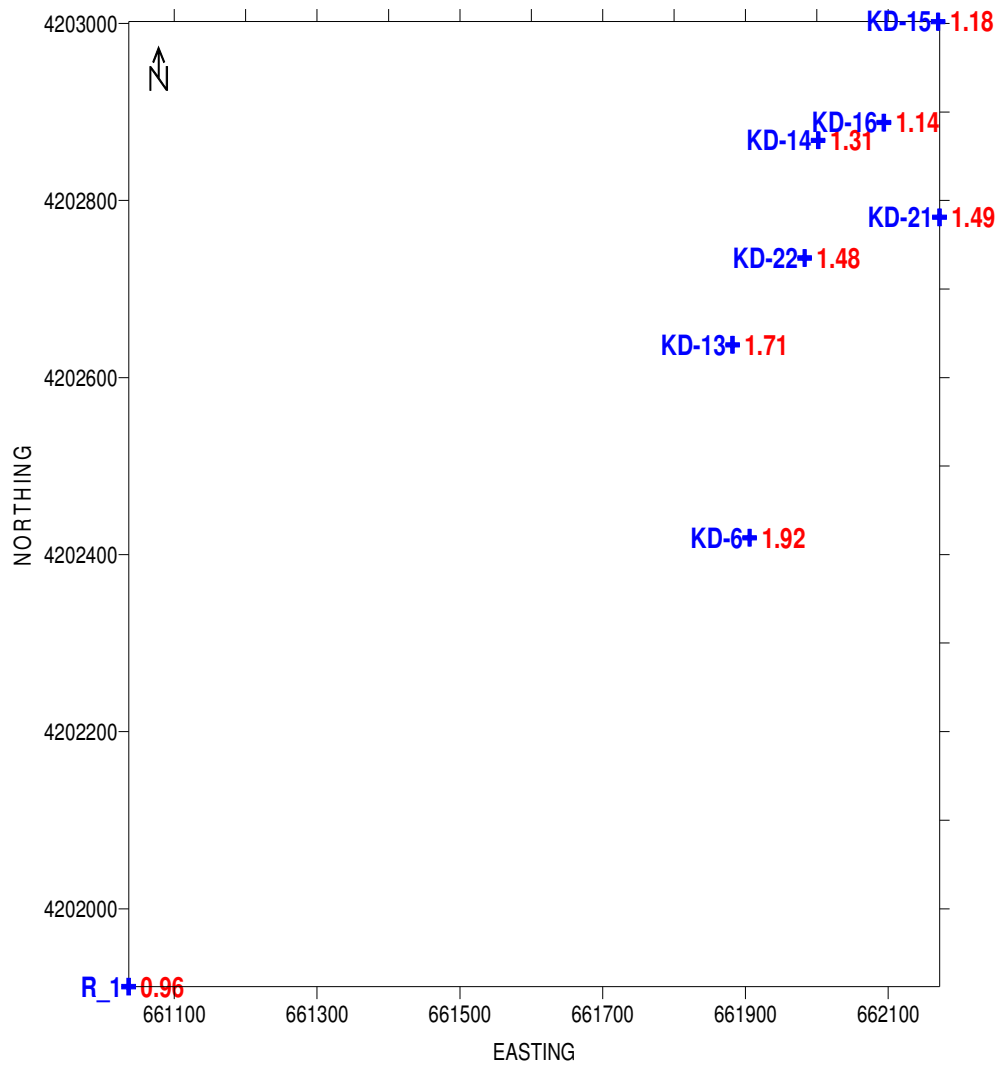
Figure 7.8a Spatial distribution of R/Ra ratios (shown in red) for the Kızıldere geothermal field.
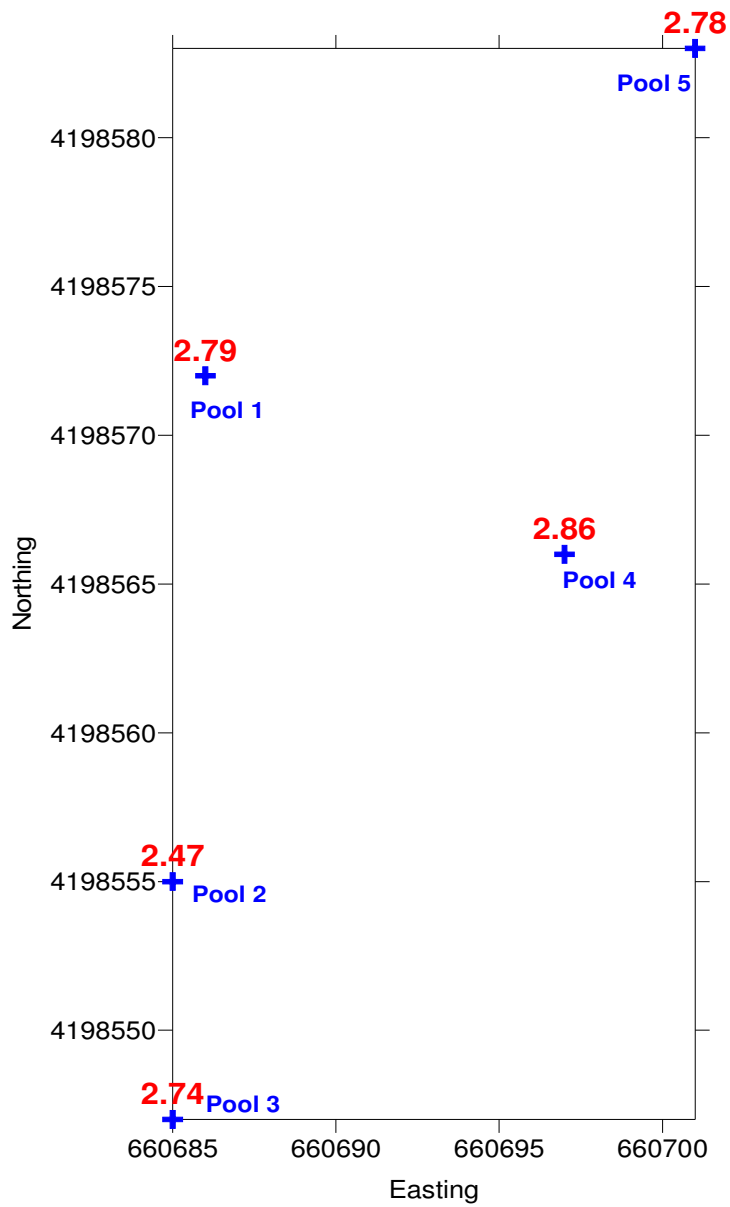
Figure 7.8b Spatial distribution of R/Ra ratios (shown in red) for the Tekke Hamam geothermal field.
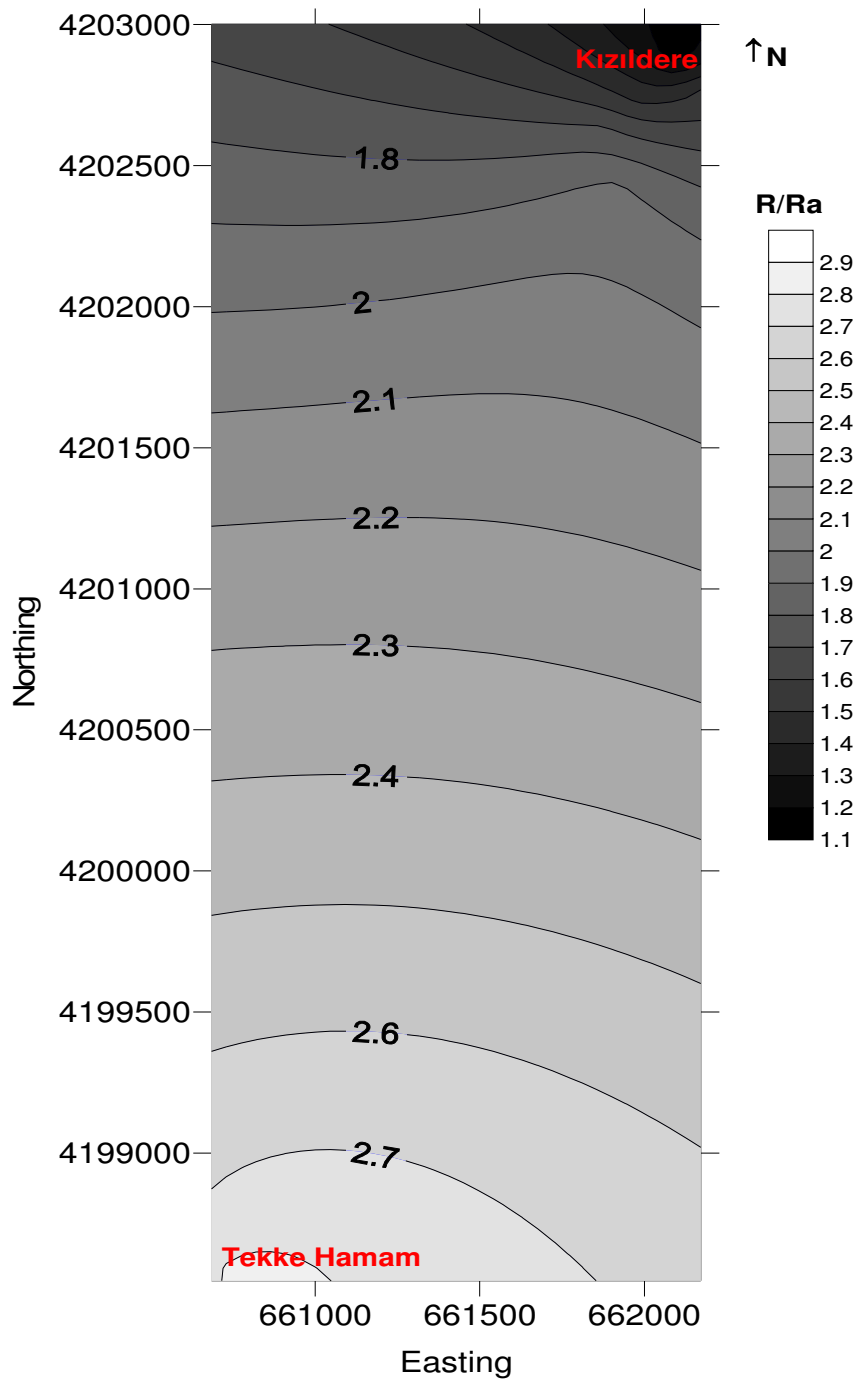
Figure 7.9 Spatial distribution of R/Ra ratios for both fields.
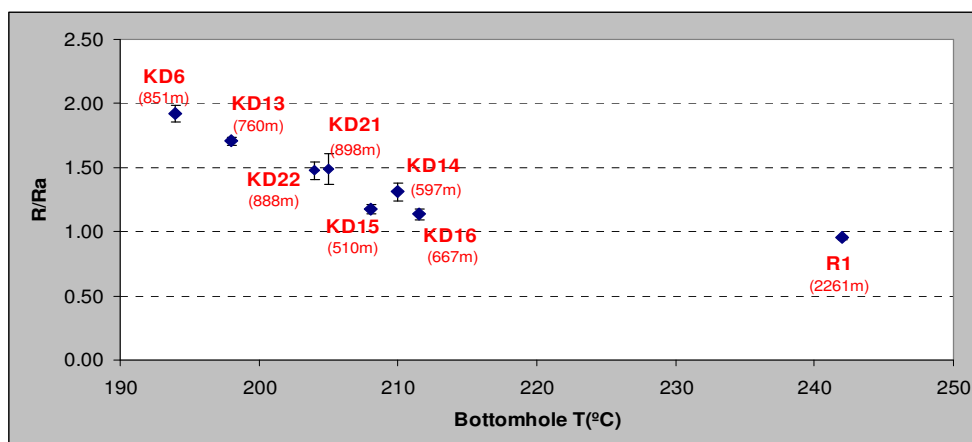
Figure 7.10 R/Ra versus bottom-hole temperature for the Kızıldere well samples.

The two stable isotopes of helium, ^{3}He and ^{4}He, have different origins. ^{3}He is essentially primordial and is retained in the Earth's interior at the time of its formation, whereas ^{4}He is mainly produced in the crust via the decay of uranium and thorium (Ozima and Podosek, 2002). Each isotope has both atmospheric and non-atmospheric components. The atmospheric components of helium can be introduced during sampling or during air equilibrium. The non-atmospheric components of helium, on the other hand, can originate from different terrestrial reservoirs, such as lithospheric mantle, asthenospheric mantle, continental crust etc. Therefore, helium in the subsurface can basically be described as a mixture of atmospheric and non-atmospheric components, each represented by specific ^{3}He/^{4}He ratios (atmospheric ^{3}He/^{4}He ratio = $1.4*10^{-6}$ (Clarke et al., 1976), crustal ^{3}He/^{4}He ratio $\sim 2*10^{-8}$ (Mamyrin and Tolstikhin, 1984), and astenospheric mantle ^{3}He/^{4}He ratio = $1.1*10^{-5}$ (Graham, 2002)). However, in any attempt to evaluate the individual components of helium present in a sample (water or gas), a conceptual model must be first created, specifying which components are assumed or possible to be present in the context of the geology/hydrogeology of the field of concern.

In order to quantify the non-atmospheric helium components in the gases collected, as a first step, air correction should be undertaken. During sampling, atmospheric

contamination may occur and can severely affect the original/deep noble gas signature of a sample. This is the case which can be most pronounced for argon, which has a concentration of about 1% in the atmosphere, while helium, being the lightest noble gas, can be lost very easily from a sample due to its small molecular size and high diffusion rate. In addition to sampling, gases can also attain an atmospheric component during air-water equilibrium (from atmospheric air or air-saturated water). Therefore, the two possible atmospheric sources of helium should be eliminated before determining the mantle component present in a sample.

In this regard, the measured ^{3}He/^{4}He ratios of the gas samples collected from the Kızıldere and Tekke Hamam geothermal fields were corrected assuming that the measured ^{20}Ne is completely atmospheric, which is also confirmed by the neon isotopic analysis (^{21}Ne/^{22}Ne and ^{20}Ne/^{22}Ne). The measured ^{3}He/^{4}He ratios were air corrected, assuming a ^{4}He/^{20}Ne ratio of 0.319 (Ballentine et al., 2002) for the atmospheric component, by using the equation given below (Poreda and Craig, 1989).

$$(^3He/^4He)_{cor} = [(^3He/^4He)_m - (^3He/^4He)_{air} * r]/(1 - r) \qquad (7.1)$$

$$r = (^4He/^{20}Ne)_{air} / (^4He/^{20}Ne)_m \qquad (7.2)$$

where the subscript cor stands for the corrected value; m is the measured value. The air corrected helium isotope ratios are given in Table 7.3. Most of the samples exhibit slightly higher helium isotope ratios when normalized to air after air correction. The calculated ratio should now represent only the mixture of the mantle and crustal helium.

After correction for air contamination, the separate contributions of mantle and crustal components for all samples were calculated assuming a simple binary mixing between an asthenospheric mantle (R/Ra = 8) and a crustal (R/Ra = 0.02) endmember component, utilizing the formula given below

$$R_c/R_a = 8.0 \, a + 0.02 \, (1 - a) \qquad (7.3)$$

where the subscript c stands for the corrected ^{3}He/^{4}He ratio; a is the percentage of mantle component involved in the sample and (1 – a) denotes the percentage of crustal contribution.

In Figure 7.11, the percentages of mantle-He and crustal-He are presented as a bar diagram for both fields. The mantle-He component in the samples ranges from 31 to 36% for Tekke Hamam (an average of about 34%) and 12 to 24% for Kızıldere (an average of about 18%). Therefore, it is apparent that mantle-derived fluids play an important role in the origin of the gases reaching the surface, although in slightly different percentages for both fields.
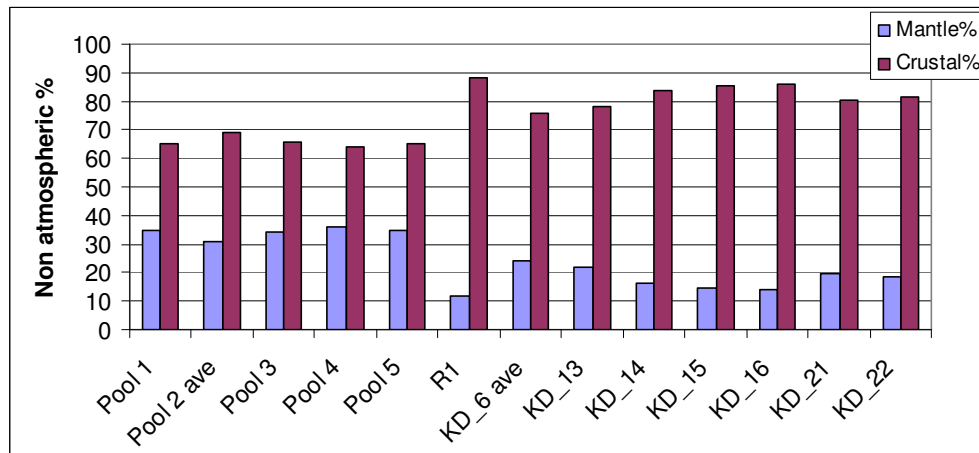
Figure 7.11 Mantle and crustal helium components for the samples.

7.6 Concluding Remarks

The ^{3}He/^{4}He and ^{4}He/^{20}Ne ratios of the Tekke Hamam and Kızıldere geothermal fields reveal that their helium sources highly exceed helium introduced by atmospheric components and suggest the existence of contributions from some other extraneous

sources (crustal and/or mantle). The other isotopes of noble gases, on the other hand, reveal a highly atmospheric component, possibly attained during sampling and/or air equilibrium.

The helium component resolutions done according to the simple binary mixing calculations reveal that the mantle helium component seems to be higher in the gas samples taken from the Tekke Hamam geothermal field than those in Kızıldere. The lower helium isotope ratios of the Kızıldere gas samples are accompanied by lower helium abundances than those of Tekke Hamam. The possible reason for this distribution can be a different mantle helium flux variably contaminated by different radiogenic helium input, during differing subsurface conditions such as solubility differences owing to different subsurface temperatures or interaction with shallow groundwater or different pathways for gases. The different mantle-He flux can be related to a deeper and less degassed mantle source for Tekke Hamam, and a mixture of two different mantle sources (one deep and less degassed as proposed for Tekke Hamam and the other representing a shallower mantle source, that has already undergone degassing) for the Kızıldere geothermal site. The distinctly lower R/Ra value for well R-1, very close to that of air, on the other hand, can be related to the accumulation of radiogenic helium due to hampered migration through a possible non-active fault, which might have acted as a barrier for fluid flow.

The presence of mantle-derived helium components observed in both Kızıldere and Tekke Hamam geothermal fields is not surprising as both fields are situated on the boundary faults of the Büyük Menderes Graben formed in relation to the currently active extension in western Anatolia. This extension is believed to be associated with mantle upwelling, leading to the continuous release of mantle volatiles (Mutlu et al., 2008). Therefore, the gases coming from depth in the area can be represented by a mixture of non-atmospheric sources, variably contaminated by atmospheric components.

Regarding the transfer of mantle-He to the shallow crust in the region, the most probable mechanism seems to be melting related to volcanic and/or plutonic activity, as proposed by Güleç and Hilton (2006). Degassing of mantle melts emplaced at deep levels of the crust is an increasingly accepted mechanism of mantle-He transfer in extensional terrains

characterized by deep fault planes but with little or no surface evidence of recent magmatic activity (e.g. Kennedy and Van Soest, 2006). Since both Kızıldere and Tekke Hamam fields are located in an extensional province, the magmatic volatiles are assumed to be supplied from deep penetrating faults in the region which may act as either conduits or barriers of mantle volatiles, and therefore mantle helium. The different character of the faults can lead to different mantle-crustal interactions. For example, a slow migration through a low permeable fault may result in the accumulation of radiogenic helium, and a further dilution of the deep mantle signal (Wiersberg and Erzinger, 2007). On the other hand, a fast migration owing to the higher permeability of a fault may result in a lower dilution of the mantle signal by shallow crustal helium sources. Therefore, any possible interaction between deep gases and tectonic features (faults, fractures, shear zones, etc.) of the region may in turn develop different helium isotopic ratios, owing to the existence of different stages of mantle-crustal interaction within the subsurface.

CHAPTER 8

REAL-TIME MONITORING OF GASES FROM
THE TEKKE HAMAM GEOTHERMAL FIELD

Starting from the end of November 2007 till the end of October 2008, a real-time gas monitoring experiment was carried out near a gas discharging pool (Mofette) in the Tekke Hamam geothermal field. During the course of the nearly year round on-line gas monitoring experiment, a Quadrupole Mass Spectrometer (QMS) was set to measure the composition of the released gases, that is, CO_2, CH_4, O_2, H_2S, H_2, He, Ar and N_2 (vol.%) simultaneously, at intervals of one minute. In addition to the gas compositions, the gas flow rate (l/min) and the pool temperature (ºC) were also measured at the same time intervals (in one minute) by a flowmeter and a temperature sensor, respectively.

The average (together with the minimum and maximum values) gas composition and gas flow rate range is given as a comparison for Pool 2 (representing the time interval between November 2007 - August 2008) and Pool 3 (the time interval between September 2008 – October 2008) in Table 8.1 and presented in Figure 8.1(a,b) as pie diagrams. As can be seen from the table and figure, the major component of the gases discharging from the pools is represented by CO_2, with values changing mainly around 96 vol.% for Pool 2 and 98 vol.% for Pool 3. The second most abundant component in the gas mixture coming from the pools is N_2, changing around 2.9 vol.% for Pool 2 and 1.2 vol.% for Pool 3. Other gases, from the most abundant to the least, are represented by CH_4, O_2, H_2S, Ar, H_2 and He.

As can be seen from their compositions, Pool 2 is characterized by slightly higher CH_4, Ar, He, N_2 and O_2 compositions than Pool 3. Pool 3, on the other hand, has higher CO_2, H_2 and a higher gas flow rate. The most likely reason for the high gas flow rate observed in Pool 3 can be probably related to a higher gas flux rate from depth. The lower Ar, N_2 and O_2 concentrations in Pool 3 is possibly related to a relatively lower air contamination

due to a slightly higher gas flux from the pool or may be a tighter connection to the station.

Table 8.1 Range of gas compositions for Pool 2 and Pool 3 (given in vol.%).

	Pool 2			Pool 3		
	min	**max**	**ave**	**min**	**max**	**ave**
CO_2	95.3	97.2	96.3	98.1	98.6	98.3
CH_4	0.36	0.46	0.41	0.27	0.29	0.28
H_2	0.00088	0.00286	0.00187	0.00226	0.00360	0.00293
He	0.000437	0.000802	0.000619	0.000395	0.000453	0.000424
N_2	1.8	3.9	2.9	1.0	1.4	1.2
O_2	0.24	0.36	0.30	0.12	0.13	0.12
H_2S	0.029	0.119	0.074	0.061	0.090	0.075
^{40}Ar	0.012	0.020	0.016	0.009	0.011	0.010
Gas Flow rate	around 0.2 - 0.4 l/min			around 0.7 l/min		
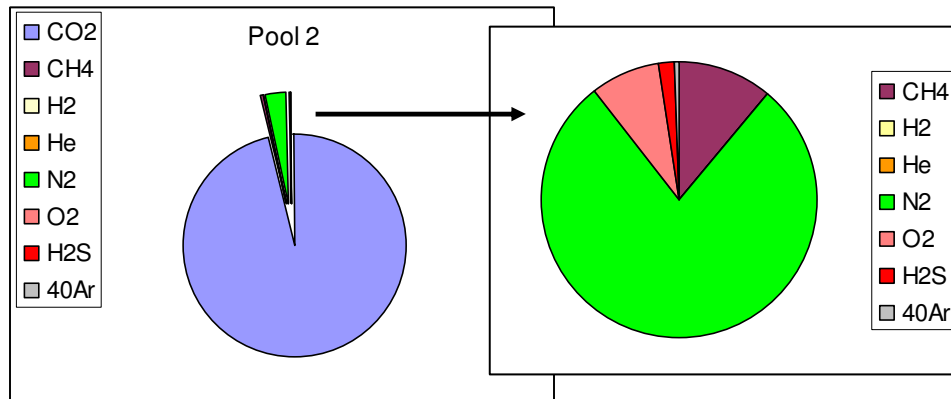
Figure 8.1a Gas composition of Pool 2 shown in a Pie chart.
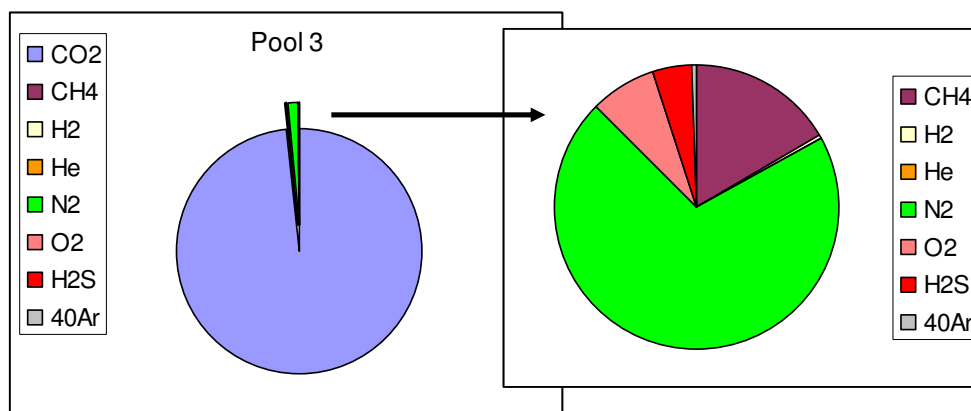
Figure 8.1b Gas composition of Pool 3 shown in a Pie chart.

8.1 Origin of the Monitored Gases

Geothermal fluids may contain gases originating from different sources. The gases mostly observed in geothermal environments are CO_2, CH_4, H_2S and H_2, which can have both deep and shallow sources. Other gases such as N_2 and O_2, on the other hand, are dominant in air, but can also be observed within the deep discharging crustal fluids. Noble gases can also derive from different sources within the Earth, particularly Helium being the most deep gas indicative one and Argon mostly introduced by air contamination. Therefore, every monitored gas originates from a different compartment of the Earth. The best way for the evaluation of the possible sources of gases (e.g., crustal, mantle, atmospheric, organic etc.) is the analysis of isotopes of elements such as Carbon (^{13}C, ^{14}C), Hydrogen (D/H), Sulfur (^{34}S), Helium (^{3}He, ^{4}He), Oxygen (^{18}O) and Nitrogen (^{15}N). Isotopes have characteristic values for different sources of gases and thus provide valuable insights into the evaluation of the possible sources for the gases discharging from the Earth. The molecular composition of a discharging gas can also be indicative for the source of a gas, but only isotope data can finally clarify its origin.

The monitored gases (CO_2, CH_4, H_2, He, N_2, O_2, H_2S, Ar) discharging from the bubbling pools in the Tekke Hamam geothermal field possibly have different origins. The high

CO_2 content, nearly close to pure CO_2, of the gases coming from the bubbling pools in the Tekke Hamam geothermal field possibly points to the deep origin of these gases. The low O_2 and N_2 contents detected in the gas composition during most of the time of monitoring suggest only low air contamination in the gas line of the monitoring setup. CH_4 and H_2S are also typical gases representing geothermal systems and can possibly point to organic and/or deep origins.

Below is a brief discussion regarding the possible sources of the gases present in the pools.

8.1.1 Sources of CO_2 and He

CO_2 is one of the most abundant gas species in hydrothermal to volcanic environments. CO_2 can derive from different sources: the mantle (exsolution from magma, volcanic activity), carbonate metamorphism (thermal decarbonation of carbonate minerals), decomposition of organic material (organic sources) and surface biological activity (biogenic origin) (Irwin and Barnes, 1980). In addition to these sources, CO_2 can also be mechanically produced in relation to seismic activities (Martinelli and Plescia, 2005; Italiano et al., 2009).

The analysis of carbon isotopes ($^{13}C/^{12}C$) in CO_2 allows the differentiation between different sources, owing to the large isotopic variations in the various carbon reservoirs. Lower CO_2 concentrations are usually related to organic/biogenic sources and are characterized by $\delta^{13}C$-depleted gases. Values closer to 0 ‰ may be related to several different sources, like marine carbonates, carbon from thermometamorphic processes and/or deeper origin.

CO_2 rich spring gases, having high gas fluxes, generally occur in seismically active areas (Irwin and Barnes, 1980). High CO_2 concentrations, generally exceeding 50%, are seen in deep crustal or mantle sources of volcanogenic (exsolution from magmas) or metamorphic (thermal destruction of marine carbonates) origin. Especially geothermal waters in volcanic settings or along fault zones associated with plate boundaries will often have elevated P_{CO2} values that reflect a subsurface mantle source. This mantle

derived CO_2 has been observed in geothermal waters and fumaroles from seismically active belts and has been found to have a $\delta^{13}C$ value of about -6 ‰ (Marty and Jambon, 1987). In addition to its mantle source, high amounts of CO_2 can also originate from crustal compartments. There are basically two major sources for crustal carbon: thermal metamorphism of limestone and organic carbon from sedimentary rocks. When rising magma interacts with carbonate strata, decarbonation of $CaCO_3$ takes place, with the preferential loss of heavy CO_2. Such reactions can take place at temperatures as low as 600 ºC. Metamorphic CO_2 is several permil enriched above carbonate precursor (Marine carbonates, $\delta^{13}C_{CO2}$ =0‰), with values typically between 5 and 10‰ (Clark and Fritz, 1997). Lower CO_2 concentrations are usually related to organic sources from sedimentary rocks and are characterized by $\delta^{13}C$-depleted gases generally varying around -25‰ (Allard, 1986).

Shallow biogenic sources of CO_2 are generally low in abundance and are characterized by lighter isotopic compositions depending on the kind of vegetation (ranging around -20‰; Drever, 1997). For example, in soil, CO_2 is strongly influenced by biogenic activities. The typical levels of biogenic CO_2 in soils change around 2 and 6 vol.% during the growing season, depending on the type of vegetation (Buyanovsky and Wagner, 1983). In addition to deep and shallow sources, CO_2 can also have an atmospheric component, with an average concentration of some 360 ppmv or a partial pressure of $10^{-3.5}$ ($\delta^{13}C$ close to -6.4‰; Clark and Fritz, 1997).

Therefore CO_2 fluxes can derive from different sources: abiogenic: magmatic or thermometamorphic (having high CO_2 abundances and heavier carbon isotope data) and organic/biogenic (characterized by lower CO_2 abundances and lighter isotopic compositions). However, it should be kept in mind that, the gases originally having a pristine magmatic signal will be contaminated by both crustal and shallow organic/biogenic sources of CO_2. High CO_2 abundances with high gas flux rates mostly observed in seismically active regions of the crust will possibly mask the shallow CO_2 contribution. Thus, the CO_2 abundance should not simply imply a single source, but more likely a mixture of different sources.

Regardless of the source of the CO_2 in an accumulation, its abundance is controlled not only by its origin, but also by its reaction in the subsurface. CO_2 is a highly soluble and chemically reactive gas that undergoes large chemical and isotopic modifications when interacting with shallow fluids; that is, in contrast to other gases, CO_2 is very vulnerable to fractionation processes. These modifications strongly depend on the temperature and pH of the groundwater. However, due to the high solubility of CO_2 in water and the HCO_3 formation, fractionations of the CO_2-rich gases takes place (Weinlich et al., 1999). Therefore, the CO_2 gas composition can be altered solely by solubility fractionation.

Helium is the lightest noble gas in nature and is mainly used as a powerful indicator of deep origined gases in both continental and oceanic terrains. Helium has a low and constant concentration in the atmosphere (5.24 ppm, Ozima and Podosek, 2002). Any concentration of helium exceeding that of the atmosphere possibly indicates the existence of a non-atmospheric component.

The helium isotope composition provides useful genetic information about one of the three possible helium sources: atmosphere, mantle and crust. In active volcanic terrains, helium mainly originates from the mantle (^{3}He-primordial helium, represented by a high ratio of ^{3}He/^{4}He), whereas in regions devoid of volcanic activity helium is considered to be primarily originated from the radioactive decay of uranium and thorium within the crust (^{4}He-radiogenic helium; lower ^{3}He/^{4}He ratios), with also varying contributions from the atmosphere and the mantle. Therefore, helium in the subsurface can basically be described as a mixture of atmospheric and non-atmospheric components, each represented by specific ^{3}He/^{4}He ratios (atmospheric ^{3}He/^{4}He ratio= $1.40*10^{-6}$ (Clarke et al., 1976), crustal ^{3}He/^{4}He ratio = $2*10^{-8}$ (Mamyrin and Tolstikhin, 1984), and mantle ^{3}He/^{4}He ratio = $1.1*10^{-5}$ (Graham, 2002).

The coupled usage of CO_2 and He in evaluating the possible origins of gases has proved to be very useful in several studies (Du et al., 2005; Inguaggiato et al., 2005; Mutlu et al., 2008). Both gases are essentially deep origined, especially in geothermal environments. Helium travels with CO_2 and other components and, in many springs, CO_2 can comprise over 99% of the gas phase. The origin of the carbon in fluid emissions can be resolved by coupling He to C measurements in the form of the $CO_2/^3$He ratio. This approach has been

widely exploited in studies of the carbon inventory of arc-related volcanoes (Hilton et al., 2002). In addition, the combination of $\delta^{13}CO_2$ measurements and the $CO_2/^3He$ ratio has been used successfully to resolve the relative contribution of mantle, carbonate and sedimentary CO_2, organically derived CO_2, and atmospheric CO_2 (Sano and Marty, 1995; Sherwood Lollar et al., 1997; Ballentine and Sherwood Lollar, 2002; Mutlu et al., 2008). The typical values of $CO_2/^3He$ ratio for mantle is 2×10^9, and 10^{13} for both sedimentary organic carbon and marine carbonates (Sano and Marty, 1995).

The major component of the gases discharging from the pools in the Tekke Hamam geothermal field is represented by CO_2. The high CO_2 content (nearly 97% on the average) most probably depicts a deep origin for this component since high CO_2 abundances were generally related to deep sources. The high CO_2 concentration of the gases most likely rules out the possibility of a biogenic source, which is generally characterized by a lower CO_2 abundance. Therefore it is likely that the CO_2 coming from the deep crust masks the biogenic production in the shallow crust.

The deep origin of CO_2 is also confirmed by the relatively high $^3He/^4He$ ratio found in the gas samples (R/Ra = 2.46-2.86), suggesting a contribution of about 34% of mantle helium (taking R/Ra = 8 as the average mantle ratio) admixture into the crustal fluids.

As another constraint on the evidence of the origin of CO_2, the $CO_2/^3He$ ratio was evaluated together with the $^3He/^4He$ ratio. The $CO_2/^3He$ ratios are estimated by observed $^3He/^4He$ ratios, and helium and CO_2 concentrations. The $CO_2/^3He$ ratio of the mofette gas (from both Pool 2 and Pool 3) is higher than the asthenospheric mantle value (2×10^9), hence an additional source of CO_2 is indicated (e.g. crustal contamination of the magma source or fluid-carbonate interaction during fluid migration or organic). Therefore, CO_2 is partly from the mantle and partly from fluid-rock-interaction. However, since there is not any carbon isotope measurement performed on the CO_2 content of the gases discharged, it is not possible to clarify the exact origin of CO_2 (whether it is organic/biogenic, mantle, thermometamorphic). In fact, the high CO_2 and He contents measured in the pools, coupled with the respective isotopic compositions ($^3He/^4He$)— clearly indicating the contribution of an appreciable magmatic component— indicate a

high gas–water interaction between deep CO_2-rich gases and shallow fluids. Therefore, high contents of magmatic gases of He and CO_2 are present as dissolved gases.

The high values of $CO_2/^3He$ ratios observed in western Anatolian geothermal fluids, generally exceeding values typical of an upper mantle source value (2×10^9; Marty and Jambon, 1987), together with the carbon isotope measurements ($\delta^{13}C(CO_2)$ = −8.04 to +0.35‰) were attributed to mixing between mantle and various crustal sources, with a dominant crustal input controlling the CO_2 inventory (Mutlu et al., 2008). The high crustal-carbon flux was related to marble lithologies of Menderes Massif metamorphics which comprise the basement in most parts of the western Anatolian region.

In Figure 8.2, the $CO_2/^3He$ ratio is plotted vs. the isotopic composition of He. As can be seen from the graph, Pool 3 is associated with a higher $CO_2/^3He$- R/Ra couple, whereas Pool 2 has relatively lower ratios.

The transfer of mantle-He into the crust is probably associated with (extension related) mantle melting while the fault systems of the grabens appear to have acted as conduits for the geothermal fluids to carry the mantle-He to the surface (Mutlu et al., 2008). Therefore, large emissions of CO_2 in the Tekke Hamam geothermal field can act as a carrier gas for trace gases such as He. Other studies have also shown the possibility of CO_2 to act as a carrier gas for gases such as radon (Etiope et al., 2005). Furthermore, the monitoring records in the present study demonstrate that both CO_2 and He show opposite variations, that is, an increasing trend in CO_2 coupled with a decreasing trend in He. This can strengthen the possibility that CO_2 is acting as a carrier gas for He, and that the He concentration is depending on the CO_2 flux.
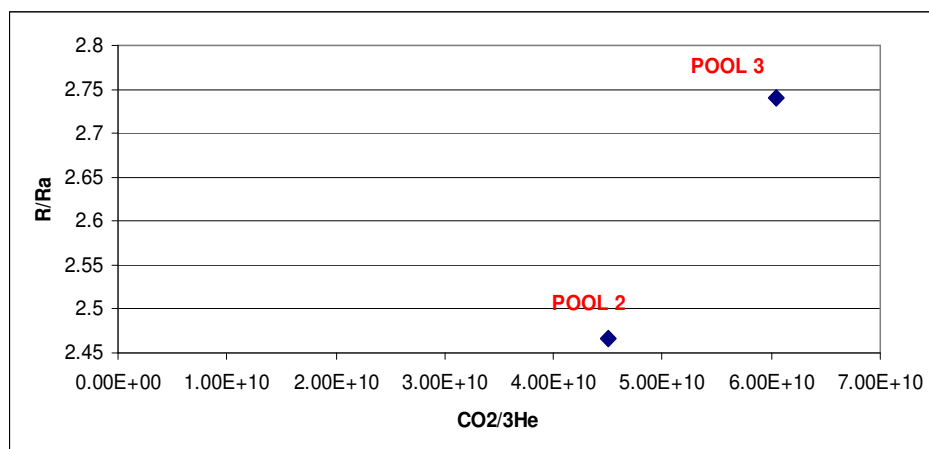
Figure 8.2 R/Ra versus $CO_2/^3He$ for Pool 2 and Pool 3.

8.1.2 Sources of N_2 and CH_4

Methane is an ubiquitous gas found in natural environments ranging from deep crustal settings and sedimentary basins to soils, surface waters and the atmosphere. As a component of carbonate evolution in groundwaters, it participates in the carbon cycle and contributes to the greenhouse gases. CH_4, like He, has also proved to be a good indicator of deep gas leaks along crustal discontinuities.

There are three principal origins of methane in groundwater:

i)   biogenic methane is the most common in shallow low temperature groundwater systems in anaerobic environments, forming from the bacterial reduction of organic matter. Biogenic methane commonly occurs in recent anoxic sediments and is well documented in both freshwater environments, such as lakes and swamps, and in marine environments, such as estuaries and shelf regions. Two primary metabolic pathways are generally recognized for metanogenesis: fermentation of acetate and reduction of CO_2. Although both pathways may occur in marine and freshwater environments, CO_2 reduction is dominant in the sulfate-free zone of marine sediments, while acetate

fermentation is dominant in freshwater sediments. Typical $\delta^{13}C$ ranges for marine sediments are between -110 and -60‰, while those for methane from freshwater sediments are from -65 to -50‰ (Hoefs, 2004).

ii) Thermogenic methane forms by the breaking down of higher mass hydrocarbons at elevated temperatures (organic matter deeply buried) and represents the natural gas in sedimentary basins (Welhan, 1988). Increasing temperatures modify the organic matter due to various chemical reactions, such as cracking and hydrogen disproportionation in the kerogen. Thermogenic gas typically has $\delta^{13}C$ values between -50 and -20 ‰.

iii) Abiogenic (geogenic) methane is defined as methane that does not involve organic precursors. It can be produced within the involvement of bacteria when strongly reducing conditions and inorganic catalysts such as Fe are found (Clark and Fritz, 1997). Methane emanating in Mid Ocean Ridge hydrothermal systems is one of the occurrences for abiogenic methane. Deep crustal or mantle methane is typically enriched in $\delta^{13}C$ (-20 to 15‰) due to exchange at high temperatures with mantle carbon. It also has enriched δ^2H values reflecting high temperature equilibrium with water. Geothermal water may incorporate high temperature methane providing insights into the movement of volatile fluids in the crust (Clark and Fritz, 1997).

The combination of carbon and hydrogen isotope analysis of methane is a powerful tool to discriminate different origins of gases.

Nitrogen is a trace phase in rocks and the major component of air (nearly 78%). Nitrogen is also a biologically active element and participates in a multitude of reactions that are important to life. N_2, like O_2 and Ar, can be considered to be derived from the atmosphere upon dissolution in groundwater during meteoric recharge of geothermal systems. However, other sources of N_2 can also be present, such as organic, hydrothermal, sedimentary, etc. For example, decay of biomass releases nitrogen, which oxidizes to nitrate. NO_X is produced by nitrification and denitrification processes in soils. Although nitrogen can also be derived from magmatic sources, magmatic nitrogen is not

a common component of high-nitrogen gases. Therefore, high concentrations of N_2 in subsurface gases may be derived basically from thermal alteration of sedimentary organic matter (Jenden et al., 1988).

In order to evaluate different origins of nitrogen, $\delta^{15}N$ isotope measurement techniques on Nitrogen should be performed, however, there are still some difficulties with the measurement techniques of the nitrogen isotope ratios. Another point is that, the determination of nitrogen isotopes in terrestrial materials (such as basaltic glasses) is severely complicated by its low concentration, which makes nitrogen sensitive to atmospheric contamination and to addition of surface-derived materials, i.e., organic matter.

The N_2 content of the discharging gases in Tekke Hamam varies generally around 1.8-2.8 vol.%. When this N_2 is also compared with the O_2 content of the mofette gas, it can be clearly seen that there is some excess N_2 within the total N_2 content, that is, if the N_2/O_2 ratio of air is taken as 3.727, then the excess N_2 can be calculated according to the equation 8.1 given below

$$N_2 \text{ (excess)} = N_2 \text{ (measured)} - [(O_2 \text{ (measured)} \times (N_2/O_2)air)] \qquad (8.1)$$

N_2 and Ar are two of the basic components of atmosphere. The abundance ratio of nitrogen to argon has also been used as an indicator for the origin of nitrogen in natural gases (Zartman et al., 1961), volcanic gases (Matsuo et al., 1978; Kiyosu, 1986) and sedimentary rocks (Sano and Pillinger, 1990). The N_2/Ar ratio of air saturated water is equal to 38 (at 20ºC) and that of air is equal to 83.6 (Giggenbach, 1986).

The N_2/Ar ratio of the gases discharging from the pools in Tekke Hamam are greater than the atmospheric ratio (generally varying around 110-250). The N_2/O_2 ratio of the gas mixture discharging from Tekke Hamam (varying around 7-14) is also clearly higher than that of the atmospheric ratio, most probably indicating that oxygen was consumed by microbial and/or chemical reactions in the groundwater.

The high N_2/Ar ratio can also be explained by either an argon deficiency or a nitrogen excess in the gases discharging, the latter being more likely. Based on $^{40}Ar/^{36}Ar$ ratios indistinguisable from the atmospheric value, could demonstrate that no excess Ar with respect to air is expected to be present in the gases discharging from the pools. Therefore, there is likely to be a non-atmospheric N_2 component present in the gases; an additional uptake of N_2 was identified. Sedimentary gases generally have N_2/Ar ratios higher than air ($N_2/Ar = 83$). The higher ratios than air can imply that the additional source of N_2 can be of a sedimentary origin (shallow organic) or may even have a deeper source from the mantle. However, only isotope studies would be able to finally clarify the most likely origin of nitrogen.

The CH_4 content, on the other hand, is likely to be derived from shallow organic sources. The occurrence of methane generally indicates crustal component in thermal fluids. In addition, methane is not among the gaseous species in volcanic vapors nor does it occur in meteoric water, but methane is common in sedimentary formation fluids. Organic material, which produces methane, also contains nitrogen. Therefore, all the CH_4 contents are possibly related to the excess N_2, suggesting a shallow organic source for CH_4 and an atmospheric and shallow organic/mantle source for N_2.

8.1.3 Sources of H_2

H_2 can originate from reactions between fractured rocks and groundwater (Sugisaki et al., 1983; Sugisaki, 1987). Several laboratory studies have shown that freshly generated silicate mineral surfaces can catalyse the synthesis of H_2 from water. Since H_2 is probably generated within faulted zones at fresh mineral interfaces, it can be used as a good indicator of fault activity (Sugisaki et al., 1983). Other sources of hydrogen can include the serpentinization of ultramafic rocks (Sato et al., 1986), production via biogenic processes such as bacterial oxidation of H_2S (Nagamine, 1994) and organic sources. To distinguish different H_2 sources, D/H ratios should be analyzed.

Generally, the occurrence of hydrogen can be observed in active volcanic environments and in geothermal areas as a final product of many reactions involving the presence of light hydrocarbons (Capaccioni et al., 1993; Darling et al., 1995). Hydrogen can also

produce as a result of chemical reactions between H_2S and CH_4 (Giggenbach, 1980). Reducing conditions may allow for hydrogen generation through several oxidation reactions of the Fe^{2+} species on the basis of reactions (Neal and Stanger, 1983) such as:

$$2Fe(OH)_2 = Fe_2O_3 + H_2O + H_2 \qquad\qquad (8.2)$$

and

$$3Fe(OH)_2 = Fe_3O_4 + 2H_2O + H_2 \qquad\qquad (8.3)$$
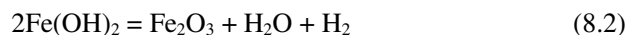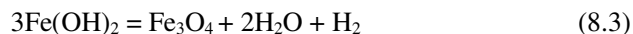
The H_2 gas composition of the pools varies around a value of 0.00187-0.00293 vol.%. H_2 in the mofette gas can be possibly related to deep origins. However, the exact origin of H_2 cannot be determined since there is no D/H determination in the mofette gas. As mentioned above, H_2 can form by interaction of water with fresh mineral surfaces generated by tectonic activities. However, with the current knowledge, it is not possible to evaluate the relation between seismicity and hydrogen production, and therefore origin of H_2 cannot be fully understood.

8.1.4 Sources of O_2 and Ar

Oxygen is the second most abundant gas found in air (around 20%). Argon, as a noble gas, on the other hand, is the most abundant in air and it is characterized by a composition around 1%. Other sources of Argon can include mantle and crustal production (via the decay of K).

Generally, the presence of oxygen in geothermal gases is taken as an evidence of atmospheric contamination. Both O_2 and Ar are considered to be derived from the atmosphere upon dissolution in groundwater during meteoric recharge of geothermal systems. The relatively low oxygen concentrations are due to atmospheric contamination of the gas flow line. The low oxygen content of the discharging fluid is consistent with the gas originated from deep sources because oxygen is a highly active gas which is easily consumed below the depth of a few meters. Like O_2, the Ar concentration in the gas mixture coming from the pools most probably depicts air abundance. This is also evident from the isotopic measurements on Ar; the $^{40}Ar/^{36}Ar$ ratios of the gases sampled from Tekke Hamam reveal an atmospheric origin (near 295.5). Therefore Ar and O_2 can

be accepted as shallow origined gases and their presence in the gas mixture can be attributed solely to air introduction.

8.1.5 Sources of H$_2$S

H$_2$S is found in most geothermal areas and in some oil and natural gas fields. Hydrogen sulphide can have a volcanic origin, as in geothermal areas, or is formed by the decomposition of organic material by bacteria. On reaching the surface, most of the hydrogen sulphide is released from the geothermal fluid along with steam at boiling temperature. At lower temperatures, much of the H$_2$S gas remains dissolved in the geothermal fluid.

A variety of discrete sources for H$_2$S can include: (i) bacterial reduction of sulfate to H$_2$S. The sulfate can be from connate waters, anhydrite dissolution, injected seawater, or pyrite oxidation by injected water; (ii) thermal decomposition of sulfides in kerogen and/or oil (especially in clay-poor, sulfur-rich source rocks). This process typically does not result in gases containing >5% H$_2$S; (iii) thermochemical reduction of sulfate to H$_2$S (TSR), is the reaction of sulfate minerals (primarily anhydrite) and hydrocarbons (beginning at temperatures of 120-140 ºC) to form H$_2$S and calcium carbonate. TSR is the most important process for formation of high-H$_2$S gases (>10% H$_2$S) (Machel, 1998). Because anhydrite is often associated with carbonate sequences, TSR is commonly associated with deep, hot, carbonate reservoirs and/or source rocks. Therefore, the highest concentrations of H$_2$S are found in deep, post-mature gases from carbonate sources.

The H$_2$S concentration of the bubbling pools in Tekke Hamam varies around 0.075 vol.%, and there is a very characteristic smell around the geothermal field, calling for the existence of H$_2$S. The content of H$_2$S is possibly related to a deep origin, that is magmatic. However, since there is no isotopic analyses on hydrogen and sulfur, it is not possible to decide on the exact source of H$_2$S with the current knowledge.

8.1.6 Conclusive Remarks on the Sources of Gases

The block diagram showing the proposed mixing model for the gas emission in Tekke Hamam geothermal site is given in Figure 8.3. The He and CO_2 possibly derive from deep sources, H_2 can be introduced via the faults, proposing that H_2 can be continuously produced in respect to seismic activities, CH_4 appears to be shallow organic, the excess N_2 can be of sedimentary (shallow organic) or mantle origin, O_2, Ar and some part of N_2 are purely atmospheric.

Typical components of the atmosphere, such as O_2, Ar and N_2, are common shallow contaminants of deep rising gases and they can be used as reference components to evaluate the meaning of the more typical hydrothermal geo-indicator gases, such as H_2, CO_2 and He. In conclusion, there is likely to be an interaction between the deep magmatic/crustal and shallow/atmospheric fluids and/or gases.

In addition to the above mentioned possible sources for the discharging gases, there appears to be slight differences observed between the gas compositions of the two pools, Pool 2 and Pool 3. The slight differences observed in the gas composition between the pools located near each other show itself as a similarity for their chemical and isotopic compositions (see Chapter 6). Both pools have similar chemical compositions, that is, they are both Na-Ca-SO_4 in character. In addition, the helium isotope ratios of the gases discharging from the pools appear to be similar. However, regarding the stable isotope composition, Pool 3 appears to be characterized by a more negative stable isotopic composition. Since both pools are characterized by similar helium isotope ratios, they possibly represent gases originating from the same source which have undergone slightly different physico-chemical processes (different pathways and different interaction intervals with rocks leading to different gas compositions) on their way to the surface. Both pools may possibly interact with similar rocks, but they may have different recharging mechanisms leading to slightly different stable isotopic compositions. Therefore, these pools possibly originate from the same source and stay under the effects of slightly different shallow and deep processes (different circulation pathways, different recharging altitudes) leading to slight differences observed in their gas and stable isotopic compositions.
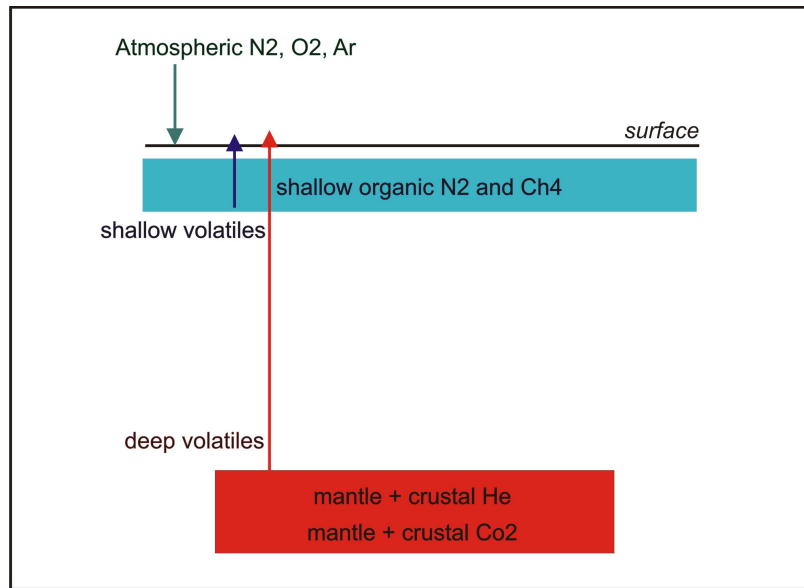
Figure 8.3 Simplified block diagram showing the proposed gas mixing model for the Tekke Hamam pools.

8.2 Gas Monitoring Results

8.2.1 Handling of the Monitoring Data

The raw data (comprising gas compositions (in ASCI format), gas flow rate and pool temperature) from the QMS and the data logger were all gathered into separate monthly files using the EXCEL (Microsoft) software. In addition to these data, meteorological data (air temperature (maximum, minimum, average ºC), air pressure (mbar), precipitation (mm) and evaporation) taken from the Denizli Meteorology Station, and seismic events recorded by the Kandilli Observatory in İstanbul were also incorporated into the monthly raw data files. The data files in EXCEL were then plotted as temporal variation diagrams for every single monitored parameter using the GRAPHER (graphical design) software (Golden Software).

As a result of some technical problems encountered during the course of monitoring, for some time intervals, there is a lack of data. Especially during the months of January and February, 2008, due to the frequent power cut offs and the lacking response of the UPS in the station, data gaps appeared. Also for the whole months of July and August 2008, due to the air contamination in the monitoring setup, data were eliminated. Moreover, owing to an electronical problem encountered in the temperature probe inside the bubbling pool, negative temperature values were recorded for some time intervals during monitoring and these erroneous values were later eliminated from the raw data files. As a result of these inconveniences, lengthy time/data gaps appear in the temporal variation diagrams, and therefore the temporal variations are dealt as temporal variation data blocks.

The temporal variation diagrams are evaluated as 3 separate data blocks:

    i.   Data Block - I: November 2007 – February 2008

    ii.   Data Block - II: March - August 2008

    iii.   Data Block - III: September - October 2008

During the second sampling campaign conducted between 28 August and 2 September 2008, due to the low gas flow rates observed in Pool 2, as another alternative, Pool 3, just next to Pool 2, was used for monitoring. The same monitoring setup was constructed for Pool 3 and monitoring was initiated on the first days of September. Therefore, the first two data blocks represent Pool 2, whereas the third data block represents the variations recorded in the gas composition and flow rate for Pool 3.

8.2.2 Temporal Variations

The nearly year round continuous operation of the gas monitoring setup in the Tekke Hamam geothermal field demonstrates that the gas compositions, as wells as the gas flow rate and pool temperature, show significant variations.

While dealing with the presentation of seismic events in the temporal variation diagrams, a new arbitrary parameter, "**Relative Seismicity**", was created and calculated for each seismic event. This parameter was simply calculated by M/d^2, where M is the magnitude of the event and d the distance from the epicenter to the station (in km). For the sake of presentation this arbitrary value was shown on a logarithmic scale in the temporal variation diagrams. During the year round continuous monitoring, there was not any record of a seismic event having a magnitude exceeding M: 5.0. In addition, seismic events with magnitude M < 3.0 were not given by the Kandilli observatory and therefore were not taken into consideration. During the course of monitoring, a total of 530 earthquakes were recorded. Most of the seismic activities were recorded near the Çameli-Denizli district, which is about 100 km away from the monitoring site. The earthquakes having relative seismicities higher than 1 were considered to be the most significant ones.

The list of seismic events compiled from the website records of the Kandilli observatory are given in Table B.1 in the Appendix B. The temporal variation diagrams of the gas compositions, as well as gas flux and pool temperature, for the whole duration of monitoring are shown in the Appendix C as three separate data blocks (Figure C.1, C.2, C.3).

The general temporal variation characters of the monitored parameters are briefly summarized below for each data block.

Data Block – I

The first data block covers the time interval between 25/11/2007 and 29/2/2008 (Figure C.1). Within this data block two routine field visits were conducted, one on the 29th of December, 2007 and the other on the 23rd of February, 2008. During these field visits the data record was stopped for a short time interval to do some adjustments and data collected during these time intervals were therefore not discussed here.

The variations recorded just after the beginning of monitoring (first two weeks) may indicate ongoing equilibration of the monitoring setup and are dealt with caution. The variations recorded during January are not explained due to the intense air contamination.

Since the data belonging to February is also problematic (owing to the power cut offs), only the variations recorded in the pool temperature are taken into evaluation and shown in the figures.

During this data block, the gas flow rate appears to be nearly constant till the 17th of December, with values changing around 0.2 l/min. A significant increase in the gas flow rate, from 0.2 to 0.35 l/min, is observed around the 17th of December. This sudden increase is followed by a continuous, gradual decrease towards values even lower than 0.2 l/min ($\approx$ 0.1 l/min). Gas flow rate is nearly zero for the whole month of January.

Temporal variations are also observed in the gas compositions during this data block. There seems to be some period of equilibration in the gases for the first days of monitoring, that is, every monitored gas parameter either increases or decreases and later remains constant with values fluctuating. During this data block, CO_2 generally shows a decreasing character from values as high as 96.6 to 95.0 vol.%. In CH_4 there seems to be an increase from 0.38 to 0.44 vol.% towards the end of the data block and values generally change around 0.41 vol.%. Ar, after a slight decrease, varies constantly and generally fluctuates around 0.015 vol.%. H_2 shows a slightly increasing trend from 0.00100 to 0.00170 vol.%. H_2S shows a slight increase and later becomes constantly fluctuating around values of 0.050 vol.%. He shows an increasing trend towards the first half of December and later stays constant with values changing around 0.000660 vol.%. A significant increase and later a constant trend is seen in N_2, with values changing around 3.5 vol.%. O_2 shows a slightly increasing trend towards the end of December and values change around 0.26 vol.%. The pool temperature, on the other hand, shows a slight decreasing trend, possibly in accordance with the decrease in the air temperature.

Data Block – II

During this data block, the field was visited on 8 March, 18 April and 21 June, and the variations belonging to these time intervals are therefore dealt with caution. Problematic data (having the signals of intense air contamination and/or power cut offs) belonging to the first weeks of March and April, and for the whole months of July and August are all eliminated to avoid data confusion.

170

During this data block, the gas flow rate generally varies around 0.4 l/min in March and after the mid of April it changes around 0.2 l/min on the average (Figure C.2). CO_2, CH_4 and N_2 generally show a constant trend for the whole data block and vary around 96.0 vol.%, 0.38 vol.% and 3.5 vol.%, respectively. A slightly increasing trend is seen in He (from 0.000600 to 0.000800 vol.%), H_2S (0.080 to 0.120 vol.%), H_2 (0.00100 to 0.00220 vol.%), O_2 (0.28 to 0.32 vol.%) and Ar (0.012 to 0.016 vol.%) towards the end of the data block. The pool temperature, on the other hand, shows a slightly increasing trend towards the end of the data block, this time in accordance with the increasing air temperature.

Data Block-III

The third data block covers the months of September and October 2008 (Figure C.3). As a result of the slight differences observed between the gas compositions of Pool 2 and Pool 3, for this data block the scale of the y-axis was reorganized for the gas compositions. Since the temperature sensor did not function during this time interval, there is no record of pool temperature data for this data block.

During this data block, the gas flow rate generally varies between 0.6 and 0.8 l/min. In CO_2 for the first week of September a slightly increasing trend and later a decreasing trend is seen and values generally decrease from 98.5% to 98.1%. In CH_4 there is a slightly increasing trend with CH_4 concentration increasing from 0.27 to 0.29% during the data block. A slightly increasing trend is seen in Ar and generally the values change around 0.010 vol.%. A prominent decrease in H_2 values from 0.00340 to 0.00240 vol.% is seen for the whole data block. H_2S shows a constant but very fluctuating variation with values generally changing around 0.075 vol.%. He changes around 0.000410 vol.%. In N_2 after a decrease in the first week there appears to be a slightly increasing trend from 1.0 to 1.4% and later it stays nearly constant. O_2 varies nearly constant and changes around 0.13 vol.%.

As an overall inspection of the whole monitoring data, it can be seen that there exists some interrelation between the variation trends of the gases. For example, variations of CO_2 and He appear to be negatively correlated; that is, an increasing trend in CO_2 is generally seen as a decreasing trend in He. Some gases also seem to exhibit similar

variation trends. The most prominent interrelation in this respect appears between N_2 and CH_4, the former having a dominantly atmospheric and an additional shallow organic/mantle component, and the latter mainly derived from a similar shallow organic source. There seems to be a positive correlation between the variation trends of the two gases, which can be due to their similar sources. For the other gases, on the other hand, no significant interrelation can be identified.

There seems to be no major correlation between the gas flow rate and the gas concentrations. However, it is seen that variations in the gas flow rate can also appear as variations in the gas compositions, that is, variations in the gas flow rate seem to couple with variations in the gas compositions for some periods. The response of change of gas composition to some of the changes in the gas flux can arise from the possibility of changing mixing ratios of gases of different origins in relation to an increase or decrease in the deep gas flux. Such a change in the mixing ratios owing to a change in the gas flux can be the result of (i) an increase or decrease in permeability of deep faults/fractures in relation to seismic activities and an accompanying change in the mixing ratios of deep and shallow gas reservoirs, (ii) air dilution and the corresponding air derived gas introduction into the deep gas flux. However, no basic generalization can be made with the current data.

8.2.2.1 Possible External Factors

Before going into the discussion regarding the observed temporal variations and their possible causes, the external factors that can affect the temporal gas behavior should be first assessed. In this respect, a brief discussion of the possible external factors that can affect the temporal gas behavior within the crust is summarized below.

8.2.2.1.1 Meteorological Factors

The meteorological parameters that were compiled during the course of monitoring comprise the daily air temperature (maximum, minimum and average values), daily air pressure and precipitation. When looked at the possible interrelation between the compiled meteorological parameters, it can be seen that especially times of intense

rainfall is associated with a distinct decrease in the atmospheric air pressure. During drier periods, on the other hand, no significant fluctuation can be observed in the atmospheric air pressure.

Within the meteorological parameters, air temperature can have direct influence on the pool temperature. This is clearly evident from the temporal variations observed in the pool temperature: decreasing values during lower air temperatures and increasing values during higher air temperatures.

Atmospheric air pressure can also affect the gas flow coming from depth. For example, higher atmospheric air pressure may result in the lowering of the gas flow, however, no such relation can still be observed in the data. Also a general relationship is not ascertainable between the air pressure and the variations in the gas compositions, although there appears to be some variations corresponding to the significant atmospheric air pressure fluctuations.

Intense precipitation can also affect the gas behavior. For instance, during periods of intense precipitation, the groundwater table level can fluctuate and can induce some variations in the gases discharging from the ground. Groundwater table or shallow aquifers may affect gas migration from depth. Groundwater table can also buffer any short-term variations in the gas flow from greater depths. The gas solubility of water is temperature dependent; at low temperatures more gas is dissolved. Therefore, a long period of rain can result in an increase in cold meteoric water input into the groundwater, making more gas dissolved in the water table. After the cooling effect of draining water stops, the groundwater can heat up again and can release the additional gases as a result of the decrease in gas dissolution. Therefore, deep gas fluxes can vary in relation to intense precipitation events, most prominently observed in gases that are chemically reactive such as CO_2, which has a solubility very much dependent on the temperature and pH conditions of the environment. Another effect of high amounts of precipitation can be the introduction of air-derived gas components into the groundwater system, such as N_2, O_2 and Ar. Air derived gases can dissolve in groundwater following the solubility law of gases (Henry's coefficient of gas solubility; mainly dependent on the temperature). This can result in the dilution of the composition of the deep gases via admixing of the air

derived gases. In addition to the introduction of air derived gases during rainy periods, biological activities within the pools can also be activated in response to high rainfall, therefore introducing biogenic gases such as CH_4. Consequently, the bubbling gases may be contaminated with atmospheric air and/or dissolved air (O_2, N_2, Ar), and organic gases (CH_4) released from the organic rich sediments at the bottom of the mud pool due to the disturbances by intense rainfall. In fact, during the rainy season, some soapy materials were seen to cover the surface of the pools. These can probably be related to an increased biological activity in the pools owing to the increase in the precipitation or different meteorological conditions.

As an overall inspection, no major correlation can be conceptualized between the variations observed in the gas compositions/flux and the meteorological parameters. However, it is likely that drier periods (having no significant precipitation events) of monitoring, with no significant air temperature and air pressure fluctuations will be more representative of the pure changes of deep gases discharging from the pools. Since the meteorological data were taken from the Denizli Meteorology station, located approximately 40 km away from the monitoring facility, the meteorological parameters can roughly reflect the possible effects of meteorological events on the monitored gas data and it may not be correct to expect one-to-one relation between the variations in the meteorological parameters and the variations observed in the monitored gas data.

8.2.2.1.2 Tidal Effects versus Seismicity

Earth tides and seismicity can generally represent deep earth processes. Earth tides are cyclical, small, and slow ground movements, and are caused by the gravitational attraction of the solar system bodies; primarily the Moon and the Sun, and, to a much lesser extent, the other planets. Earth tides can cause a daily cycle of compressive and tensile stress along faults/fractures within the crust and this can increase or decrease the permeability of faults and can control the migration of gases and/or fluids coming from depth. Seismicity, in contrast to tidal activity, is an instant natural earth process that can occur in any environment. Seismicity can trigger the opening or sealing of new or present pathways for the ascending fluids and can therefore lead to an increase or decrease in the flow of gases from depth, which in turn can appear as abnormal variations in the gas

composition and flow rate. These signals can suggest variations related to the modifications of local permeability as a result of seismic activities. Furthermore a seismic shock may provoke desorption of gas or in gas bearing fluids gas exsolution. The further will result in either an increase or decrease, the latter only in an increase of gas concentration.

Seismic shocks generally release more energy than tidal activities and can therefore override the tensile-compressive effects of tides on the fault/fractures within the crust and may in this regard lead to anomalous variations that cannot be correlated with the cyclic variations induced by the earth tides. Another fact that should be considered is the effect of tides on seismic activities. Although there are some studies that have shown the triggering effects of tides on seismicity, many other studies have revealed that there is no direct correlation between the two deep earth processes (Knopoff, 1964).

Since both seismicity and tides are related to deep earth processes, they can have more profound effects on the deep origined gases, such as CO_2 and He. However, since the gases discharging from depth is representing a mixture of variable sources in different levels of the crust, the effects of both deep processes (seismicity and tidal effects) and shallow processes (meteorological factors, groundwater cooling and the further gas dissolution) can have cumulative effects on the temporal variations of the gases discharged and can therefore mask pure deep or shallow origined variations.

In addition to the deep gases, some studies have shown the production of gases in relation to seismicity. In this respect, especially H_2 has proved to be a good indicator of fault activity since it has been shown by many studies that it can be produced in relation to seismic activities (Sato et al., 1986). Therefore, any significant variation in H_2 can also be correlated with seismicity. However, there is no basic method conceptualized until now how to evaluate which gas is more responsive to which conditions and thus, every monitored site is specific to its own environment and any significant correlation methodology cannot be generalized with the current knowledge.

8.2.2.1.3 Effects of Methodology on the Gas Variations

The gases monitored by the Quadrupole Mass Spectrometer are arranged to sum up to 100 vol.%, that is, any variation in one gas component will produce a direct variation in another gas component. Therefore, during the evaluations of the temporal variations observed in the gas compositions, these mass spectrometer induced variations should also be taken into consideration. It should be kept in mind that, the gases observed in higher compositions will show these variations more prominently than the trace gases. However, there is no way to eliminate the variations induced by the methodology of the monitoring. Only the overall inspection of the possible external factors and their possible influences will show which variations are expected to be real and which are not. It is certain that every variation in the gas composition will bear the methodology induced variations, until they mask it with the earth/meteorology related external factors.

8.2.2.1.4 Air Contamination in the Gas Line

The gases coming from the pools in Tekke Hamam are dominant in CO_2. The increase in N_2, O_2 and Ar and the corresponding decrease in CO_2 composition in the gas mixture coming from the pools, towards values characterizing that of air, can possibly reveal the existence of an increasing air contamination in the gas line (for example January 2008). The main reason for the observed air contamination during monitoring is most probably related to the not fully gas tight connections in the gas line. Since the pools seem to be highly active during the year, even tight connections can deteriorate within time and can lead to air leaks into the system. However, the degree of air contamination is constant, but becomes relatively higher (not absolute) with a lower flow rate from the pools. Therefore, times of lower flow rates are more susceptible to relatively higher air contamination. Also it should be kept in mind that, since the pools represent dynamic systems, the gas fluxes within the pools seem to change spatially with time, sometimes even closed or interrupted by for example biogenic activities or physical blocking (due to mud accumulation in front of the funnel) on the ground of the pools. The decline in the gas fluxes are often associated with a constant and significant increase in the air contamination.

Therefore, the major concerns during the evaluation of the temporal variation diagrams are the possible effects of meteorological factors and earthquakes/tides on the gas composition and flux. After a reconnaissance for possible meteorological influence and/or air contamination, the variations are correlated with the seismic events occurring nearby and any possible significant relation is tried to be evaluated.

8.2.2.2 Components of Variation

The continuous monitoring of the gas compositions, gas flow rate and pool temperature have revealed the existence of different types of variation profiles within the temporal variation diagrams. There are three main components that have been identified from the temporal variation diagrams: daily/diurnal variations, short-term variations and Multi-day variations. Some of them might be linked with geogenic signals.

8.2.2.2.1 Daily/Diurnal Variations

The real-time monitoring of gases revealed the existence of different daily/diurnal variation profiles for all of the monitored geochemical parameters. The daily variation profiles appear as 24-hour, cyclic, symmetrical or asymmetrical shaped variations, frequently changing within the time interval, and are characterized by daily variation amplitudes (distance between the adjacent low and high peak value) which differ for each specific parameter (Figure 8.4).

All gases have different minimum and maximum peaks during different times of the day. For example, O_2, He, H_2 and CO_2 appear to have high peaks at noon and low peaks close to midnight (00:00), whereas N_2 and CH_4 appear to have a low peak at noon and a high peak close to midnight. H_2S and Ar seem to have less identifiable peaks, but still appear to be having a high peak at noon. Pool temperature has a high peak at midday, in conformity with the air temperature maximum. The gas flow rate, on the other hand, seems to have peaks and lows, but frequently changing with time; that is there is no exact daily variation profile identified for the gas flow rate.

The different daily variation profiles of the monitored gas parameters can be correlated with their origin. For example, in soils the biological CO_2 production is enhanced at mean day time, showing a maximum around midday and minimum in the night. However, it should be kept in mind that, since the CO_2 discharging from the pools is mainly deep origined, the shallow induced variations are most probably masked by the deep high CO_2 gas flux. Another example is the peaks observed for N_2 and CH_4. The daily variations in N_2 and CH_4 can be linked to biogenic activities, that is, they may get produced at night and consumed during the day by shallow biogenic activities. Therefore, positive peaks in N_2 and CH_4 are mostly seen towards midnight and lower peaks are seen during the day.

Keeping the above mentioned daily variation characteristics of some of the gases in mind, the nearly 24-hour cycle of the daily variation profiles observed in the monitored parameters are probably linked with shallow processes, such as atmospheric/meteorological parameters and/or biogenic production, rather than deeper ones (tides and seismic activities). However, since the meteorological data is taken daily, not minute wise, a direct correlation cannot be assumed with the current observations.

8.2.2.2.2 Geogenic Signals

There appears to be distinctive variations in the cyclic behavior of the daily variation signals for some parameters, that is, the daily variation profiles are not constant throughout time. These variations can appear as changing daily variation amplitudes, varying shapes of the daily profiles (changing peak positions, changing symmetry), closing and opening of the daily variations and also significant diminishing in the daily variation cycles (Figure 8.5a). In addition to the variations in the geometry of the daily signals, some distinct variations, appearing as positive or negative peaks (sometimes lasting for a couple of days) that superimpose the daily variation can be identified in the data recordings (Figure 8.5b). These abnormal signals do not have any trend and mostly appear as spot-like and sharp variations for short time durations (short-term variations). In addition to the peaks, there appears to be also Multi-day variations, that is, variations that generally last for nearly 2 or more days and appear mostly beyond the limits of the daily variation profiles (Figure 8.5b). Multi-day signals, different than peaks, still bear

the daily variation profiles. After these variations the values sometimes return to the initial values or appear as following a different variation trend.

The above mentioned abnormal variations, superimposing the daily variation profiles, appear to be beyond the effects of tides and can be correlated with either meteorological events (for example periods of intense precipitations) or more likely with geogenic events, that is, seismicity and the resulting effects of stress-strain redistribution within the crust. However, the fact that the multi-day signals bear also the daily variation trend can suggest that, if there is a kind of redistribution within the stress field of the crust in relation to a deep earth process, the effects of shallow processes can be still active and can still be kept within the abnormal signals. In case of peaks exceeding the daily variation profiles, however, it seems that the effects of seismicity overrides the cyclic effects imposed by the shallow processes, that is the daily variation signals appear to disappear for a short time interval. After such anomalous variations, the monitored parameters seem to follow a slightly or distinctly different trend. If the anomalous variations appear to be followed by a similar trend to the pre-anomaly trend, then it can be assumed that the deep or shallow process affecting the gas behavior returns to its original distribution, however, if it appears that the anomalous variations are followed by a disturbed trend, significantly different than the pre-anomaly trend, then the deep/shallow process may have a profound effect on the gas behavior and equilibrium within the crust may have been disturbed for a long time.
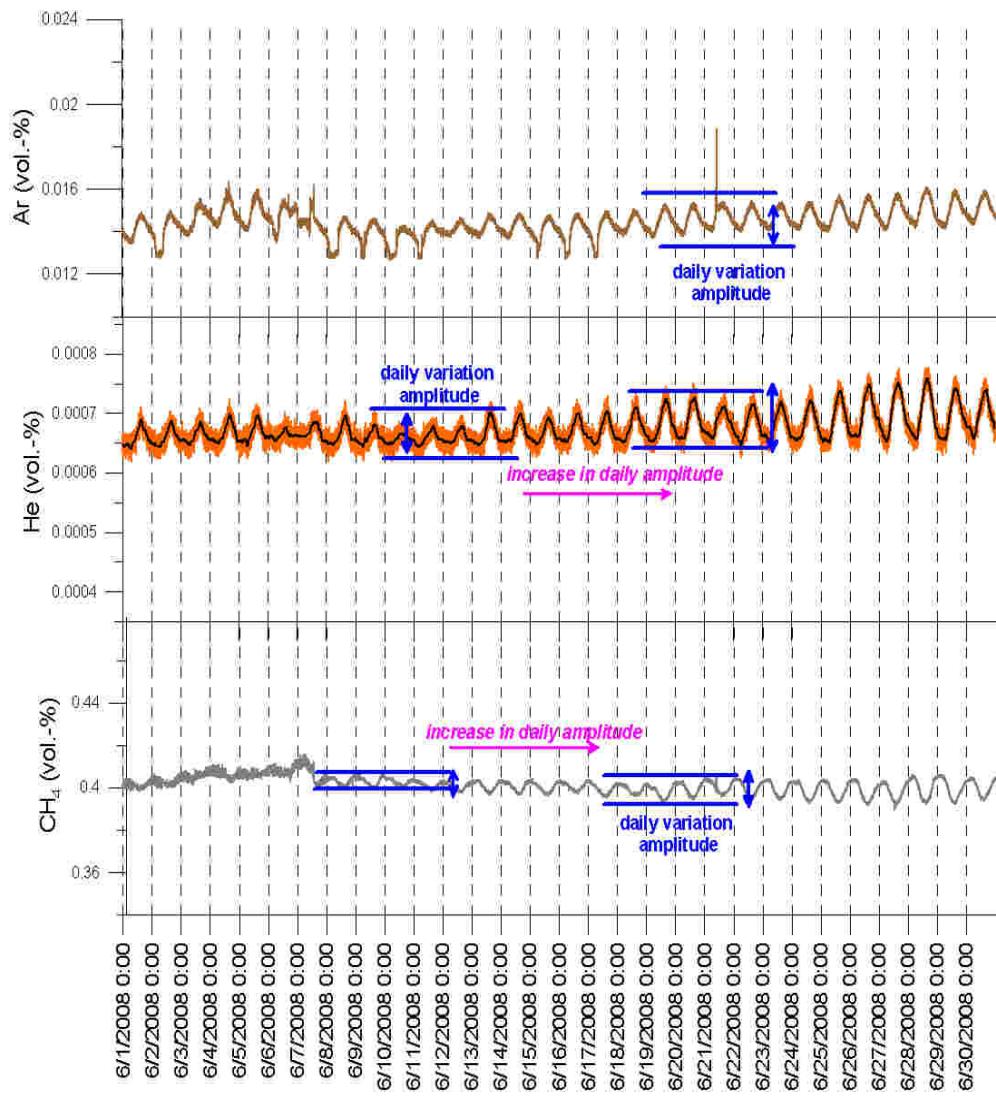
Figure 8.4 Daily variation profiles and varying daily amplitudes.
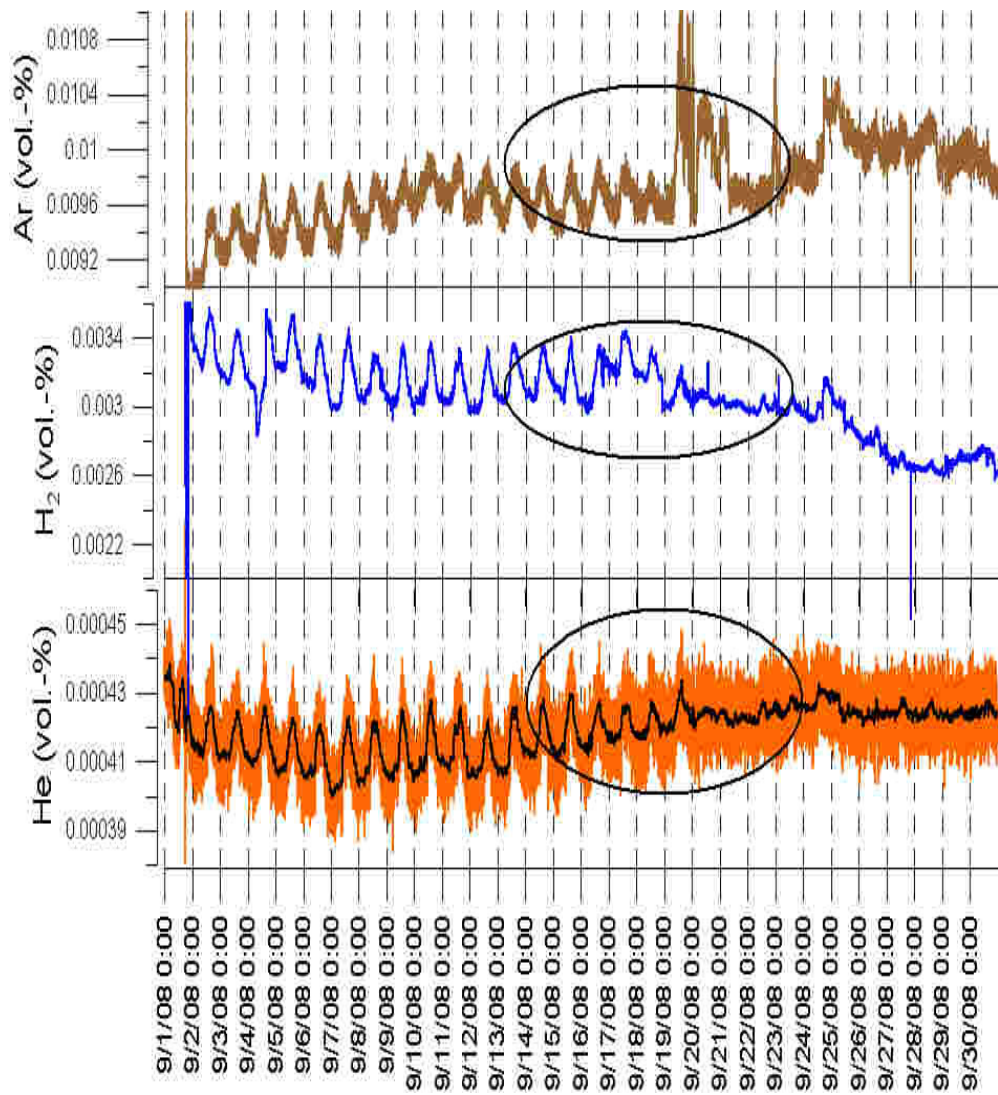
Figure 8.5a Changing shapes of daily variation profiles.
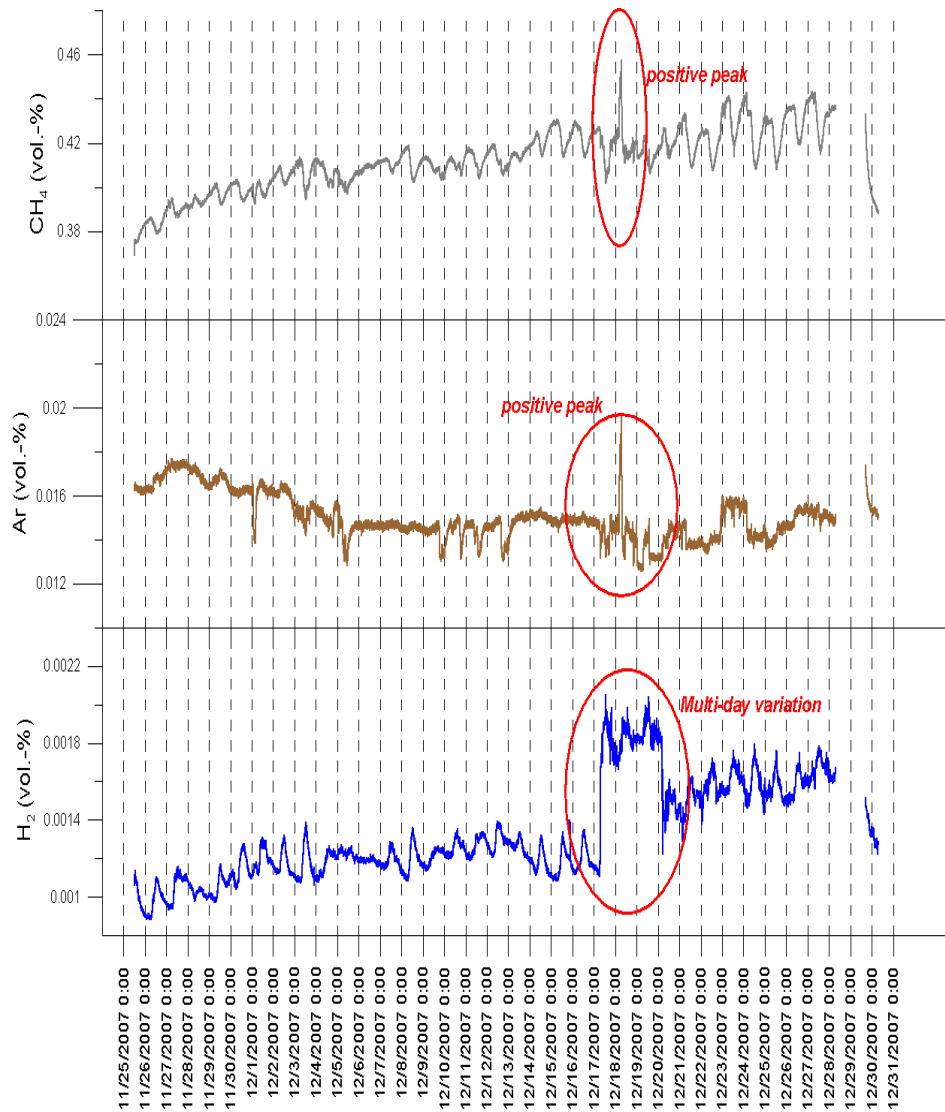
Figure 8.5b Peaks and Multi-day signals in the temporal variation diagrams.

8.2.2.3 Significant Temporal Variations

Gas compositions along with the gas flow rate and pool temperature show significant variations, that is, variations that can be accepted as anomalies. In addition to the gas

compositions, temporal variations in some of the gas ratios are also used as a further earthquake surveillance in the area, since gas ratios can be sensitive parameters to earthquake events, and previous studies in this respect have shown the usefulness of the evaluation of gas ratios (e.g. Kawabe, 1985; Yang et al., 2006). While dealing with gas ratios, in order to identify any possible interaction between deep and shallow derived gases, the best way can be the utilization of different origined gas ratios, such as the ratios of deep versus shallow or shallow versus deep gases. In this respect, the concentration ratios of the deep gas components to Ar, for example, can be used in order to evaluate any possible interaction between deep and shallow gases. Ar can be effectively used in this respect since it is a principal rare gas component that cannot be lost in chemical reactions in the ground. Groundwater usually retains the atmospheric Ar as well as the other rare gases, once dissolved in the original meteoric waters, unless extensive boiling or bubbling occurs underground. The actual contributions of ^{40}Ar from ^{40}K in the subsurface rocks to the total Ar dissolved in groundwaters are negligibly small, because Ar is the most abundant rare gas in the atmospheric air and the solubility of Ar in water is quite large. Therefore, the relative concentrations normalized by the Ar concentration are very useful as showing how much the gas components other than Ar are added to the circulating water/gas or lost from it underground (Kawabe, 1985). The ratios of CO_2 and He to Ar, in this respect, can be used as useful parameters to monitor any possible changes within the deep and shallow gas interaction. In addition to deep versus atmospheric gas ratios, deep versus shallow origined gas ratios can also be used, for example, the CO_2/CH_4 and He/CH_4 ratios. An increase in the deep component can be related to a permeability increase triggered by seismicity, whereas an increase in the shallow gas component can be related to a meteorological and a further biogenic influence.

While dealing with the evaluation of the temporal variations in the monitored data, the variations exceeding the daily variation profiles (peaks, multi-day signals) and variations within the daily variation profiles (changing amplitude and shape) are first tried to be identified. Especially variations observed in more than one parameter at the same time interval is taken into consideration during the evaluation stage. The potentially anomalous signals are first roughly correlated with the observed variations in the meteorological events, that is rainfall events, atmospheric pressure modifications, etc.

After looking for any possible meteorological influence on the gas compositional variations, the next stage is the investigation of seismicity at the times of interest.

The most striking variations detected during the course of monitoring can be summarized as follows:

2-17 December 2007

- The most prominent variations that were recorded during this time interval include the variations in H_2S, Ar, He, CH_4 and O_2. In H_2S there appears to be positive peaks between 4 to 5 December, exceeding the daily variation profile. In Ar there appears to be negative peaks starting from the 2nd of December till the 5th. There are also positive peaks that appear in O_2. Some variations in the daily variation profiles of CH_4 and He can also be observed (a very slight response of the disappearing of the daily variation amplitude). The gas flow rate seems to slightly increase in this time interval, however, no significant variation can still be identified (Figure 8.6a).

Between the dates 2-17 December intense precipitation is observed. Especially for the time interval between 5-7 December, precipitation increases significantly. These precipitations can be the triggering mechanism for the variations observed in the gases mentioned above. High amounts of precipitation can affect the groundwater table level, inducing water table fluctuations. This in turn may disturb the stable structure of the water table and may therefore result in different gas behaviors. As it is known, the solubility of gases in water is a temperature dependent process; at lower temperatures more gas tends to dissolve, whereas at higher temperatures the gases that were initially dissolved in water prefer to stay in the volatile phase and are released from the water. The release of gas from the groundwater may appear as peaks or even disruptions in the daily variation signals. Therefore, a long period of rain in December may have disturbed the groundwater table level and may have resulted in a cold meteoric water admixing to the groundwater, making more gas dissolved in the water table due to the cooling effect of the meteoric water recharge. The cold water recharge may have also introduced air

derived gases into the subsurface and may therefore result in the dilution of the deep gas signal. In addition to the increased amount of precipitation, it is also clearly seen that there is a decrease in the atmospheric air pressure values during this time interval. The decrease in the atmospheric air pressure may have also triggered variations in the gas flux coming from the pool, however, no significant variation can be identified in the gas flow rate corresponding to the decrease in the atmospheric pressure.

In addition to the variations observed in the meteorological parameters, the mentioned time interval also corresponds to an increased seismic activity frequency with seismic events characterized by high Relative Seismicity (RS) values (RS > 1). Especially, there are three seismic events (7, 8, 9th of December) with high Relative Seismicity values. These seismic events can be also the triggering mechanisms of the above mentioned variations. However, it should be kept in mind that, the time interval under consideration is very close to the beginning of monitoring and the variations can actually be within the equilibration stage of the monitoring setup (corresponding to the first two weeks of monitoring).

17 December 2007

- Around the 17th of December, 2007, significant variations are recorded in some of the parameters. Around this date, a very rapid and sharp increase is detected in the gas flow rate, with values increasing from nearly 0.2 l/min to 0.35 l/min, followed by a gradual decrease towards the end of December. The fading of the flow rate also continues in 2008. The increase in the gas flow rate is also coupled with variations in some of the gases. For CO_2, CH_4 and O_2 daily variation amplitude seems to increase after this date. Multi-day variations, lasting for about 2 to 3 days, are seen in H_2 (increase) and H_2S (increases and decreases). Positive and negative peak like variations (short-term variations) are recorded in CH_4 and Ar. The instant increase and the gradual decrease in the gas flow rate seems to be correlated with the variations detected in the gases (Figure 8.6a).

- In addition to the variations in the pure gas compositions, there seems to be also significant variations in the gas ratios corresponding to this time interval (Figure 8.6b). There appears to be instant decrease (within a couple of hours) in the CO_2/Ar and He/Ar ratio, just corresponding to the instant increase in the gas flow rate. Although not as significant, the decrease can also be seen in the CO_2/CH_4 and N_2/Ar ratio. Other gas ratios do not show significant variations around this date. The instant decrease in the gas ratios then follows as positive peak like variations for a couple of days.

As also mentioned above, before the intense variations observed on the 17th of December, a nearly two week period of rain that immediately stopped before the 17th can be seen. Since gas solubility is a temperature dependent process, the intense rainfall might have cooled the groundwater and might have resulted in a higher dissolution of gas. After the rain events, the groundwater may have heated up again and the gases could have been released, therefore leading to intense variations appearing as abnormal peaks in the gas composition. However, the instant variation in the gas flow rate, possibly highlighting the existence of a deep event, can result in the variations observed in the gas composition. If it were the meteorological factors that have induced the variations, then we would expect an earlier signal of the gas flow rate variation, possibly corresponding to the beginning of the rain events. However, the gas flow rate appears as an instant anomaly followed by a gradual decrease to values near zero during the whole data block. Such a significant and instant variation in the gas flow rate may not be linked with a shallow process like precipitation. Therefore, the instant variations observed in the gas flow rate most probably depicts a deep dynamic process, such as a seismicity induced opening or closing of pathways for gases. The instant variations in the gas flow rate can therefore appear as variations in the gas composition/ratio, possibly superimposing the effects of shallow biogenic and/or meteorological processes acting on the gas composition. Especially the increase in the CO_2/Ar and He/Ar ratios of the gases after a sharp decrease can possibly point to an increasing fault permeability that may be occurring in relation to crustal relaxation and an accompanying deep gas input into the shallow gases as a result of seismic triggering. These variations can probably be correlated with the seismic activities that occurred in the area around the 7th, 8th and 9th of December. The frequent

nature of seismic activities in the vicinity of the field leads us to consider the variations related to the composite effect of seismic activities, instead of the effects of a single seismic event. However, there should still be a triggering seismic event that resulted in the instant flow rate variation and the further gas composition variations. The three seismic activities with high Relative Seismicity values may be the triggering earthquakes of the observed coupled variations.

Another interesting point that can be mentioned is the similar variation trends observed in He/Ar and CO_2/Ar ratios. Since both are deep gases, they may be controlled by the same transport processes; possibly CO_2 acting as a carrier gas for the trace He component. Therefore any increase or peak in the variations of the ratios can be related to a flux of deep gas from depth, whereas any decrease may be related to a decrease in fault permeability or a closure of a deep discontinuity in relation to a seismic triggering.

First days of May

- Around the 4th of May there appears to be a small positive peak in the gas flow rate. The daily variation amplitude of H_2S increases in the first 10 days of May and later returns to its normal pattern (Figure 8.7a).

May seems to be dominated by high Relative Seismicity events and since there is no significant meteorological event observed for this month, the variations can probably point the effects of seismic activities. However, since no significant variations are identified in other gases and gas ratios, the observed variations only in a limited monitored data may not be significant.

- There appears to be positive peaks in He/Ar and CO_2/Ar around the mid of May. Also there is a slightly increasing trend in He/CH_4 and He/N_2 ratios. A significant increase and later a decrease is seen in CO_2/CH_4 (Figure 8.7b).

There are high relative seismicity events occurring in May. The mentioned peaks in the gas ratios may result from an increase in the deep gas ratio, since especially He increases

with respect to shallow and atmospheric derived gases. There is also an increase in CO_2, however, later it decreases. In May there are insignificant rainfall events. Therefore the variations observed in the gas ratios can be related to a seismically triggered variation in the mixing ratio of deep and shallow gas components. When we look at gas flow rate, however, there seems to be step wise increases, reaching a flat peak towards the mid of May. The increase in gas flow rate can also be due to an increasing deep gas flux coming from depth (in relation to seismicity), therefore disrupting the mixing ratio of shallow and deep gas in favor of deep gases. On the other hand, when we look at the absolute gas compositions during this time interval, we cannot see any significant variation, therefore it is likely that the variations are amplified when considering the gas ratios.

First week of June

- During the first week of June 2008, distinct variations are observed in some parameters. There appears to be slight variations in the gas flow rate. There appears to be a slight decrease in CO_2 between 3-7 June and an accompanying change in the daily variation profile for the time interval. There is a negative Multi-day variation in H_2S for these time intervals. For Ar there is an increase lasting for a couple of days. Also for CH_4 there is an increasing trend with a closing daily profile. H_2 also shows a slight increase during this time interval. The variations in the gas flow rate seem to be coupled with the variations observed in the gases (Figure 8.8a).

- In the gas ratios a significant decrease can be seen in CO_2/CH_4, CO_2/N_2, CO_2/Ar, He/Ar, He/N_2, N_2/Ar and CH_4/N_2 ratios during the first week of June. These variations are also coupled with a decrease in the gas flow rate (Figure 8.8b).

During the first week of June there are high relative seismicity earthquakes. The decrease in the ratios of He/Ar and CO_2/Ar can be related to a decrease in the deep gas mixing ratio, that is can be related to a decrease in the gas flux from depth in relation to a permeability reduction as a result of seismicity triggering. Deep pathways may be closed

in accordance with compressive stress induced by high relative seismicity events. It is also apparent that there is no significant rainfall event during the first week, with no significant variation in the atmospheric air pressure. The slight increase in the H_2 content can be related to H_2 formation in relation to seismic activities, however, with the current knowledge it is not possible to verify this correlation. Therefore, the observed variations can be the precursory signals of the high relative seismicity events around the 10th of June. Also it is seen that with a gradual decrease in the gas flow rate, the daily variation amplitudes of the gases seem to become significantly disturbed and increase. This can point to the continuing effects of the seismic events, disrupting the general behavior of the gases.

19-20 September 2008

- Around the 19th of September there appears to be an increase in the gas flow rate which lasts for nearly 5 days and after the 24th there is a decrease. For this time interval there are significant variations in CH_4, Ar, H_2, H_2S and He, differing from their daily variation profiles. For the time between 19-20 September there is a rapid increase of about 2 days for CH_4 and Ar. There appears to be a gradual decrease after the 18th of September for H_2, and especially after the 20th of September daily variation amplitude decreases significantly. There appears to be a negative peak lasting for 2 days for H_2S. After the 18th of September the daily variation amplitude of He decreases and follows nearly constant towards the end of the data block. For O_2 the daily variation amplitude also seems to decrease and closes up after the 19th of October (Figure 8.9a).

- In addition to the variations observed in the gas compositions, a decrease is observed in the CO_2/Ar and He/Ar ratio (negative peaks or negative multi-day signals) around the 19th of September. A very slight decrease is also seen in He/N_2. A slight decreasing trend is seen during 19-20 September also in CO_2/CH_4. The other gas ratios seem to be constant with no significant variations (Figure 8.9b).

189

The variations in the gas compositions and gas ratios correspond to an increased precipitation event (starting after the 20th). There seems to be a decrease in the atmospheric air pressure (after the 18th) in relation to the high precipitation. Also a sharp decrease appears in the average air temperature. Keeping in mind that there is no significant variation in the gas flow rate, the observed variations can be related to the shallow processes. Especially the increase in Ar, N_2, and O_2 can suggest that there can be an input of cold meteoric water recharge, in relation to a precipitation event. The decreases observed in the gas ratios, CO_2 and the disappearing of the daily signal in He can also suggest an increase in the shallow origined gases, thereby disrupting the mixing ratios of deep and shallow gases, in favor of the shallow ones. The decrease in the atmospheric air pressure may induce a slight increase in the gas flow rate. Therefore the increased gas flow rate for a duration of a couple of days may have been triggered by the variations in atmospheric pressure in relation to the increased rainfall.

In addition to a possible meteorological influence, there are also seismic activities recorded during this time interval. Between the mentioned dates the seismic frequency is not so high, however, there are seismic events with Relative seismicities exceeding or close to 1. Since there is no significant variation observed in the gas flow rate, the variations detected in the gas compositions and gas ratios mentioned above may not be related to a deep dynamic process. However, there can also be a cumulative effect of both seismicity and meteorological factors on the gas variations, possibly the meteorological factors masking any possible influence of seismicity.
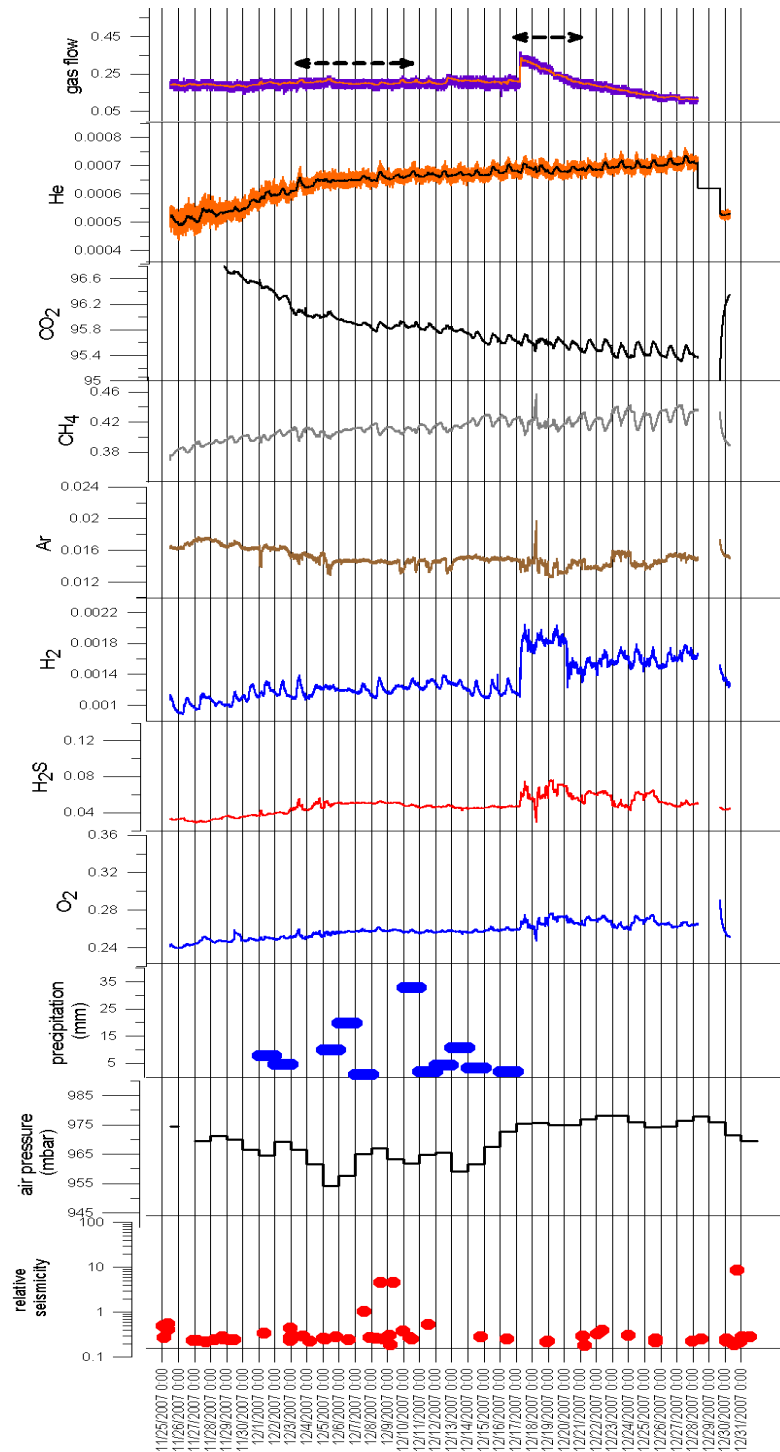
Figure 8.6a Temporal variations around 2-17 December and the significant variations around the 17th of December, gases in vol.%.
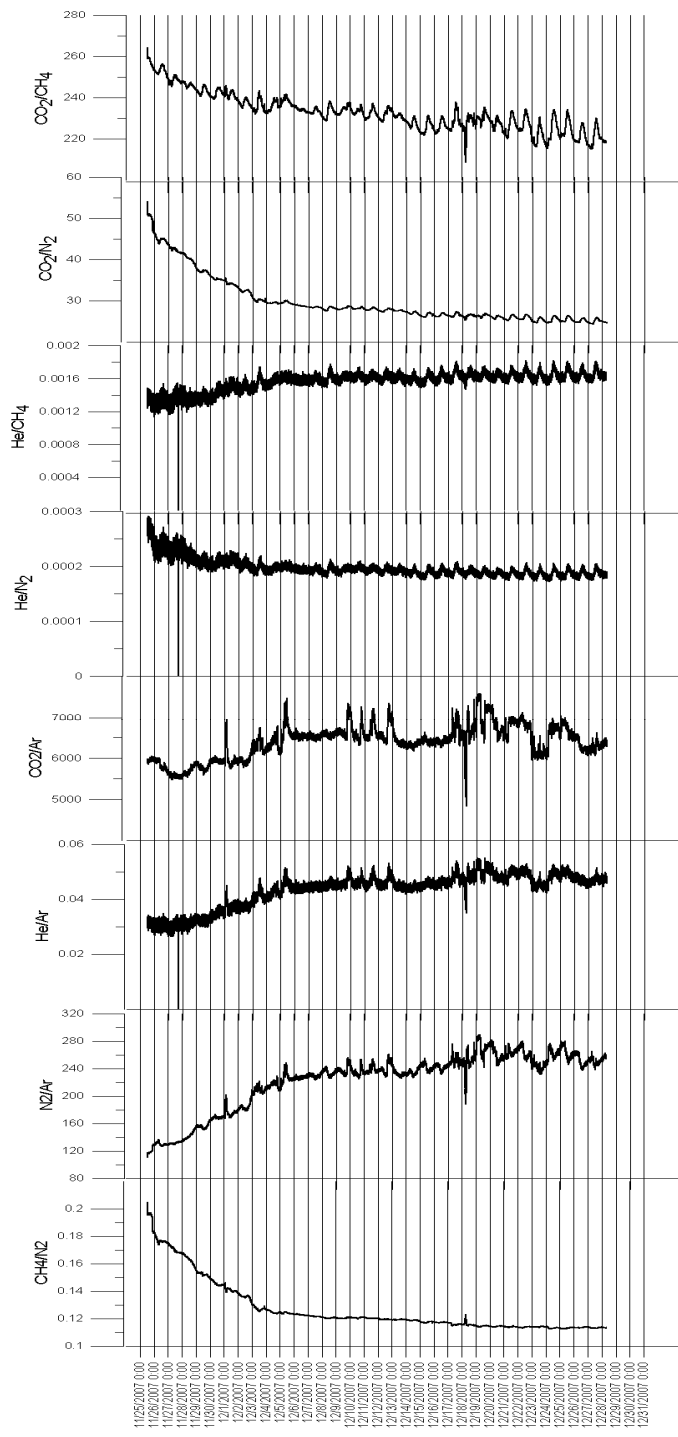
Figure 8.6b Temporal variations in the gas ratios around the 17th of December.
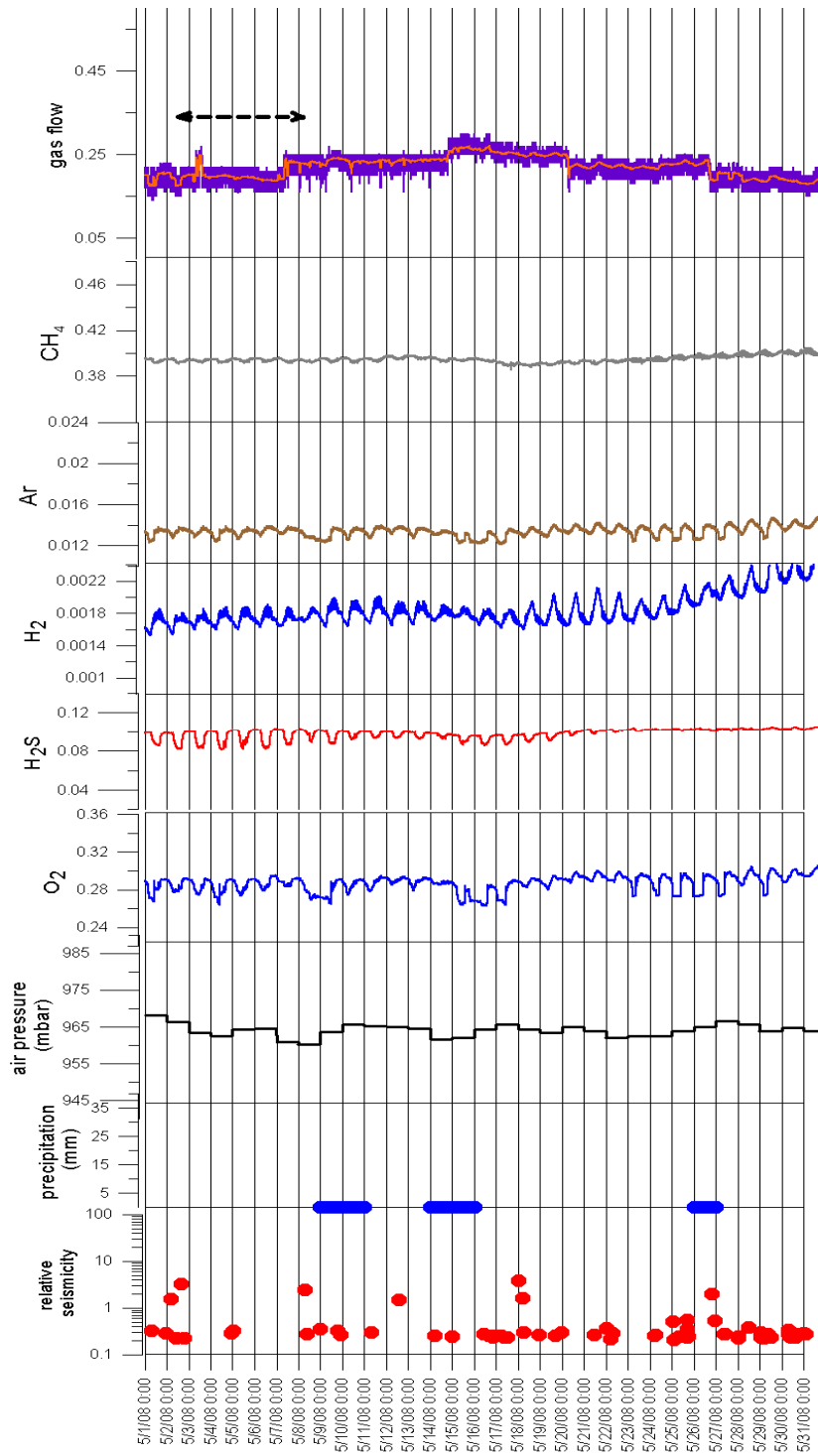
Figure 8.7a Temporal variations around the first days of May, gases in vol.%.
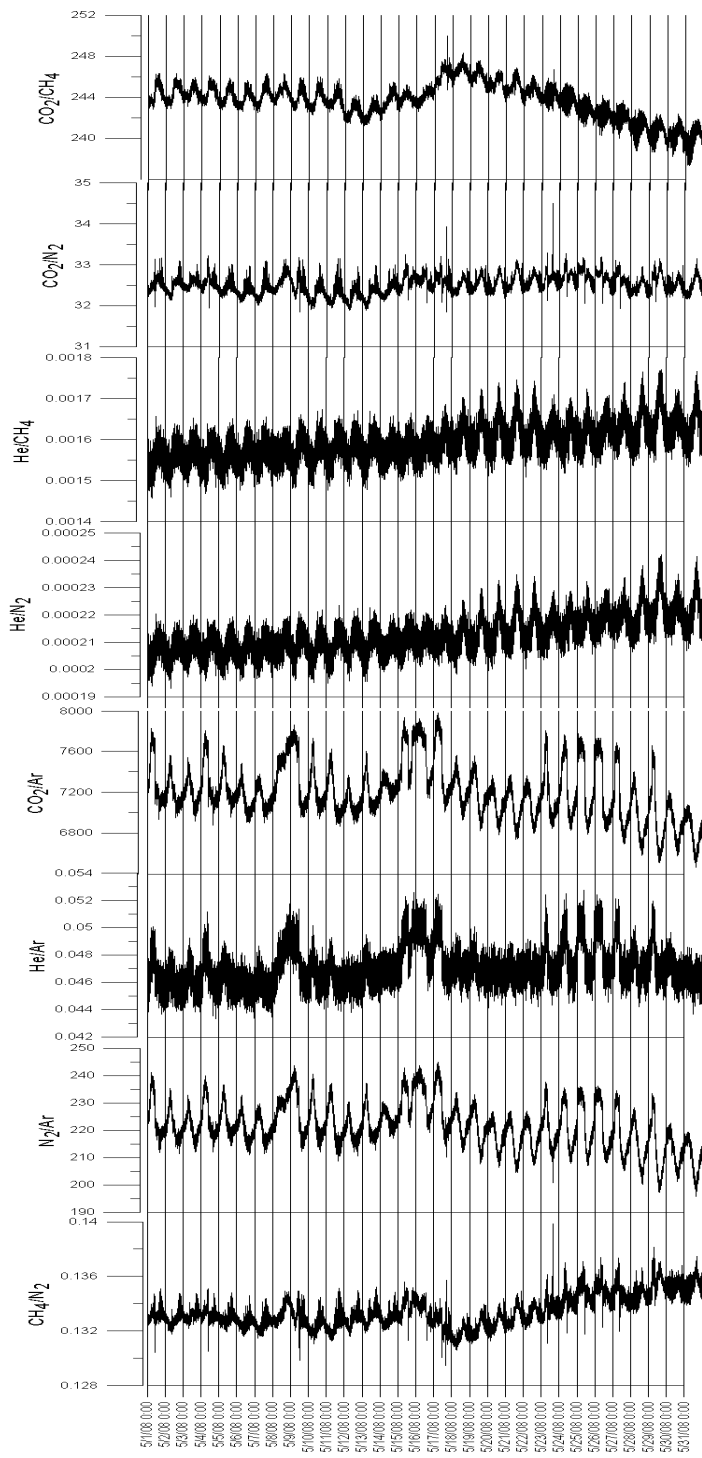
Figure 8.7b Temporal variations in gas ratios around the mid of May.
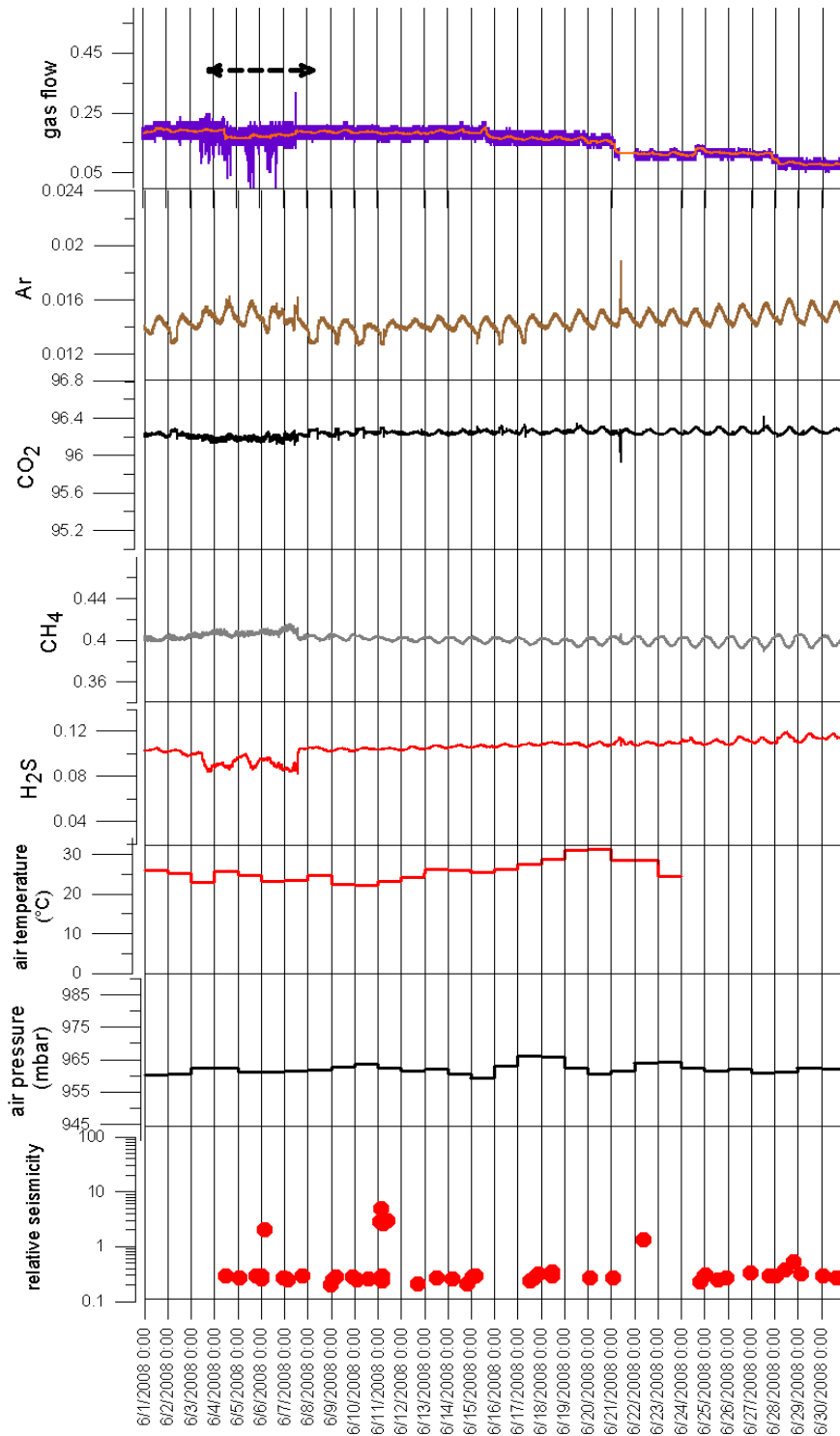
Figure 8.8a Temporal variations around the first week of June, gases in vol.%.
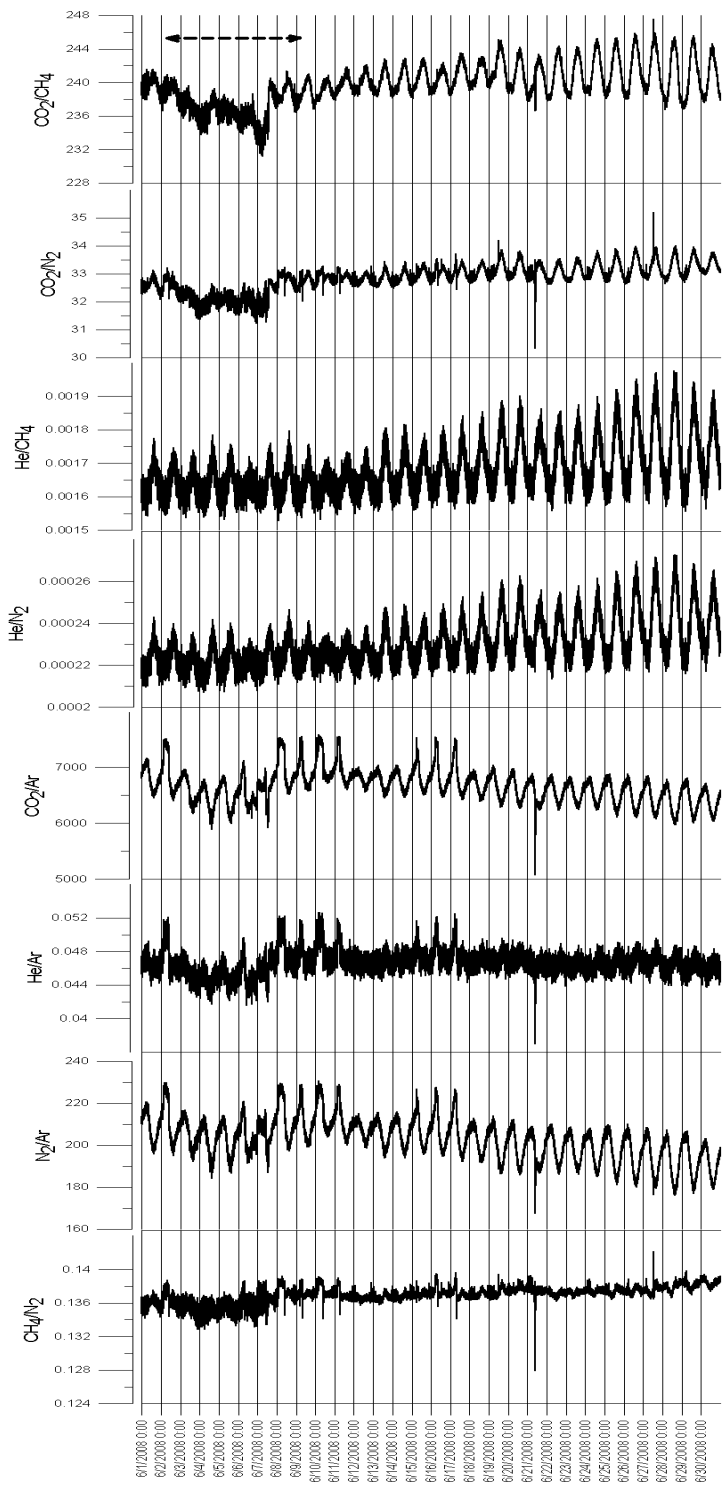
Figure 8.8b Temporal variations in gas ratios around the first week of June.

196
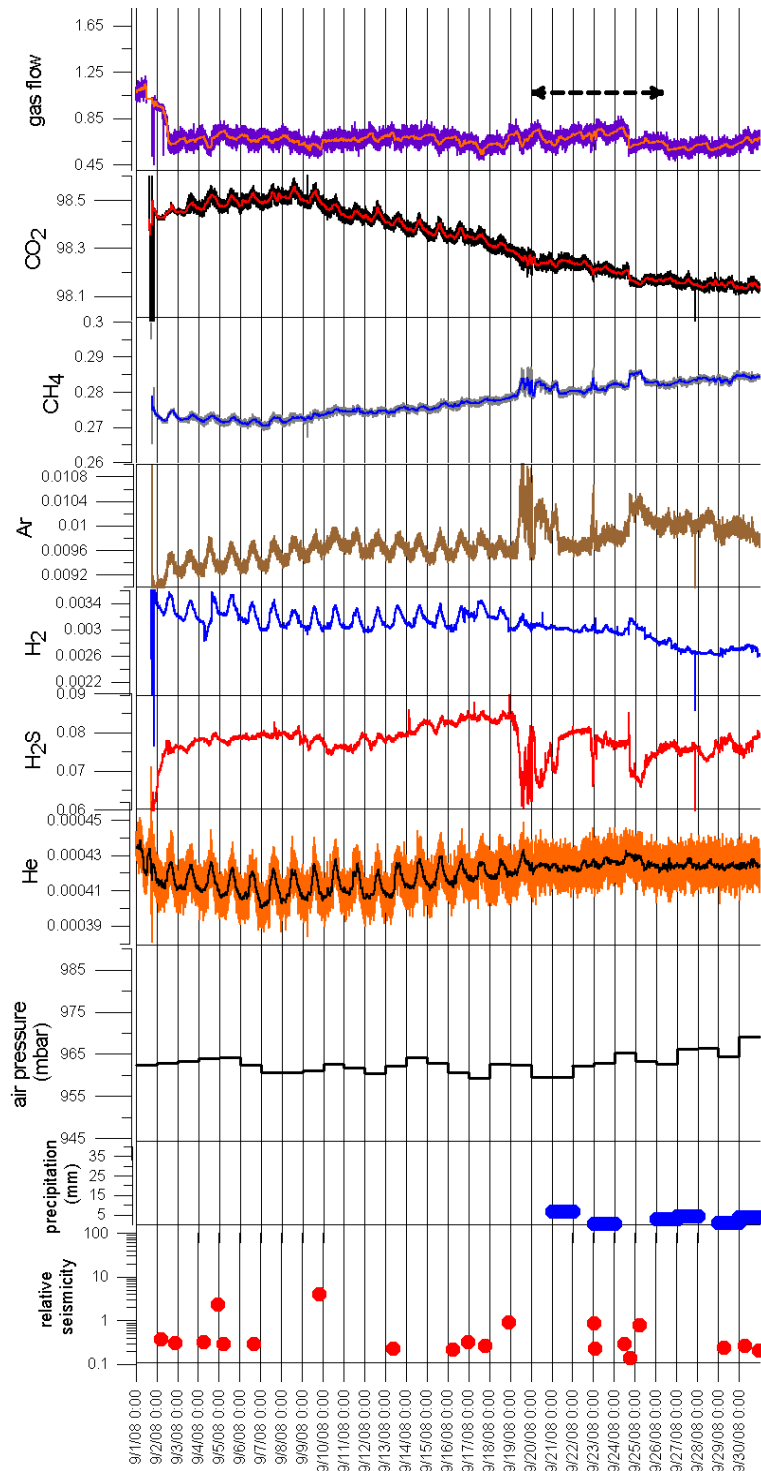
Figure 8.9a Temporal variations around 19-24 September, gases in vol.%.

197
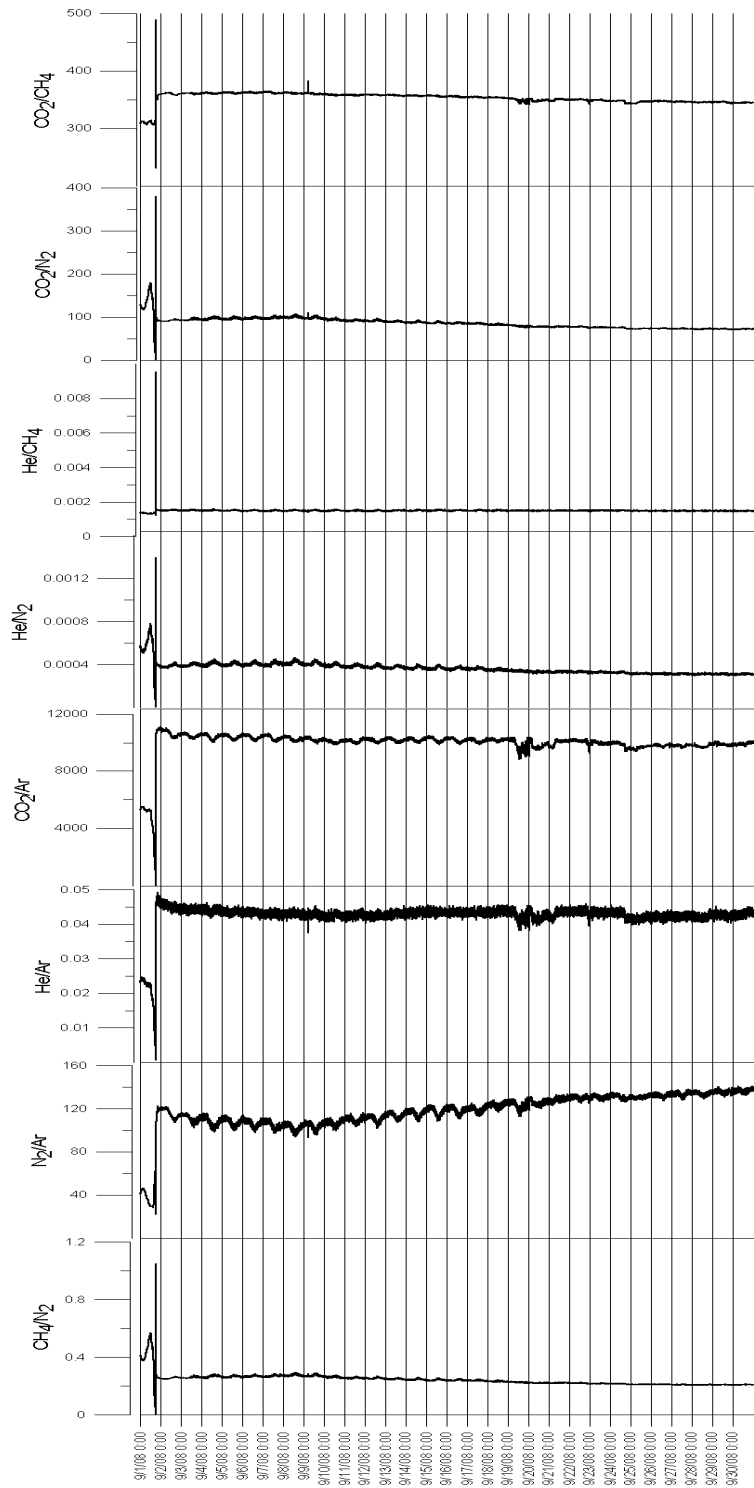
Figure 8.9b Temporal variations in gas ratios around 19-24 September.

8.2.2.4 Concluding Remarks on Gas Monitoring Results

The foregoing discussion regarding the observed temporal variations and their possible triggering mechanisms can therefore be summarized as follows:

- The temporal variation diagrams have revealed the existence of different variation patterns for every monitored parameter. Of these the daily/diurnal variation profiles are the most prominent ones observed for all of the monitored parameters. The symmetrical or asymmetrical distribution of the daily variation profiles in the temporal variation diagrams appear to be shallow related, that is, appear most probably in relation to the meteorological effects such as daily production and consumption of gases.

- The abrupt variations in the gas compositions/gas ratios and flow rate is probably not correlated with the cyclic tidal activities and can therefore be related either to seismic events occurring nearby or to the meteorological influences, especially during heavy rainfalls.

- Seismicity is a mechanical deep process, it leads to fracture/fault opening or closing, therefore if a seismic event is to affect the gases, it can probably show itself as a variation in the gas flux from depth. The variation in the gas flow rate can then lead to different mixing proportions between gases in deep and shallow reservoirs. For example, an increase in the CO_2 composition may not suggest that there is a higher CO_2 flux coming from depth, it can actually mean that there is some kind of redistribution in the mixing proportions of the gases from deep and shallow reservoirs. The observed variations could have been induced by varying mixing ratios of deep and shallow origined gases as a result of a permeability modification due to rock fracturing in response to seismic energy release during or prior to the earthquakes.

- Meteorological factors can be assumed as shallow processes. They can induce variations in the gas composition/ratio through change in groundwater temperature or introduction of air derived gas components or even through the triggering of biogenic activities, thereby introducing atmospheric or biological gases, mainly N_2, O_2, Ar and CH_4. However, a significant variation in the gas flow rate is not expected from such shallow processes.

- Any coupled variation in the gas flow rate and gas composition/ratio can possibly reflect the existence of a deep dynamic process, however, if there is only variation in the gas composition/ratio during a meteorologically anomalous period, then it can be correlated with the meteorological events. However, there is no conceptualized method to discriminate the possible effects of meteorology and seismicity.

- Both gas compositions and ratios appear to be useful in evaluation of the temporal variation diagrams. However, the gas ratios seem to impose an advantage regarding the possible interaction between deep and shallow origined gases in that the absolute concentration of a subsurface gas component could be altered by dilution of the other component, such as CO_2 formed in the ground, or by preferential loss of another major component, such as the chemical consumption of O_2 under reducing subsurface conditions. But these effects do not influence the concentration ratio of the gases being monitored. Therefore, gas ratios seem to highlight possible deep crustal interactions better than the gas compositions.

- Since the area of interest experiences several frequent low-medium magnitude seismic events (magnitudes generally varying between 3.0 and 4.0), the observed abnormal signals or variations in the temporal variation diagrams are possibly related to the composite/cumulative effect of the seismic events, rather than the effect of a single event. Nevertheless, there should be a seismic event that triggers the gas

200

discharge. When looked in detail, no direct correlation can still be identified; gas composition variations do not seem to follow the seismic activity occurrences and it is hard to identify a direct correlation since the area is mostly active in terms of seismicity, avoiding the chance of seeing the gas composition representing a seismically quiescent period.

The nearly one year real-time monitoring study conducted in the Tekke Hamam geothermal field showed the importance of mainly two aspects:

i)   discrimination of possible external factors that can affect the deep gas behavior. In this regard, importance should be given to the elimination of possible meteorological influences in such studies. In order to catch a pure earth-related variation, monitoring equipments should be installed deep into the crust, deep enough to be absent from the effects of shallow processes, such as meteorological events. Since the monitoring equipment installed near the pools in the Tekke Hamam geothermal field does not penetrate into the deeper portions of the crust (the inverted funnel dipped inside the pools not deeper than 1 m), the gases discharging should possibly be under the effects of both shallow and deep processes. However, it is possible that sometimes deep and sometimes shallow processes may mask important variations.

ii)   accumulation of background data of gas compositions during relatively seismically quiescent periods. Unfortunately, the high frequency of seismic activities in the vicinity of Denizli makes it a difficult task to decide on the background values of the recorded gas compositions. Nevertheless, sudden variations in the gas compositions, gas ratios and gas flow rates can be accepted as anomalies and can be correlated with the seismic activities occurring nearby, during times without any significant meteorological event.

Therefore, in order to better evaluate the possible relationships between instant gas signals and seismicity, monitoring studies adopting longer monitoring periods, with less data gaps, and with the least possible meteorological influence is necessary.

CHAPTER 9

CONCLUSIONS AND RECOMMENDATIONS

The main conclusions drawn from the thesis study can be summarized in two separate headings, as follows:

1. Gas Monitoring in the Tekke Hamam geothermal field

- Different components of variations are observed in the compositions the gases discharging from the ground of the bubbling pools in the Tekke Hamam geothermal field. Within these, the most prominent ones are the daily variation profiles and peak/Multi-day signals. The daily variation profiles observed in each monitored parameter is probably correlated with shallow processes, most likely meteorological events such as rainfall and the accompanying variations in the atmospheric pressure. The variations appearing as either positive or negative peaks or Multi-day signals, beyond the limits of the daily variation profiles, are mainly correlated with seismic events occurring nearby, particularly at times of no significant meteorological events (e.g. intense rainfall). Especially the coupled variations in the gas flow rate and composition can be interpreted as variations due to permeability modifications within the subsurface as a result of seismic triggering. In addition to gas compositions, some gas ratios also show significant variations that seem to be coupled with those detected in the gas flow rate. However, no direct correlation can be conceptualized regarding the variations in the monitored gas data and the compiled meteorological and seismic events, owing to the different time scale of the meteorological parameters (daily data, not in minute scale as for the gas monitoring data) and the frequent nature of seismicity in the vicinity of the fields.

- The gases emanated from the ground of the pools in the Tekke Hamam geothermal field are evaluated as shallow and/or deep origined gases. Especially the high composition of CO_2 (nearly 96-98%) in the gas mixture and the high mantle-He flux (calculated to be around 34% from the helium isotopic compositions) possibly reveals a deep origin for these gases; a magmatic and/or thermometamorphic component for CO_2 as revealed by the $CO_2/^3He$ ratios, and a mantle-crustal admixture for helium. Ar and O_2 are mainly atmospheric in origin owing to the high abundance of Argon in air (close to 1%) and the very low abundance of O_2 in deep environments. The atmospheric origin for Argon can also be suggested from the Argon isotopic ratios, $^{40}Ar/^{36}Ar$ and $^{38}Ar/^{36}Ar$, which appear to be close to that characterizing air. The N_2 content of the discharging gas appears to be a mixture of atmospheric and nonatmospheric (sedimentary and/or mantle) sources. The CH_4 is probably shallow organic (sedimentary) in origin as the excess N_2 since it appears to correlate with the excess N_2. The H_2S and H_2 possibly have deep origins. However, since there is no isotopic analyses except for He and Ar, it is not possible to define the exact origin of the gases discharging from the Tekke Hamam geothermal field.

2. Geochemical evaluation of the Kızıldere and Tekke Hamam geothermal fields

- The well waters in the Kızıldere geothermal field are all $Na-HCO_3$ in character with relatively high SO_4 contents, whereas the well waters in the Tekke Hamam geothermal field are $Na-HCO_3-SO_4$ in character. The Tekke Hamam pool waters, on the other hand, are mainly SO_4 dominated. Both fields are characterized by high boron, silica and low Sr contents. The cold waters collected from the vicinity of the fields show different compositions, but appear to be mainly $Ca-Mg-HCO_3-SO_4$ in character, with low B, Si and high Sr contents. The chemical composition of the well waters from both fields possibly reflect the existence of deep water-rock interaction processes and the accompanied effects of deep origined gases, mainly CO_2 and H_2S. The pool waters in Tekke Hamam, on the other hand, can be interpreted as the shallow surface expressions of the deep thermal reservoir, which appear to evolve as a result of interaction with gypsum

204

levels and the near surface H$_2$S oxidation, accompanied by leaching of the wall rocks through which gas/fluid circulates.

- The δ^{18}O and δD compositions of the thermal/cold waters reveal an essentially meteoric origin for both Kızıldere and Tekke Hamam geothermal waters. The Tekke Hamam pool waters appear to be intensely affected by evaporation and show significant compositional variations possibly due to seasonal changes and the further change in the ambient air temperature. The well waters from both fields, on the other hand, possibly reflect deep high temperature water-rock interaction processes leading to oxygen isotope shifts, and they do not show any significant temporal variation, as also verified by their chemical compositions.

- The noble gas concentrations of the gas samples collected from both fields reveal the existence of an appreciable mantle helium component prevailing in the gases dissolved in the deep fluids. The mantle helium component in the Tekke Hamam geothermal field appears to be higher than that dissolved in the Kızıldere waters. There appears to be a slight increasing trend in the mantle helium component from Kızıldere to the Tekke Hamam site; however, since there is no known geothermal field existing between the two fields, it is not possible at this stage to define the nature of the increase, whether it is a continuous increase or a discontinuous, irregular increase possibly affected by the alignment of tectonic features. It is possible, however, to attribute the R/R$_a$ ratio of well R-1 (the lowest ratio recorded within the wells) to a possible non-active fault constituting a barrier between R-1 and the other wells in the Kızıldere geothermal field. The high R/Ra ratios and relatively higher helium abundances of the Tekke Hamam gas samples (compared to Kızıldere) can possibly suggest different mantle-He flux variably contaminated by radiogenic helium for the geothermal fields. However, conceptualization of this model requires more He data with a broader spatial distribution. The other noble gases (Ne, Ar, Kr and Xe), on the other hand, are probably atmospheric in origin owing to their isotopic ratios close to the air values.

The present thesis study has shown the importance of real-time geochemical monitoring studies in relation to earthquake prediction. The frequent nature of seismicity in the Tekke Hamam geothermal site has made it difficult to catch variations related to seismic events. Also the different time scale for the meteorological data prevents a more precise direct correlation with the monitored gas data. Nevertheless, anomalous variations, both in the gas flow rate and composition/ratio, can be observed and can be correlated with earthquakes, mainly at times of insignificant shallow surface processes (e.g. in the absence of high rainfall), since it is possible that sometimes even shallow processes can mask deep gas flux possibly triggered by seismicity.

Therefore, it should be kept in mind that, in order to better evaluate the possible relations between earthquakes and gas behavior within the crust, monitoring sites should be devoid of external factors as much as possible to see the purest earth-related variations, and longer monitoring durations should be adopted. Also it is of great importance to decide on the location of the monitoring setup, for it is better to be constructed near tectonic features which are the best known transport media for the deep reaching gases and can thus reflect instant variations in the gas flux triggered by seismicity.

REFERENCES

Aeschbach-Hertig, W., Peeters, F., Beyerle, U. and Kipfer, R., 1999. Interpretation of dissolved atmospheric noble gases in natural waters. Water Resources Research, 35, 2779-2792.

Aeschbach-Hertig, W., Peeters, F., Beyerle, U. and Kipfer, R., 2000. Palaeotemperature reconstruction from noble gases in groundwater taking into account equilibration with entrapped air. Nature, 405, 1040–1044.

Akkök, R., 1983. Structural and metamorphic evolution of the northern part of the Menderes massif: new data from the Derbent area and their implication for the tectonics of the massif. Journal of Geology, 91, 342–350.

Allard, P., 1986. The origin of hydrogen, carbon, sulfur, nitrogen and rare gases in volcanic exhalations: evidence from isotope geochemistry, in Tazieff, H., and Sabroux, J.-C., eds., Forecasting Volcanic Events: Elsevier, Amsterdam, 337-386.

Allegre, C.J., Staudacher, T. and Sarda, P., 1986. Rare gas systematics:formation of the atmosphere, evolution and structure of the Earth's mantle. Earth and Planetary Science Letters, 81, 127–150.

Allègre, C.J., Hofmann, A. and O'Nions, K., 1996. The Argon constraints on mantle structure: Geophysical Research Letters, 23, 3555-3557.

Alparslan, T., 1970. Denizli Sarayköy Kızıldere sahası sismik etüdü. MTA Ön Rapor.

Anderson, D.L., 2007. New Theory of the Earth. Cambridge University Press. 377p.

Andrews, J.N. and Lee, D.J., 1979. Inert gases in groundwater from the Bunter sandstone of England as indicators of age and paleoclimatic trends. Journal of Hydrology, 41, 233–252.

Andrews, J.N., 1992. Mechanisms for noble gas dissolution by groundwaters In: Isotopes of Noble Gases as Tracers in Environmental Studies. IAEA, Vienna, 87–110.

Arpat, E. and Bingöl, E., 1969. The rift system in western Turkey: thoughts on its development. Mineral Research and Exploration Institute of Turkey Bulletin, 79, 1-9.

Attendorn, H.G. and Bowen, R.N.C., 1997. Radioactive and Stable Isotope Geology. Chapman & Hall, London, 522 p.

Ayan, M., 1973. Gördes migmatitleri. MTA Dergisi no. 81, 132-155.

Ballentine, C.J., O'Nions, R.K., Oxburgh, E.R., Horvath, F. and Deak, J., 1991. Rare gas constraints on hydrocarbon accumulation, crustal degassing and groundwater flow in the Pannonian Basin. Earth and Planetary Science Letters, 105, 229–246.

Ballentine, C.J. and Burnard, P.G., 2002. Production, release and transport of noble gases in the continental crust. In Noble Gases in Geochemistry and Cosmochemistry (eds. D. R. Porcelli, C. J. Ballentine, and R. Weiler). 47, 481–538.

Ballentine, C.J. and Sherwood Lollar, B., 2002. Regional groundwater focusing of nitrogen and noble gases into the Hugoton-Panhandle giant gas field, USA. Geochimica et Cosmochimica Acta, 66, 2483-2497.

Ballentine, C.J., Burgess, R. and Marty, B., 2002. Tracing fluid origin, transport and interaction in the crust. In Noble Gases in Geochemistry and Cosmochemistry (eds. D. R. Porcelli, C. J. Ballentine, and R. Weiler), vol. 47, 539–614.

Ballentine, C.J., Marty, B., Lollar, B. S. and Cassidy, M., 2005. Neon isotopes constrain convection and volatile origin in the Earth's mantle. Nature, 433, 33–38.

Borchiellini, S., Campredon, R. and Bernat, M., 1991. Ground variatin of Radon 222 for location of hidden structural features. Examples of the South of France (Alpes Maritimes). Pure and Applied Geophysics, 135, 625-638.

Bozkurt, E., 1996. Metamorphism in the Palaeozoic schists of the Southern Menderes Massif: field, petrographic, textural and fabric data from Selimiye (Milas-Muğla) area. Turkish Journal of Earth Sciences, 5, 105−121.

Bozkurt, E., 2000. Timing of extension on the Büyük Menderes Graben, western Turkey, and its tectonic implications, in: Bozkurt, E., Winchester, J.A., Piper, J.D.A. (Eds.),

Tectonics and magmatisim in Turkey and the surrounding area, Geological Society Special Publication no. 173, Geological Society, London, 385-403.

Bozkurt, E., 2001. Neotectonics of Turkey – a synthesis. Geodinamica Acta, 14, 3–30.

Bozkurt, E., 2002. Discussion on the extensional folding in the Alaşehir (Gediz) Graben, western Turkey. Journal of the Geological Society, London, 159, 105-109.

Bozkurt, E., 2003. Origin of NE trending basins in western Turkey. Geodinamica Acta, 16, 61-81.

Bozkurt, E., 2004. Granitoid rocks of the Southern Menderes Massif (southwest Turkey): field evidence for Tertiary magmatism in an extensional shear zone. International Journal of Earth Sciences, 93, 52−71.

Bozkurt, E., 2007. Extensional vs Contractional Origin for the Southern Menderes Shear Zone, Southwest Turkey: Tectonic and Metamorphic Implications. Geological Magazine, 144, 191−201.

Bozkurt, E. and Park, R.G., 1994. Southern Menderes Massif: an incipient metamorphic core complex in western Anatolia, Turkey. Journal of the Geological Society, London, 151, 213−216.

Bozkurt, E. and Park, R.G., 1997. Evolution of a mid-Tertiary extensional shear zone in the Southern Menderes Massif, western Turkey. Bulletin of Geological Society of France, 168, 3−14.

Bozkurt, E. and Mittwede, S.K., 2001. Introduction to the geology of Turkey-a synthesis. International Geology Review, 43, 578-591.

Bozkurt, E. and Sözbilir, H., 2004. Tectonic evolution of the Gediz Graben: field evidence for an episodic, two-stage extension in western Turkey. Geological Magazine, Cambridge Univ. Pres, 141, 63–79.

Bozkurt, E. and Mittwede, S.K., 2005. Introduction: evolution of Neogene extensional tectonics of western Turkey. Geodinamica Acta, 18, 153−165.

Bozkurt, E. and Rojay, B., 2005. Episodic two-stage Neogene extension and short-term intervening compression in Western Turkey: field evidence from the Kiraz Basin and Bozdağ Horst. Geodinamica Acta, 18, 299-316.

Bozkurt, E., Winchester, J.A. and Park, R.G., 1995. Geochemistry and tectonic significance of augen gneisses from the southern Menderes Massif (West Turkey). Geological Magazine, 132, 287–301.

Brauer, K., Kampf, H., Strauch, G. and Weise, S.M., 2003. Isotopic evidence (^{3}He/^{4}He, ^{13}C$_{CO2}$) of fluid triggered intraplate seismicity. Journal of Geophysical Research, 108 (B2), 2070.

Buyanovsky, G.A. and Wagner, G.H., 1983. Annual cycles of carbon dioxide level in soil air, Soil Sci. Soc. Am. J., 47, 1139– 1145.

Candan, O., 1995. Menderes Masifinde kalıntı granulit fasiyesi metamorfizmasi. International Journal of Earth Sciences, 4, 35-55.

Candan, O., Dora, O.Ö., Oberhänsli, R., Çetinkaplan, M., Partzsch, J. H., Warkus, F. C. and Dürr, S., 2001. Pan-African high-pressure metamorphism in the Precambrian basement of the Menderes Massif, western Anatolia, Turkey. International Journal of Earth Sciences, 89(4), 793–811.

Capaccioni, B., Martini, M., Mangani, F., Giannini, L., Nappi, G. and Prati, F., 1993. Light hydrocarbons in gas-emissions from volcanic areas and geothermal fields. Geochemical Journal, 27, 7-17.

Caracausi, A., Italiano, F., Martinelli, G., Paonita, A. and Rizzo, A., 2005. Long-term geochemical monitoring and extensive/compressive phenomena: case study of the Umbria region (central Apennines, Italy). Annals of Geophysics, 48, 43-53.

Castro, M.C., 2004. Helium sources in passive margin aquifers—new evidence for a significant mantle ^{3}He source in aquifers with unexpectedly low in situ ^{3}He/^{4}He production. Earth and Planetary Science Letters, 222, 897–913.

Chen, C. and Thomas, D.M., 1994. Soil processes and chemical transport. Journal of Environmental Quality, 23, 173–179.

Chen, C., Thomas, D.M. and Green, R.E., 1995. Modelling of Radon transpot in unsaturated soil, Journal of Geophysical Research, 100, 15517-15525.

Ciancabilla, N., Ditta, M., Italiano, F. and Martinelli, G., 2007. The Porretta thermal springs (Northern Apennines): seismogenic structures and long-term geochemical monitoring. Annals of Geophysics, 50, 513-526.

Cioni, R., Guidi, M., Pierotti, L. and Scozzari, A., 2007. An automatic monitoring network installed in Tuscany (Italy) for studying possible geochemical precursory phenomena. Natural Hazards and Earth System Sciences, 7, 405–416.

Clark, I.D. and Fritz, P., 1997. Environmental isotopes in hydrogeology: Boca Raton, Florida, Lewis Publishers, 328 p.

Clarke, W.B., Beg, M.A. and Craig, H., 1976. Excess ^{3}He in the sea: evidence for terrestrial primordial helium. Earth and Planetary Science Letters, 6, 213–220.

Clauser, C., Griesshaber, E. and Neugebauer, H.J., 2002. Decoupled thermal and mantle helium anomalies: Implications for the transport regime in continental rift zones. Journal of Geophysical Research, 107/B11, 2669, doi:10.1029/2001JB000675.

Clements, W.E. and Wilkening, M.H., 1974. Atmospheric pressure effects on ^{222}Rn transport across the earth-air interface. Journal of Geophysical Research, 79, 5025-5029.

Craig, H., 1961. Isotopic variations in meteoric waters. Science, 133, 1702-1703.

Crovetto, R., Fernandez-Prini, R. and Japas, M.L., 1982. Solubilities of inert gases and methane in H_2O and in D_2O in the temperature range of 300 to 600 K, Journal of Chemical Physics, 76, 1077-1086.

Çemen, İ., Catlos, E.J., Göğüş, O. and Özerdem, C., 2006. Postcollisional extensional tectonics and exhumation of the Menderes massif in the Western Anatolia extended terrane, Turkey. Geological Society of America, Special Paper 409, 333-380.

Darling, W.G., Griesshaber, E., Andrews, J.N., Armannsson, H. and O'Nions, R., 1995. The origin of hydrothermal and other gases in the Kenya Rift Valley. Geochimica et Cosmochimica Acta, 59 (12), 2501 - 2512.

Das, N.K., Choudhuryb, H., Bhandaria, R.K., Ghoseb, D., Senb, P. and Sinhaa, B., 2006. Continuous monitoring of ^{222}Rn and its progeny at a remote station for seismic hazard surveillance. Radiation Measurements, 41, 634 – 637.

De Gregorio, S., Gurrieri, S. and Valenza, M., 2005. A PTFE membrane for the in situ extraction of dissolved gases in natural waters: Theory and applications. Geochem. Geophys. Geosyst., 6, Q09005, doi:10.1029/2005GC000947.

Demirörer, M., 1967. Denizli-Sarayköy gradyent etüdleri. MTA Rapor No. 4141.

Dewey, J. F. and Şengör, A. M. C., 1979. Aegean sea and surrounding regions: complex multiplate and continuum tectonics in a convergent zone. Geological Society of America Bulletin, Part I, 90, 84-92.

Dewey, J.F., 1988. Extensional collapse of orogens, Tectonics, 7, 1123-1139.

Dora, O.Ö., 1975. Menderes masifinde alkali feldspatların yapısal durumları ve bunların petrojenetik yorumlarda kullanılması. TJK Bült. C.18, sayı 2.

Dora, O.Ö., Candan, O., Dürr, S.T. and Oberhanslı, R., 1995. New evidence on the geotectonic evolution of the Menderes Massif. In: Pişkin, Ö., Ergün, M., Savaşçın, M.Y., Tarcan, G. (Eds.), Proceedings of the International Earth Sciences Colloquium on the Aegean Region, İzmir, 53–72.

Drever, J.I., 1997. The Geochemistry of Natural Waters (3rd ed), New Jersey, Prentice-Hall Inc. 436p.

Du, J., Liu, C., Fu, B., Ninomiya, Y., Zhang, Y., Wang, C., Wang, H. and Sun, Z., 2005. Variations of geothermometry and chemical-isotopic compositions of hot spring fluids in the Rehai geothermal field, southwestern China. Journal of Volcanology and Geothermal Research, 142, 243-261.

Duenas, D. and Fernandez, M.C., 1987. Dependence of radon-222 flux on concentrations of soil gas and air gas and an analysis of the effects produced by several atmospheric variables. Annals Geophysics, 5, 533-537.

Dürr, S., 1975. Über Alter und geotektonische Stellung des Menderes-Kristallins/SW-Anatolien und seine Aequivalente in der mittleren Aegaeis. Habilitation thesis, University of Marburg/Lahn, 106 pp.

Dürr, S., Altherr, R., Keller, J., Okrusch, M. and Seidel, E., 1978. The median Aegean crystalline belt: Stratigraphy, structure, metamorphism, magmatism. IUCG Sci. Rep., 38, 455-477.

Ekingen, A., 1970. Kızıldere (Denizli) sondaj alanı detay gravimetrik etüdü. MTA Der. Rap. No: 2325, Ankara.

Ellis, A.J. and Mahon, W.A.J., 1977. Chemistry and geothermal systems. Academic Press, New York, 392p.

ENEL, 1988. Optimization and Development of the Kızıldere Geothermal Field: Final report. Unpublished report of ENEL, Pisa, Italy.

Ercan, T., Erdogdu, G. and Bas, H., 1983. Petrology and plate tectonic implications of Denizli volcanics. Geological Society of Turkey Bulletin, 26, 153-159.

Erzinger, J., Wiersberg, T. and Dahms, E., 2004. Real-time mud gas logging during drilling of the SAFOD Pilot Hole in Parkfield, CA. Geophysical Research Letters, 31, L15S18, doi:10.1029/ 2003GL019395.

Erzinger, J., Wiersberg, T. and Zimmer, M., 2006. Real-time mud gas logging and sampling during drilling. Geofluids, 6, 225 – 233.

Eşder, T., Çağlav, F. and Pekatan, R., 1994. Kızıldere jeotermal sahasındaki KD-20, KD-21, KD-22 üretim kuyuları (1985-1986) ve sistemin yeni verilerle yorumlanması. MTA Rapor.

Etiope, G., Guerra, M. and Raschi, A., 2005. Carbon dioxide and radon geohazards over a gas-bearing fault in the Siena Graben (Central Italy). Terr. Atmos. Ocean. Sci., 16, 885-896.

Faure, G., 1986. The K-Ar method of dating, in Principles of Isotope Geology, second edition, John Wiley, New York, 66-92.

Favara, R., Grassa, F., Inguaggiato, S. and Valenza, M., 2001. Hydrogeochemistry and stable isotopes of thermal springs: earthquake-related chemical changes along Belice Fault (Western Sicily). Applied Geochemistry, 16, 1-17.

Federico, C., Aiuppa, A., Favara, R., Gurrieri, S. and Valenza, M., 2004. Geochemical monitoring of groundwaters (1998-2001) at Vesuvius Volcano (Italy). Journal of Volcanology and Geothermal Research, 133, 81-104.

Fytikas, M., Innocenti, F., Manetti, P., Mazzuoli, R., Peccerillo, A. and Villari. L., 1984. Tertiary to Quaternary evolution of volcanism in the Aegean region. In The Geol. Evolution of the Eastern Mediterranean, Dixon JE, Robertson AHF (eds). Spec. Publ., Geol. Soc. London 17, 687–699.

Gat, J.R. and Carmi, I., 1970. Evolution of the isotopic composition of atmospheric waters in the Mediterranean Sea area. Journal of Geophysical Research, 75, 3039-3048.

Gessner, K., Ring, U., Johnson, C., Hetzel, R., Passchier, C.W. and Güngör, T., 2001. An active bivergent rolling-hinge detachment system. Central Menderes metamorphic core complex in western Turkey. Geology, 29, 611-614.

Gessner, K., Collins, A.S., Ring, U. and Güngör, T., 2004. Structural and thermal history of poly-orogenic basement: U-Pb gecohronology of granitoid rocks in the southern Menderes Massif, western Turkey. Journal of the Geological Society, London, 161 93-101.

Giggenbach, W.F., 1980. Geothermal gas equilibria. Geochimica et Cosmochimica Acta, 44, 2021-2032.

Giggenbach, W.F., 1986. The use of gas chemistry in delineating the origin of fluids discharges over the Taupo Volcanic Zone: A review. International Volcanological Congress, Hamilton, New Zealand, Proceedings Symposium 5, 47-50.

Gilfillan, S.M.V., Holland, G., Blagburn, D., Sherwood Lollar, B., Stevens, S., Schoell, M. and Cassidy, M., 2008. The noble gas geochemistry of natural CO_2 gas reservoirs from the Colorado Plateau and Rocky Mountain provinces,USA. Geochimica et Cosmochimica Acta, 72, 1174 -1198.

Graciansky, P.C., 1965. Menderes Masifi güney kıyısı boyunca görülen metamorfizma hakkında açıklamalar. MTA Dergisi, 64, 88-121.

Graham, D. W., 2002. Noble Gas Isotope Geochemistry of Mid-Ocean Ridge and Ocean Island Basalts: Characterization of Mantle Source Reservoirs, in Porcelli, D., Ballentine, C. J., and Wieler, R., eds., Noble Gases in Geochemistry and

Cosmochemistry, Washington DC, Geochemical Society & American Society of America, 247-315.

Güleç, N., 1988. He-3 distribution in western Turkey. Bulletin of the Mineral Research and Exploration Institute of Turkey, 108, 35–42.

Güleç, N., 1991. Crust–mantle interaction in western Turkey: implications from Sr and Nd isotope geochemistry of Tertiary and Quaternary volcanics. Geological Magazine, 125, 417–435.

Güleç, N. and Hilton, D.R., 2006. Helium and heat distribution in Western Anatolia, Turkey. Relationship to active extension and volcanism. Geological Society of America Special Paper, 409, 305–319.

Güleç, N., Hilton, D.R. and Mutlu, H., 2002. Helium isotope variations in Turkey: relationship to tectonics, volcanism and recent seismic activities. Chemical Geology, 187, 129–142.

Gürer, Ö.F., Sarıca, N., Özburan, M., Sangu, E. and Doğan, B., 2009. Progressive development of the Büyük Menderes Graben based on new data, western Turkey. Geological Magazine, 146, 1-22.

Hartmann, J., Berner, Z., Stüben, D. and Henze, N., 2005. A statistical procedure for the analysis of seismotectonically induced hydrochemical signals: A case study from the Eastern Carpathians, Romania. Tectonophysics, 405, 77– 98.

Heaton, T.H.E. and Vogel, J.C., 1981. Excess air in groundwater. Journal of Hydrology, 50, 201–216.

Heinicke, J. and Koch, U., 2000. Slug flow, a possible explanation for hydrogeochemical earthquake precursors at Bad Brambach, Germany. Pure and Applied Geophysics, 157, 1621–1641.

Heinicke, J., Italiano, F., Lapenna, V., Martinelli, G. and Nuccio, P.M., 2000. Coseismic Geochemical Variations in some Gas Emissions (Central Italy). Phys. Chem. Earth, 25, No. 3. 289-293.

Hetzel, R., Ring, U., Akal, C. and Troesch, M., 1995. Miocene NNE-directed extensional unroofing in the Menderes massif, southwestern Turkey. London, Journal of the Geological Society, 152, 639-654.

Hetzel, R., Romer, R.L., Candan, O. and Passchier, C.W., 1998. Geology of the Bozdağ area, central Menderes Massif, SW Turkey: Pan-African basement and Alpine deformation. Geologische Rundschau, 87, 394–406.

Hilton, D.R., 1996. The helium and carbon isotope systematics of a continental geothermal system: results from monitoring studies at Long Valley Caldera (California, U.S.A.). Chemical Geology, 127, 269-295.

Hilton, D.R., Fischer, T. and Marty, B., 2002. Noble gases and volatile recycling at subduction zones. MSA Special Volume: Noble Gasses, 47, 319–370.

Hirabayashi, J. and Kusakabe, M., 1985. A review on the chemical precursors of volcanic eruption, Bull. Volcanol. Soc. Jpn., 30, 171—183.

Hoefs, J., 2004. Stable isotope geochemistry. Springer-Verlag, 5th Edition, 244p.

Honda, M., McDougall, I., Patterson, D.B., Doulgeris, A. and Clague, D.A., 1991. Possible solar noble-gas component in Hawaiian basalts. Nature, 349, 149–151.

Igarashi, G., Saeki, S., Takahata, N., Sumikawa, K., Tasaka, S., Sasaki, Y., Takahashi, M. and Sano, Y., 1995. Groundwater Radon anomaly before the Kobe earthquake in Japan. Science, 269, 60–61.

Inguaggiato, S., Martin, A.L., Del Pozzo, Aguayo, A., Capasso, G. and Favara, R., 2005. Isotopic, chemical and dissolved gas constraints on spring water from Popocatepetl volcano (Mexico): evidence of gas–water interaction between magmatic component and shallow fluids. Journal of Volcanology and Geothermal Research, 141, 91– 108.

Innocenti, F., Manetti, P., Mazzuoli, R., Pasquare, G. and Villari, L., 1982. Regional distribution and character of active andesite volcanism- Anatolia and Northwestern Iran. In orogenic Andesites and Related Rocks, R.S. (Thorpe (ed.), J. Wiley and Sons, New York, 327-349.

Irwin, W.P. and Barnes, I., 1980. Tectonic relations of CO_2 discharges and earthquakes. Journal of Geophysical Research, 85, 3115–3121.

Italiano, F. and Martinelli, G., 2001. Anomalies of mantle-derived helium during the 1997-1998 seismic swarm of Umbria-Marche, Italy. Geophysical Research Letters, 28(5), 839-842.

Italiano, F., Martelli, G., Nuccio, P.M. and Paternoster, M., 2001a. Significance of earthquake-related anomalies in fuids of Val D'Agri (southern Italy). Terra Nova, 13, 249-257.

Italiano, F., Martinelli, G. and Nuccio, P.M., 2001b. Anomalies of mantle-derived helium during the 1997-1998 seismic swarm of Umbria-Marche, Italy. Geophysical Research Letters, 28, 839-842.

Italiano, F., Martinelli, G. and Plescia, P., 2008. CO_2 degassing over seismic Areas: The Role of Mechanochemical Production at the Study Case of Central Apennines. Pure and Applied Geophysics, 165, 75–94.

Italiano, F., Bonfanti, P., Ditta, M., Petrini, R. and Sleijko, F., 2009. Helium and carbon isotopes in the dissolved gases of Friuli region (NE Italy): Geochemical evidence of CO_2, production and degassing over a seismically active area. Chemical Geology, 266 (1–2), 76–85.

Jenden, P.D., Kaplan, I.R., Poreda, R.J. and Craig, H., 1988. Origin of nitrogen-rich natural gases in the Great Valley, California. Evidence from stable isotope ratios of helium, carbon and nitrogen. Geochimica et Cosmochimica Acta, 52, 851–861.

Jin, A. and Aki, K., 1986. Temporal change in coda Q before the Tangshan earthquake of 1976 and the Haicheng earthquake of 1975. Journal of Geophysical Research, 91, 665–673.

Kawabe, I., 1985. Anomalous changes of CH_4/Ar ratio in subsurface gas bubbles as seismo-geochemical precursors at Matsuyama, Japan. Pure and Applied Geophysics, 122, 194–214.

Kaymakçı, N., 2006. Kinematic development and paleostress analysis of the Denizli Basin (Western Turkish): implications of spatial varition of relative paleostress magnitudes and orientations. Journal of Asian Earth Sciences, 27, 207–222.

Kennedy, B.M. and Truesdell, A.H., 1996. The Northwest Geysers high-temperature reservoir: Evidence for active magmatic degassing and implications for the origin of The Geysers geothermal field. Geothermics, 25, 365–387.

Kennedy, B.M. and Van Soest, M.C., 2006. A helium isotope perspective on the Dixie Valley, Nevada, hydrothermal system. Geothermics, 35, 26–43.

Kennedy, B.M., Kharaca, Y.K., Evans, W.C., Ellwood, A., DePaolo, D.J., Thordsen, J., Ambats, G. and Mariner, R.H., 1997. Mantle fluids in the San Andreas fault system, California, Science, 278, 1278-1281.

Keskin, B., 1972. Kızıldere hidrojeoşimisi ve 3. Rezervuar. MTA Rap. 5269, Ankara.

King, C.Y., 1978. Radon emanation on San Andreas Fault. Nature, 271, 516–519.

King, C.Y., 1980. Episodic radon changes in subsurface soil gas along active faults and possible relation to earthquakes. Journal of Geophysical Research, 85 (B6), 3065-3078.

King, C.Y., 1986. Gas geochemistry applied to earthquake prediction: An overview. Journal of Geophysical Research, 91, 12269–12281.

King, C.Y. and Minissale, 1994. Seasonal variability of soil gas radon concentration in central California. Radiation Measurements, 23, 683-692.

Kipfer, R., Aeschbach-Hertig, W., Peeters, F. and Stute, M., 2002. Noble Gases in Lakes and Groundwaters, in Noble Gases in Geochemistry and Cosmochemistry, Rev. Mineral. Geochem., vol. 47, edited by D. Poorcelli, C. Ballentine, and R. Wieler, 615-700.

Kiyosu, Y., 1986. Variations in N_2/Ar and He/Ar ratios of gases from some volcanic areas in Northeastern Japan. Geochemical Journal, 19, 275-281.

Klusman, R.W. and Webster, J.D., 1981. Preliminary analysis of meteorological and seasonal influences on crustal gas emission relevant to earthquake prediction. Bulletin of the Seismological Society of America, 71, 211–222.

Knopoff, L., 1964. Earth tides as a triggering mechanism for earthquakes, Bulletin of the Seismological Society of America, 54, 1865–1870.

Koch, U. and Heinicke, J., 2007. Hydrological influences on long-term gas flow trends at locations in the Vogtland/NW Bohemian seismic region (German-Czech border). Annals of Geophysics, 50, 557-568.

Koçyiğit, A., 2005. The Denizli graben-horst system and the eastern limit of western Anatolian continental extension: basin-fill, structure, deformational mode, throw amount and episodic evolutionary history, SW Turkey. Geodinamica Acta, 18 (3/4), 167–208.

Koçyiğit, A., Yusufoğlu, H. and Bozkurt, E., 1999. Evidence from the Gediz graben for episodic two-stage extension in western Turkey. Journal of the Geological Society, London, 156, 605−616.

Kulongoski, J.T., Hilton, D.R. and Izbicki, J.A., 2003. Helium isotope studies in the Mojave Desert, California: implications for groundwater chronology and regional seismicity. Chemical Geology, 202, 95–113.

Kulongoski, J.T., Hilton, D.R. and Izbicki, J.A., 2005. Source and movement of helium in the eastern Morongo groundwater Basin: the influence of regional tectonics on crustal and mantle helium fluxes. Geochimica et Cosmochimica Acta, 69, 3857–3872.

Kulongoski, J.T., Hilton, D.R., Cresswell, R.G., Hostetler, S. and Jacobson, G., 2008. Helium-4 characteristics of groundwaters from Central Australia: Comparative chronology with chlorine-36 and carbon-14 dating techniques. Journal of Hydrology, 348, 176– 194.

Le pichon, X. and Angelier, J., 1979. The Hellenic arc and trench system; A key to the neotectonic evolution of the eastern Mediterranean: Tectonophysics, 60, 1-42.

Lehmann, B.E., Love, A., Purtschert, R., Collon, P., Loosli, H.H., Kutschera, W., Beyerle, U., Aeschbach-Hertig, W., Kipfer, R., Frape, S.K., Herczeg, A.L., Moran, J., Tolstikhin, I.N. and Groning, M., 2003. A comparison of groundwater dating with [81]Kr, [36]Cl and [4]He in four wells of the Great Artesian Basin, Australia. Earth and Planetary Science Letters, 211, 237–250.

Lippmann, J., Stute, M., Torgersen, T., Moser, D.P., Hall, J.A., Lin, L., Borcsik, M., Bellamy, R.E.S. and Onstott, T.C., 2003. Dating ultra-deep mine waters with noble gases and ^{36}Cl, Witwatersrand Basin, South Africa. Geochimica et Cosmochimica Acta, 67, 4597–4619.

Lippmann, J., Erzinger, J., Zimmer, M., Schloemer, S., Eichinger, J.L. and Faber, E,. 2005. On the geochemistry of gases and noble gas isotopes (including ^{222}Rn) in deep crustal fluids: The 4000 m KTB-pilot hole fluid production test 2002-03. Geofluids, 5 , 52-66.

Lupton, J. E. and Craig, H., 1975. Excess ^{3}He in oceanic basalts: evidence for terrestrial primordial helium. Earth and Planetary Science Letters, 26, 133-139.

Lupton, J.E., 1983. Terrestrial inert gases : Isotope tracer studies and clues to primordial components in the mantle. Ann. Rev. Earth and Planetary Science Letters, 11, 371 -414.

Machel, H.G., 1998. Gas souring by thermochemical sulfate reduction at 140ºC: discussion. American Association Petroleum Geology Bulletin, 82, 1870–1873.

Mahara Y. and Igarashi T., 2003. Changes in isotope ratio and content of dissolved helium through groundwater evolution. Applied Geochemistry, 18(5), 719-738.

Mahara, Y., Igarashi, T., Hasegawa, T., Miyakawa, K., Tanaka, Y. and Kiho, K., 2001. Dynamic changes in hydrogeochemical conditions caused by tunnel excavation at the Aspo Hard Rock Laboratory (HRL), Sweden. Applied Geochemistry, 16, 291–315.

Mamyrin, B.A. and Tolstikhin, I.N., 1984. Helium isotopes in Nature: Elsevier, 273p, Amsterdam.

Martinelli, G. and Plescia, P., 2005. Carbon dioxide and methane emissions from calcareous-marly rock under stress: experimental test results. Annals of Geophysics, 48, 40-57.

Marty, B. and Craig, H., 1987. Cosmic-ray-produced neon and helium in the summit lavas of Maui. Nature, 325, 335-337.

Marty, B. and Jambon, A., 1987. C/^{3}He in volatile fluxes from the solid Earth: implication for carbon geodynamics. Earth and Planetary Science Letters, 83, 16–26.

Matsuo, S., Suzuki, M. and Mizutani, Y., 1978. Nitrogen to argon ratio in volcanic gases. In: E.C.J. Alexander and M. Ozima (Editors), Terrestrial rare gases. Japan Sci. Soc. Press, Tokyo, 17-25.

Mattson, M. D. and Likens, G.E., 1990. Air pressure and methane fluxes. Nature, 347, 718-7 19.

Mazor, E., 1972. Paleotemperatures and other hydrological parameters deduced from noble gases dissolved in groundwaters: Jordan Rift Valley, Isreal. Geochimica et Cosmochimica Acta, 36, 1321-1336.

Mazor, E., 1997. Chemical and isotopic groundwater hydrology, Applied Approach, 158-166.

Mc Kenzie, D.P., 1972. Active tectonics of the Mediterranean region. Geophys. J. R. Astron. Soc., 30, 109-185.

McKenzie, D.P., 1978. Some remarks on the development of sedimentary basins. Earth and Planetary Science Letters, 40, 25–32.

McKlusky, S., Balassanian, S., Barka, A.A., Demir, C., Ergintav, S., Georgiev, I., Gürkan, O., Hamburger, M., Hurst, K., Kahle, H.G., Kastens, K., Kekelidze, G., King, R., Kotzev, V., Lenk, O., Mahmoud, S., Mishin, A., Nadariya, M., Ouzounis, A., Paradissis, D., Peter, Y., Prilephin, M., Reilinger, R.E., Sanlı, İ., Seeger, H., Tealeb, A., Toksöz, M.N. and Veis, G., 2000. Global Positioning System constraints on plate kinematics and dynamics in the Eastern Mediterranean and Caucasus. Journal of Geophysical Research, 105, 5695–5720.

Morikawa, N., Kazahaya, K., Fourre, E., Takahashi, H.A., Jean-Baptiste, P., Ohwada, M., LeGuern, F.J. and Nakama, A., 2008. Magmatic He distribution around Unzen volcano inferred from intensive investigation of helium isotopes in groundwater. Journal of Volcanology and Geothermal Research, 175, 218-230.

Mutlu, H., Güleç, N. and Hilton, D.R., 2008. Helium-Carbon Relationships in Geothermal Fluids of Western Anatolia, Turkey. Chemical Geology, 247, 305-321.

Nagamine, K., 1994. Origin and coseismic behavior of mineral spring gas at Byakko, Japan, studied by automated gas chromatographic analyses. Chemical Geology, 114, 3-17.

Neal, C. and Stanger, G., 1983. Hydrogen generation from mantle souce rocks in Oman. Earth and Planetary Science Letters, 66, 315-320.

Nicholson, K., 1993. Geothermal Fluids, Chemistry and Exploration Techniques. Springer-Verlag, Berlin, 263p.

Nishizawa, S., Igarashi, G., Sano, Y., Shoto, E., Tsaka, S. and Sasaki, Y., 1998. Radon, Cl^- and SO_4^{-2} anomalies in hot-spring water associated with the 1995 earthquake swarm of the East Coast of the Izu Peninsula, Central Japan, Applied Geochemistry, 13, 89-94.

Oberhänsli, R., Candan, O., Dora, O.Ö. and Dürr, S.H., 1997. Eclogites within the Menderes Massif/western Turkey. Lithos, 41, 135–150.

Okay, A.I., 1986. High pressure/low temperature metamorphic rocks of Turkey: Geological Society of America Bulletin, 164, 333-347.

Okay, A.I. and Tüysüz, O., 1999. Tethyan sutures of nothern Turkey, in Durand, B., Jolivet, L., Horvath, D., and Serranne, M., eds., The Mediterranean basins: Tertiary extension within the Alpine Orogen: Geological Society of London, Special Publication, no. 156, 475-515.

Oxburgh, E.R. and O'Nions, R.K., 1987. Helium loss, tectonics and the terrestrial heat budget. Science, 237, 1583–1588.

Oxburgh, E.R., O'Nions, R.K. and Hill, R., 1986. Helium isotopes in sedimentary basins. Nature, 324, 632 -635.

Ozima, M. and Podosek, F.A., 1983. Noble gas geochemistry. Cambridge Univ. Press, Cambridge, 367p.

Ozima, M. and Podosek, F.A., 2002. Noble Gas Geochemistry, Cambridge Univ. Press, Cambridge, 286p.

Ölmez, E., Yıldız, B., Çetinel, L., Akıllı, H. ve Yıldırm, N., 1998. Denizli-Sarayköy-Kızıldere R-1 reenjeksiyon sondajı kuyu bitime raporu: MTA Der. Rap. No: 10192, 16s (yayımlanmamış), Ankara.

Ölmez, E., Akıllı, H., Uygur, N., Çiçekli, K. ve Yıldırm, N., 2001. Denizli-Kızıldere R2 nolu reenjeksiyon sondajı kuyu bitirme raporu: MTA Enerji Dairesi Arşiv No: 1010, Ankara.

Özgüler, M.E., Turgay, M.I. and Şahin, H., 1984. Geophysical investigations in Denizli geothermal fields. Bulletin of MTA, No. 99/100, 80–99, Ankara.

Özgür, N., 2001. Origin of high boron contents of the thermal waters of Kızıldere and vicinity, Western Anatolia, Turkey. International Geology Review, 43, 910-920.

Parkhurst, D.L., and Appelo, C.A.J., 1999. User's Guide to PHREEQC (Version 2-A) Computer Program for Speciation, Batch-Reaction, One-Dimensional Transport, and Inverse Geochemical Calculations.

Porcelli, D. and Ballentine, C.J., 2002. Models for the Distribution of Terrestrial Noble Gases and Evolution of the Atmosphere, in Porcelli, D., Ballentine, C. J., and Wieler, R., eds., Noble Gases in Geochemistry and Cosmochemistry: Reviews in Mineralogy and Geochemistry, Washington D. C., Geochemical Society & Mineralogial Society of America, 411-480.

Porcelli, D., Ballentine, C.J. and Wieler, R., 2002. Noble Gases in Geochemistry and Cosmochemistry. Reviews in Mineralogy and Geochemistry, Vol. 47, Geochemical Society and Mineralogical Society of America, 1-19.

Poreda, R.J. and Craig, H., 1989. Helium isotope ratios in circum-Pacific volcanic arcs. Nature, 338, 473-478.

Reddy, M.P.M. and Affholder, M., 2001. Descriptive physical oceanography: State of the Art. Taylor and Francis. 249p.

Reimer, G.M., 1980. Use of soil-gas helium concentrations for earthquake prediction: limitations imposed by diurnal variation. Journal of Geophysical Research, 85, 3107–3114.

Sano, Y. and Pillinger, C.T., 1990. Nitrogen isotopes and N_2/Ar ratios in cherts: An attempt to measure time evolution of atmospherid $\delta^{15}N$ value. Geochemical Journal, 24, 315–325.

Sano, Y. and Marty, B., 1995. Origin of carbon in fumarolic gas from island arcs. Chemical Geology, 119, 264–274.

Sano Y., Nagao K. and Pillinger C. T., 1994. Carbon and noble gases in Archean chert. Chemical Geology, 112, 327–342.

Sano, Y., Takahata, N., Igarashi, G., Koizumi, N. and Sturchio, N.C., 1998. Helium degassing related to the Kobe earthquake. Chemical Geology, 150, 171-179.

Sarda, P., Staudacher, T. and Allegre, C. J., 1985. $^{40}Ar/^{36}Ar$ in MORB glasses: constraints on atmosphere and mantle evolution. Earth and Planetary Sciences Letters, 72, 357–75.

Sarda, P., Staudacher, T. and Allegre, C.J., 1988. Neon isotopes in submarine basalts. Earth and Planetary Science Letters, 91, 73–88.

Satır, M. and Friedrichsen, H., 1986. The origin and evolution of the Menderes Massif, Turkey: A rubidium/strontium and oxygen isotope study, Geol. Rundschaus 75/3, 703-714.

Sato, M., Sutton, A.J., McGee, K.A. and Russel-Robinson, S., 1986. Monitoring of hydrogen along the San Andreas and Calaveras faults in central California in 1980-1984. Journal of Geophysical Research, 91, 12315-12326.

Savaşçın, M.Y. and Güleç., N. 1990. Relationship between magmatic and tectonic activities in western Turkey: geological and geochemical features with examples from the coastal section. Proceedings of International Earth Sciences Congress on Aegean Regions (IESCA 1990), V.II, 300-313.

Schery, S.D. and Gaeddert, D.H., 1982. Measurements of the effect of cyclic atmospheric pressure variation of the flux of 222Rn from the soil, Geophysical Research Letters 9, 835-838.

Schlosser, P., Stute, M., Sonntag, C. and Munnich, K.O., 1989. Tritiogenic ^3He in shallow groundwater. Earth and Planetary Sciences Letters, 94, 245-256.

Schuiling, K.D., 1962. On the petrology, age and structure of the Menderes migmatites complex (SW Turkey). Min. Res. Exp. Inst. Turkey Bull., 58, 71- 84.

Seyitoğlu, G. and Scott, B.C., 1991. Late Cenozoic crustal extension and basin formation in west Turkey. Geology Magazine, 28, 155−166.

Seyitoğlu, G. and Scott, B.C., 1992. The age of the Büyük Menderes Graben (west Turkey) and its tectonic implications. Geological Magazine, 129, 239–242.

Seyitoğlu, G. and Scott, B.C., 1996. The age of the Alaşehir graben (west Turkey) and its tectonic implications. Geological Journal, 31, 1-11.

Seyitoğlu, G., Tekeli, O., Çemen, İ., Şen, Ş. and Işık, V., 2002. The role of flexural rotation/rolling hinge model in the tectonic evolution of the Alaşehir graben, western Turkey. Geology Magazine, 139, 15−26.

Shapiro, M.H., Rice, A., Mendenhall, M.H., Melvin, D. and Tombrello, T.A., 1985. Recognition of environmentally cause variations in radon time series. Pure and Applied Geophysics, 122, 309–326.

Sherwood Lollar, B., O'Nions, R.K. and Ballentine, C.J., 1997. The fate of mantle-derived carbon in a continental sedimentary basin: Integration of C/He relationships and stable isotope signatures. Geochimica et Cosmochimica Acta, 61, 2295-2307.

Shi, Y. and Zhang, W., 1995. The correlation between radon variation and earth solid tide change in rock-groundwater system-the mechanical foundation for using radon change to predict earthquake, Journal of Earthquake Prediction research, 4, No. 3, 423-430.

Smith, S.P. and Kennedy, B.M., 1985. Noble gas evidence for two fluids in the Baca (Valles Caldera) geothermal reservoir. Geochimica et Cosmochimica Acta, 49, 893– 902.

Song, S.R., Chen, Y.L., Liu, C.M., Ku, W.Y., Chen, H.F., Liu, Y. J., Kuo, L.W., Yang, T. F., Chen, C. H., Liu, T. K. and Lee, M., 2005. Hydrochemical changes of spring waters in Taiwan: implications for evaluating sites for earthquake precursory monitoring. Terr. Atmos. Ocean. Sci., 16, 745-762.

Song, S.R., Ku, W.Y., Chen, Y.L., Liu, C.M., Chen, H.F., Chan, P.S., Chen, Y.G., Yang, T.F., Chen, C-H., Liu, T.K. and Lee, M., 2006. Hydrogeochemical anomalies in the springs of the Chiayi Area in West-central Taiwan as possible precursors to earthquakes. Pure and Applied Geophysics, 163, 675-691.

Steinitz, G., Vulkan, U. and Lang, B., 1999. The Radon flux at the northwestern segment of the Dead Sea (Dead Sea Rift) and its relation to earthquakes. Israel Jour. Earth Sci., 48, 283-299.

Stute, M. and Deak, J., 1989. Environmental isotope study (^{14}C, ^{13}C, ^{18}O, D, Noble gases) on deep groundwater circulation systems in Hungary with reference to paleoclimate: Radiocarbon, 31, no. 3, 902-918.

Stute, M., Sonntag, C., Deak, J. and Schlosser, P., 1992. Helium in deep circulating groundwater in the Great Hungarian Plain: Flow dynamics and crustal and mantle helium fluxes. Geochimica et Cosmochimica Acta, 56, 2051-2067.

Stute, M., Forster, M., Frischkorn, H., Serejo, A., Clark, J. F., Schlosser, P., Broecker, W. S. and Bonani, G., 1995. Cooling of tropical Brazil during the last glacial maximum. Science, 269, 379–383.

Sugisaki, R., 1978. Changing He/Ar and N_2/Ar ratios of fault air may be earthquake precursors. Nature, 275, 209–211.

Sugisaki, R., 1981. Deep seated gas emission induced by the earth tide: A basic observation for geochemical earthquake prediction. Science, 212, 1264-1266.

Sugisaki, R., 1987. Behavior and origin of helium, neon, argon and nitrogen from active faults. Journal of Geophysical Research, 92, 12523-12530.

Sugisaki, R. and Sugiura, T., 1986. Gas anomalies at three mineral springs and a fumarole before an inland earthquake, central Japan. Journal of Geophysical Research, 91, 12,296–12,304.

Sugisaki, R., Ido, M., Takeda, H., Isobe, Y., Hayashi, Y., Nakamura, N., Satake, H., and Mizutani, Y., 1983. Origin of hydrogen and carbon dioxide in fault gases and its relation to fault activity. Journal of Geology, 91, 239-258.

Süer, S., Güleç, N., Mutlu, H., Hilton, D.R., Çifter, C. and Sayın, M., 2008. Geochemical Monitoring of Geothermal Waters (2002–2004) along the North Anatolian Fault Zone, Turkey: Spatial and Temporal Variations and Relationship to Seismic Activity. Pure and Applied Geophysics, 165, 17–43.

Şengör, A.M.C., 1984. The Cimmeriden orogenic system and the tectonics of Eurasia. Geological Society of America, Special Paper, 195, p. 82.

Şengör, A.M.C., 1987. Cross-faults and differential stretching of hanging walls in regions of low-angle normal faulting: examples from western Turkey. In: Coward, M.P., et al. (Eds.), Continental Extensional Tectonics. Geological Society of London Special Publication, 28, 575–589.

Şengör, A.M.C. and Yılmaz, Y., 1981. Tethyan evolution of Turkey: a plate tectonic approach. Tectonophysics, 75, 181-241.

Şengör, A.M.C., Satır, M. and Akkök, R., 1984. Timing of the tectonic events in the Menderes Massif, western Turkey: implications for tectonic evolution and evidence for Pan-African basement in Turkey. Tectonics, 3, 693-707.

Şengör, A.M.C., Görür, N. and Şaroğlu, F., 1985. Strike–slip deformation, basin formation and sedimentation: Strike–slip faulting and related basin formation in zones of tectonic escape: Turkey as a case study. In: Strike-Slip Deformation, Basin Formation and Sedimentation (Ed. by K. Biddle & N. Christie-Blick), Society of Economic Palaeontologists and Mineralogists, Special Publication 37, 227–264.

Şimşek, Z., 1978. Tekke Hamam jeotermal alanı gradyent sondajları değerlendirilmesi, MTA Rapor No. 6236.

Şimşek, Ş., 1984. Denizli, Kızıldere, Tekkehamam, Tosunlar, Buldan ve Yenice Alanları Jeolojisi ve Jeotermal Enerji Olanakları. MTA Rapor No 7486, Ankara.

Şimşek, Ş., 1985. Geothermal Model of Denizli, Sarayköy-Buldan Area. Geothermics, 14, No.2/3 , 393-417.

Şimşek, Ş., 2005. Research on Isotope Techniques for Exploitation of Geothermal Reservoirs in Western Turkey, Use of isotope techniques to trace the origin of acidic fluids in geothermal systems. IAEA TECDOC Publication, p. 155-169. ISBN 92-0-102805-9, ISSN 1011-4289, Vienna.

Şimşek, Ş., Yıldırım, N. and Gülgör, A., 2005. Development and Environmental effects of the Kızıldere Geothermal Power project, Turkey, Geothermics, 34, 239-256.

Tezcan, A.K., 1967. Denizli-Sarayköy jeotermik enerji araştırmaları gravite ve rezistivite etütleri. MTA Der. Rap. No: 3896, Ankara.

Thomas, D., 1988. Geochemical Precursors to Seismic Activity. Pure and Applied Geophysics, 126, 241-266.

Torgersen, T., 1993. Defining the role of magmatism in extensional tectonics: He-3 fluxes in extensional basins. Journal of Geophysical Research, 98, 16257–16269.

Torgersen, T. and Clarke, W.B., 1985. Helium accumulation in groundwater. 1. An evaluation of sources and the continental flux of crustal He-4 in the Great Artesian Basin, Australia: Geochimica et Cosmochimica Acta, 49, 1211–1218.

Toutain, J.P., Munoz, M., Poitrasson, F. and Lienard, A.C, 1997. Springwater chloride ion anomaly prior to a M = 5.2 Pyrenean earthquake. Earth and Planetary Science Letters, 149, 113-119.

Tretner, A., Zimmer, M., Erzinger, J., Nakada, S. and Saito, M., 2008. Real-time drill mud gas logging at the USDP-4 drilling, Unzen volcano, Japan. Journal of Volcanology and Geothermal Research, 175, 28-34.

Tsunogai, U. and Wakita, H., 1995. Precursory chemical changes in ground water: Kobe earthquake, Japan. Science, 269, 61–63.

Turgay, I., Özgüler, M.E. ve Şahin, H., 1980. Denizli Buldan-Pamukkale jeotermal enerji aramaları rezistivite etüdü. MTA Der. Rap. No: 6958, Ankara.

Uysallı, H. and Keskin, B., 1971. Denizli-Sarayköy-Kızıldere jeotermal sahası KD13 ve KD15 derin jeotermik enerji sondajları bitirme raporu. MTA Der. Rap. No: 4717, Ankara.

Wakita, H., 1996. Chemical Challenge to Earthquake Prediction. Proceedings Natural Academic Science, 93, 3781-3786.

Walia, V., Virk, H.S. and Bajwa, B.S., 2006. Radon precursory signals for some earthqaukes of magnitude > 5 occurred in N-W Himalaya. Pure and Applied Geophysics, 163, 711-721.

Weinlich, F.H., Brauer, K., Kampf, H., Strauch, H., Tesar, J. and Weise, S.M., 1999. An active subcontinental mantle volatile system in the western Eger Rift, Central Europe: gas flux, isotopic (He, C and N) and compositional fingerprints, Geochimica et Cosmochimica Acta, 63, 3653-3671.

Weinlich, F.H., Faber, E., Bouskova, A., Horalek, J., Teschner, M. and Poggenburg, J., 2006. Seismically induced variations in Marianske Lazne fault gas composition in the NW Bohemian swarm quake region, Czech Republic - A continuous gas monitoring. Tectonophysics, 421, 89-110.

Welhan, J.A., 1988. Origins of methane in hydrothermal systems. Chemical Geology, 71, 183–198.

Westaway, R., 2003. Kinematics of the Middle East and Eastern Mediterranean Updated. Turkish Journal of Earth Sciences, 12, 5-46.

Westaway, R., Guillou, H., Yurtmen, S., Demir, T., Scaillet, S. and Rowbotham, G., 2005. Constraints on the timing and regional conditions at the start of the present phase of crustal extension in western Turkey, from observations in and around the Denizli region. Geodinamica Acta, 18 (3–4), 209–238.

Wetherill, G.W., 1954. Variations in the isotopic abundances of neon and argon extracted from radioactive minerals. Phys. Rev., 96, 679-683.

Whitney, D.L. and Bozkurt, E., 2002. Metamorphic history of the southern Menderes massif, western Turkey. Geological Society of America Bulletin, 114, 829−838.

Wiersberg, T. and Erzinger, J., 2007. A helium isotope cross-section study through the San Andreas Fault at seismogenic depths. Geochem. Geophys. Geosyst. 8. doi:10.1029/2006GC00138, Q01002.

Wiersberg, T. and Erzinger, J., 2008. Origin and spatial distribution of gas at seismogenic depths of the San Andreas Fault from drill-mud gas analysis. Applied Geochemistry, 23, 1670 – 1695.

Yang, T.F., Fu, C.C., Walia, V., Chen, C.H., Chyi, L.L., Liu, T.K., Song, S.R. Lee, M., Lin, C.W. and Lin, C.C., 2006. Seismo-Geochemical Variations in SW Taiwan: Multi-Parameter Automatic Gas Monitoring Results. Pure and Applied Geophysics, 163, 693–709.

Yatsevich, I. and Honda, M., 1997. Production of nucleogenic neon in the Earth from natural radioactive decay. Journal of Geophysical Research, 102, 10291–10298.

Yılmaz, Y., Genç, S.C., Gürer, Ö.F., Bozcu, M. Yılmaz, K., Karacık, Z., Altunkaynak, Ş. and Elmas, A., 2000. When did western Anatolian grabens begin to develop. In: Tectonics and Magmatism in Turkey and the Surrounding area (Ed. by E. Bozkurt, J.A. Winchester, & J.D.A. Piper), Geological Society, London, Special Publications 173, 353–384.

Zartman, R.E., Wasserburg, G.J. and Reynolds, J.H., 1961. Helium, argon and carbon in some natural gases. Journal of Geophysical Research, 66, 277-306.

Zimmer, M. and Erzinger, J., 1995. On the geochemistry of gases in formation and drilling fluids-Results from the KTB. Sci. Drill., 5, 101-110.

Zimmer, M. and Erzinger, J., 2003. Continuous H_2O, CO_2, [222]Rn and temperature measurements on Merapi Volcano, Indonesia. Journal of Volcanology and Geothermal Research, 125, 25-38.

APPENDIX A

INFORMATION ON THE QUADSTAR SOFTWARE

1. The connection between the QMS and the computer was established via the Service menu of the Quadstar software.

   <Quadstar-SERVICE-Comm-Connect>

2. The valve of the QMS was opened electronically from the Manual menu of Quadstar.

   <Quadstar-MEASURE-Manual>

3. Following the opening of the valve, the filaments and the SEM (Secondary Electron Multiplier) were turned on by the Setup menu.

   <Quadstar-SERVICE-Setup-SEM/Emission Control>

4. The SEM voltage was set to 1400.

5. After these steps, the buttons in front of the QMS showing the i) power, ii) maximum speed achieved by the Turbo Molecular Pump and iii) valve where all checked before proceeding any further.

Before starting the measurements, the inlet capillary of the QMS was heated as a major step to prevent the condensation of water vapour coming from the gas line. A baking procedure was also performed for the QMS in order to reduce the background pressure inside the gas chamber. During heating and baking, the filaments and SEM were turned off.

APPENDIX B

SEISMIC EVENT LIST OF DENİZLİ AND ITS VICINITY

Table B.1 Seismic event list of Denizli and its vicinity.

DATE-TIME	Latitude N	Longitude E	Depth (km)	Magnitude Md	Relative Seismicity
25.11.2007 00:51	37.56	29.56	11	3.2	0.49
25.11.2007 01:42	37.03	29.25	3	3.1	0.28
25.11.2007 07:57	37.2	28.9	4	3.6	0.56
25.11.2007 08:05	37.13	28.91	5	3.2	0.41
27.11.2007 03:23	36.94	29.21	11	3.1	0.24
28.11.2007 05:46	36.94	29.21	9	3.2	0.24
28.11.2007 16:41	36.99	29.09	5	3.2	0.28
29.11.2007 02:57	36.93	29.24	6	3.3	0.24
29.11.2007 03:53	36.96	29.23	8	3.1	0.24
29.11.2007 10:22	36.99	29.33	14	3.2	0.25
01.12.2007 07:23	37.09	29.21	7	3.3	0.34
02.12.2007 22:21	37.07	29.22	6	4.5	0.44
02.12.2007 22:27	36.97	29.23	5	3	0.24
02.12.2007 22:38	37.02	29.25	5	3	0.26
02.12.2007 22:47	37.04	29.23	4	3	0.28
02.12.2007 23:49	37.01	29.27	5	3	0.25
03.12.2007 01:32	37.04	29.25	1	3.4	0.31
03.12.2007 18:12	37	29.23	10	3.6	0.3
04.12.2007 04:28	36.95	29.34	4	3.1	0.23
04.12.2007 23:25	36.99	29.26	10	3.3	0.27
05.12.2007 02:40	37	29.23	12	3	0.25
05.12.2007 19:26	37.02	29.23	3	3.2	0.28
06.12.2007 13:35	36.99	29.27	7	3	0.24
07.12.2007 12:20	37.84	29.48	8	3.6	1.05
08.12.2007 06:37	36.94	29.24	8	3.5	0.26
08.12.2007 14:18	38.12	28.97	5	3.1	4.59
09.12.2007 08:55	38.14	28.73	4	3.2	4.65
09.12.2007 22:29	37.05	29.23	5	4.2	0.39

Table B.1 (continued).

DATE-TIME	Latitude N	Longitude E	Depth (km)	Magnitude Md	Relative Seismicity
10.12.2007 09:10	37.03	29.32	6	3.2	0.27
10.12.2007 12:22	37.01	29.29	8	3.1	0.26
11.12.2007 12:10	38.57	28.65	5	3	0.55
14.12.2007 18:49	37	29.22	3	3.4	0.29
16.12.2007 09:50	36.94	29.26	14	3.5	0.26
18.12.2007 21:55	36.89	29.16	9	3.1	0.22
18.12.2007 22:59	36.93	29.17	12	3	0.23
21.12.2007 02:57	37.04	29.2	10	3.2	0.30
21.12.2007 05:25	36.85	29.36	7	3	0.18
22.12.2007 00:54	37.08	29.2	8	3.3	0.33
22.12.2007 07:45	37.16	29.07	5	3.1	0.41
23.12.2007 23:56	37.03	29.23	6	3.4	0.31
25.12.2007 15:41	36.93	29.23	9	3	0.22
25.12.2007 15:58	36.98	29.19	9	3.1	0.26
27.12.2007 23:43	36.95	29.33	5	3.1	0.23
28.12.2007 12:34	36.86	29.1	9	3.8	0.26
30.12.2007 01:17	36.99	29.29	7	3.2	0.26
30.12.2007 01:37	36.97	29.34	8	3	0.23
30.12.2007 13:41	36.87	29.31	1	3	0.19
30.12.2007 17:11	37.93	29.03	5	3	8.78
30.12.2007 19:03	36.93	29.35	10	3.1	0.22
30.12.2007 19:10	36.97	29.36	13	3	0.22
30.12.2007 22:39	36.96	29.34	13	3	0.22
31.12.2007 00:55	37.01	29.08	10	3.1	0.29
31.12.2007 12:54	37.01	29.27	5	3.4	0.29
01.01.2008 22:16	36.98	29.18	7	3	0.25
03.01.2008 00:55	37.25	28.67	7	3.1	0.53
05.01.2008 00:47	36.98	29.33	10	3.1	0.24
08.01.2008 08:04	37.07	29.81	10	3.3	0.20
08.01.2008 17:57	36.99	29.22	4	3.5	0.29
08.01.2008 18:32	37	29.18	3	3	0.26
09.01.2008 01:58	36.99	29.13	4	3.1	0.27
10.01.2008 02:03	37.02	28.3	9	3	0.24
10.01.2008 04:11	37.9	28.78	5	3	61.53

Table B.1 (continued).

DATE-TIME	Latitude N	Longitude E	Depth (km)	Magnitude Md	Relative Seismicity
10.01.2008 05:17	36.86	29.37	9	3	0.18
10.01.2008 05:34	37.22	28.64	5	3.4	0.53
10.01.2008 19:52	37.94	28.76	5	4.3	64.22
10.01.2008 20:04	37.93	28.78	3	3.2	108.99
10.01.2008 20:49	37.96	28.77	5	3.2	44.80
10.01.2008 20:57	37.91	28.78	2	3	123.15
11.01.2008 01:37	37.92	28.75	3	3.2	56.35
11.01.2008 03:06	37.94	28.75	5	3.4	43.76
11.01.2008 08:17	36.98	29.24	10	3.1	0.25
12.01.2008 08:38	37	29.21	10	3	0.26
13.01.2008 23:23	37.02	29.1	7	3.3	0.31
14.01.2008 03:21	37.9	28.73	5	3.2	30.42
15.01.2008 18:00	36.98	28.81	10	3	0.27
15.01.2008 21:59	37.02	29.21	4	3.1	0.28
16.01.2008 11:17	37.02	29.3	8	3	0.25
16.01.2008 12:21	36.97	29.21	2	3.2	0.26
16.01.2008 21:11	36.98	29.32	5	3.3	0.26
19.01.2008 00:33	37.01	29.13	7	3	0.27
19.01.2008 11:34	36.93	29.35	5	3.1	0.22
20.01.2008 19:08	37	29.21	14	3.1	0.26
21.01.2008 00:36	36.99	29.11	8	3.2	0.28
21.01.2008 01:43	36.99	29.09	7	3	0.27
21.01.2008 11:11	36.95	29.25	7	3.1	0.24
21.01.2008 20:36	37	29.07	5	3.6	0.33
24.01.2008 17:44	36.97	29.05	6	3.3	0.28
25.01.2008 02:45	37	29.24	5	3	0.25
27.01.2008 20:18	37.02	29.09	8	3.2	0.30
28.01.2008 17:24	37.02	29.19	9	3.1	0.28
29.01.2008 11:48	37.02	29.23	5	3.1	0.27
30.01.2008 06:39	36.98	29.22	8	3.2	0.26
30.01.2008 07:50	37	29.2	7	3.1	0.27
30.01.2008 11:08	36.98	29.21	11	3.2	0.26
30.01.2008 14:53	36.96	29.18	18	3.2	0.25
01.02.2008 00:02	37.05	29.15	5	3.2	0.31

Table B.1 (continued).

DATE-TIME	Latitude N	Longitude E	Depth (km)	Magnitude Md	Relative Seismicity
01.02.2008 01:53	37.15	28.4	5	3.1	0.35
01.02.2008 04:38	36.99	29.17	5	3.1	0.27
01.02.2008 23:34	36.95	29.23	9	3	0.23
03.02.2008 02:21	36.9	29.14	7	3.1	0.23
03.02.2008 04:13	38.22	28.86	6	3	2.59
03.02.2008 13:34	36.96	29.22	8	3	0.24
03.02.2008 17:59	37.24	28.19	7	3	0.34
04.02.2008 05:33	37.87	29.31	2	3.2	1.75
05.02.2008 20:39	36.99	29.11	3	3.2	0.28
05.02.2008 22:53	36.99	29.21	3	3.2	0.27
06.02.2008 03:41	36.96	29.18	5	3.3	0.27
06.02.2008 04:10	36.97	29.2	4	3.1	0.25
06.02.2008 04:23	36.97	29.19	5	3.2	0.26
06.02.2008 06:08	36.99	29.18	8	3.2	0.27
06.02.2008 12:49	36.96	29.19	6	3.3	0.26
08.02.2008 04:05	36.97	29.22	8	3	0.24
08.02.2008 05:20	36.97	29.23	6	3.1	0.25
08.02.2008 10:01	36.97	29.2	8	3.3	0.27
08.02.2008 10:31	36.98	29.2	6	3.1	0.26
08.02.2008 11:26	36.98	29.21	4	3.1	0.26
08.02.2008 16:20	36.97	29.19	11	3	0.24
08.02.2008 21:23	36.97	29.2	8	3.1	0.25
08.02.2008 23:40	36.94	29.26	11	3	0.22
09.02.2008 06:45	36.96	29.21	8	3.3	0.26
10.02.2008 03:29	36.94	29.25	9	3	0.22
10.02.2008 06:31	36.98	29.21	11	3.2	0.26
10.02.2008 12:23	37.99	29.28	5	3.2	1.93
11.02.2008 04:00	37	29.18	7	3.2	0.28
12.02.2008 08:24	37.13	28.24	5	3	0.29
12.02.2008 10:14	36.99	29.22	5	3.1	0.26
13.02.2008 03:11	36.94	29.26	6	3.4	0.25
13.02.2008 05:01	36.95	29.26	3	3.8	0.29
13.02.2008 10:00	36.98	29.2	7	3.2	0.26

Table B.1 (continued).

DATE-TIME	Latitude N	Longitude E	Depth (km)	Magnitude Md	Relative Seismicity
13.02.2008 11:29	36.97	29.2	5	3.3	0.27
17.02.2008 14:48	37	29.21	4	3.2	0.27
18.02.2008 04:35	36.97	29.23	9	3	0.24
21.02.2008 02:12	36.95	29.23	8	3.1	0.24
24.02.2008 12:09	37.25	28.22	6	3.1	0.37
25.02.2008 03:14	37.66	29.9	8	3.1	0.32
27.02.2008 16:45	36.92	29.09	7	3.1	0.24
28.02.2008 05:53	37.02	29.15	7	3	0.28
29.02.2008 19:37	37.82	29.64	12	3.2	0.60
02.03.2008 07:26	37.17	28.97	7	3.1	0.43
02.03.2008 20:34	37.96	29.15	9	3	3.33
05.03.2008 20:18	36.98	29.22	2	3.1	0.25
06.03.2008 05:49	36.97	29.18	10	3	0.24
07.03.2008 05:43	36.92	29.21	7	3	0.22
07.03.2008 11:44	36.63	29.89	10	3.1	0.10
07.03.2008 16:05	36.76	29.04	15	3.1	0.18
13.03.2008 06:33	37.92	28.98	13	3.1	8.90
16.03.2008 15:00	37.17	28.75	7	3	0.42
23.03.2008 13:34	36.98	29.16	10	3.7	0.31
28.03.2008 16:48	36.97	29.23	7	3.2	0.26
29.03.2008 04:32	37	29.18	8	3.1	0.27
30.03.2008 01:52	36.97	29.21	6	3	0.24
01.04.2008 00:26	37.73	29.51	7	3	0.73
01.04.2008 13:14	37.96	28.94	6	3.4	22.13
01.04.2008 16:24	36.93	29.22	7	3	0.22
03.04.2008 02:33	36.94	29.25	3	3.1	0.23
03.04.2008 20:06	36.98	29.2	7	3.2	0.26
06.04.2008 05:04	36.93	29.24	10	3.1	0.23
06.04.2008 20:48	36.72	28.78	9	3.2	0.18
09.04.2008 07:45	36.96	29.22	10	3	0.24
09.04.2008 07:45	36.97	29.25	3	3.1	0.25
09.04.2008 16:51	36.98	29.21	7	3	0.25

Table B.1 (continued).

DATE-TIME	Latitude N	Longitude E	Depth (km)	Magnitude Md	Relative Seismicity
10.04.2008 01:35	36.95	29.24	7	3.2	0.25
10.04.2008 06:24	36.93	29.22	11	3.1	0.23
11.04.2008 07:00	37	29.21	5	3	0.26
11.04.2008 11:54	37	29.21	7	3.2	0.27
12.04.2008 02:10	36.96	29.23	10	3.1	0.24
12.04.2008 11:04	36.98	29.21	10	3.1	0.25
12.04.2008 20:17	36.95	29.23	10	3.2	0.25
13.04.2008 02:27	36.97	29.21	1	3	0.24
13.04.2008 04:22	36.96	29.19	10	3	0.24
13.04.2008 06:20	36.98	29.19	10	3.1	0.26
13.04.2008 06:24	36.98	29.2	10	3.7	0.30
13.04.2008 07:00	36.97	29.2	10	3.2	0.26
13.04.2008 07:34	36.98	29.21	10	3.2	0.26
13.04.2008 07:50	36.97	29.2	6	3.1	0.25
13.04.2008 09:20	36.97	29.21	10	3.1	0.25
13.04.2008 10:39	36.99	29.18	2	3.1	0.27
13.04.2008 14:05	36.95	29.2	5	3.1	0.24
13.04.2008 16:38	36.96	29.22	10	3.2	0.25
13.04.2008 21:08	36.95	29.23	10	3	0.23
13.04.2008 22:04	36.95	29.23	7	3.1	0.24
13.04.2008 22:25	36.97	29.2	1	3.1	0.25
14.04.2008 00:11	36.97	29.2	10	3	0.24
14.04.2008 03:31	36.98	29.22	18	3.1	0.25
14.04.2008 10:46	36.95	29.22	5	3.2	0.25
14.04.2008 12:14	36.96	29.21	6	3.1	0.25
14.04.2008 18:54	36.96	29.21	1	3.1	0.25
14.04.2008 19:32	36.95	29.19	10	3.2	0.25
14.04.2008 22:27	36.94	29.25	1	3	0.23
15.04.2008 04:40	36.99	29.19	8	3	0.25
15.04.2008 05:31	36.96	29.23	1	3.1	0.24
15.04.2008 20:06	36.99	29.18	10	3	0.25
15.04.2008 20:49	36.96	29.22	2	3.1	0.25
15.04.2008 22:31	36.97	29.21	3	3	0.24
16.04.2008 03:06	36.95	29.24	7	3.1	0.24
16.04.2008 03:24	36.97	29.22	10	3.1	0.25

Table B.1 (continued).

DATE-TIME	Latitude N	Longitude E	Depth (km)	Magnitude Md	Relative Seismicity
16.04.2008 03:45	36.94	29.25	7	3	0.22
16.04.2008 17:28	36.98	29.19	10	3.6	0.30
16.04.2008 21:17	36.96	29.22	9	3.2	0.25
16.04.2008 22:11	36.98	29.22	5	3	0.25
16.04.2008 22:46	36.99	29.18	10	3.1	0.26
18.04.2008 01:46	36.95	29.27	6	3.1	0.23
18.04.2008 03:46	36.95	29.21	18	3	0.23
18.04.2008 04:22	36.99	29.19	1	3.2	0.27
18.04.2008 04:28	36.96	29.19	5	3	0.24
18.04.2008 20:56	36.95	29.28	15	3	0.22
18.04.2008 22:07	36.98	29.24	17	3	0.24
20.04.2008 02:21	36.96	29.21	10	3.5	0.28
20.04.2008 03:34	36.99	29.19	6	3.2	0.27
20.04.2008 14:53	36.97	29.25	6	3	0.24
20.04.2008 16:25	36.96	29.27	20	3	0.22
21.04.2008 16:25	36.96	29.21	8	3	0.24
21.04.2008 21:11	36.99	29.22	7	3	0.25
21.04.2008 21:47	37.72	29.31	10	3.1	1.29
22.04.2008 02:04	36.95	29.25	19	3	0.22
22.04.2008 03:13	36.97	29.22	10	3.1	0.25
24.04.2008 00:30	36.97	29.25	5	3.1	0.25
24.04.2008 21:15	36.99	29.11	10	3.1	0.27
25.04.2008 06:48	37.82	29.25	10	4.8	3.00
25.04.2008 07:43	37.81	29.25	10	3.1	1.91
26.04.2008 14:27	36.99	29.16	4	3	0.26
26.04.2008 15:45	37.79	29.26	10	3	1.71
26.04.2008 20:26	37.79	29.23	6	3	2.02
27.04.2008 01:38	36.99	29.19	10	3.3	0.28
27.04.2008 10:29	36.97	29.27	19	3	0.23
28.04.2008 22:04	37.32	28.48	6	3	0.55
28.04.2008 23:23	37.8	29.27	11	3.3	1.83
29.04.2008 20:49	36.99	29.19	9	3.7	0.31
29.04.2008 22:31	36.96	29.23	5	3.1	0.24

Table B.1 (continued).

DATE-TIME	Latitude N	Longitude E	Depth (km)	Magnitude Md	Relative Seismicity
29.04.2008 22:41	36.97	29.23	8	3	0.24
30.04.2008 01:44	36.99	29.17	11	3	0.26
30.04.2008 02:22	36.96	29.21	10	3	0.24
30.04.2008 05:40	36.93	29.27	20	3	0.21
01.05.2008 06:42	37.59	29.82	7	3	0.33
01.05.2008 22:34	36.99	29.21	3	3.5	0.29
02.05.2008 04:29	37.71	29.27	7	3.3	1.57
02.05.2008 10:03	36.97	29.35	6	3	0.22
02.05.2008 15:08	38.15	28.63	2	3.2	3.33
02.05.2008 19:21	36.97	29.33	5	3	0.23
04.05.2008 21:54	37.01	29.12	3	3.2	0.29
05.05.2008 00:08	37.08	28.99	11	3	0.33
08.05.2008 06:34	37.86	29.21	7	3	2.46
08.05.2008 09:15	37.02	29.18	7	3.1	0.28
08.05.2008 23:30	37.31	28.11	22	3.2	0.35
09.05.2008 19:01	37.07	29.1	8	3.1	0.32
09.05.2008 21:24	37.02	29.14	21	3	0.27
11.05.2008 06:50	37.06	29.07	22	3	0.30
12.05.2008 13:07	37.56	29.05	2	3	1.50
14.05.2008 05:09	36.99	29.21	3	3	0.25
14.05.2008 23:54	36.96	29.22	5	3.1	0.25
16.05.2008 10:29	36.99	29.17	2	3.2	0.28
16.05.2008 16:01	37	29.18	6	3	0.26
16.05.2008 20:17	36.96	29.24	5	3	0.23
16.05.2008 21:06	36.96	29.19	5	3.2	0.26
17.05.2008 05:12	36.96	29.2	3	3.2	0.26
17.05.2008 08:02	36.97	29.22	8	3	0.24
17.05.2008 11:35	36.96	29.25	5	3	0.23
18.05.2008 00:12	38.09	28.6	5	3	3.84
18.05.2008 04:19	37.81	29.31	5	3.2	1.62
18.05.2008 05:41	36.99	29.2	5	3.5	0.30
18.05.2008 22:05	37.02	29.16	10	3	0.27
19.05.2008 16:13	36.98	29.2	7	3.1	0.26

Table B.1 (continued).

DATE-TIME	Latitude N	Longitude E	Depth (km)	Magnitude Md	Relative Seismicity
19.05.2008 22:48	37.02	29.12	6	3.2	0.30
21.05.2008 10:37	36.98	29.22	5	3.2	0.26
22.05.2008 00:27	37.12	28.88	14	3	0.37
22.05.2008 05:10	36.93	29.31	6	3	0.21
22.05.2008 07:03	37.03	29.1	8	3	0.29
24.05.2008 04:15	36.99	29.19	9	3	0.25
24.05.2008 06:01	36.99	29.19	5	3.1	0.26
25.05.2008 01:20	37.83	29.7	6	3.1	0.52
25.05.2008 02:07	36.92	29.34	13	3	0.21
25.05.2008 07:46	36.98	29.21	8	3	0.25
25.05.2008 16:02	37.01	29.17	6	3.4	0.30
25.05.2008 16:35	37.35	29.31	5	3.3	0.56
25.05.2008 17:04	36.97	29.22	8	3	0.24
25.05.2008 17:05	37.24	28.21	7	3.1	0.35
25.05.2008 17:35	36.96	29.24	8	3.2	0.25
26.05.2008 19:44	37.83	29.25	6	3	1.98
26.05.2008 22:28	37.21	28.76	5	3.4	0.54
27.05.2008 08:42	36.97	29.23	5	3.4	0.27
27.05.2008 09:32	36.97	29.2	4	3.4	0.28
27.05.2008 23:56	36.94	29.24	5	3	0.23
28.05.2008 00:18	36.96	29.24	8	3.1	0.24
28.05.2008 11:01	37.27	28.23	5	3.1	0.38
29.05.2008 00:35	36.96	29.19	5	3.7	0.30
29.05.2008 00:44	36.95	29.21	3	3	0.23
29.05.2008 04:29	36.94	29.24	4	3	0.23
29.05.2008 08:26	36.97	29.18	5	3.2	0.26
29.05.2008 08:35	36.98	29.19	5	3.3	0.28
29.05.2008 11:40	36.96	29.23	7	3	0.24
30.05.2008 07:34	36.98	29.21	5	4.1	0.34
30.05.2008 07:38	36.97	29.21	6	3.4	0.28
30.05.2008 07:56	36.97	29.22	2	3.1	0.25
30.05.2008 08:36	37.02	29.13	4	3	0.28
30.05.2008 10:44	36.97	29.22	10	3	0.24
30.05.2008 13:48	36.95	29.24	8	3.2	0.25

Table B.1 (continued).

DATE-TIME	Latitude N	Longitude E	Depth (km)	Magnitude Md	Relative Seismicity
30.05.2008 14:57	36.97	29.23	7	3	0.24
30.05.2008 15:17	37	29.14	7	3.1	0.27
30.05.2008 23:57	36.97	29.24	12	3.7	0.29
31.05.2008 01:42	36.99	29.16	6	3.2	0.28
04.06.2008 11:10	36.99	29.2	2	3.4	0.29
05.06.2008 01:07	36.98	29.17	5	3.2	0.27
05.06.2008 01:13	36.98	29.16	9	3.2	0.27
05.06.2008 18:37	37.03	29.14	9	3.1	0.29
05.06.2008 23:45	36.98	29.18	5	3.1	0.26
06.06.2008 00:03	36.99	29.19	7	3.5	0.30
06.06.2008 03:02	38.17	28.58	15	3	2.04
06.06.2008 23:12	36.99	29.1	5	3.1	0.27
07.06.2008 02:16	36.97	29.19	3	3.1	0.25
07.06.2008 03:19	36.97	29.21	5	3.1	0.25
07.06.2008 18:25	36.96	29.21	5	3.6	0.29
07.06.2008 18:48	36.96	29.19	5	3.6	0.29
08.06.2008 23:02	36.9	29.37	4	3.1	0.20
09.06.2008 01:26	36.98	29.21	5	3	0.25
09.06.2008 04:45	36.97	29.21	5	3.4	0.28
09.06.2008 21:50	37.01	29.16	3	3.1	0.28
10.06.2008 02:16	36.96	29.24	5	3.2	0.25
10.06.2008 13:47	37	29.22	8	3	0.26
11.06.2008 02:14	37.87	29.2	5	3.2	2.85
11.06.2008 03:30	37.9	29.11	3	3.1	4.96
11.06.2008 04:13	36.97	29.22	10	3	0.24
11.06.2008 04:25	37.03	29.2	5	3.2	0.29
11.06.2008 05:40	37.82	29.21	5	3.4	2.67
11.06.2008 05:50	37.89	29.18	5	3.1	3.12
11.06.2008 09:10	37.87	29.19	4	3.2	3.02
12.06.2008 16:38	36.92	29.32	2	3	0.21
13.06.2008 12:50	37	29.16	5	3.1	0.27
14.06.2008 04:41	36.99	29.2	7	3.1	0.26
14.06.2008 19:21	36.93	29.32	6	3	0.21

Table B.1 (continued).

DATE-TIME	Latitude N	Longitude E	Depth (km)	Magnitude Md	Relative Seismicity
15.06.2008 00:55	36.99	29.2	6	3.3	0.28
15.06.2008 04:29	37.01	29.17	6	3.3	0.29
17.06.2008 12:48	36.95	29.27	7	3.2	0.24
17.06.2008 17:20	37.01	29.23	10	3.1	0.27
17.06.2008 21:29	37.05	29.19	5	3.3	0.32
18.06.2008 10:35	37.05	29.21	9	3.1	0.29
18.06.2008 10:42	37.09	29.18	6	3.3	0.35
20.06.2008 02:07	36.97	29.16	8	3.2	0.26
21.06.2008 01:35	37.01	29.2	8	3.1	0.27
22.06.2008 08:46	37.73	29.34	7	3.4	1.33
24.06.2008 19:11	36.94	29.2	5	3	0.23
25.06.2008 00:04	37.04	29.22	10	3.2	0.29
25.06.2008 00:35	37.04	29.17	4	3.2	0.30
25.06.2008 14:04	36.99	29.2	12	3	0.25
25.06.2008 22:02	37.01	29.18	5	3	0.27
26.06.2008 23:03	37.03	29.15	8	3.5	0.33
27.06.2008 18:13	37.03	29.18	2	3.1	0.29
28.06.2008 01:20	37	29.18	9	3.4	0.29
28.06.2008 11:03	37.28	28.21	3	3	0.37
28.06.2008 19:12	37.38	28.32	5	3	0.53
29.06.2008 02:57	37.03	29.18	8	3.5	0.32
30.06.2008 01:50	37.04	29.18	8	3.1	0.29
30.06.2008 15:51	37	29.25	8	3.2	0.27
02.07.2008 05:56	37.02	29.19	6	3.1	0.28
03.07.2008 10:30	37.02	29.19	8	3	0.27
03.07.2008 17:17	37.02	29.22	5	3.1	0.28
03.07.2008 19:16	36.99	29.19	2	3.2	0.27
03.07.2008 19:37	37.04	29.15	5	4.4	0.42
03.07.2008 20:01	37.05	29.15	2	3.2	0.31
03.07.2008 20:50	37.03	29.22	11	3	0.27
03.07.2008 22:18	37.02	29.22	5	3.1	0.28
04.07.2008 01:10	36.99	29.16	8	3	0.26
04.07.2008 07:36	37.08	29.2	9	3.2	0.32

Table B.1 (continued).

DATE-TIME	Latitude N	Longitude E	Depth (km)	Magnitude Md	Relative Seismicity
04.07.2008 11:57	36.97	29.18	6	3.2	0.26
04.07.2008 12:04	37.11	29.22	2	3.1	0.33
04.07.2008 12:09	37.02	29.23	6	3.3	0.29
04.07.2008 12:17	37.06	29.23	5	3.1	0.30
04.07.2008 16:56	37.01	29.23	4	3	0.26
04.07.2008 18:19	36.99	29.27	5	3	0.24
05.07.2008 01:45	37.09	29.25	2	3.1	0.31
05.07.2008 02:20	37.05	29.26	5	3	0.28
05.07.2008 10:13	37.09	29.16	9	3.1	0.33
05.07.2008 22:10	37	29.24	6	3.1	0.26
05.07.2008 23:55	37.07	29.19	5	3	0.30
06.07.2008 03:29	37.07	29.16	5	3.5	0.36
06.07.2008 03:38	36.98	29.23	7	3.1	0.25
06.07.2008 04:25	37.04	29.16	5	3	0.29
06.07.2008 16:58	37.05	29.18	6	3.5	0.34
06.07.2008 19:37	37.04	29.22	2	3.2	0.30
08.07.2008 09:20	37.03	29.15	11	3	0.28
08.07.2008 12:33	37.03	29.23	7	3	0.27
09.07.2008 04:07	37.06	29.2	9	3.1	0.30
10.07.2008 21:46	36.96	29.19	6	3.7	0.30
11.07.2008 12:12	37.03	29.15	5	3	0.28
11.07.2008 16:11	37.05	29.15	6	4.1	0.40
11.07.2008 18:25	36.97	29.24	8	3	0.24
11.07.2008 19:04	37.07	29.19	9	3	0.30
11.07.2008 21:45	37.04	29.2	9	3	0.28
12.07.2008 03:02	37.04	29.22	9	3	0.28
12.07.2008 18:13	36.95	29.27	7	3	0.23
12.07.2008 18:48	37.01	29.18	8	3.1	0.27
13.07.2008 07:33	37.01	29.2	5	3.1	0.27
14.07.2008 00:38	37.02	29.17	12	3	0.27
14.07.2008 01:17	37.04	29.18	9	3.1	0.29
14.07.2008 02:10	37.07	29.19	9	3	0.30
14.07.2008 07:09	37.03	29.17	9	3.1	0.29
15.07.2008 04:44	37.05	29.22	6	3.1	0.29

Table B.1 (continued).

DATE-TIME	Latitude N	Longitude E	Depth (km)	Magnitude Md	Relative Seismicity
15.07.2008 10:38	37.01	29.22	3	3.2	0.28
18.07.2008 03:35	37.01	29.18	8	3.1	0.27
18.07.2008 14:12	36.96	29.16	16	3	0.24
18.07.2008 18:54	37.11	29.17	7	3	0.33
20.07.2008 04:09	37.01	29.14	8	3	0.27
20.07.2008 09:59	37.04	29.12	5	3.2	0.31
20.07.2008 11:23	37.01	29.16	7	3	0.27
22.07.2008 00:54	37.03	29.14	7	3	0.28
22.07.2008 10:55	36.96	29.17	11	3.1	0.25
24.07.2008 04:36	36.98	29.21	8	3	0.25
24.07.2008 22:09	37.06	29.17	7	3.2	0.32
24.07.2008 22:29	37	29.15	5	3.2	0.28
25.07.2008 00:39	36.99	29.27	10	3	0.24
25.07.2008 12:04	36.97	29.2	8	3	0.24
25.07.2008 23:33	37	29.25	17	3.1	0.25
26.07.2008 12:05	37.02	29.19	9	3.1	0.28
26.07.2008 16:52	37.15	29.83	6	3.6	0.24
26.07.2008 20:42	37.03	29.15	6	3	0.28
27.07.2008 00:07	37.16	29.86	5	3.3	0.21
27.07.2008 03:07	37.07	29.13	8	3.1	0.32
27.07.2008 03:56	37.03	29.22	10	3	0.27
27.07.2008 05:04	37.02	29.14	12	3.1	0.28
28.07.2008 09:14	37.02	29.2	6	3.2	0.29
28.07.2008 16:53	37	29.18	8	3.4	0.30
29.07.2008 22:50	37.05	29.21	9	3	0.28
31.07.2008 07:09	37.06	29.14	7	3.3	0.33
03.08.2008 18:01	37.17	29.87	8	3.8	0.25
06.08.2008 04:27	37	29.18	8	3	0.26
06.08.2008 11:00	37.24	28.19	13	3	0.33
07.08.2008 04:26	37.01	29.21	8	3	0.26
08.08.2008 05:46	37.03	29.25	8	3	0.27
12.08.2008 01:41	38	29.1	5	3.4	5.07
17.08.2008 09:13	37.01	29.16	11	3.5	0.31
17.08.2008 09:30	37.04	29.13	3	3.5	0.34

Table B.1 (continued).

DATE-TIME	Latitude N	Longitude E	Depth (km)	Magnitude Md	Relative Seismicity
17.08.2008 09:43	37.03	29.17	6	3.2	0.30
17.08.2008 13:10	37.03	29.15	5	3.1	0.29
17.08.2008 20:13	37.11	29.13	8	3.1	0.35
17.08.2008 22:40	37.08	29.17	9	3	0.31
18.08.2008 03:33	36.96	29.06	8	3	0.25
18.08.2008 04:40	37.05	29.14	6	3.4	0.33
18.08.2008 05:42	37.06	29.12	7	3.7	0.38
18.08.2008 05:53	37.07	29.15	9	3	0.30
18.08.2008 16:07	37.01	29.19	2	3.2	0.28
19.08.2008 05:46	37.12	28.33	8	3.1	0.31
19.08.2008 05:56	37	29.23	6	3.2	0.27
19.08.2008 14:57	37.05	29.19	7	3	0.29
19.08.2008 17:49	37.04	29.15	13	3.1	0.29
20.08.2008 00:46	37.04	29.13	13	3	0.29
20.08.2008 21:46	37	29.2	9	3	0.26
21.08.2008 04:43	37.02	29.17	10	3.2	0.29
21.08.2008 18:53	37.04	28.21	15	3.1	0.24
22.08.2008 00:30	36.9	28.26	66	3.4	0.17
22.08.2008 08:55	37.02	29.16	6	3	0.27
23.08.2008 23:41	37.03	29.17	12	3	0.28
25.08.2008 00:52	36.98	29.19	5	3.5	0.29
25.08.2008 02:39	37.01	29.19	3	3	0.27
25.08.2008 02:50	36.99	29.2	6	3.2	0.27
25.08.2008 04:57	37.01	29.18	5	3.7	0.33
25.08.2008 06:01	37	29.22	5	3	0.26
25.08.2008 08:59	36.98	29.22	9	3.2	0.26
26.08.2008 01:35	36.72	28.25	62	3.2	0.13
27.08.2008 03:12	37.05	29.16	10	3.1	0.30
28.08.2008 14:55	37	29.21	9	3.2	0.27
28.08.2008 23:02	36.98	29.07	6	3.1	0.27
28.08.2008 23:07	37.12	29.11	7	3	0.35
31.08.2008 13:36	37.07	29.18	9	3.1	0.31
02.09.2008 04:28	37.1	29.13	3	3.4	0.38

Table B.1 (continued).

DATE-TIME	Latitude N	Longitude E	Depth (km)	Magnitude Md	Relative Seismicity
02.09.2008 20:50	37.03	29.1	3	3.2	0.31
04.09.2008 06:20	37.05	29.1	7	3.3	0.33
04.09.2008 22:29	37.9	29.25	4	3.2	2.31
05.09.2008 04:47	37.02	29.12	5	3.2	0.30
06.09.2008 15:34	37	29.14	6	3.3	0.29
09.09.2008 19:00	38.15	28.83	10	3	3.99
13.09.2008 09:07	36.97	29.29	5	3	0.23
16.09.2008 05:41	37.04	28.13	8	3	0.22
16.09.2008 23:34	37.09	29.12	8	3.1	0.33
17.09.2008 18:52	36.99	29.17	9	3.2	0.27
18.09.2008 21:51	37.84	29.49	10	3.3	0.93
23.09.2008 00:54	37.85	29.51	8	3.2	0.86
23.09.2008 01:16	37.04	28.11	6	3.1	0.23
24.09.2008 11:15	37.55	29.86	5	3	0.30
24.09.2008 18:16	36.81	28.12	81	3.6	0.14
25.09.2008 04:54	37.87	29.55	5	3.3	0.81
29.09.2008 05:57	36.96	29.16	8	3	0.24
30.09.2008 06:25	36.97	29.15	5	3.3	0.27
30.09.2008 06:44	36.98	29.14	5	3.2	0.27
30.09.2008 22:36	36.89	28.34	19	3.3	0.21
01.10.2008 05:53	37.02	29.11	5	3.7	0.35
01.10.2008 12:39	37.08	29.15	2	3.2	0.34
01.10.2008 20:26	36.98	29.11	5	3.2	0.28
01.10.2008 23:52	37.01	29.11	5	3.5	0.32
02.10.2008 01:06	36.95	29.14	5	3.1	0.25
02.10.2008 02:28	36.95	29.14	5	3.2	0.26
02.10.2008 03:35	37	29.12	5	3.2	0.29
02.10.2008 05:22	37	29.17	6	3	0.26
02.10.2008 05:55	36.98	29.09	2	3.4	0.30
02.10.2008 06:02	36.98	29.11	5	3	0.26
02.10.2008 10:26	36.99	29.11	5	3.1	0.27
03.10.2008 09:28	37	29.09	5	3.1	0.28
08.10.2008 14:31	36.97	29.13	5	3.5	0.29

Table B.1 (continued).

| DATE-TIME	Latitude N	Longitude E	Depth (km)	Magnitude Md	Relative Seismicity
08.10.2008 15:11	36.97	29.11	5	3.4	0.29
08.10.2008 15:15	36.97	29.14	8	3.2	0.27
08.10.2008 20:25	36.97	29.17	8	3	0.25
08.10.2008 21:08	36.96	29.16	8	3	0.24
09.10.2008 03:42	36.95	29.13	8	3.2	0.26
09.10.2008 19:47	36.96	29.13	5	3	0.25
10.10.2008 15:02	37.02	29.14	10	3.2	0.29
10.10.2008 16:26	36.98	29.17	6	3	0.25
10.10.2008 16:40	36.97	29.09	7	3	0.26
11.10.2008 11:34	36.98	29.16	6	3	0.25
11.10.2008 22:55	36.94	29.17	5	3	0.23
13.10.2008 12:54	37	29.06	7	3	0.27
17.10.2008 21:51	37	29.09	8	3.1	0.28
17.10.2008 21:53	36.94	29.14	7	3	0.24
19.10.2008 00:58	36.98	29.1	4	3	0.26
19.10.2008 17:02	37.25	28.15	7	3.1	0.34
20.10.2008 09:12	36.95	29.19	5	3	0.24
20.10.2008 10:10	36.98	29.07	7	3	0.26
22.10.2008 17:02	37.21	28.18	7	3	0.31
22.10.2008 20:37	36.94	29.12	5	3	0.24
23.10.2008 22:26	36.94	29.23	4	3.2	0.24
24.10.2008 07:03	36.94	29.13	7	3	0.24
24.10.2008 10:49	36.97	29.09	26	3	0.24
24.10.2008 17:51	37	29.06	5	3	0.27
27.10.2008 06:25	38.9	28.21	5	3.3	0.22
28.10.2008 22:11	37.02	29.07	10	3	0.28
30.10.2008 23:29	36.96	29.1	11	3.6	0.30

APPENDIX C

TEMPORAL VARIATION DATA BLOCKS
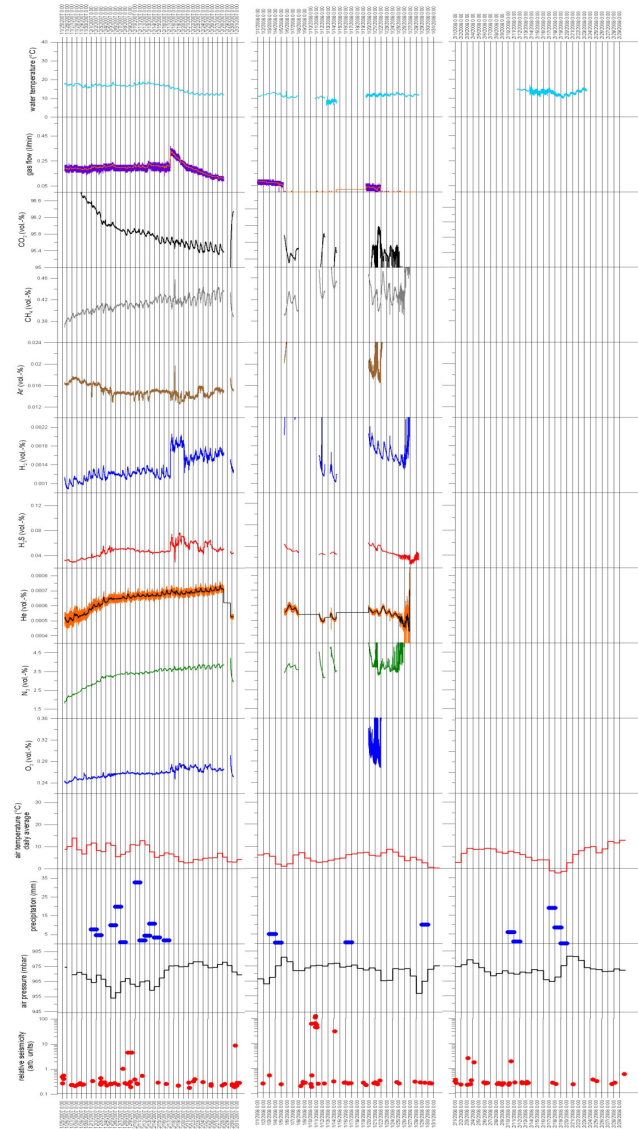
Figure C.1 Temporal variation diagram for Data Block I.
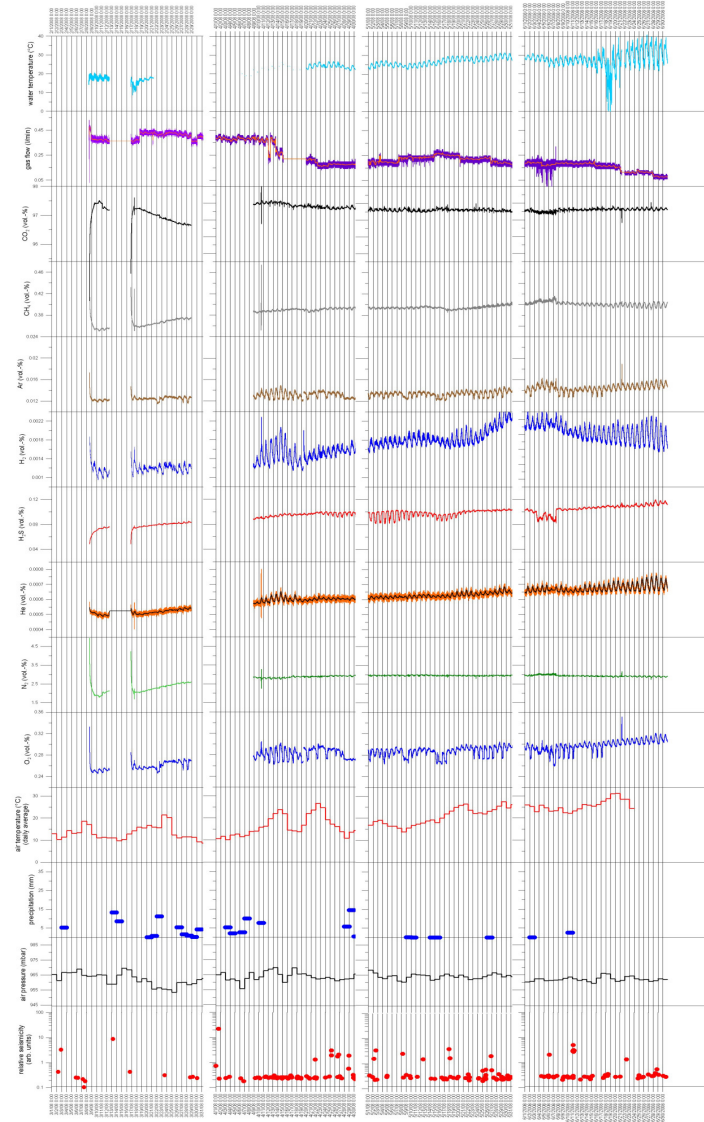
Figure C.2 Temporal variation diagram for Data Block II.
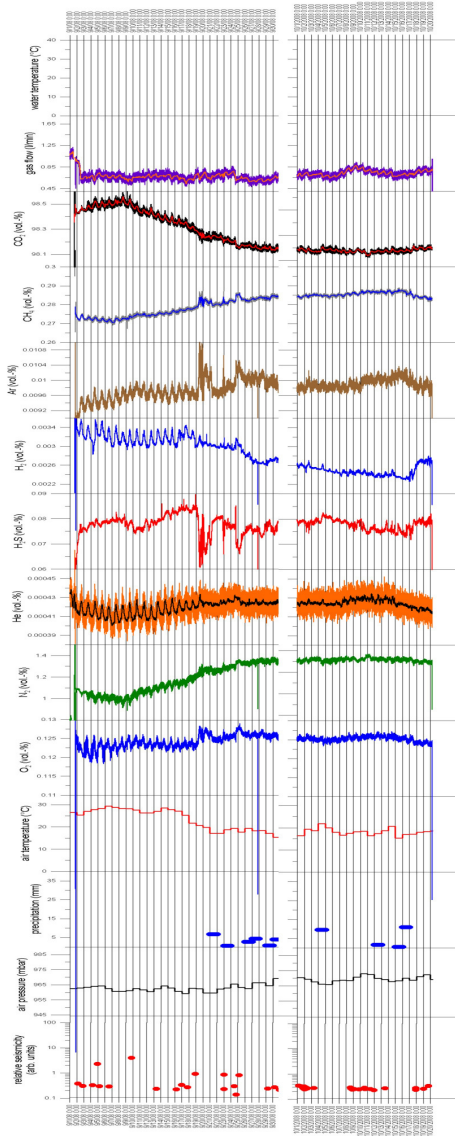
Figure C.3 Temporal variation diagram for Data Block III.

CURRICULUM VITAE

PERSONAL INFORMATION

Surname, Name: Süer, Selin
Nationality: Turkish (TC)
Date and Place of birth: 23 December 1979, Ankara
Marital Status: Single
Phone: +90 533 413 20 13
Fax: +90 312 285 36 19
E-mail: selsuer@gmail.com

EDUCATION

Degree	Institution	Year of Graduation
MS	METU Geological Engineering	2004
BS	METU Geological Engineering	2001
High School	METU College, Ankara	1997

WORK EXPERIENCE

Year	Place	Enrollment
2008-Present	General Directorate of Mineral Research & Exploration	Engineer
2001-2008	METU Department of Geological Engineering	Research Assistant

FOREIGN LANGUAGES

Advanced English, Poor German

PUBLICATIONS

Süer, S., Güleç, N., Mutlu, H., Hilton, D.R., Çifter, C., and Sayın, M., 2008. Geochemical Monitoring of Geothermal Waters (2002–2004) along the North Anatolian Fault Zone, Turkey: Spatial and Temporal Variations and Relationship to Seismic Activity. Pure appl. geophys. 165, 17–43.

Süer, S., Güleç, N., Mutlu, H., Çifter, C., Sayın, M., and Hilton, D.R., 2005. Sismik Etkinliklerin Izlenmesinde Hidrojeokimyasal ve İzotopik Parametreler: Kuzey Anadolu Fay Zonu. II. Ulsual Hidrolojide İzotop Teknikleri Sempozyumu, 26-30 Eylül 2005, Gümüldürİzmir. Bildiri Metinleri Kitabı, s. 11-23.

Süer, S., Güleç, N., Mutlu, H., Çifter, C., Hilton, D.R., 2003. Monitoring of Chemical and Isotopic Composition of Geothermal Waters along the North Anatolian Fault Zone. International Workshop on the North Anatolian, East Anatolian and Dead Sea Fault Systems: Recent Progress in Tectonics and Paleoseismology, and Field Training Course in Paleoseismology (Abstract Volume, p.52).

HOBBIES

Drawing, Traveling, Volleyball